1990 Thesis/Dissertation

Prediction of Tropical Cyclone Rapid Intensification Events

Dan B. Mundell

AD-A227 668

AFIT Student at: Colorado State University

AFIT/CI/CIA - 90-104

AFIT/CI
Wright-Patterson AFB OH 45433

186

UNCLASSIFIED

GENERAL INSTRUCTIONS FOR COMPLETING SF 298

The Report Documentation Page (RDP) is used in announcing and cataloging reports. It is important that this information be consistent with the rest of the report, particularly the cover and title page. Instructions for filling in each block of the form follow. It is important to **stay within the lines to meet optical scanning requirements.**

Block 1. Agency Use Only (Leave Blank)

Block 2. Report Date. Full publication date including day, month, and year, if available (e.g. 1 Jan 88). Must cite at least the year.

Block 3. Type of Report and Dates Covered. State whether report is interim, final, etc. If applicable, enter inclusive report dates (e.g. 10 Jun 87 - 30 Jun 88).

Block 4. Title and Subtitle. A title is taken from the part of the report that provides the most meaningful and complete information. When a report is prepared in more than one volume, repeat the primary title, add volume number, and include subtitle for the specific volume. On classified documents enter the title classification in parentheses.

Block 5. Funding Numbers. To include contract and grant numbers; may include program element number(s), project number(s), task number(s), and work unit number(s). Use the following labels:

C	- Contract	**PR**	- Project
G	- Grant	**TA**	- Task
PE	- Program Element	**WU**	- Work Unit Accession No.

Block 6. Author(s). Name(s) of person(s) responsible for writing the report, performing the research, or credited with the content of the report. If editor or compiler, this should follow the name(s).

Block 7. Performing Organization Name(s) and Address(es). Self-explanatory.

Block 8. Performing Organization Report Number. Enter the unique alphanumeric report number(s) assigned by the organization performing the report.

Block 9. Sponsoring/Monitoring Agency Names(s) and Address(es). Self-explanatory.

Block 10. Sponsoring/Monitoring Agency. Report Number. (If known)

Block 11. Supplementary Notes. Enter information not included elsewhere such as: Prepared in cooperation with...; Trans. of ..., To be published in .... When a report is revised, include a statement whether the new report supersedes or supplements the older report.

Block 12a. Distribution/Availablity Statement. Denote public availability or limitation. Cite any availability to the public. Enter additional limitations or special markings in all capitals (e.g. NOFORN, REL, ITAR)

DOD - See DoDD 5230.24, "Distribution Statements on Technical Documents."
DOE - See authorities
NASA - See Handbook NHB 2200.2.
NTIS - Leave blank.

Block 12b. Distribution Code.

DOD - DOD - Leave blank
DOE - DOE - Enter DOE distribution categories from the Standard Distribution for Unclassified Scientific and Technical Reports
NASA - NASA - Leave blank
NTIS - NTIS - Leave blank.

Block 13. Abstract. Include a brief (Maximum 200 words) factual summary of the most significant information contained in the report.

Block 14. Subject Terms. Keywords or phrases identifying major subjects in the report.

Block 15. Number of Pages. Enter the total number of pages.

Block 16. Price Code. Enter appropriate price code (NTIS only).

Blocks 17. - 19. Security Classifications. Self-explanatory. Enter U.S. Security Classification in accordance with U.S. Security Regulations (i.e., UNCLASSIFIED). If form contains classified information, stamp classification on the top and bottom of the page.

Block 20. Limitation of Abstract. This block must be completed to assign a limitation to the abstract. Enter either UL (unlimited) or SAR (same as report). An entry in this block is necessary if the abstract is to be limited. If blank, the abstract is assumed to be unlimited.

THESIS

PREDICTION OF TROPICAL CYCLONE RAPID INTENSIFICATION EVENTS

Submitted by

Dan B. Mundell

Department of Atmospheric Science

In partial fulfillment of the requirements

for the degree of Master of Science

Colorado State University

Fort Collins, Colorado

Summer, 1990

COLORADO STATE UNIVERSITY

May 3, 1990

WE HEREBY RECOMMEND THAT THE THESIS PREPARED UNDER OUR SUPERVISION BY DAN B. MUNDELL ENTITLED PREDICTION OF TROPICAL CYCLONE RAPID INTENSIFICATION EVENTS BE ACCEPTED AS FULFILLING IN PART REQUIREMENTS FOR THE DEGREE OF MASTER OF SCIENCE.

Committee on Graduate Work

Adviser

Department Head

ABSTRACT OF THESIS

PREDICTION OF TROPICAL CYCLONE RAPID INTENSIFICATION EVENTS

The largest errors in tropical cyclone intensity forecasting are usually the result of rapid intensification events, where rapid intensification is defined as a change in minimum central pressure of at least 42 hP_a in a 24 hour period, or a satellite-inferred increase in maximum sustained winds of at least 23 ms^{-1} per day when no measurement of central pressure is possible.

An observational and theoretical study is made of the unique characteristics of rapidly intensifying typhoons in the western North Pacific. Climatological data, digital infrared satellite imagery and composited rawinsonde sounding data within 5° of the center of tropical cyclones were used to identify the distinctive features associated with rapid intensifiers when compared to other stratifications of non-rapid intensifiers and non-intensifiers. Results show that rapidly intensifying tropical cyclones develop at latitudes equatorward of the seasonal mean in favored regions of the western North Pacific during the primary typhoon season from July to November. Rapid intensity change is indicated on satellite imagery as an extreme concentration of convection near the cyclone center. Relative concentrations of inner and outer deep cumulus convection reveal a predictive relationship between the ratio of inner core to outer core convection and the onset of rapid intensity change 12 hours later. This prediction technique was found to successfully forecast rapid or non-rapid intensification in over 90% of the cases in a three-year study of 70 northwest Pacific tropical cyclones

A physical explanation of the likely processes associated with rapid intensification is also presented. Rapid intensification is believed to be the result of weak asymmetrical

wind flow across the cyclone center at upper levels of the troposphere. Rapid intensifiers are shown to have large warm anomalies near the tropopause and weak vertical shear of tangential winds below 150 hP_a.

Dan B. Mundell
Department of Atmospheric Science
Colorado State University
Fort Collins, Colorado 80523
Summer, 1990

ACKNOWLEDGEMENTS

William Taylor was the inspiration for this intensification study. The author is indebted to the previous, unpublished work of Roger Edson and James Kossin for their efforts to discover a physical explanation of the rapid intensification process. The author would like to thank Dr. William M. Gray for his guidance and instruction. The author extends his appreciation to Raymond Zehr, William Thorson, Barbara Brumit, and Judy Sorbie/Dunn for data analysis, typing, manuscript preparation, and drafting. The support and understanding of Marquita and the boys was a major reason for the successful completion of this study. The author's research was supported by the United States Air Force Institute of Technology.

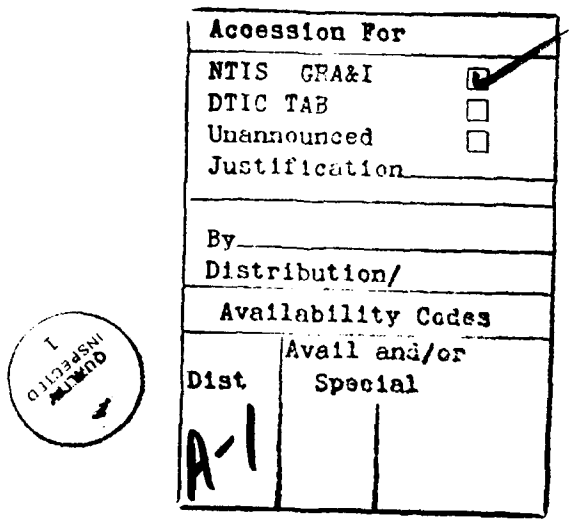

TABLE OF CONTENTS

LIST OF FIGURES

LIST OF TABLES

LIST OF SYMBOLS AND ACRONYMS

24FI = 24 Hour Forecast Intensity

AC = Aircraft

ARW Vector = Asymmetric Relative Wind Vector

ATCR = Annual Tropical Cyclone Report

ATR = Annual Typhoon Report

CI = Current Intensity

DMSP = Defense Meteorological Satellite Program

EIR = Enhanced Infrared

FI = Forecast Intensity

GMS = Geostationary Meteorological Satellite

GR = Genesis Region

I = Intensifiers

I/O Ratio = Inner to Outer Convection Ratio

IR = Infrared

JTWC = Joint Typhoon Warning Center

Julian Month = Overlapping 30 day climatological period centered on 15 day

MOT = Storm-relative cylindrical coordinate system

MSLP = Minimum Sea Level Pressure

N = Non-intensifiers

NOAA = National Oceanic and Atmospheric Administration

NWPAC = Northwest Pacific

OCS = Outer Core Wind Strength

OPEVAL = Modified Operations Evaluation

R = Rapid Intensifiers

RMW = Radius of Maximum Wind

SAT = Satellite

SCS = South China Sea

STY = Supertyphoon

T-Number = Tropical Cyclone Intensity Number

TC = Tropical Cyclone

TS = Tropical Storm

TS Lat = Latitude of Initial Tropical Storm Classification

TY = Typhoon

TY Lat = Latitude of Initial Typhoon Classification

Chapter 1

INTRODUCTION

1.1 A Personal Experience

On 19 November 1987, a rather ordinary tropical cyclone in the western Pacific attained tropical storm intensity and was named Nina. Over the next several days it continued to develop at a normal rate, reaching 90 knot (46 ms^{-1}) intensity on 24 November. Residents of Samar and southern Luzon in the Philippines did what they could to prepare for yet another typhoon. Like most tropical cyclones, Nina was not expected to intensify further, even weakening some, due to its proximity to land. But something unusual happened on 24 November 1987. Instead of weakening, Nina abruptly intensified, reaching winds estimated in excess of 150 kt (77 ms^{-1}) in less than 24 hours. The preparations for Nina's passage were not sufficient for the fury of its incredible winds. Hundreds died and about half a million people were homeless in the aftermath of one of the most destructive typhoons in recent memory (JTWC, 1987).

Could the magnitude of this disaster have been prevented or even reduced? Is it possible to forecast rapid intensification? These and other similar questions are the subject of this research.

1.2 The Present State of Intensity Forecasting

There are two basic forecast problems which daunt the tropical cyclone forecaster. The first is cyclone motion and the second is intensification. Numerous recent studies have concentrated on the first problem, but much less research has been devoted to the question of whether a given tropical cyclone will intensify or not, and to the rate of future intensification. The purpose of this study is to determine the primary factors which can

be used by the operational tropical forecaster to accurately predict intensification rates of tropical cyclones. The focus of this research is rapid intensification, a phenomena that occurs often without any prior warning, and can devastate large population and industrial centers due to a large, sudden increase in destructive potential in conjunction with inadequate warning lead time.

Of particular interest will be intensity forecasts based primarily on available satellite data. Since the discontinuance of aerial reconnaissance in the northwest Pacific Ocean (NWPAC) in August 1987, only a small percentage of tropical cyclones are monitored using aircraft. Thus, satellite-based intensity forecasting techniques would be in greater demand and have more worldwide application. Currently the only intensity forecasting techniques used by tropical cyclone forecast centers are based on persistence or extrapolation of past trends. The Dvorak intensity forecast model (Dvorak, 1984) is globally accepted as the best method available to forecast future intensity changes without the benefit of cyclone intensity measurements by aircraft. Yet the Dvorak model is simply an extrapolation forward of the past 24 hour trend unless the cloud pattern or its environment indicate strong favorable or unfavorable signs for future development. The objective of this research is to provide operational forecasters with more skillful forecasting techniques that are an improvement over intensity forecasts based on extrapolation and persistence.

1.3 Previous Research

Most of the studies conducted over the past 20 years concerning rapid intensification of tropical cyclones have been primarily climatological in nature. Probably the most in-depth research of the climatology of rapidly intensifying typhoons were done by Holliday and Thompson (1979) (see also Brand, 1972; Brand and Gaya, 1971). The climatological facts revealed in these papers have been used extensively in this research. The climatology of rapid intensifiers discussed in this research will be an extension of previous studies. With the demise of aerial reconnaissance in 1987, it is assumed that this climatological record can be considered complete inasmuch as verifiable, measured intensity changes used to distinguish rapid versus non-rapid intensifying typhoons in the western North Pacific is

concerned. Very little intensity forecasting research outside of climatological studies has been conducted over the past twenty years. A study of the cloud top equivalent blackbody temperatures of tropical cyclones and intensity change revealed that there was a strong relationship between cloud top temperatures with both current and future intensity (Gentry *et al.*, 1980; Steranka *et al.*, 1986). Gentry developed a set of regression equations used to predict intensity change based on an observed lag between convection and intensity change. Pike (1985) referred to geopotential height changes as a predictor of future intensity. Both of these methods are not used in an operational sense by any major tropical cyclone forecast center. Dunnavan (1981) found a relationship between the 700 hP_a equivalent potential temperature and the sea level pressure. An intersection of the traces of each variable was considered a predictive signal for further intensification to sea level pressure values below 925 hP_a. This technique was routinely used by JTWC forecasters on Guam to predict super typhoons (maximum sustained winds of 67 ms^{-1} or more) and rapid intensification with a reasonable amount of success. The measurement of the 700 hP_a equivalent potential temperature and surface pressure was accomplished using Air Force reconnaissance aircraft. Without aircraft, this method of intensity forecasting is no longer used in the NWPAC. Chen and Gray (1985) and Merrill (1988) tied intensity changes to environmental outflow patterns but without any specific intensity forecast scheme. A statistical intensity forecast scheme developed for the Atlantic by Merrill (1987) was unable to demonstrate forecast skill over the SHIFOR climatology and persistence forecast model by Jarvinen and Neumann (1979).

1.4 Motivation

In comparison to the amount of research effort to improve track forecasts, there has been a lack of research in the field of intensity forecasting. Consequently, there are few operationally useful methods that can be applied to predict future intensity. Accurate prediction of intensity is equally as important as small track forecast errors. In the recent example of Hurricane Hugo, the sudden pressure drop which occurred shortly before landfall was not forecast, creating a situation where the maximum winds and the size of the

hurricane-force wind field were significantly greater than the warnings just a few hours before landfall had indicated. The net effect of under-forecasting accelerated rates of intensification cannot be calculated. But clearly if rapid intensification could be accurately predicted at least 0 to 12 hours in advance of the onset of intensification, advance warning would allow more adequate preparation for stronger winds in the threat areas and likely help reduce the number of deaths and damage.

Why isn't more being done to address the intensity forecast problem? The author suspects that numerical and statistical modeling attempts to predict intensity change have not been able to demonstrate significant improvement over climatology and persistence models. The factors which affect intensity change may not be adequately resolved by the grid region used in the numerical and statistical methods. But as (or more) important, a complete understanding of the distinctive characteristics of rapid intensifiers versus non-intensifiers is lacking. It is likely that a better understanding of rapid intensity change characteristics and how they can be applied to numerical/statistical models will aid in the development of new intensity forecast models which will be an improvement over climatology/persistence forecasts.

Therefore, the motivation for this research is threefold:

1. Update the climatology of rapid intensifiers in the NWPAC, and show how knowledge of climatological probability can reduce large forecast errors .

2. Since satellites are the primary reconnaissance tool for most tropical cyclone forecast centers, develop ways the satellite data can be better used by forecasters to predict future intensity change. In particular, this study attempts to compensate for the loss of aerial reconnaissance in the NWPAC by finding a replacement for the Dunnavan technique used to predict rapid intensification.

3. Identify the unique characteristics of rapidly intensifying cyclones, and present a theory that explains the process of rapid intensification. Better measurements of rapid intensifiers and newer fine mesh resolution models of these distinctive characteristics might be used to improve our understanding of the rapid intensification process.

Chapter 2

DATA SET AND STRATIFICATIONS

2.1 The Climatological Data Set

The period from 1972 to 1987 was selected to determine the climatology of western North Pacific (NWPAC) intensity change. Starting in 1972, satellite data was routinely used by the Joint Typhoon Warning Center (JTWC) to locate tropical disturbances and monitor their development (intensity change). The bulk of the climatological information discussed in this thesis is based on the latitude at which tropical storm and typhoon intensity were first attained, so it was deemed prudent to limit the size of the climatology data set to a 16 year period where concurrent satellite and aircraft reconnaissance data were available to ensure position and intensity consistency. The availability of aerial reconnaissance, (discontinued on 15 August 1987 in the NWPAC), is vital for verification of intensity change measurements.

In addition, the rapid intensifiers which occurred in the NWPAC between 1956 and 1971 were included in the climatological data set, primarily to increase the number of rapid intensifiers studied. A total of 119 tropical cyclones were classified as rapid intensifiers during this 33 year period, and are listed in Appendix B. Intensity measurement data, as published in the Annual Typhoon Reports (ATR) from 1956-79 and the Annual Tropical Cyclone Reports (ATCR) from 1980-87, were used to determine intensification rates and to classify tropical cyclones as rapid intensifiers and non-rapid intensifiers. The 24 hour change of minimum sea level pressure was the primary classification factor.

2.2 Stratifications of the Climatological Data Set

Tropical cyclones which occurred in the NWPAC during the period of study were stratified into rapid intensifier, non-rapid intensifier, and non-intensifier categories. Addi-

tionally, regional differences were considered by distinguishing whether initial development happened in the western North Pacific (NWPAC) or in the South China Sea (SCS). All storms were categorized by initial tropical storm latitude (TS Lat), initial typhoon latitude (TY Lat), maximum intensity, and intensification rate. The number of hours required to reach maximum intensity (peaking hour) was used to determine intensification rate.

2.3 The Satellite Data Set

Satellite imagery is the primary reconnaissance tool used to monitor tropical cyclone intensity in all ocean basins worldwide with the exception of the western Atlantic and Gulf of Mexico regions, where aircraft are utilized by the United States government for positioning and intensity measurements. Of the various satellite platforms available for tropical cyclone observation, the Japanese Geostationary Meteorological Satellite (GMS), National Oceanographic and Atmospheric Administration (NOAA) and Defense Meteorological Satellite Program (DMSP) satellite data were used to distinguish unique characteristics of NWPAC rapid intensifiers which are apparent on routinely available satellite imagery. The data set used for this research included a 4 year sample of GMS digital infrared satellite data on magnetic tape supplied by the NOAA satellite applications branch at Fort Collins, Colorado for the primary June to December seasons of 1983 to 1986. This data which is available to William M. Gray's tropical cyclone research project, has a spatial resolution of 10 km and a temporal resolution of once every three hours (8 per day) with the exception of July and August 1984, where it is only once every six hours (4 per day). "Hardcopy" visual and infrared NOAA and DMSP data for the 1986 and 1987 tropical seasons was obtained from the JTWC.

Both DMSP and NOAA satellites are in a polar orbiting low-earth orbit. Typically, two passes are available per day for each satellite over a given tropical cyclone, one in the daytime and one at night. For the 1986-87 seasons, the DMSP satellites F6, F7 and F8 were operational in addition to the NOAA 9 and 10 spacecraft. Three to four spacecraft were operational at the same time, which means that high resolution satellite reconnaissance of a tropical disturbance was possible 6 to 8 times per day. For the purposes

of this research, satellite intensity estimates using the Dvorak EIR (enhanced infrared) and digital IR techniques were taken approximately every three hours to determine the rate of intensification as measured from satellite. In addition, for the digital IR GMS data it is possible to count the number of individual data points (pixels) with a brightness temperature colder than a particular value to determine the amount of deep convection for a given octant or radial band. This technique was extensively used in this study to determine relative concentrations of convection around the cyclone center.

2.4 The Composite Rawinsonde Sounding Data Set

For several years, Gray and his research group at Colorado State University have used composited rawinsonde soundings for tropical cyclone studies. Individual soundings and rawinsonde composites were extensively used to determine the unique characteristics of rapidly intensifying tropical cyclones. All composites are based on a cylindrical grid fixed on the cyclone center, divided into eight octants and extending out to 15° (1665 km) radius (Fig. 2.1). The primary radial bands used from the composite data set were 0 to 2° (0 to 222 km) for inner core and 3 to 5° (333 to 555 km) for outer core research. The outer circulation region beyond 5° was not studied extensively because most of the significant differences between rapid and non-rapid deepeners were expected to be found close to the cyclone center. Individual soundings were assigned an octant and radial band for averaging purposes based on the distance and direction of the rawinsonde site relative to the cyclone center. In the vertical, composite data is available for 22 pressure levels, from the surface to 50 hP_a (Fig. 2.2). At each pressure level, all soundings in a particular octant grid space or radial band are averaged to obtain mean values of such meteorological parameters as temperature, wind, moisture content, and geopotential height. In addition, by subtracting out the motion of the tropical cyclone, it is possible to determine such factors as radial and tangential wind components relative to a moving center. The primary composite parameters utilized in this research were the tangential winds, radial winds, temperatures and geopotential heights.

Tropical cyclones were stratified according to intensity, the rate of 24 hour intensity change, and time period relative to the intensity change.

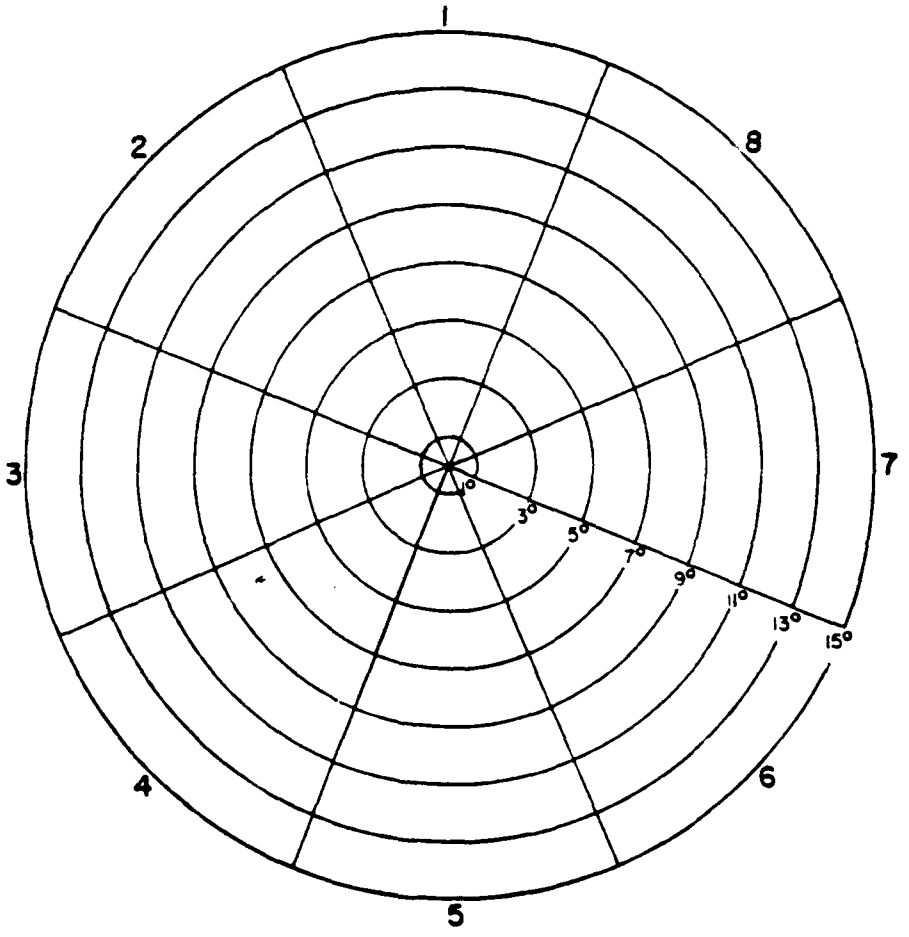

Figure 2.1: Cylindrical coordinate grid used to composite rawinsonde data relative to a fixed cyclone at the center. Octant is oriented to the north. Tangential and radial components of the wind were computed relative to the moving cyclone center by subtracting the storm motion vector. Temperature and height measurements were in a stationary coordinate system (Frank, 1977).

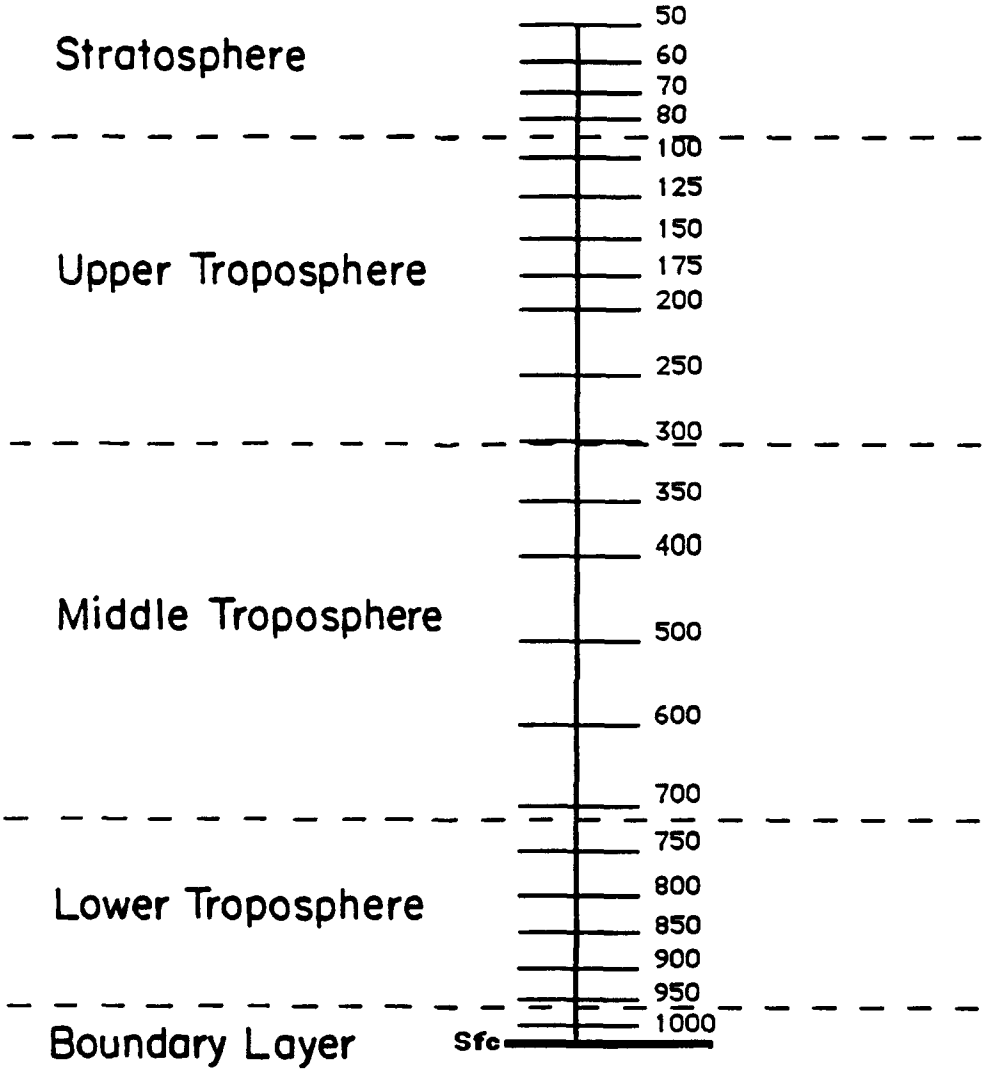

Figure 2.2: Illustration of the vertical resolution available in the composited rawinsonde stratifications utilized in this research.

Rapid intensifiers were defined by an intensity change of $\geq 42\ hP_a$ in 24 hours. This is the same definition used by Holliday and Thompson (1979). Storms were classified as non-rapid intensifiers if Δp was between 15 and 35 hP_a, and non-intensifiers if intensity change was 10 hP_a or less. A total of 13 stratifications listed in Table 2.1 were identified in this manner. These stratifications and the time period involved are presented graphically in Fig. 2.3.

2.5 Limitations of the Composite Data Set

It is an accepted fact that large variation is possible within each composite stratification. Averaging of data will tend to smooth outlying data that may (or may not) be of importance when considering individual sounding cases. The premise upon which compositing methods are based is that, given a sufficient number of individual soundings, it is possible to get an accurate vertical and horizontal representation of the average tropical cyclone in a particular stratification. When comparing one stratification to another, such as "Before Rapid Intensification" to "After Rapid Intensification", it is implicitly assumed that it is the same as comparing two soundings, one before the onset of rapid deepening, and a second after rapid intensity change has commenced. It must be noted that all before/after stratifications are independent. Two soundings are not paired together so that one is part of the "before" category and the other in the "after" column.

Since tropical cyclones occur in the data sparse open ocean regions, a lack of rawinsonde data extremely close to the cyclone center is to be expected. Soundings both within 1° (111 km) of the center and during a period of rapid intensity change are a rare but valuable source of information about the distinctive characteristics of rapid intensifiers. The number of soundings within 0-1° compared to other radial belts for the composite data set is presented in Table 2.2. For these reasons, individual soundings were used in place of composite data for the 0-1° radial belt.

Table 2.1: Description of the various composite stratifications used in this study to identify unique features of both rapid and non-rapid intensifiers. The before and after stratifications distinguish ongoing temporal changes that occur during intensification or non-intensification. Stratification by initial intensity was necessary because rapid intensifiers have tropical storm characteristics before the onset of rapid intensification and have mature typhoon characteristics afterward. $\bar{I}$ and $\bar{N}$ are mean values of the intensification and non-intensification classes, respectively.

COMPOSITE	DESCRIPTION TIME PERIOD	$\overline{\text{MSLP}}$ (hPa)
I1	Before Intensification / Tropical Storms 0 to 24 Hours Before Onset	993
I2	After Intensification / Tropical Storms 0 to 24 Hours After Onset	967
I3	Before Intensification / Typhoons 0 to 24 Hours Before Onset	966
I4	After Intensification / Typhoons 0 to 24 Hours After Onset	945
$\overline{\text{I}}$	Intensifiers 15 hPa $\leq \Delta p \leq$ 35 hPa / day 24 Hours Before to 24 Hours After Onset	967
N1	Before Non-Intensification/Tropical Storms 0 to 24 Hours Before Onset	998
N2	After Non-Intensification/ Tropical Storms 0 to 24 Hours After Onset	993
N3	Before Non-Intensification/ Typhoons 0 to 24 Hours Before Onset	963
N4	After Non-Intensification/ Typhoons 0 to 24 Hours After Onset	962
$\overline{\text{N}}$	Non - Intensifiers $\Delta p \leq$ 10 hPa / day 24 Hours Before to 24 Hours After Onset	977
R1	Before Rapid Intensification $\Delta p \geq$ 42 hPa 12 to 24 Hours Before Onset	983
R2	After Rapid Intensification $\Delta p \geq$ 42 hPa 0 to 12 Hours After Onset	956
$\overline{\text{R}}$	Rapid Intensifiers $\Delta p \geq$ 42 hPa /day 24 Hours Before to 12 Hours After Onset	969

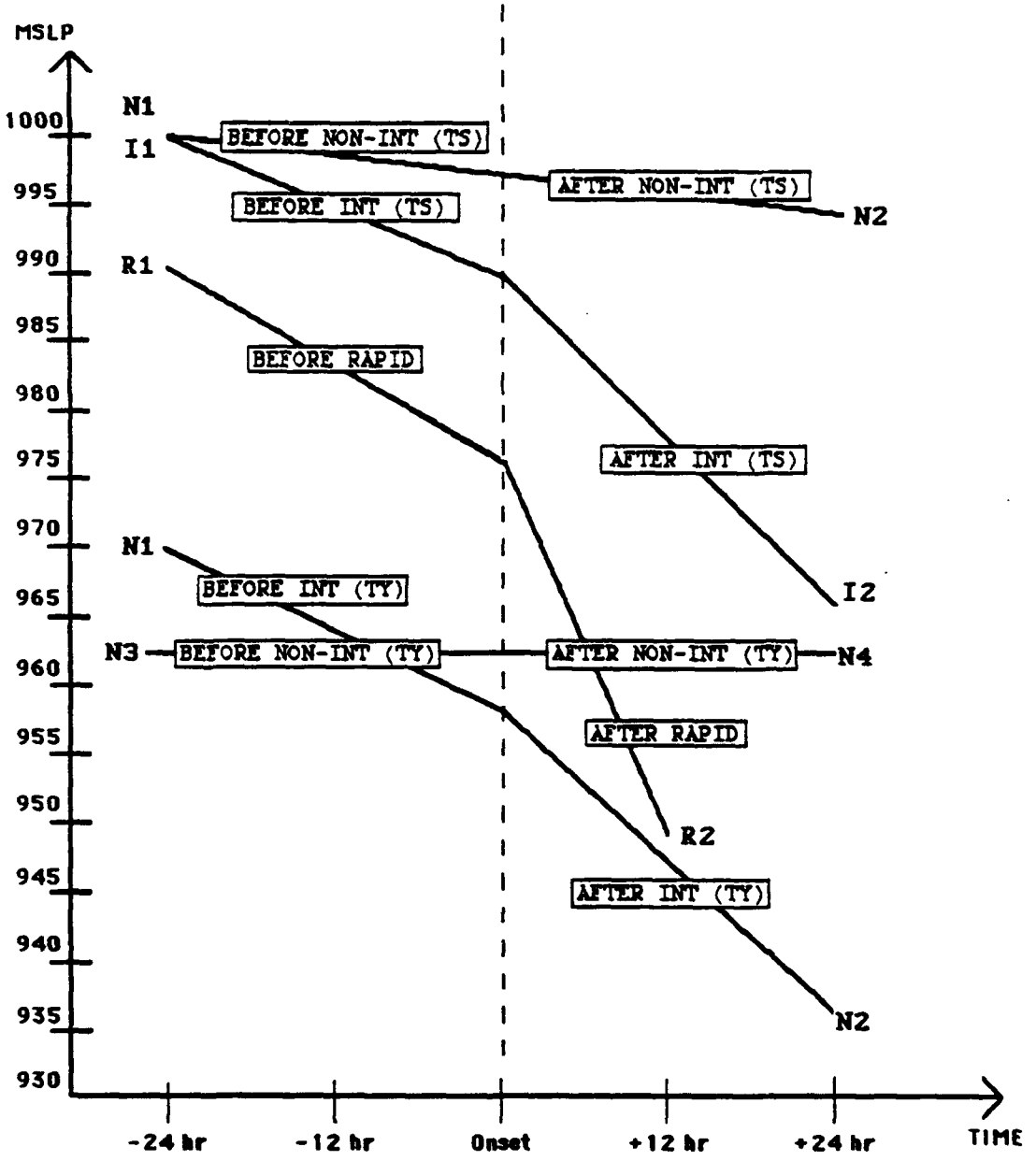

Figure 2.3: Illustration of the time versus intensity profiles for the 12 different composite stratifications used to identify distinctive characteristics of three main classes of intensification: rapid intensifiers (R), intensifiers (I), and non-intensifiers (N). The intensity range of the rapid intensifier composite is intermediate to the other classifications and does not include the time period 12 to 24 hours after onset.

Table 2.2: Availability of upper level rawinsonde soundings for a given radial band for the 12 composite data sets. The distribution of data is not uniform among radial octants within 2° of the center.

Rawinsonde Soundings per Radial Band (200 hPa)

COMPOSITE	0-1°	1-2°	2-3°	3-4°	4-5°
I1	8	25	49	65	92
I2	7	28	50	80	118
I3	4	25	56	94	132
I4	4	33	75	129	159
$\overline{I}$	23	111	230	368	501
N1	15	19	33	49	68
N2	7	38	55	78	115
N3	14	36	93	165	192
N4	8	57	126	207	248
$\overline{N}$	44	150	307	499	623
R1	3	11	19	27	35
R2	2	5	17	23	32
R	5	16	36	50	67

Chapter 3

THE CLIMATOLOGY OF INTENSIFICATION

3.1 Definitions

For the purposes of this research, rapid intensifiers were defined to be tropical cyclones which intensified at a rate of least 42 hP_a, the equivalent of 23 ms^{-1} (45 kt) per day, for a period of 24 hours or more. The basis for this rate of intensification was the measured minimum sea level pressures (MSLP) and 700 hP_a heights as published in the JTWC Annual Tropical Cyclone Reports (ATCRs). For the period of study from 1972 to 1987, 60 rapid intensifiers were identified in this manner, as compared to a total of 403 named tropical cyclones during the same period. Approximately 15% of all cyclones that reached tropical storm intensity in the NWPAC during the 70's and 80's experienced a period of rapid intensification (Appendix B).

The definition of rapid intensification is arbitrary; Holliday and Thompson (1979) selected a rate of $\geq$1.75 $mb\ hr^{-1}$ for 24 hr or $\geq$42 $mb\ d^{-1}$ to identify rapid intensification. Brand (1972) however, used a different criteria. He defined rapid intensification as "an increase in maximum surface wind of 50 knots or more in 24 hours".

JTWC (ATCR appendix) defines "rapid deepening" as a decrease in the MSLP of at least 1.25 $hP_a\ hr^{-1}$ for 24 hours, or 30 $hP_a\ d^{-1}$. The JTWC definition of "explosive deepening" is a decrease of 2.5 $hP_a\ hr^{-1}$ for 12 hours or a decrease of 5.0 $hP_a\ hr^{-1}$ for 6 hours. Another definition of rapid intensification would be a ΔV_{max} of at least 20 ms^{-1}, which is twice a mean intensification rate of 10 ms^{-1} per day. For the sake of consistency, the value of 42 hP_a (45 kt) per day was selected as being the best figure used to define "rapid intensification".

The *best track* winds are a post-analysis estimate of maximum sustained winds at 6 hour intervals, using all available wind intensity data, including aircraft, satellite, ship

and land station synoptic reports. Where aircraft measurements of MSLP or 700 hP_a level height were not available, the best track winds were used to determine the rate of intensification.

Julian Month is a climatological unit of time, defined to be an overlapping 30 day period centered about the midpoint (15th day) and taken every five days. Julian months are used instead of the terms "mid-July to mid-August", etc.

Period 0 means the point in time, as determined by the best track, that a tropical disturbance is classified as a tropical storm with maximum sustained winds of 18 ms^{-1}. The term *Period 1* is defined to be the number of hours after TS classification that the period of most rapid intensification begins. *Period 2* is the number of hours after TS classification that rapid intensification ends.

Period 3 is defined to be the number of hours after tropical storm classification that the maximum intensity is attained (as determined by the best track). Figure 3.1 is a time vs intensity depiction of these terms.

Tropical Storm Latitude (TS Lat) is the latitude at which a disturbance is initially upgraded to a tropical storm with maximum sustained winds of at least 18 ms^{-1} (34 kt), as determined in the post-analysis best track. Similarly, *Typhoon Latitude* (TY Lat) is the latitude at which a tropical storm is initially upgraded to a minimal typhoon with maximum sustained winds of at least 33 ms^{-1} (64 kt). *Genesis Region* (GR) refers to the 5° latitude belt at which a disturbance is upgraded to a named tropical storm.

3.2 Objective

The primary objective of this research is to reduce the magnitude of 24 hour forecast intensity (24 FI) errors which are the result of rapid intensification. It will be shown that the majority of 24 FI errors are relatively small. The author believes that such small intensity errors are not a serious forecast problem. In most cases, the intensity forecasting techniques currently used are adequate for non-rapid intensification and dissipation, and only small improvements are possible. Major strides can be made, however, toward reducing large 24 FI errors if the factors which precede rapid intensification can be identified

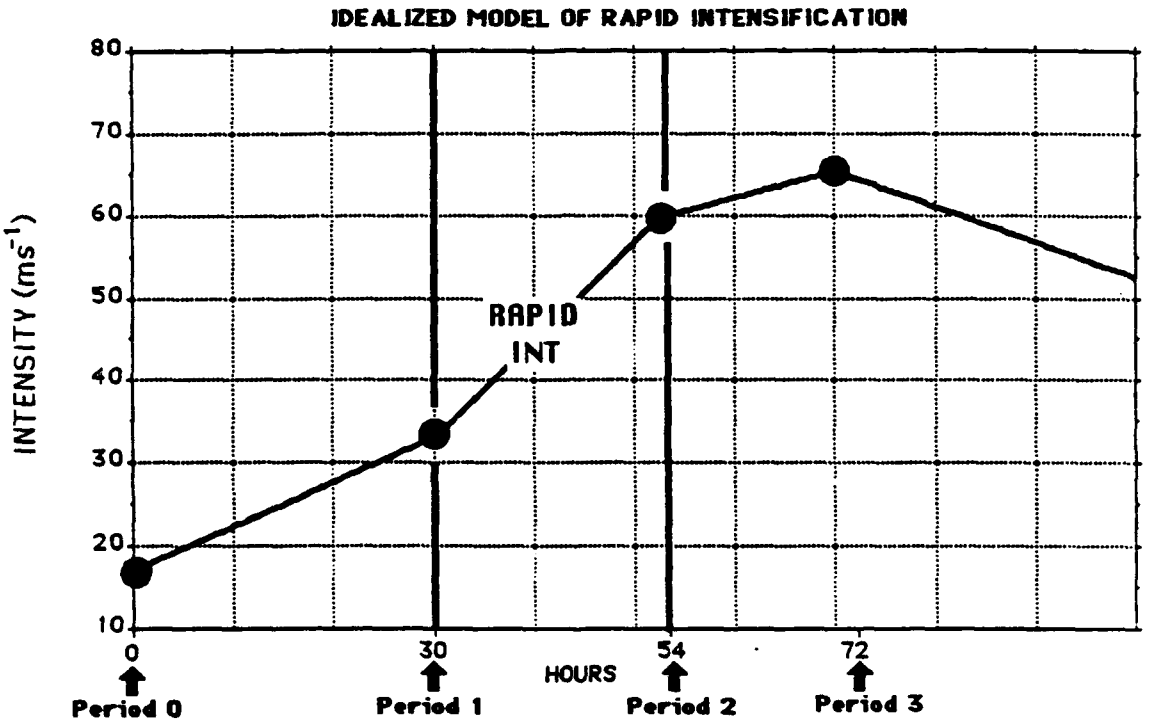

Figure 3.1: Illustration of an idealized time versus intensity model of rapid intensification. Period 0 is defined as the point that initial tropical storm intensity is attained. Periods 1 and 2 identify the onset and termination points of rapid intensity change, respectively. Period 3 occurs at maximum intensity.

and incorporated quickly into the operational forecast. The knowledge of the climatology of rapid intensifiers is the first basic factor which can be used to forecast rapid deepening.

A secondary objective is to reduce the magnitude of 48 and 72 hour forecast intensity errors. Since the long range forecasts are based even more on climatology and persistence, it is likely that a reduction of 24 FI errors would, in turn, reduce 48 and 72 FI errors. The climatology of intensification rates is especially useful for long range forecasting.

3.3 Forecast Intensity Errors

The mean 24 FI errors of the JTWC for an entire season are 6.4 ms^{-1}, with a bias of -0.3 ms^{-1}. Statistics for a sample of six NWPAC years from 1980 to 1985 are given in Table 3.1. Figure 3.2 is a frequency distribution of the 24 FI errors for this set of six consecutive seasons. The intensity errors appear to be normally distributed about a mean of 0. If we assume the true distribution is a standard normal curve with a mean of zero and a standard deviation of 8.7, then if the errors are given discrete values at 2.5 ms^{-1} intervals, this would mean that at least 68.26% of the forecast intensity errors should be within 8.7 ms^{-1} of a "perfect" forecast of 0 error. Indeed we find this to be true. Table 3.1 also lists the total percentage of 24 FI errors within ± 7.5 and 10 ms^{-1} for the 1980-85 sample. The probability of a 24 FI error of 13 ms^{-1} or more for this normal distribution is .1416.

3.4 Rapid Intensification Forecast Errors

There is a lower percentage of accurate intensity forecasts for rapid deepeners, however. Only 40 and 51 percent of the 24 FI errors are $\leq$ 7.5 and 10 ms^{-1}, respectively, during a period of rapid intensity change. During rapid intensification, much higher 24 hour forecast intensity errors are the norm. The 24 FI errors for the time period from 24 hours before "Period 1" to 24 hours after "Period 2" were tabulated to compare the magnitude of intensity forecast errors for 60 rapid intensifiers during 1972-87 versus all cases. The results for rapid deepeners are shown in Table 3.2.

The mean is nearly twice as large as the non-rapid 24 FI errors. The difference in mean values are significant at the .001 level. Note that the strong negative bias of

Table 3.1: JTWC 24 hour intensity forecast error statistics as determined by the official best track for the 1980 to 1985 NWPAC seasons. The bias is given by $\bar{x}$, the standard deviation by σ and by the mean by $|\bar{x}|$. Error values are in ms^{-1}.

Forecast Intensity Error Statistics

YEAR	% ≤ 7.5 ms^{-1}	% ≤ 10 ms^{-1}	$\bar{x}$	σ	$\lvert\bar{x}\rvert$	count
1980	75.86	84.55	-0.79	8.67	6.46	472
1981	74.41	86.14	-1.30	7.97	6.22	469
1982	75.75	84.18	-0.57	8.16	6.08	664
1983	66.56	78.77	-0.46	10.01	7.78	344
1984	74.21	82.46	+0.07	8.76	6.63	473
1985	78.26	87.22	+1.17	7.47	5.89	469
80-85	74.61	84.12	-0.32	8.48	6.43	2891

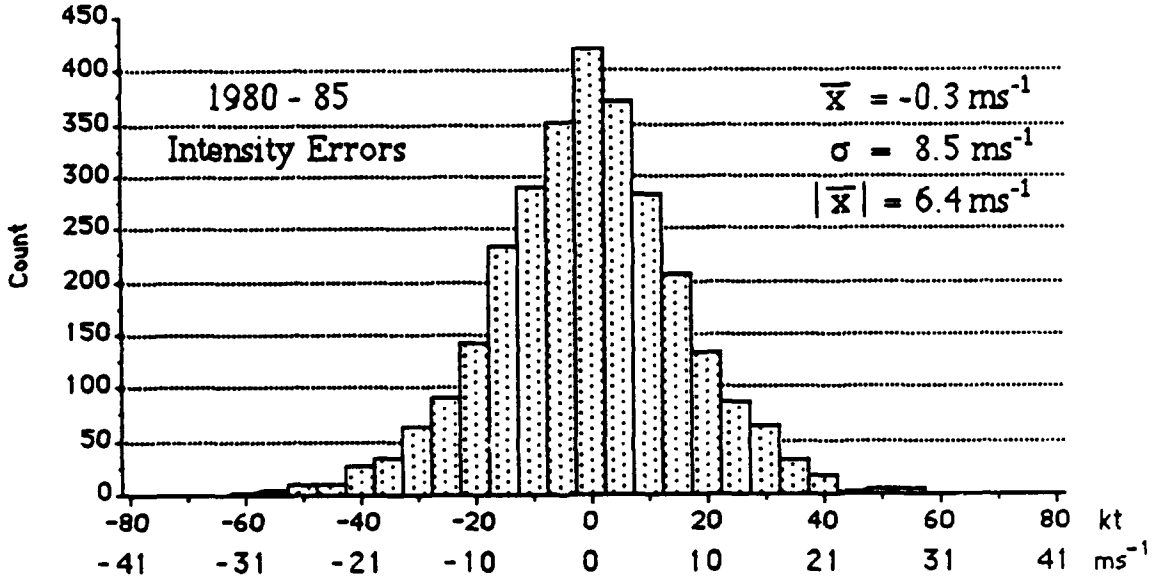

Figure 3.2: Histogram of the JTWC 24 hour intensity forecast errors for the 1980 to 1985 NWPAC seasons.

Table 3.2: Comparison of JTWC 24 hour forecast errors (in ms^{-1} for a period of rapid intensification versus all JTWC intensity forecast errors for the 1980-85 seasons. The rapid intensification period was defined as 24 hours prior to onset until 24 hours after the termination of rapid ($\geq 1.75\ hP_a\ h^{-1}$) deepening.

	MEAN	BIAS	ST. DEV.	COUNT
RAPID INTENSIFIERS 72 - 87	12.4	-9.7	11.2	468
ALL STORMS 80 - 85	6.4	-0.3	8.5	2891

-9.7 ms^{-1} reflects an inability to accurately predict rapid intensity change, resulting in under-forecasting of tropical cyclone intensity just 24 hours later. The likelihood of large ($\geq$ 13 ms^{-1}) errors in the 24 hour intensity forecast is about 50% during a period 24 hours before to 24 hours after rapid deepening. It should be noted that under-forecasting (negative bias) has more serious consequences than a positive bias. It is more dangerous, for example, to prepare for a 40 ms^{-1} typhoon that strikes at 70 ms^{-1} than to prepare for a 70 ms^{-1} storm that hits at "only" 40 ms^{-1}.

The distribution function of this set of rapid 24 FI errors is given in Fig. 3.3a. A total of 468 intensity forecasts are included in this sample, which is nearly equal to a typical full NWPAC season. The distribution function of a randomly selected full season (1984) with 473 cases is given in Fig. 3.3b for comparison. The mean absolute error of the rapid intensifiers is 12.4 ms^{-1} at 24 hours, which is about twice as large as the full season average of 6.6 ms^{-1}, and significant at the .001 level. Most of the large negative errors which occur over the course of a season are the result of rapid intensification. Eighty-five percent of the negative errors in excess of -26 ms^{-1} (50 kt) for the 1980-85 sample were from rapid intensifiers.

3.5 Geographic Distribution of Rapid Intensifiers

Rapid intensification in the NWPAC occurs mainly in the Philippine Sea region west of the Marianas Islands, east of the Philippines, and south of 25°N. The latitude and longitude of onset of rapid intensity change is influenced by the location of warm sea

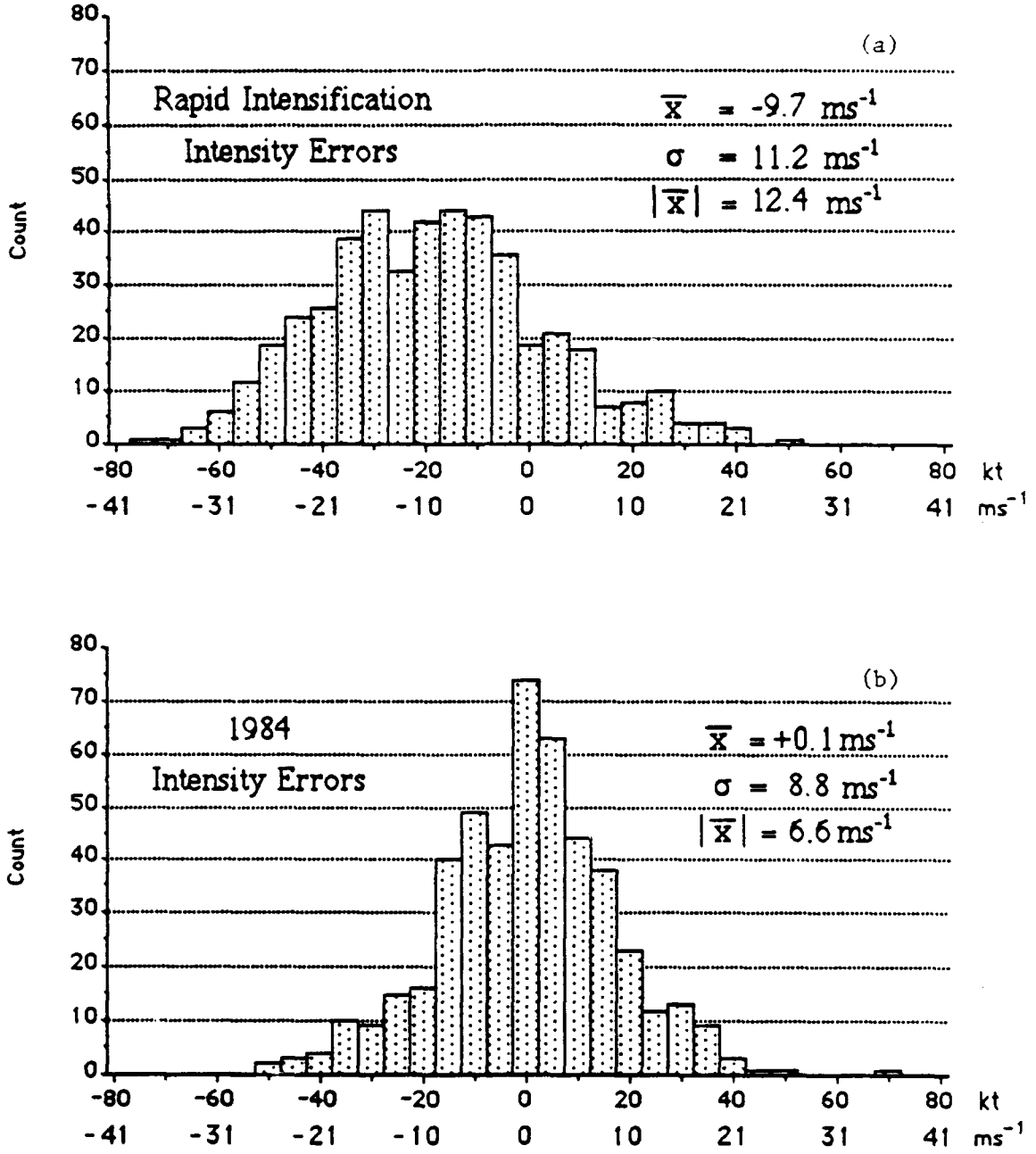

Figure 3.3: Comparison of the distribution of 24 hour forecast intensity (24 FI) errors for a period of rapid intensification (a) versus an equivalent number of intensity forecasts for the full 1984 NWPAC season (b).

surface temperatures. Figure 3.4 indicates that a minimum temperature of approximately 28.5°C is necessary for rapid intensification, which is substantially higher than the 26.5° accepted value (Palmén, 1948) needed for tropical cyclone formation. The relationship between sea surface temperature and intensity is expressed in Fig. 3.5.

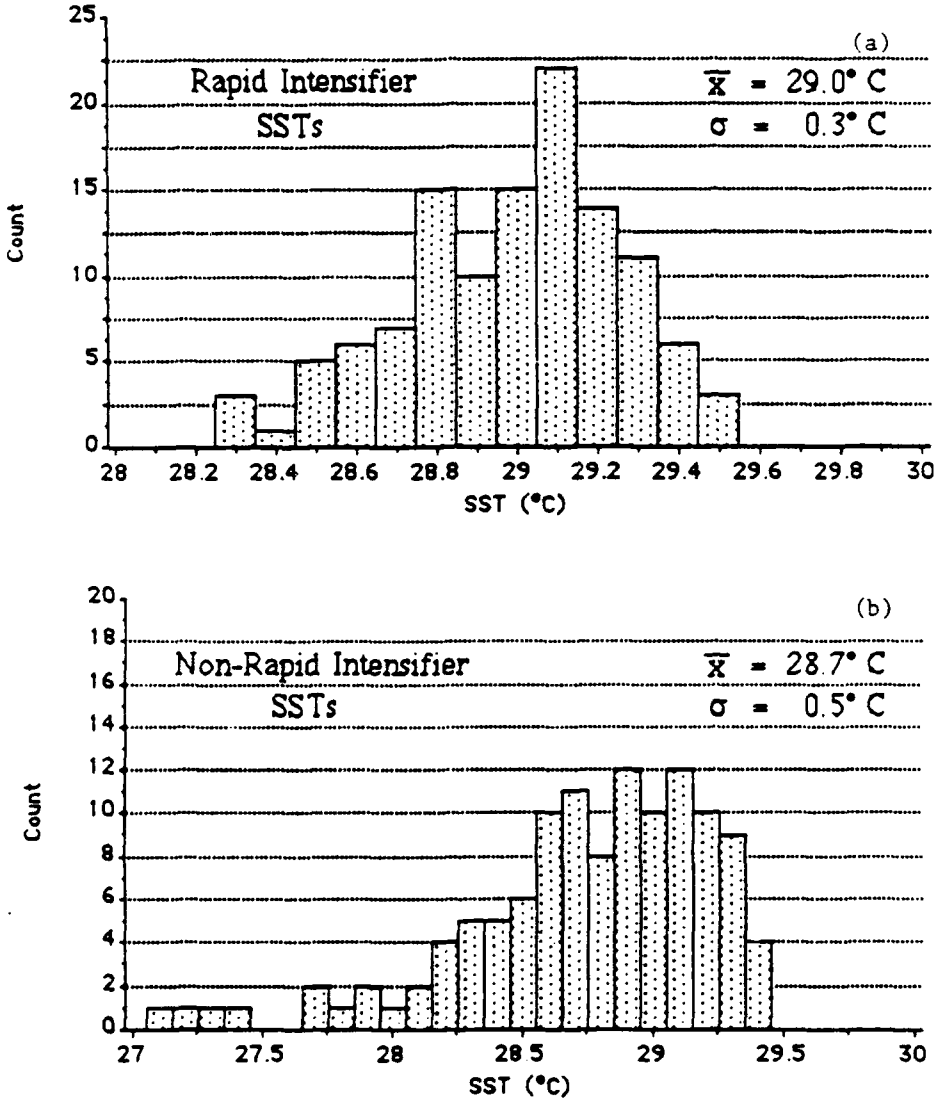

Figure 3.4: Frequency distribution of climatological sea surface temperatures at the onset of rapid (a) and non-rapid (b) intensification. Temperatures are based on the climatological parameters of location and time of year and may not reflect actual temperature in each case.

The geographic distribution of rapid intensifiers from 1956 to 1987 is shown in Fig. 3.6. The data points are at the onset of the rapid intensification period, which is the most

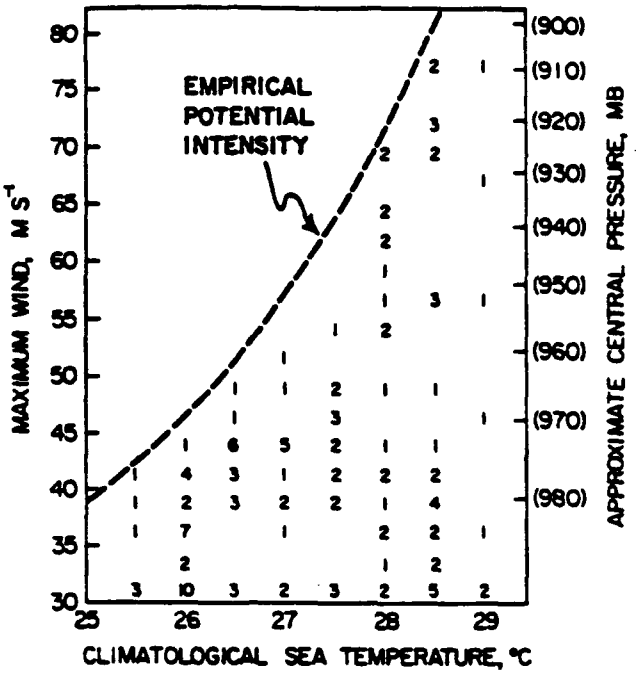

Figure 3.5: Empirical relationship between sea surface temperature and maximum intensity of North Atlantic tropical cyclones. The dashed line represents an empirical upper bound on intensity as a function of climatological SSTs (Merrill, 1988).

crucial forecast point. What is important about this climatological data is not simply where rapid intensifiers occur, but where they do not occur. The probability that rapid intensification will occur in the South China Sea region west of 125°E is less than .01. Similarly, typhoons north of 22°N or east of 158°E are not likely to rapidly intensify. Figure 3.6 shows the concentration of rapid intensifiers is within a relatively small area of the NWPAC forecast region. When seasonal SSTs are considered (Fig. 3.7 a,b), it is apparent that warm sea surface temperatures are an important factor in the geographic location of rapid intensifiers. However, most typhoons in the western North Pacific reach minimal typhoon intensity in the same region of SSTs warmer than 28°C, yet they do not rapidly intensify. The size of the 28.5° and 29°C SST regions is much larger than the area where rapid intensifiers develop. Warm SSTs are a necessary, but certainly not the only, factor that determines whether a given typhoon will rapidly deepen or not. These climatological facts presented here can be used as a filter to prevent forecasting rapid intensification at a location where it is not likely to occur.

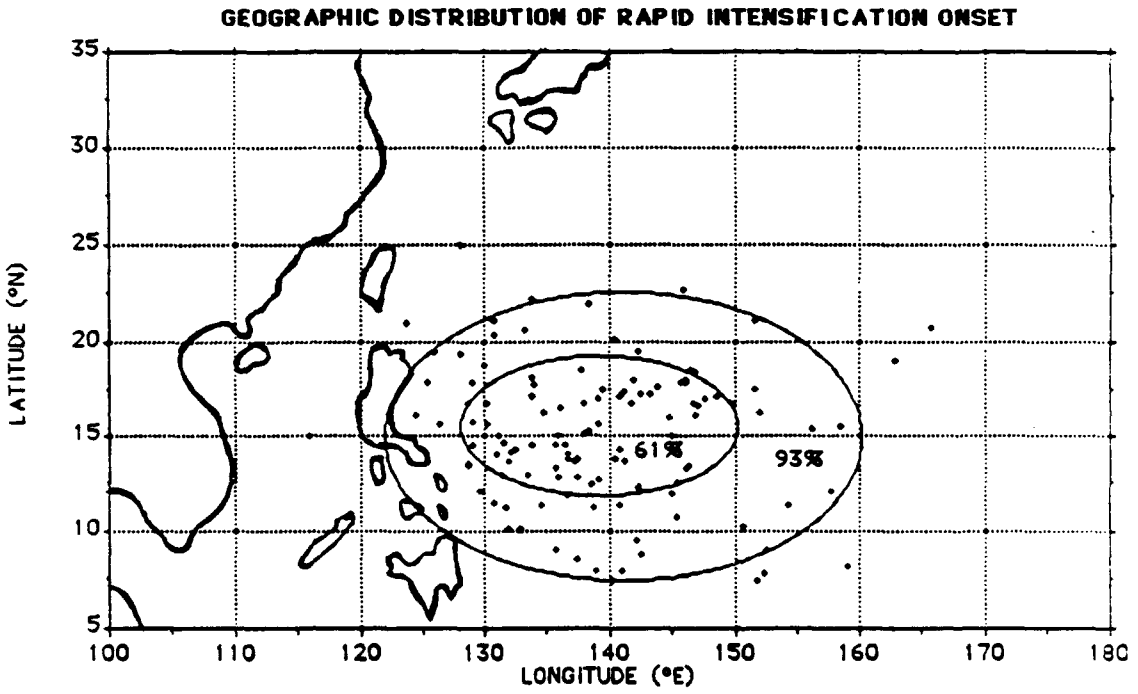

Figure 3.6: Geographic distribution of the location of onset of rapid deepening for all NWPAC rapid intensification events from 1956 to 1987. Percentages within each ellipse indicate the relative frequency of rapid intensification events. Seasonal differences are not specified.

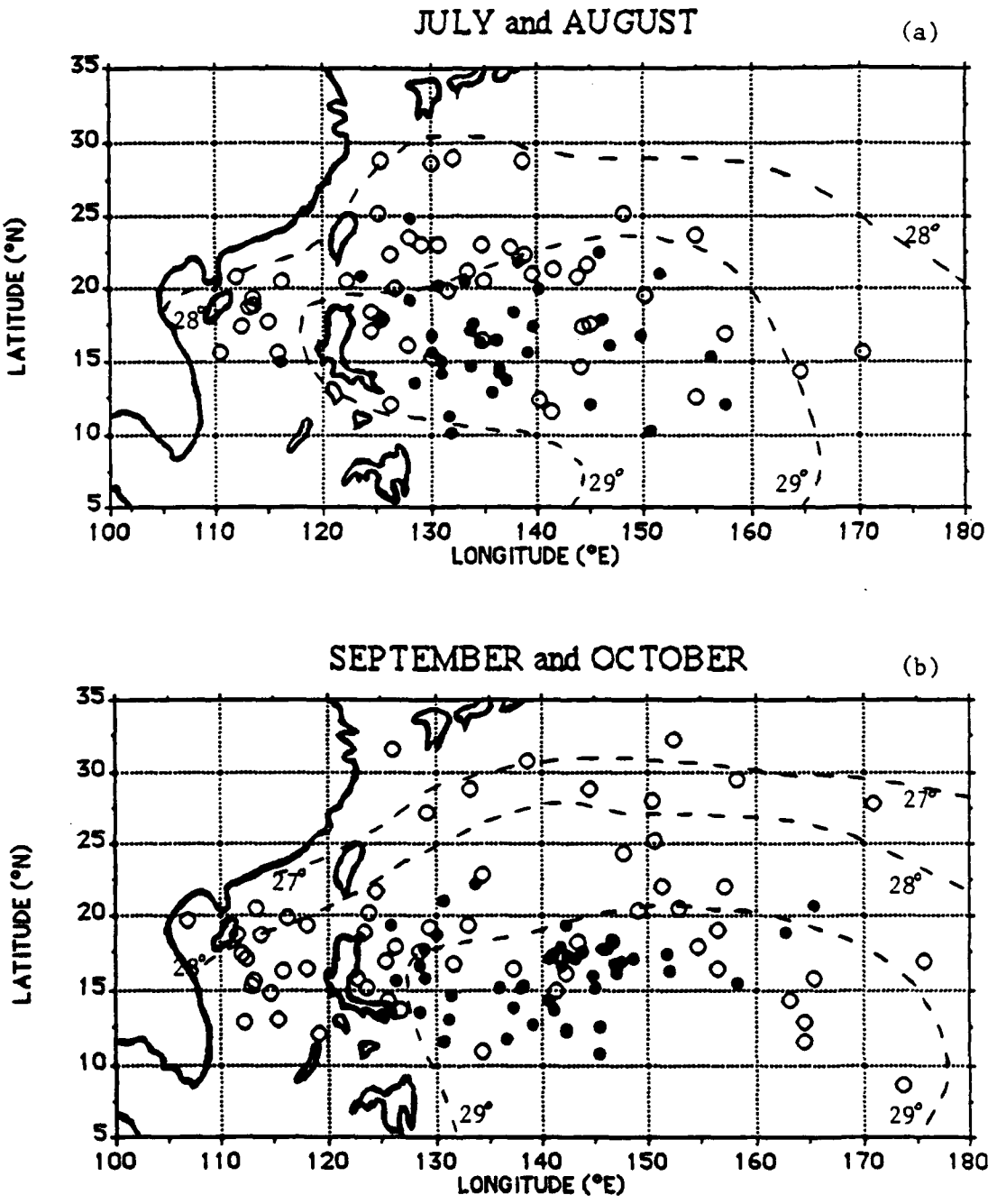

Figure 3.7: Illustration of the relationship between sea surface temperatures greater than 28.5°C and the onset of rapid (dark circles) and non-rapid (open circles) intensity change for the months of July and August (a), and September and October (b). SSTs are derived from monthly data compiled by Sadler *et al.* (1987).

3.6 Seasonal Distribution of Rapid Intensification

Another important climatological filter useful to predict rapid intensification is seasonal probability. It is possible that a certain period in the NWPAC tropical cyclone season is more favorable for rapid intensification. The daily distribution of the number of rapid intensifiers for the 1956-87 period is given in Fig. 3.8a. Of note is the fact that no rapid intensifiers have occurred in the months of February, March, or April during the past 33 years, and only once in early January (Kit, 1972). The "off season" for rapid intensification is from mid-December to mid-June (Julian dates 355 to 170). A minor peak is present during the month of May. The arbitrary division of the tropical cyclone season into the calendar months may hide true seasonal differences. For this reason, 73 overlapping 30 day periods called "julian months" were created (see Fig. 3.9). For each multiple of 5 julian days, the number of tropical cyclones occurring within ± 15 days were considered part of a "julian month" identified by the central (15th) julian date. The "monthly distribution" in this manner for 1956-87 is given in Fig. 3.8b. Most rapid intensifiers occur in the peak season of day 190 to 290 (Jul 9 to Oct 17). Most typhoons also occur during this time period (Fig. 3.10), so is the probability that a given typhoon will rapidly intensify higher during the peak season? Or is it higher in the early season of May-June or the late season of November-December? To answer these questions, the rapid intensifier count values for each of the 73 "julian months" were divided by the count values of the total number of typhoons for the same periods to determine the relative seasonal probability of rapid intensification. The results are given in Fig. 3.11. The highest probabilities of rapid intensification occur in the julian months of 205 to 215, 265 to 280, and 310 to 330. Since these "months" are defined to be the julian date ± 15 days, this means the highest probabilities are July 9 to August 18 (190 to 230) and September 7 to December 11 (250 to 345). The relative lull in late August is due to a large number of typhoons that form at latitudes north of 20°N, which is, as discussed earlier, unfavorable for rapid intensification. Forecasters should be more alert to the possibility of rapid intensification during these time periods since the probability that a given tropical cyclone of minimal typhoon intensity will experience rapid intensification is at least 1 out

of 4, while it is substantially less than this during other periods of the mean tropical cyclone season.

3.7 Geographical/Seasonal Characteristics of Rapid Intensification

The geographical and seasonal factors of rapid intensification can be used together to predict rapid intensification. The region of rapid intensification shifts slowly northward from May to September and southward again from October to December, but the longitudinal extent of this region does not vary significantly from month to month. This region of highest probability can be thought of as a box about 5 degrees of latitude in width extending from 125°E to 160°E, which moves from 7-12°N in May and December to 15-20°N in the mid-season of late August and early September. In order to more accurately define this region of highest probability, the mean latitude of the onset of rapid intensification for all rapid intensifiers occurring within each julian month was recorded along with the standard deviation. Figure 3.12 is the chronological sequence of the "monthly means" bordered by ± one standard deviation. This defines the "danger zone" of rapid intensification for a given julian date. This figure is useful for predicting whether rapid intensification is likely to occur, given a certain latitude/longitude position on a particular date.

3.8 Temporal Distribution of Rapid Intensification

The third climatological parameter of importance to the tropical cyclone forecaster is the point in time at which rapid intensification begins, and how long the rapid rate of intensification will last. Figure 3.13a is a frequency distribution of best track intensity at the beginning of rapid intensification (period 1). The initial intensity is normally distributed about a mean of 34.4 ms^{-1} with a standard deviation of 5.9 ms^{-1}. In the 1956-87 sample of 119 rapid intensifiers, 104 (87.4%) of the cases began their rapid rate of intensity change at 987 to 962 hP_a, which is equivalent to maximum sustained surface winds of 26 to 41 ms^{-1} (Atkinson and Holliday, 1977). This range of initial intensities is significant because it closely approximates the point at which a tropical cyclone develops

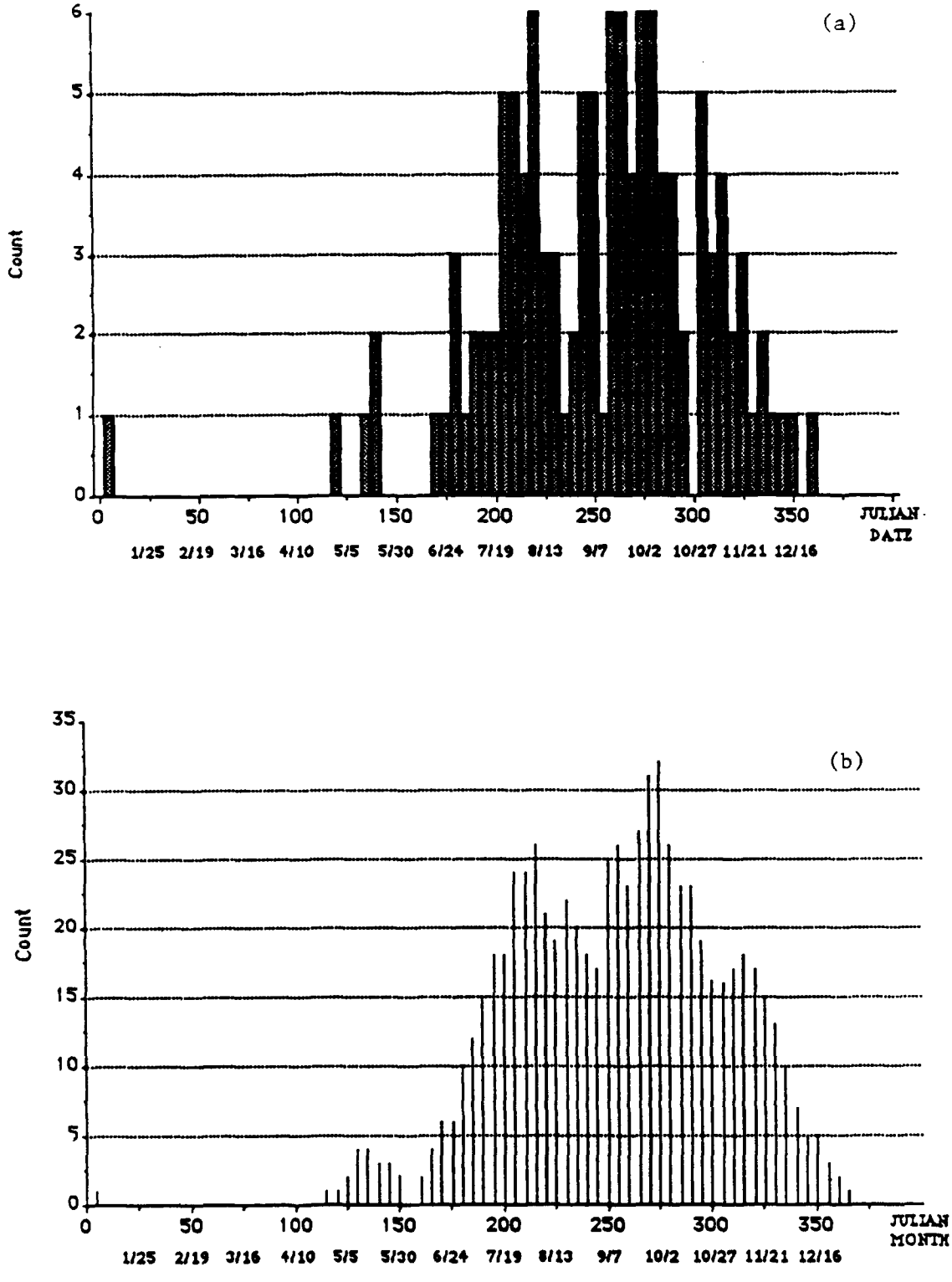

Figure 3.8: Frequency distributions of the onset of rapid intensification by date (a) and by a 30 day period called a "julian month" (b). Count values are for multiples of 5 days (pentads). Data consists of 119 rapid intensification events in the NWPAC from 1956 to 1987.

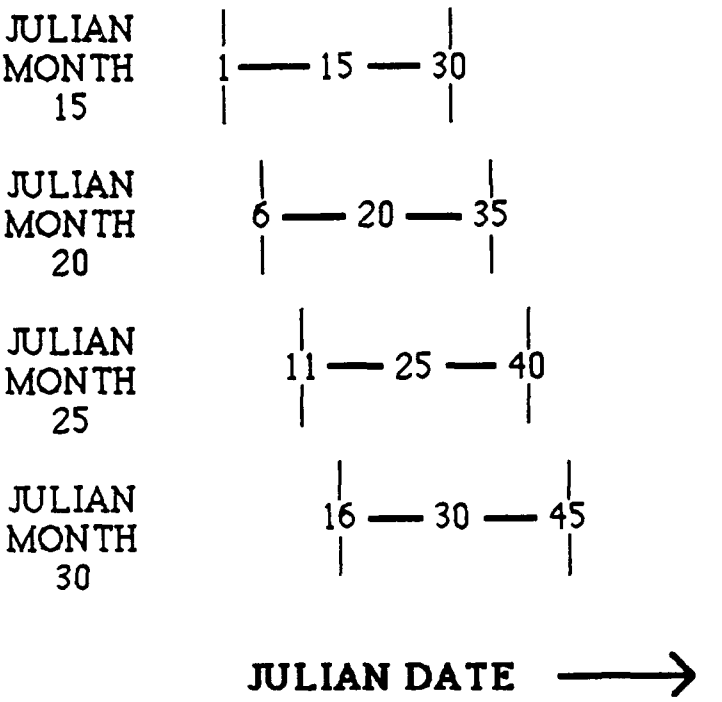

Figure 3.9: Description of the 30 day overlapping time periods used to determine tropical cyclone frequencies by julian month. A julian month is a 30 day period centered on, and identified by, the 15th day.

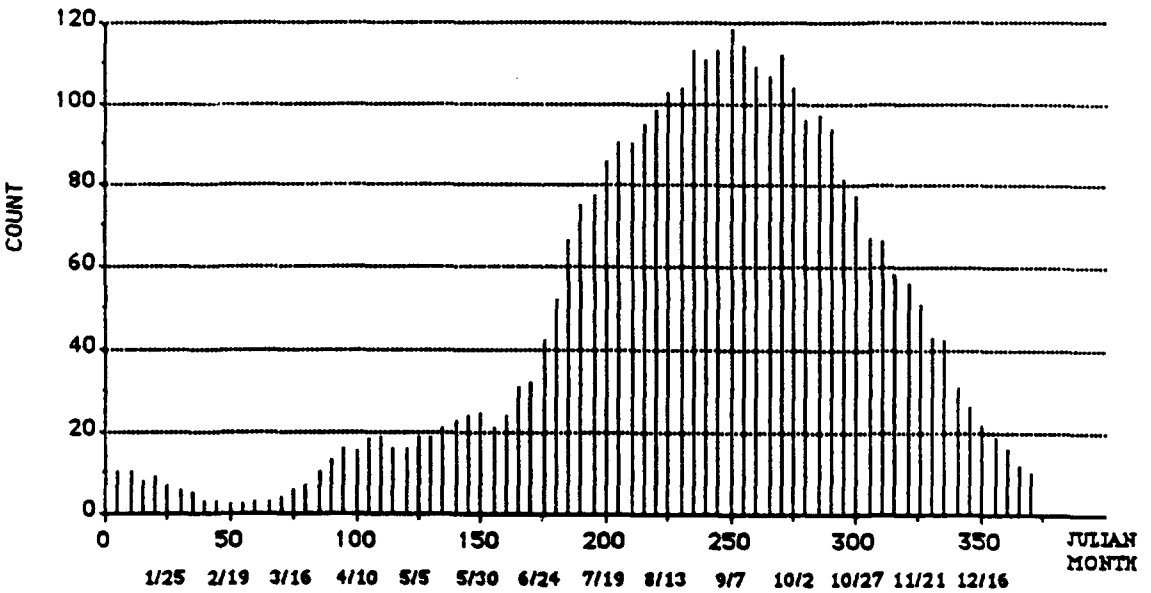

Figure 3.10: Frequency distribution of typhoons by julian month. Count values for each pentad are given by the total number of initial typhoon intensity events occurring within ± 15 days. Data consists of all NWPAC typhoons from 1956 to 1987.

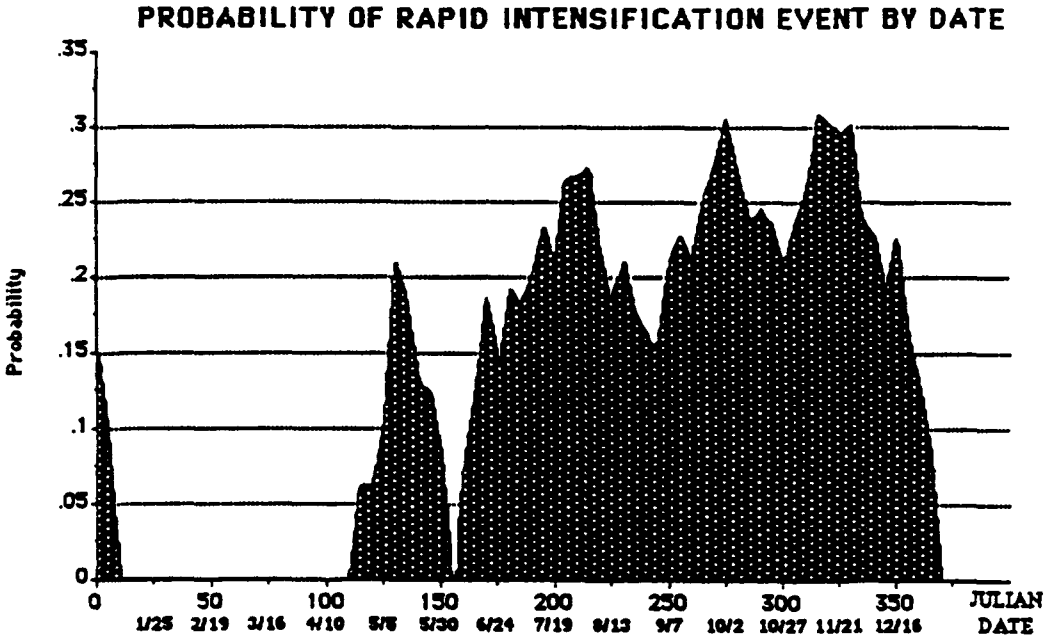

Figure 3.11: Relative probability function of rapid intensification by julian month. The relative probability is defined as the number of rapid intensification events divided by the number of initial typhoon intensity events for each overlapping julian month. This is a description of the likelihood, by date, that a particular typhoon would rapidly intensify.

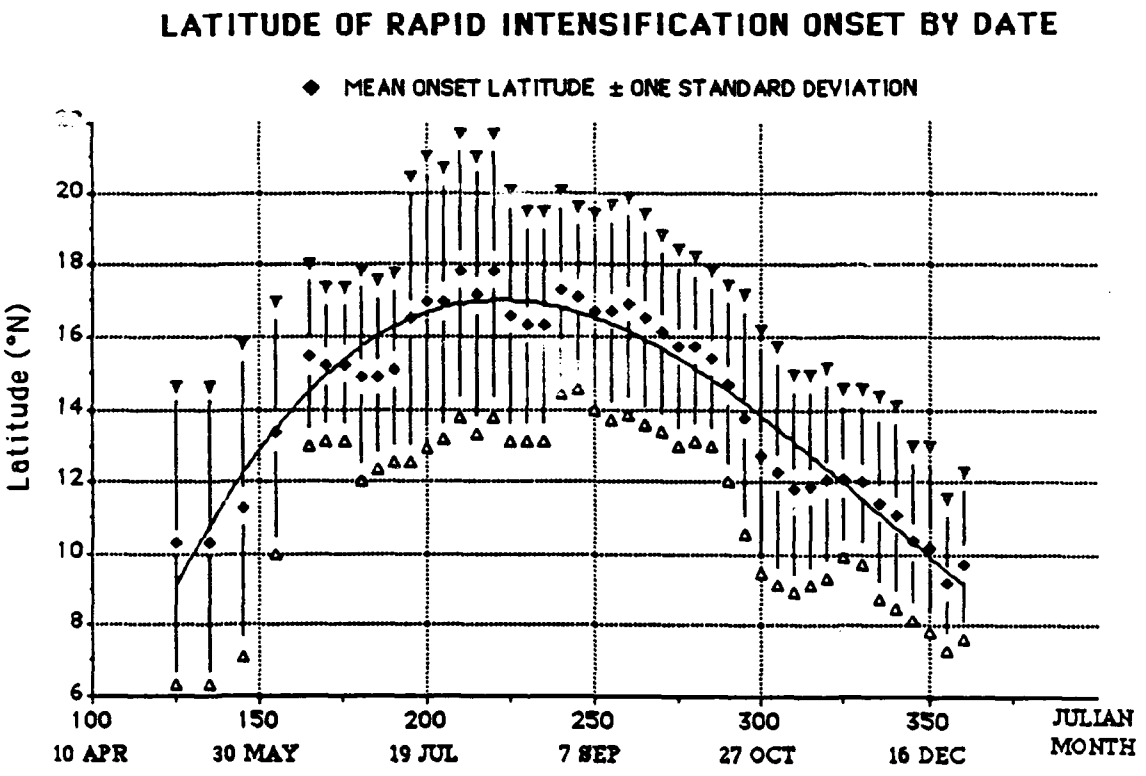

Figure 3.12: Illustration of the latitude region of highest rapid intensification probability. The mean latitude of rapid intensification onset ± one standard deviation is shown for the NWPAC season. Data consists of 119 rapid intensification events from 1956 to 1987.

a central eye which is apparent on radar and satellite imagery (Weatherford and Gray, 1988). Therefore, prediction of a rapid intensification event should be made only after development to at least 26 ms^{-1} or until an eye is apparent on satellite or radar.

The period of rapid intensification typically lasts 24 hours or less. Holliday and Thompson (1979) stated, "rapidly developing typhoons sustain the bulk of their pressure fall over short time scales, and durations of fall rates of 1.75 $mb\ hr^{-1}$ beyond 24 hours are relatively uncommon". Thus the tropical cyclone forecaster should anticipate a short term, rapid change in intensity once the criteria for rapid deepening are identified. After rapid intensity change, the period 2 intensity is usually 23 to 31 ms^{-1} greater than at period 1, which gives the intensity distribution shown in Fig. 3.13b. The distribution of the rates of rapid intensity change are given in Fig. 3.14. Ninety-one (76.5%) of the rapid intensification rates were within 22 to 32 ms^{-1} per day, with a mean of 28.

The point at which the period of rapid intensification begins is highly variable. Figure 3.15 shows the relationship between period 0 and period 1. Most rapid intensifiers begin rapid intensification 1 to 3 days after classification as a tropical storm, but the previous rate of intensification from period 0 to period 1 appears to have no relationship to the rate of intensification from periods 1 to 2. Thus the important temporal factor is intensity at period 1, not the number of hours required to develop from a weak tropical storm to a minimal typhoon. It is important to note that most rapid intensifiers develop steadily from a tropical storm to a typhoon, and before their rapid intensification period commences, the rate of intensification is not significantly different from the non-rapid intensifiers. After period 2, some rapid intensifiers intensify further at a slower rate to a peak intensity at period 3. Most rapid intensifiers have peak intensities $\geq$ 64 ms^{-1}, with a mean of 67.6 ms^{-1}, and a standard deviation of 6.7. On average, period 3 occurs 2 to 4 days after period 0.

The points of this section can be summarized into an idealized climatological model of the chronological sequence of rapid intensification that can be utilized if rapid intensification is forecast. This model of the "average rapid intensifier" was presented in Fig. 3.1. During the early stage of development from periods 0 to 1, intensification is at a

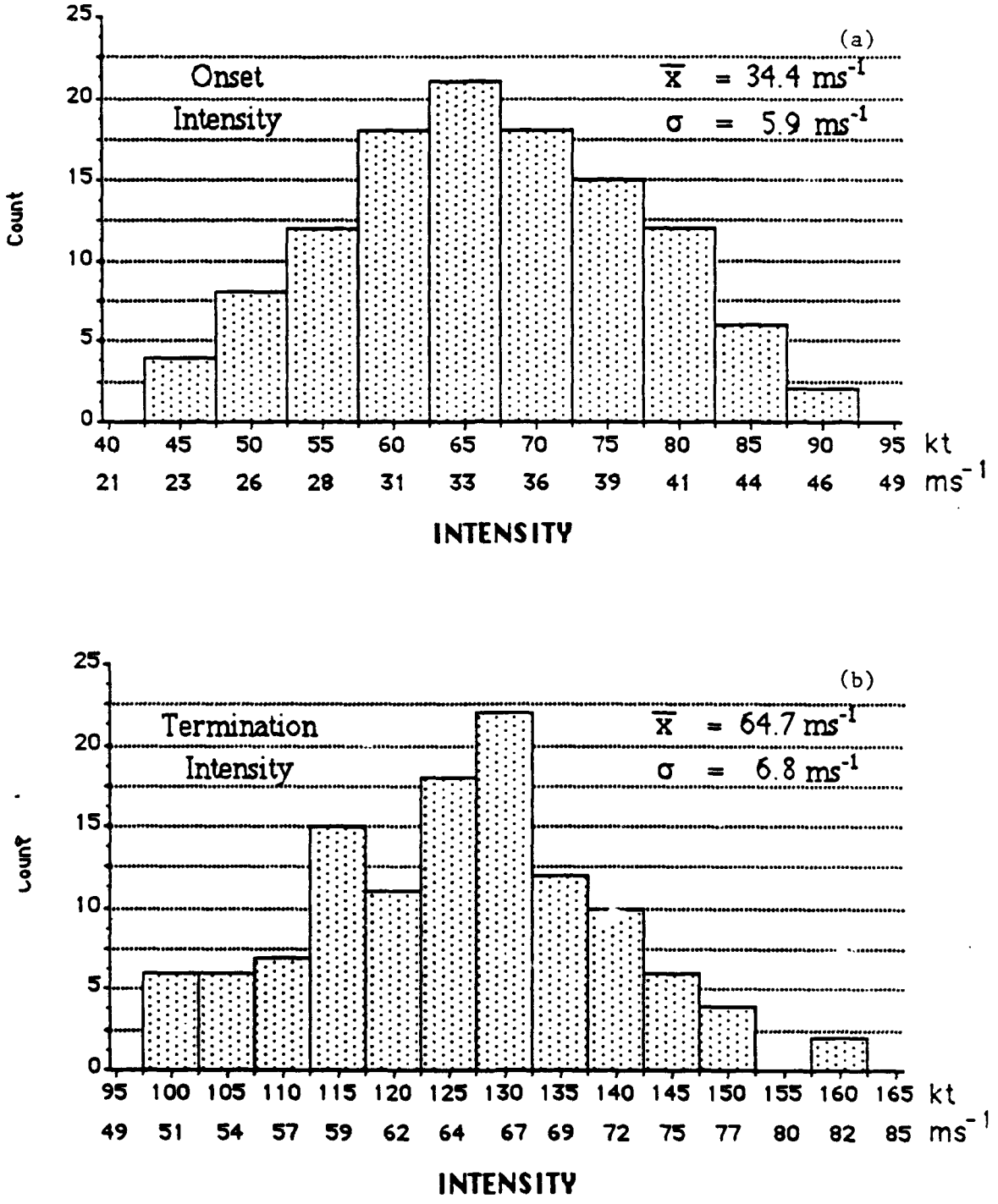

Figure 3.13: Histograms of JTWC best track intensity at the onset (a) and termination (b) of rapid intensification.

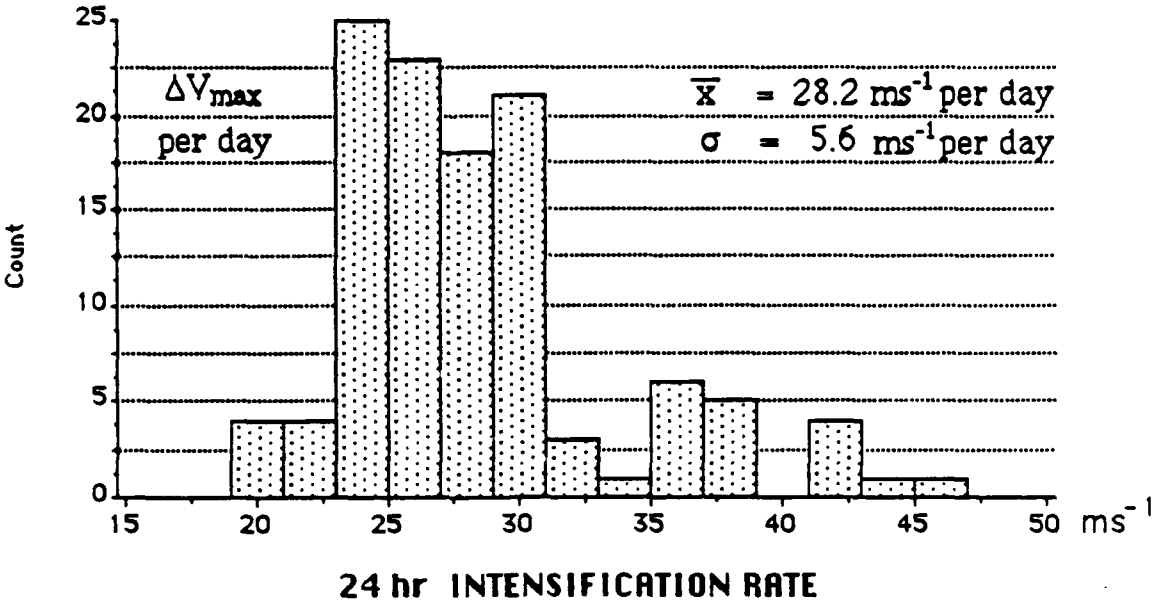

Figure 3.14: Frequency distribution of rapid intensification rates. Intensification rates are from period 1 (onset) to period 2 (termination).

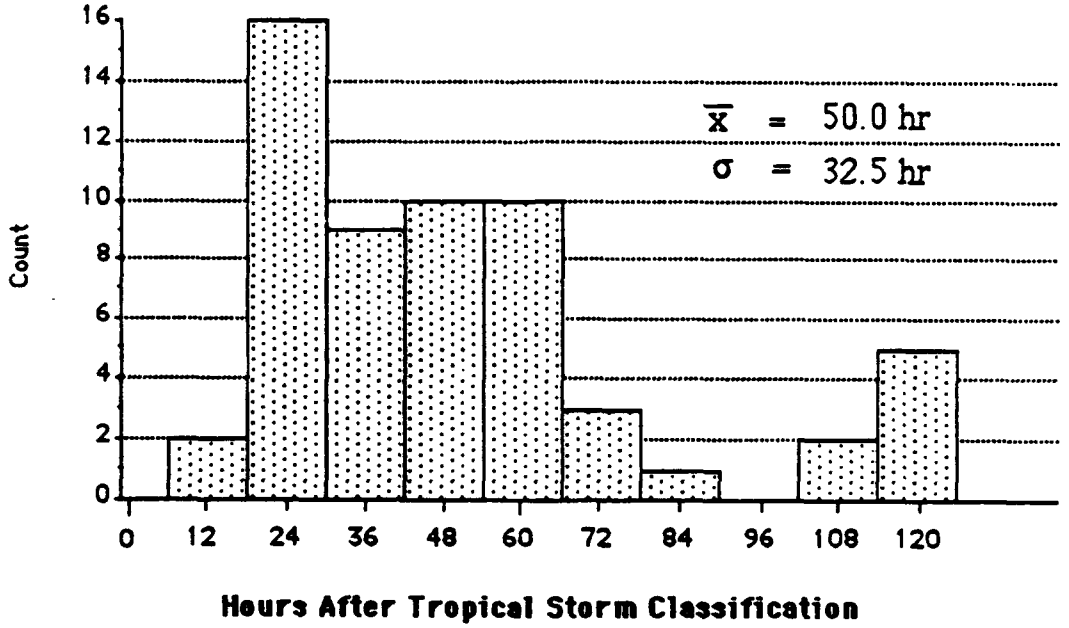

Figure 3.15: Histogram of the length of time after initial tropical storm intensity (period 0) that the onset of rapid intensification (period 1) occurs. Data consists of 60 rapid intensifiers from 1972 to 1987.

near-normal rate. Rapid intensification commences once a central eye develops, usually 1 to 2 days after period 0, during which the intensity increases by approximately 28 ms^{-1} in only 24 hours. Peak intensity occurs about 2 to 4 days after period 0 at supertyphoon ($\geq$ 67 ms^{-1}) intensity.

3.9 Longer Range Intensity Forecasting

Longer range intensity forecasting consists of two primary factors—*maximum intensity* and *peaking hour*, which is how long it takes to reach that peak intensity. Together these two factors yield the intensification rate, which is usually expressed in $kt\ hr^{-1}$ or ms^{-1} per day. At present, climatology and persistence are the best intensity forecast techniques for long range forecasts of 48 and 72 hours. A better definition to the climatological aspects of intensity change and a knowledge of intensification rates is considered essential to forecast long range intensity change and reduce the magnitude of the 48 FI and 72 FI errors. An objective of this research was to determine, based on initial position, intensity and forecast track, if accurate long range prediction of intensity change was possible. To do this, intensification rates for each genesis region (GR) were calculated from a 16 year sample of 1972-87 NWPAC tropical cyclone seasons. The latitude belts used to determine GR are shown in Fig. 3.16. The mean values and standard deviations of maximum intensity, peaking hour and intensification rates for each GR are also given in Fig. 3.16. Seasonal differences in these values for the NWPAC are shown in Table 3.3. The monthly distribution of named tropical cyclones for each GR are shown in Table 3.4. Most tropical cyclones which form in GR1 occur in the "off season" of November to May, while the majority of the TCs which form north of 15°N occur during the months of July to October. The South China Sea (SCS) region is active June to November. This information has some value in a broad sense because it shows that the most intense typhoons develop in genesis regions 1 and 2 during the months of July to November, but that the rate of intensification is only slightly higher than for other genesis regions and times of the year. However, these means have little significance for each individual long range forecast unless there can be found to be more definition to the geographic and seasonal differences.

An interesting aspect is the intensification rates of cyclones which develop significantly south of the seasonal mean latitude of development.

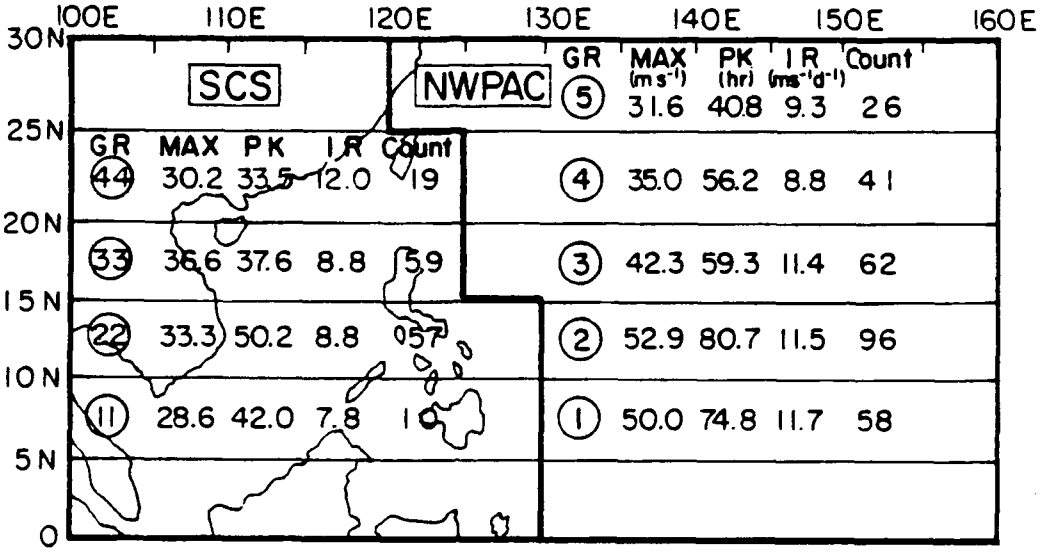

Figure 3.16: Annual mean values of maximum intensity (MAX), peaking hour (PK), and intensification rate (IR) for western North Pacific (NWPAC) and South China Sea (SCS) genesis regions (GR). Genesis regions are determined by 5° latitude belts and stratified into a western Pacific (single digit) area on the right and a South China Sea (double digit) area on the left. Count values are number of cases from 1972 to 1987.

Table 3.3: Seasonal mean values and standard deviations (σ) of maximum intensity (MAX), peaking hour (PK), and intensification rate (IR) by genesis region. Description of genesis regions is given in Fig. 3.16.

GENESIS REGION	MONTHS	$\overline{MAX}$ (ms^{-1})	σ_{mx}	$\overline{PK}$ (hr)	σ_{pk}	$\overline{IR}$ ($ms^{-1}d^{-1}$)	σ_{ir}	COUNT
3	Nov-Jun	29.3	9.9	27.8	15.4	9.6	4.6	8
3	Jul-Oct	44.2	13.2	64.0	32.7	11.1	5.7	54
2	Dec-Jun	44.6	10.5	72.1	40.3	10.3	4.8	23
2	Jul-Nov	55.4	15.7	83.3	35.3	11.4	4.3	73
1	Dec-Jun	42.4	15.6	69.4	44.9	9.8	4.8	36
1	Jul-Nov	62.3	16.4	83.7	37.4	13.2	5.2	22

Table 3.4: Monthly distribution of tropical cyclones during the 1972-87 seasons for western North Pacific (NWPAC) and South China Sea (SCS) genesis regions (GR). Only a small percentage of tropical cyclones reach minimal tropical storm intensity equatorward of 10°N during the months of July to October.

	GR	JAN	FEB	MAR	APR	MAY	JUN	JUL	AUG	SEP	OCT	NOV	DEC
NWPAC	5						1	5	14	6	1		
	4						3	11	10	15	2		
	3	1		1	1		1	7	13	18	16	3	2
	2	2		1	1	5	6	16	12	12	22	11	8
	1	7	2	5	7	5	3	3	1	3	4	11	7
SCS	44					1	1	3	12	1			
	33					2	5	9	16	16	7	3	
	22					1	9	8	1	8	14	9	7
	11						2				1	5	1

The seasonal means of latitude of initial tropical storm intensity (TS Lat) and latitude of initial typhoon classification (TY Lat) for the western Pacific region (which excludes the South China Sea) are given in Fig. 3.17. Tropical cyclones which attain minimal tropical storm status south of the seasonal mean TS Lat have an average maximum intensity of 52.2 ms^{-1} while those that develop north of the mean have a significantly lower maximum intensity of 35.3 ms^{-1}, only two-thirds as intense.

The average maximum intensity of TCs which attain initial typhoon intensity south of the seasonal mean is 58.8 ms^{-1} and those with a TY Lat poleward of the seasonal norm reach a mean maximum intensity of only 46.3 ms^{-1}, or only 79% of the mean intensity equatorward of the seasonal mean . Storms tend to intensify more if they form at lower latitudes, particularly in the primary season of July through November. This is primarily due to the fact that such storms spend a longer time in a favorable region of warm SSTs, low vertical wind shear and open ocean. In fact, a distinctive characteristic of rapid intensifiers is that they form south of the seasonal means of initial TS Lat and initial TY Lat.

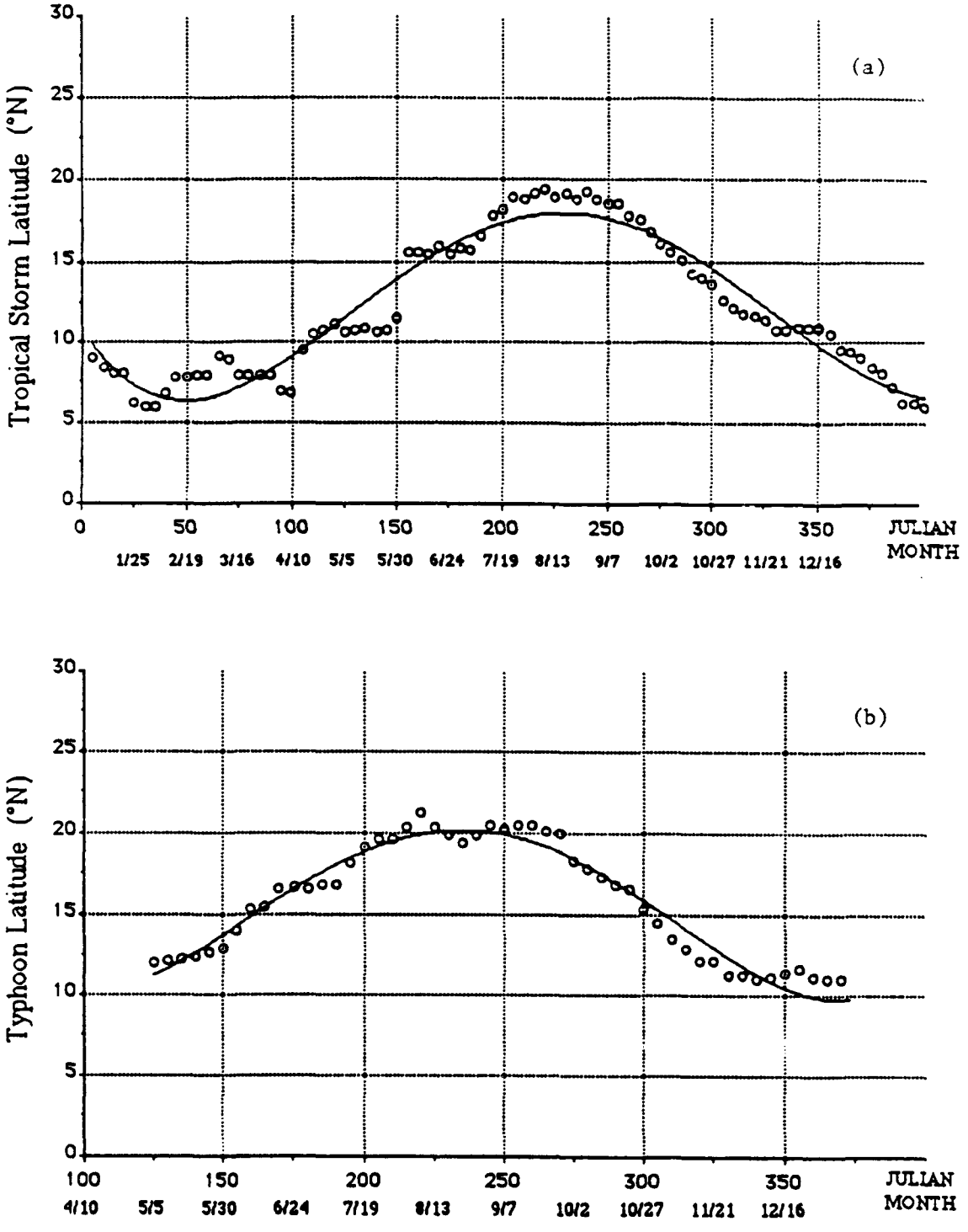

Figure 3.17: Seasonal south to north variation of mean latitudes of initial tropical storm intensity (a) and initial typhoon intensity (b) classification for the western North Pacific. Tropical cyclones that reach minimal tropical storm or minimal typhoon intensity in the South China Sea region were not included.

This relationship is shown in Fig. 3.18. Note that almost all rapid intensifiers had a TS Lat south of the seasonal norm and that the majority of rapid intensifiers reached minimal typhoon intensity before they were 1° (111 km) north of the seasonal mean of TY Lat. For the months of July to November, tropical cyclones which develop south of 10° have a high probability of attaining extreme intensities. Of 22 TCs which formed during this period, 16 (73%) had a maximum intensity of 62 ms^{-1} or greater, and most of the sixteen cases were rapid intensifiers. This relationship between the climatological mean latitudes of development and the seasonal latitudes at which rapid intensifiers form is another useful tool to determine the likelihood of rapid intensification.

To incorporate the facts given above into a scheme that can be easily applied by the operational forecaster to improve the long range intensity forecast, the latitudes of initial tropical storm (TS Lat) and typhoon (TY Lat) intensity for every tropical cyclone for the period 1972-87 were recorded and plotted against its maximum (best track) intensity, peaking hour and intensification rate from 18 ms^{-1} to maximum intensity. The mean values and standard deviations to the nearest 1° of latitude were determined to indicate the relationship between latitude and intensification. Seasonal and regional factors were considered important, so the preceding data was stratified into "off season" (Dec-Jun), "primary season" (Jul-Nov) and a South China Sea (SCS) region. For the primary season in the western Pacific region, a strong correlation between initial TS Lat and TY Lat versus maximum intensity emerges from the data (Figs. 3.19 and 3.20). Given a particular TS Lat or TY Lat, the mean (most likely) intensity can be predicted using the regression equations:

$$INT_{max} = (-1.876)(TS\ Lat) + 79.129 ms^{-1} \tag{3.1}$$

$$INT_{max} = (-1.657)(TY\ Lat) + 84.448 ms^{-1} \tag{3.2}$$

Since the majority of all NWPAC tropical cyclones occur in the primary season, these regression equations have wide application for longer range prediction of maximum intensity. Similar relationships of maximum intensity versus TS Lat and TY Lat for the off

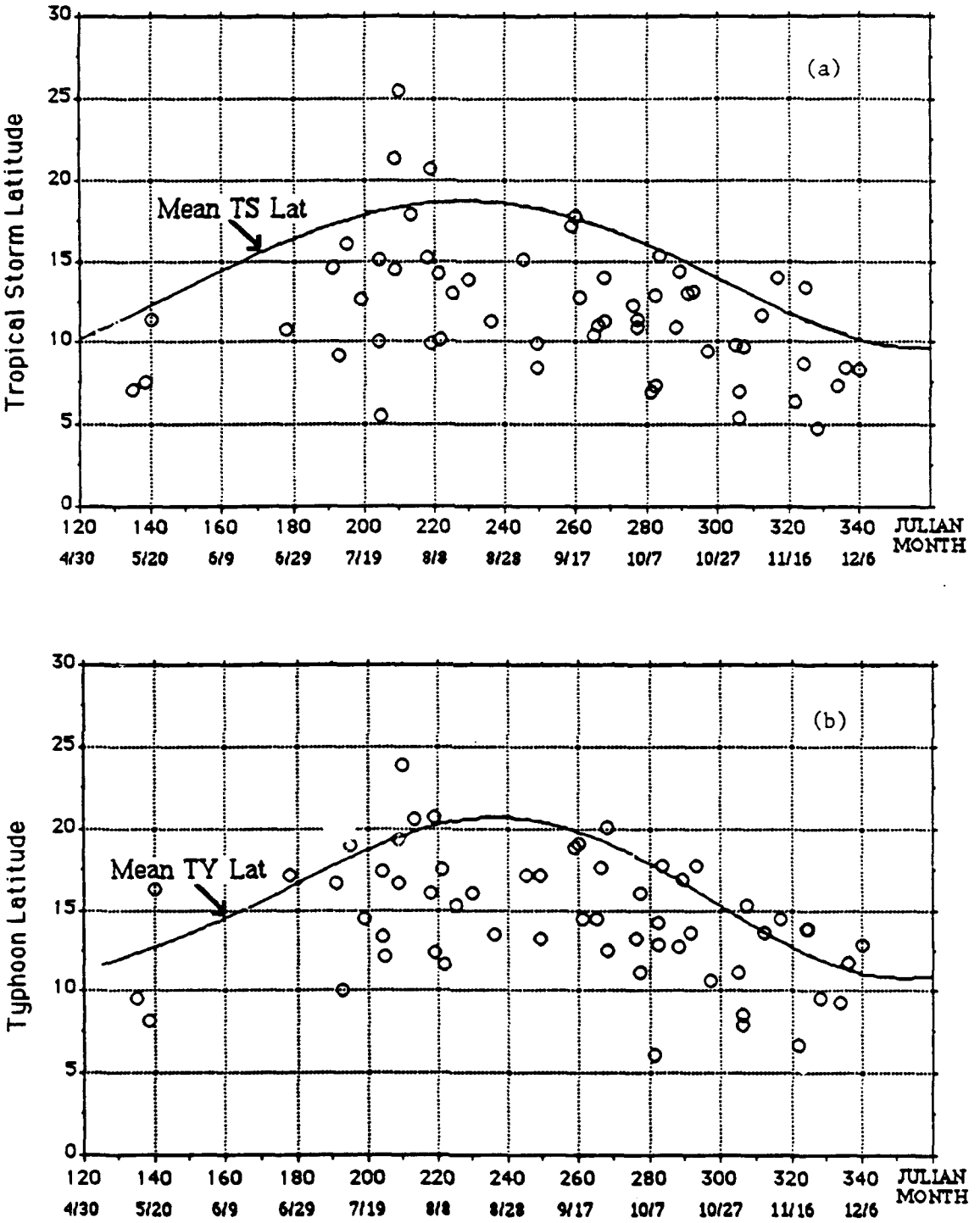

Figure 3.18: Relationship between the latitude of initial tropical storm (a) and initial typhoon (b) classification of tropical cyclones which experienced a rapid intensification event and the mean for a given julian month. Data consists of 60 rapid intensifiers from 1972 to 1987.

season and the South China Sea do not show as much of a correlation between latitude and intensity (Table 3.5), presumably due to less favorable environmental and geographic conditions.

There is also a good correlation between initial TS Lat and mean peaking hour during the primary season. A mean peaking hour for a given TS Lat can be determined from Fig. 3.19b, but the high degree of variability (as evidenced by the relatively large standard deviations) means that longer range prediction of the peaking day using only climatology is likely to be only marginally successful. The mean intensification rates are nearly the same for all latitudes in the primary season, with most falling in the range of 9.3 to 13.6 ms^{-1} per day (0.75 to 1.10 $kt\ hr^{-1}$). Therefore, a forecast of 8 to 13 ms^{-1} intensity change per day up to the expected maximum intensity given by Fig. 3.19a is probably the best initial long range forecast until an intensification rate is more clearly established at a later time. Once minimal typhoon intensity is reached, the relationship between initial TY Lat and mean intensification rates has a much higher correlation (Fig. 3.20b).

3.10 Prediction of Intensity Change Using Climatology

Summarizing, it is found that:

1. Rapid intensification is very infrequent in the South China Sea region and poleward of 22°N. Rapid Intensification is very unlikely to occur in the off season of December through June.

2. The highest probability of rapid intensification is from mid-July to mid-August and from September to November. A relative lull occurs during late August and early September when the monsoon trough is typically too far poleward to allow intensification in a favorable region of warm SSTs and open ocean.

3. A minimum intensity of 26 ms^{-1} (50 kt) is necessary before the onset of rapid intensification, with most beginning at an initial intensity of 33 ms^{-1} (65 kt). Rapid intensification is not likely to occur after an intensity of 44 ms^{-1} (85 kt) is attained.

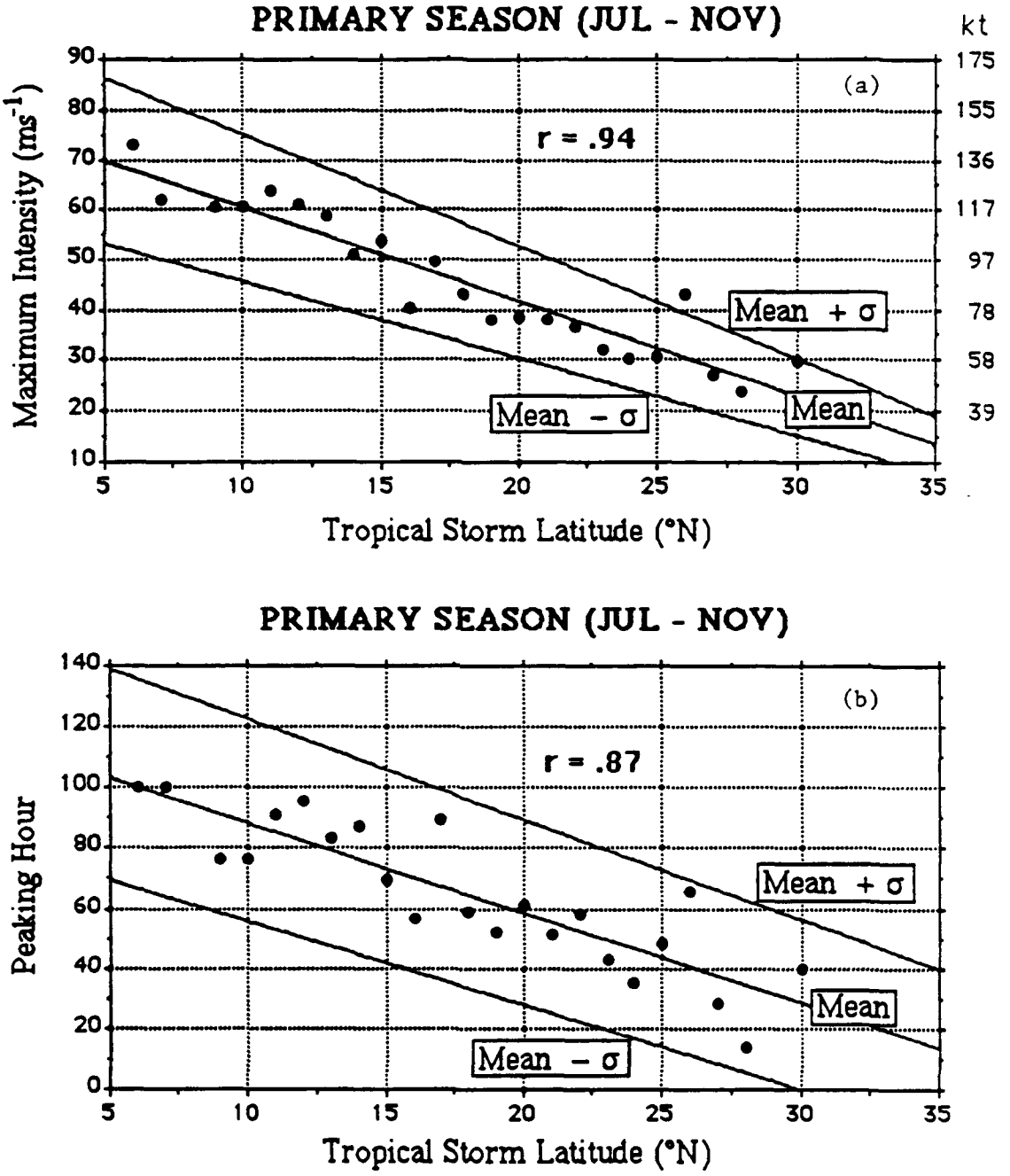

Figure 3.19: Correlation of maximum intensity (a) and peaking hour (b) to latitude of initial classification as a tropical storm (TS Lat). Variability about the mean is expressed as regression lines of ± one standard deviation.

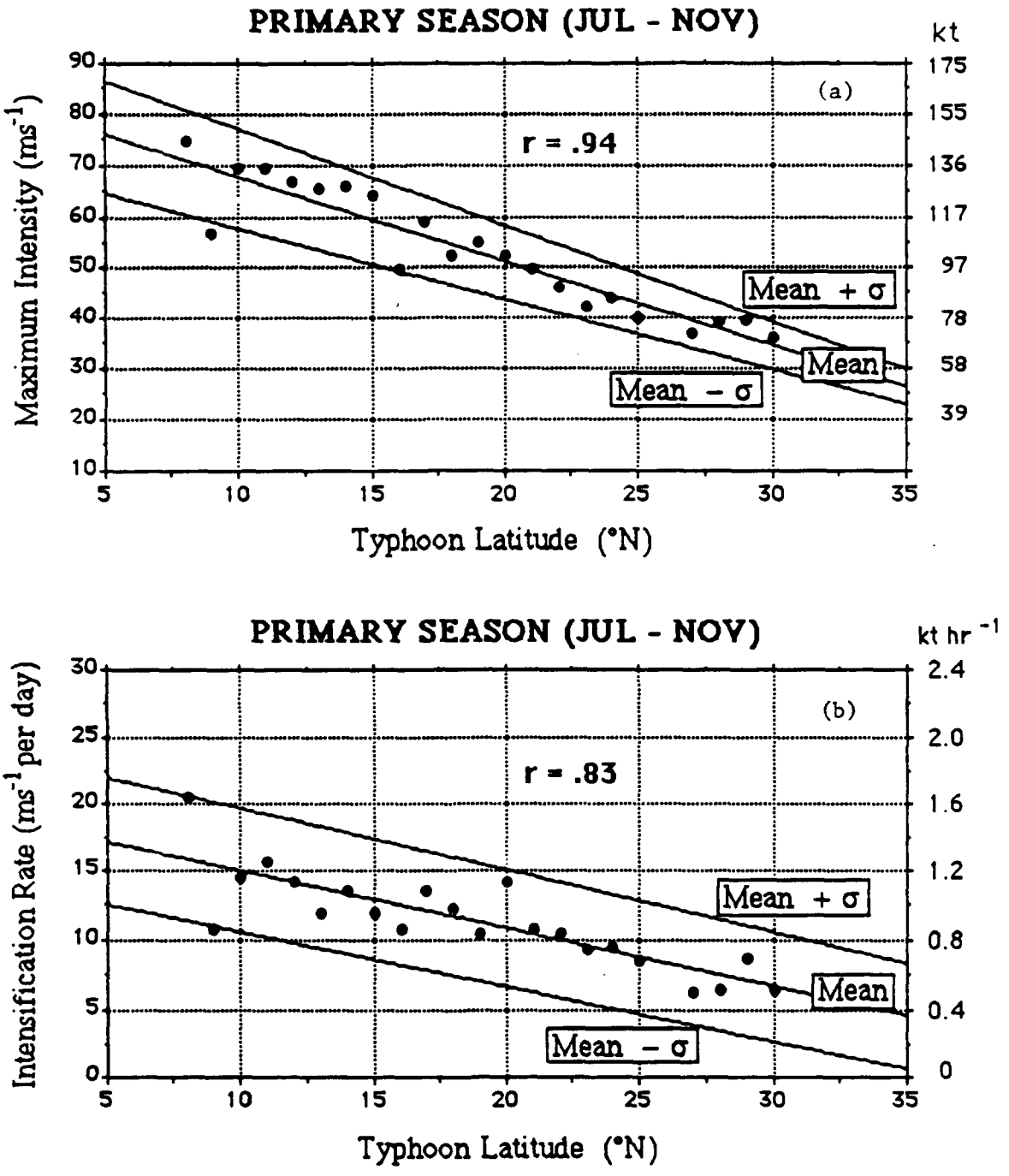

Figure 3.20: Correlation of maximum intensity (a) and intensification rate (b) to latitude of initial classification as a typhoon (TY Lat). Intensification rate is defined from period 0 (initial TS) to period 3 (maximum intensity). The mean peaking hour can be determined from the mean intensification rate. Variability about the mean is expressed as regression lines of ± one standard deviation.

Table 3.5: Mean values and standard deviations of maximum intensity, peaking hour, and intensification rate for the South China Sea region (a) and the "off season" months of December to June. Correlations between latitude of initial tropical storm classification (TS Lat) and intensification parameters were all less than 0.6.

(a) SOUTH CHINA SEA (MAY - DEC)

TS Lat	Max Intensity (ms^{-1})		Peaking Hour (hr)		Int Rate ($ms^{-1} d^{-1}$)		Count
°N	$\bar{x}$	σ	$\bar{x}$	σ	$\bar{x}$	σ	
≥ 22	27.8	5.0	27.6	15.1	9.5	3.4	5
21	28.0	15.6	21.6	32.6	8.3	7.0	10
20	29.9	8.1	47.3	50.2	7.5	2.7	8
19	28.1	5.9	31.4	26.1	9.2	5.5	11
18	29.3	7.0	33.7	22.3	8.2	4.4	13
17	37.0	8.4	55.1	25.4	8.8	2.1	11
16	32.2	11.5	36.2	21.9	8.4	5.2	16
15	28.3	6.8	39.3	21.5	6.7	2.5	9
14	37.0	11.7	56.4	52.0	10.4	3.6	14
13	29.7	11.4	34.9	34.0	7.0	4.1	11
12	31.4	10.0	50.0	51.1	8.2	3.1	15
11	33.8	9.5	39.8	22.9	9.7	2.2	8
10	29.2	10.7	44.0	46.6	7.4	2.5	3
9	32.6	3.9	34.0	6.9	10.3	2.1	3
≤ 8	32.2	10.6	71.0	48.2	6.3	3.7	6

(b) OFF SEASON (DEC - JUN)

TS Lat	Max Intensity (ms^{-1})		Peaking Hour (hr)		Int Rate ($ms^{-1} d^{-1}$)		Count
°N	$\bar{x}$	σ	$\bar{x}$	σ	$\bar{x}$	σ	
≥ 16	24.9	4.8	28.0	37.6	8.7	8.1	9
15	38.6	12.9	48.0	12.0	9.6	4.2	3
14	33.5	14.6	39.0	12.7	8.5	6.2	2
13	43.8	6.8	62.0	18.3	10.2	1.7	3
12	35.6	12.8	51.0	31.5	8.7	2.7	6
11	52.3	5.3	93.2	56.4	12.0	7.6	6
10	40.2	14.9	66.8	47.1	7.9	5.9	8
9	29.6	11.6	36.8	42.2	9.0	3.8	4
8	50.5	17.8	81.8	42.6	10.7	5.7	13
7	41.2	11.4	68.6	34.8	8.9	2.9	7
6	39.6	8.8	64.8	27.0	9.3	4.7	5
≤ 5	45.5	17.1	106.0	81.9	9.1	5.5	3

4. Rapid intensifiers reach minimal tropical storm and minimal typhoon intensities south of the seasonal mean latitude of TS Lat and not more than 1° (111 km) north of the seasonal mean latitude of TY Lat. The latitudinal "danger zone" of highest probability for onset of rapid intensification varies by the time of year.

5. The number of hours after TS classification is not a factor for prediction of rapid intensification. The primary factors are initial intensity and geographic position.

6. The period of rapid intensification typically lasts for 24 hours or less, with an intensity change of 23 to 33 ms^{-1} (45 to 65 kt) taking place over a 24 hour forecast period.

7. Maximum intensity is strongly correlated to TS Lat and TY Lat, but rates of intensification from TS classification to maximum intensity do not vary significantly according to geographic position or season.

3.11 Evaluation of Climatological Intensity Forecasting

In an effort to determine if application of these climatological parameters in an operational sense would reduce the magnitude of the forecast intensity errors, an experiment was conducted using a randomly selected sample of 90 tropical cyclones from the NWPAC for the years 1972 to 1988. Twelve rapid intensifiers were included in this sample, which roughly approximates the ratio of rapid intensifiers to named tropical cyclones during this period. A total of three separate data sets were included as part of this verification experiment. In the first two, 33 tropical cyclones from the 1972 to 1987 climatology data set were selected at random to approximate a typical NWPAC seasonal distribution. These two tests were based on the data used to develop the relationship between seasonality, location, latitude and intensification (dependent data). The third test was independent, based on the best track information published in the 1988 ATCR (JTWC, 1989)—see Appendix C.

The tropical cyclone experimental cases were selected to simulate a variety of actual forecast situations: tropical storms, typhoons and supertyphoons, rapid intensifiers and

slow developers, off season and mid-season storms, South China Sea and western North Pacific regions. Forecasts were made at two key intensity thresholds: initial tropical storm and initial typhoon classification (TS Lat and TY Lat). The predicted maximum intensity and peaking hour were calculated from the regression equations obtained from Table 3.5, Fig. 3.19 and Fig. 3.20. From the derived values of maximum intensity and peaking hour an intensity forecast was made for 24, 48, and 72 hours from the TS Lat and for 24 and 48 hours from the TY Lat. Proximity to land was the only factor used to alter the climatological forecast. The official JTWC forecast track was consulted to determine if landfall was forecast, and adjusted according to the expected point of landfall. Experimental forecast intensity errors, as measured by the best track intensity, were recorded for comparison with the official JTWC forecast intensity errors.

The results of this comparison of forecast intensity errors is presented in Tables 3.6 and 3.7. The most obvious difference between the experimental forecast and the JTWC intensity forecasts, as indicated by the bias, is the tendency to overestimate future intensity while the JTWC forecasts at initial TS and TY intensity are more likely to underestimate the intensity forecast. The mean absolute errors and standard deviations indicate the magnitude of the errors using this technique based strictly on climatology are smaller than the JTWC intensity forecasts made with the benefit of synoptic, satellite and aircraft data. This tends to support the hypothesis that the current state of intensity forecasting has very little skill if it is unable to improve on forecasts based strictly on climatology. The mean absolute errors for this technique were higher than JTWC's at 48 hours using the TS Lat but this was primarily due to the effect of off-season and SCS tropical cyclones which were shown to have poor correlation between latitude and rates of intensification.

The superiority of this forecast technique for the majority of tropical cyclones which occur during the months of July to November in the western North Pacific is apparent in Tables 3.6b and 3.7b. The tendency to slightly overestimate future intensity is negated by rapid intensifiers, resulting in lower overall forecast intensity errors, which is the primary objective of this research. The differences between the mean experimental and JTWC forecast errors were significant at the .05 level for primary season 24, 48 and 72 hour

Table 3.6: Verification statistics for a set of three experiments to test the accuracy of a climatological forecast technique based on the latitude of initial tropical storm latitude (TS Lat) versus the official JTWC intensity forecast errors. Experiments 1 and 2 were based on 1972-87 (dependent) data while experiment 3 was based on 1988 (independent) data. A total of 90 tropical cyclones were included in this verification experiment. All errors are expressed in ms^{-1}.

	24FI ERRORS			48FI ERRORS			72FI ERRORS		
(a)	$\overline{X}$	σ	$\lvert\overline{X}\rvert$	$\overline{X}$	σ	$\lvert\overline{X}\rvert$	$\overline{X}$	σ	$\lvert\overline{X}\rvert$
EXPER	+1.2	5.2	3.9	+2.8	10.1	8.6	+2.0	12.7	10.4
JTWC	-1.1	6.1	4.5	-2.5	10.1	7.6	-4.9	16.4	13.3
EX 1	+0.2	3.8	2.7	+1.9	9.4	7.7	+4.4	11.9	10.2
JT 1	-2.6	5.5	4.3	-5.1	10.9	8.4	-5.7	17.1	13.7
EX 2	+2.3	5.5	4.4	+4.8	10.1	9.2	+3.4	13.8	10.6
JT 2	+0.4	5.4	4.4	+1.1	9.7	7.4	-1.4	17.4	13.2
EX 3	+1.0	6.2	4.6	+0.8	10.9	8.9	-3.4	11.6	10.5
JT 3	-1.4	7.3	4.8	-4.7	8.2	6.8	-8.7	14.1	13.1

		24FI ERRORS			48FI ERRORS			72FI ERRORS		
	(b)	$\overline{X}$	σ	$\lvert\overline{X}\rvert$	$\overline{X}$	σ	$\lvert\overline{X}\rvert$	$\overline{X}$	σ	$\lvert\overline{X}\rvert$
PRIMARY	EXPER	+1.1	5.1	3.7	+2.2	10.3	8.4	+2.5	12.7	10.6
	JTWC	-0.9	6.7	4.6	-4.3	11.2	8.7	-6.7	18.2	15.5
RAPID	EXPER	-1.7	6.3	4.3	-5.8	12.9	11.4	-2.1	15.0	11.6
	JTWC	-3.6	8.6	6.2	-12.2	14.1	15.7	-16.9	20.9	23.4

Table 3.7: Same as Table 3.6 except based on the latitude of initial typhoon intensity (TY Lat).

(a)	24FI ERRORS $\overline{X}$	24FI ERRORS σ	24FI ERRORS $\lvert\overline{X}\rvert$	48FI ERRORS $\overline{X}$	48FI ERRORS σ	48FI ERRORS $\lvert\overline{X}\rvert$
EXPER	+0.3	9.0	6.8	+0.8	12.0	9.4
JTWC	-4.8	9.6	8.7	-6.0	13.7	12.1
EX 1	+0.3	8.8	5.7	+4.8	14.1	12.0
JT 1	-5.1	10.4	8.9	-4.1	16.4	13.4
EX 2	+2.8	8.5	7.2	-2.2	10.3	7.7
JT 2	-2.2	9.7	8.1	-5.7	12.0	10.1
EX 3	-3.6	9.4	7.9	-0.6	10.5	7.9
JT 3	-8.6	7.4	9.4	-8.8	12.6	12.7

	(b)	$\overline{X}$	σ	$\lvert\overline{X}\rvert$	$\overline{X}$	σ	$\lvert\overline{X}\rvert$
PRIMARY	EXPER	+0.6	9.7	7.7	+2.3	12.5	9.6
PRIMARY	JTWC	-6.2	9.7	9.4	-7.6	13.8	12.4
RAPID	EXPER	-6.2	9.8	9.2	-1.1	11.2	8.4
RAPID	JTWC	-13.3	7.4	13.3	-15.2	11.5	15.2

forecasts using TS Lat and TY Lat. Lower errors are possible at the critical forecast points of initial TS and TY intensity simply by using the climatological relationship between maximum intensity, peaking hour, and the TS Lat or TY Lat. This experiment found that overestimates of future intensity would be more likely, but there is less likelihood of large underestimates which were more common in the JTWC intensity forecast errors (Figs. 3.21 to 3.25). In the author's opinion, this would improve the intensity forecasts at the points of initial tropical storm and typhoon intensity because, in most cases, it is more serious if the forecast underestimates future intensity.

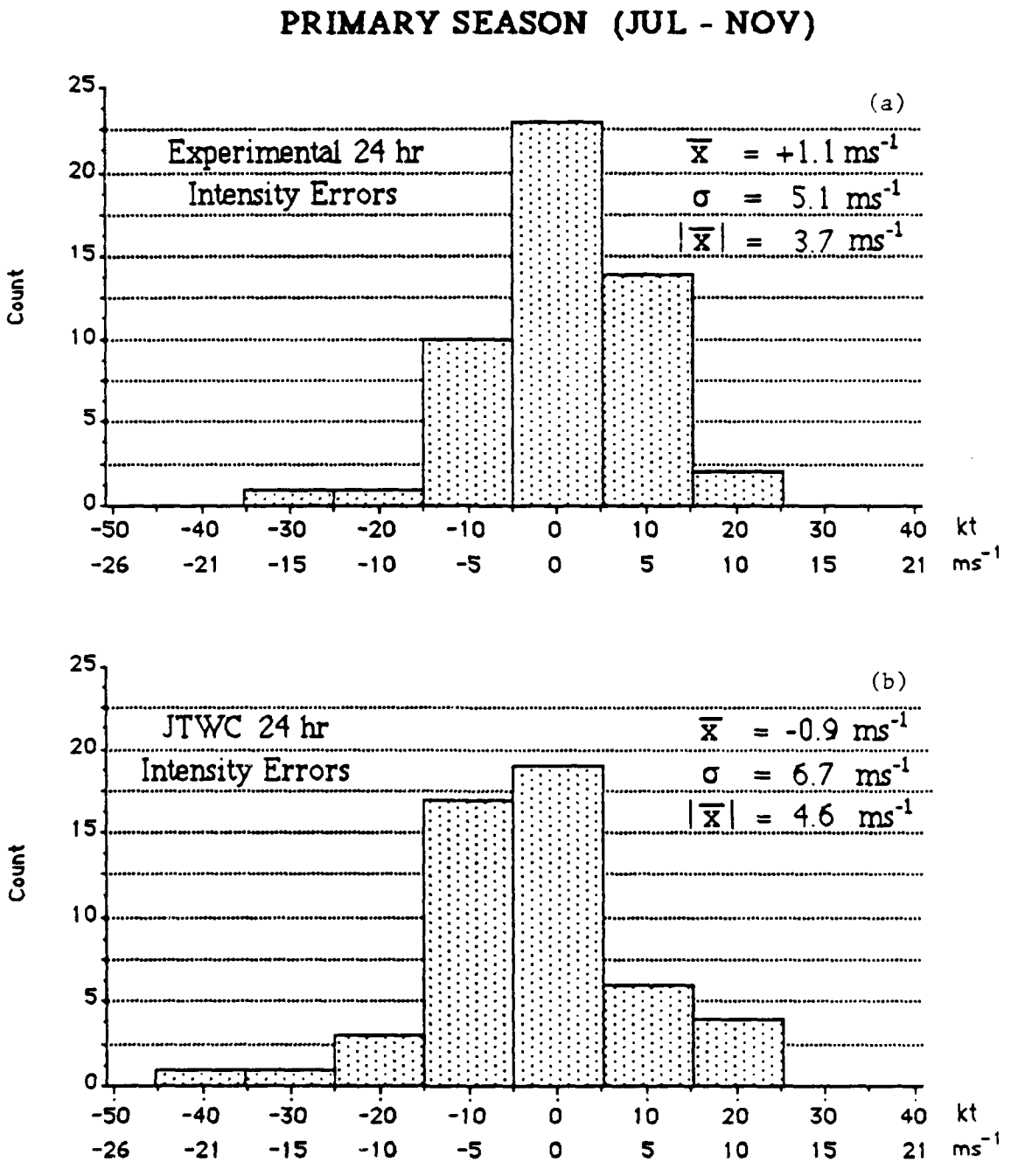

Figure 3.21: Distribution of 24 hour intensity errors based on initial TS Lat (a) and the official JTWC forecasts (b).

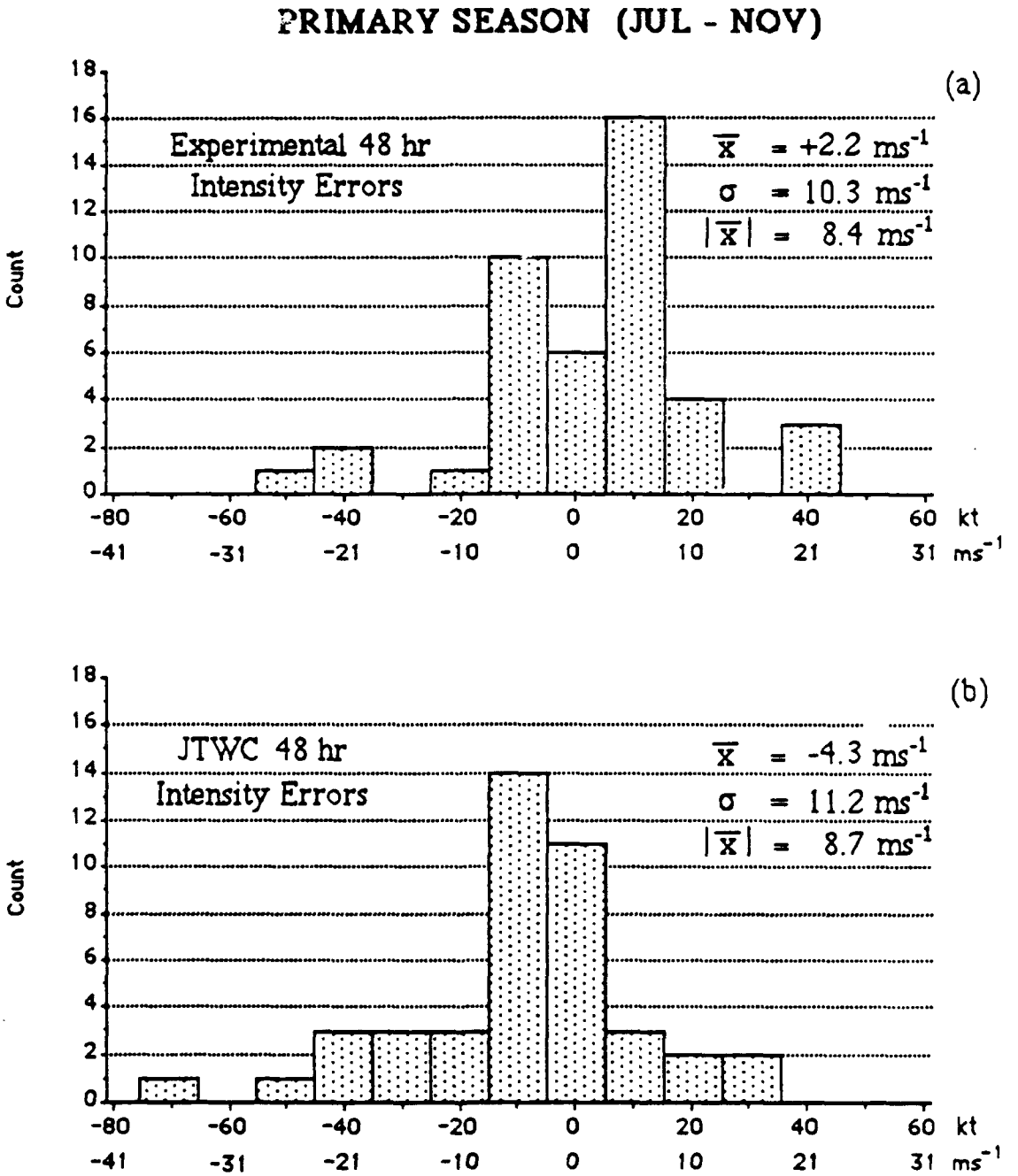

Figure 3.22: Distribution of 48 hour intensity errors based on initial TS Lat (a) and the official JTWC forecasts (b).

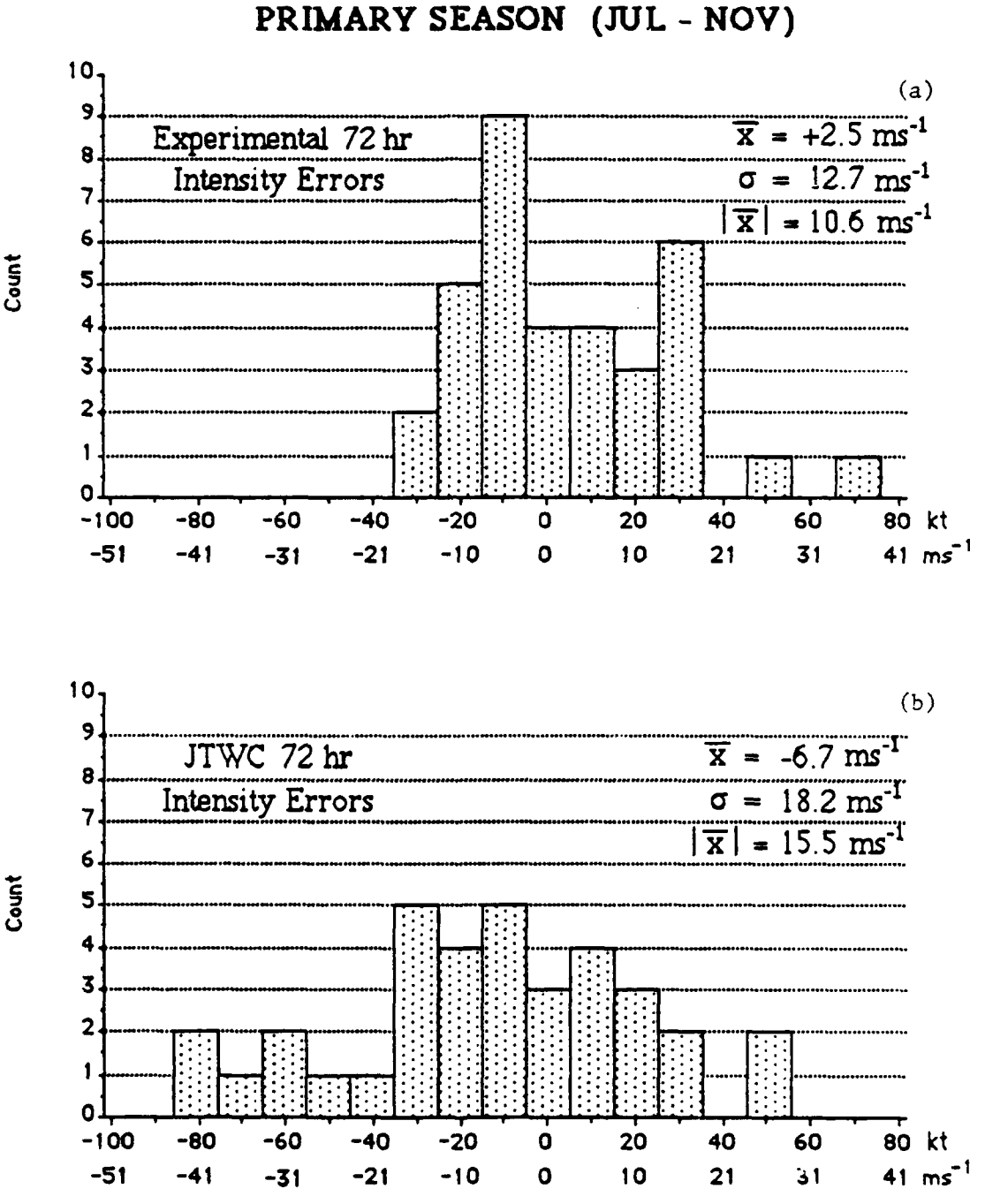

Figure 3.23: Distribution of 72 hour intensity errors based on initial TS Lat (a) and the official JTWC forecasts (b).

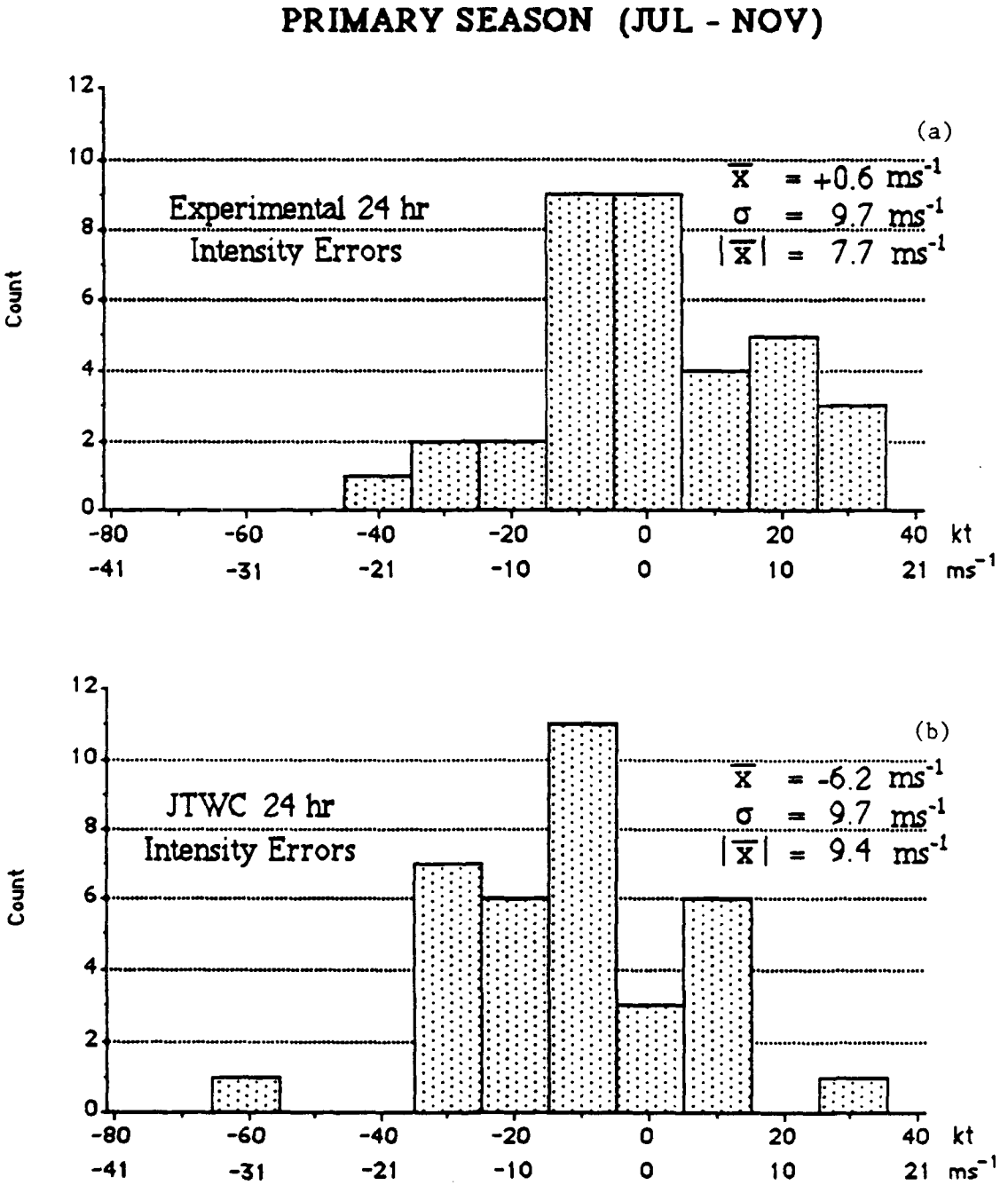

Figure 3.24: Distribution of 24 hour intensity errors based on initial TY Lat (a) and the official JTWC forecasts (b).

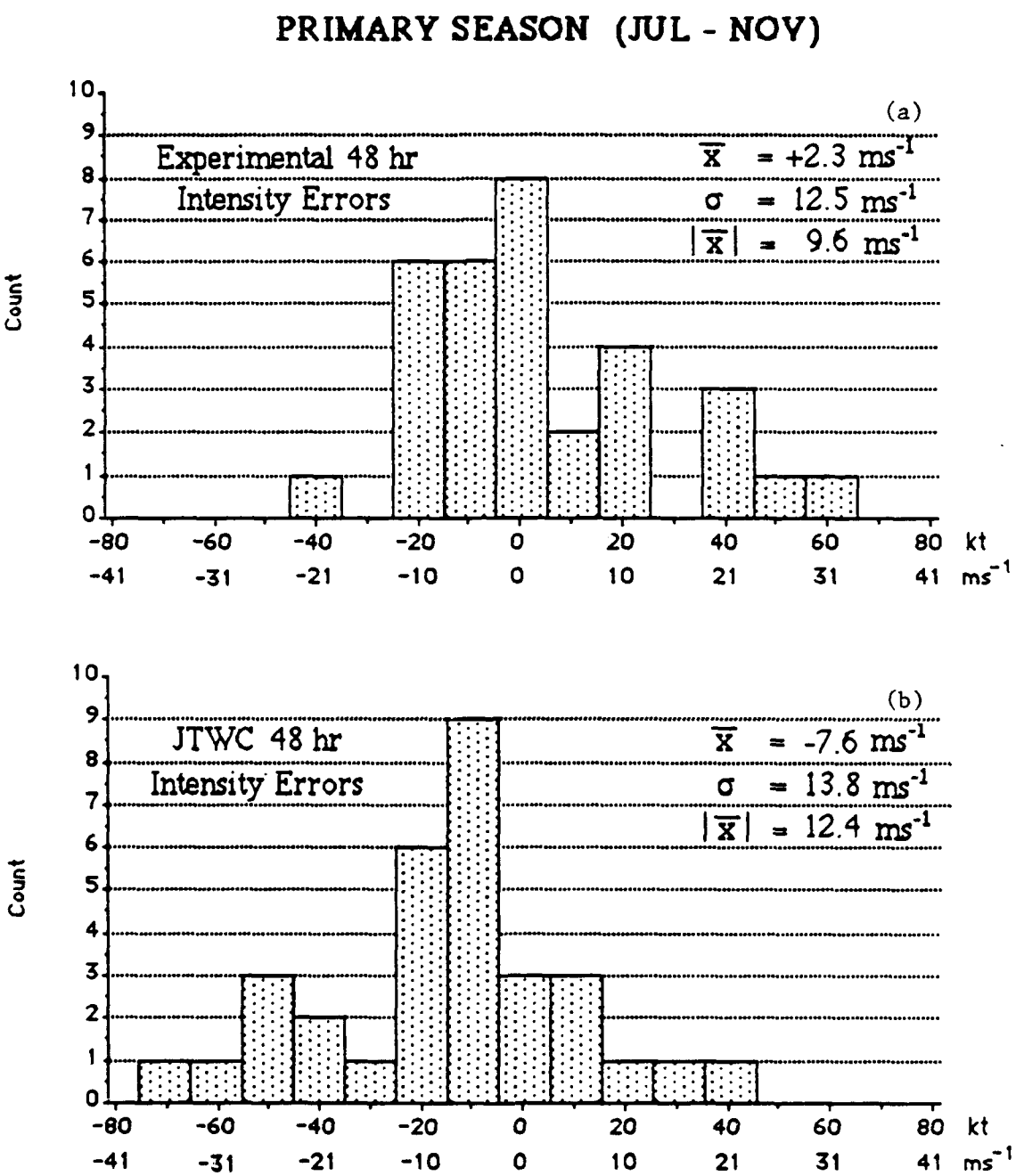

Figure 3.25: Distribution of 48 hour intensity errors based on initial TY Lat (a) and the official JTWC forecasts (b).

Chapter 4

APPLICATION OF SATELLITE IMAGERY FOR PREDICTION OF RAPID INTENSIFICATION

4.1 The Dvorak Technique

The author has extensive experience using the Dvorak satellite analysis method (Dvorak, 1984) to estimate tropical cyclone intensity and forecast future intensity. He is keenly aware of the positive aspects and the liabilities of this technique. The Dvorak method is the primary means used to estimate cyclone intensity and issue a forecast on future intensity change. It is considered important that the basic tenets of this technique be presented in enough detail to support the supposition that it is an ineffective forecast tool for rapid intensification. This is in spite of its overall merit for current intensity estimates and prediction of non-rapid intensification (Shewchuk and Wier, 1980).

The fundamental basis for the Dvorak technique is climatology (Dvorak, 1972). Hundreds of Atlantic basin satellite pictures of hurricanes and tropical storms were analyzed to distinguish common cloud patterns for a given intensity range. Each intensity range was given a "tropical number", or "T number". The distinguishing characteristics of each T-number category were found to be the amount of curvature or wrapping of the feeder bands, the size and shape of a "central dense overcast" (CDO) and the spatial definition of a central eye, if present. For a given satellite image, a "Data T-number" was assigned, based on the observed cloud features. In a later revision of his technique (Dvorak, 1984), this data T-number was based on enhanced infrared (EIR) temperatures of the eye and the surrounding ring of deep convection. The data T-number is a very important piece of information because it gives a "snapshot" view of the convective processes occurring at that point in time.

Except for the EIR technique when an eye is present, the Dvorak technique is a subjective estimate by a satellite analyst of current intensity. It is possible to have a wide range of T-numbers for the same satellite image, due to the perception and experience level of the individual analyst (Martin, 1988). Generally, experience using the Dvorak technique is the primary factor which determines the accuracy of a satellite estimate. However, when an eye is present on EIR or digital IR data, determination of the data T-number is a simple, objective process of pairing an eye temperature to a "surrounding temperature" at a radius of 111 km and obtaining a number from Dvorak's look-up tables.

The next step once a data T-number is obtained is the end product, which is called the "Final T-number". Except in unusual cases, the data T-number is exactly the same as the final T-number. It is these "unusual cases" that typically signal rapid intensification is about to occur. Another fundamental premise of the Dvorak model is that tropical cyclones intensify at a rate of 1.0 T numbers per day (see Fig. 4.1). Large deviations from this intensification rate of one T number per day are not permitted by the rules of the Dvorak model. In the western Pacific, *it is not* uncommon to see the data T-number change by 2.0 or more in 24 hours, especially for rapid intensifiers. The most interesting aspect of these large data T-number deviations is that they tend to occur several hours before the onset of rapid intensification. This tends to agree with the conclusions of several researchers (Gentry *et al.*, 1980; Zehr, 1988) that a lag exists between convection and intensity change.

The final step in the Dvorak model is the forecast intensity (FI), which is based on the past trend of intensification and is, in most cases, an extrapolation forward of the past trend for the next 24 hours. This extrapolation is tied to the model rate of 1.0 T-numbers per day. Even if the satellite data indicates an accelerated rate of intensification, the maximum FI allowed is a 24 hour change of 1.5. The reason for this is that most TCs do not develop rapidly, and such constraints prevent large forecast intensity errors. An objective of this research is to determine if the inherent intensity information contained in the data T-number can be utilized to predict rapid intensification and reduce the magnitude of large 24 FI errors.

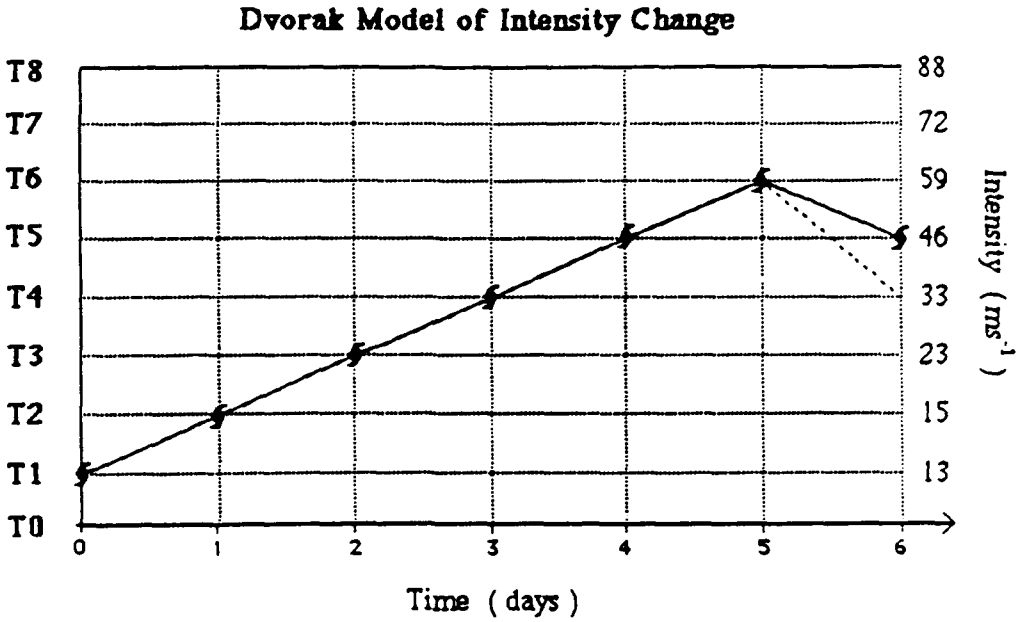

Figure 4.1: Dvorak's model of development by one T-number per day. Maximum intensity is expected about 5 days after initial T1.0 classification. Dashed line indicates intensity changes as observed by satellite after maximum intensity. Solid line indicates actual intensity change (Dvorak, 1984).

4.2 Comparison of *Dvorak Data T-number to Aircraft Intensity* Measurements

Comparisons of the accuracy of the Dvorak intensity estimate to NWPAC aircraft measurements of intensity (MSLP and/or 700 hP_a height) were conducted by Dvorak (1984) and Martin (1988). Shewchuk and Wier (1980) presented a similar study with errors based on the JTWC best track.

Their research concluded that, on average, the final T-number estimates of current intensity using the Dvorak method closely approximate the intensities from aircraft in situ measurements, especially since the T-numbers are reported in multiples of 0.5 (Table 4.1) and represent a range of intensities on the order of $\pm$ 4 ms^{-1}. Only a small bias was indicated in the data. As noted earlier, the final T-number is not necessarily the same as the data T-number. To determine if there is any predictive signal in the data T-number, enhanced IR (11.5 μm) satellite imagery in the data set were analyzed to obtain an objective data T-number for each image where an eye was present. These data and the corresponding aircraft intensity data were plotted as equivalent maximum sustained

winds using the Atkinson–Holliday (1977) wind/pressure relationship and the NWPAC Dvorak T-number to wind conversion (see Table 4.1), with time as the other axis.

Table 4.1: Empirical relationship between Dvorak T-number current intensity, maximum mean wind speed, and minimum sea level pressure for the western North Pacific (Dvorak, 1984).

Current Intensity	Max Winds (ms^{-1})	Central Pressure (hPa)
T1.0	13	1005
T1.5	13	1003
T2.0	15	1000
T2.5	18	997
T3.0	23	991
T3.5	28	984
T4.0	33	976
T4.5	40	966
T5.0	46	954
T5.5	53	941
T6.0	59	927
T6.5	65	914
T7.0	72	898
T7.5	80	879
T8.0	88	858

A list of the tropical cyclones studied in this manner and the time periods included is given in Appendix D. Comparisons of satellite data T-numbers with aircraft measured intensities are given in Figs. 4.2 to 4.4.

A characteristic feature of the rapid intensifiers in Fig. 4.2 is the rapid change of data T-numbers which precedes the rapid drop in surface pressure. Also note that the aircraft measured intensity changes tend to mirror those observed by satellite, and that a lag on the order of 6 to 18 hours exists between the two. For these rapid intensifiers, large differences between the two measurements of intensity at any point during the period of rapid intensity change are possible. Differences of 10 to 15 ms^{-1} are not unusual. The non-rapid intensifiers shown in Fig. 4.3 also seem to indicate that smaller intensity changes are detected on satellite first before they are measured by aircraft. Based on this data it

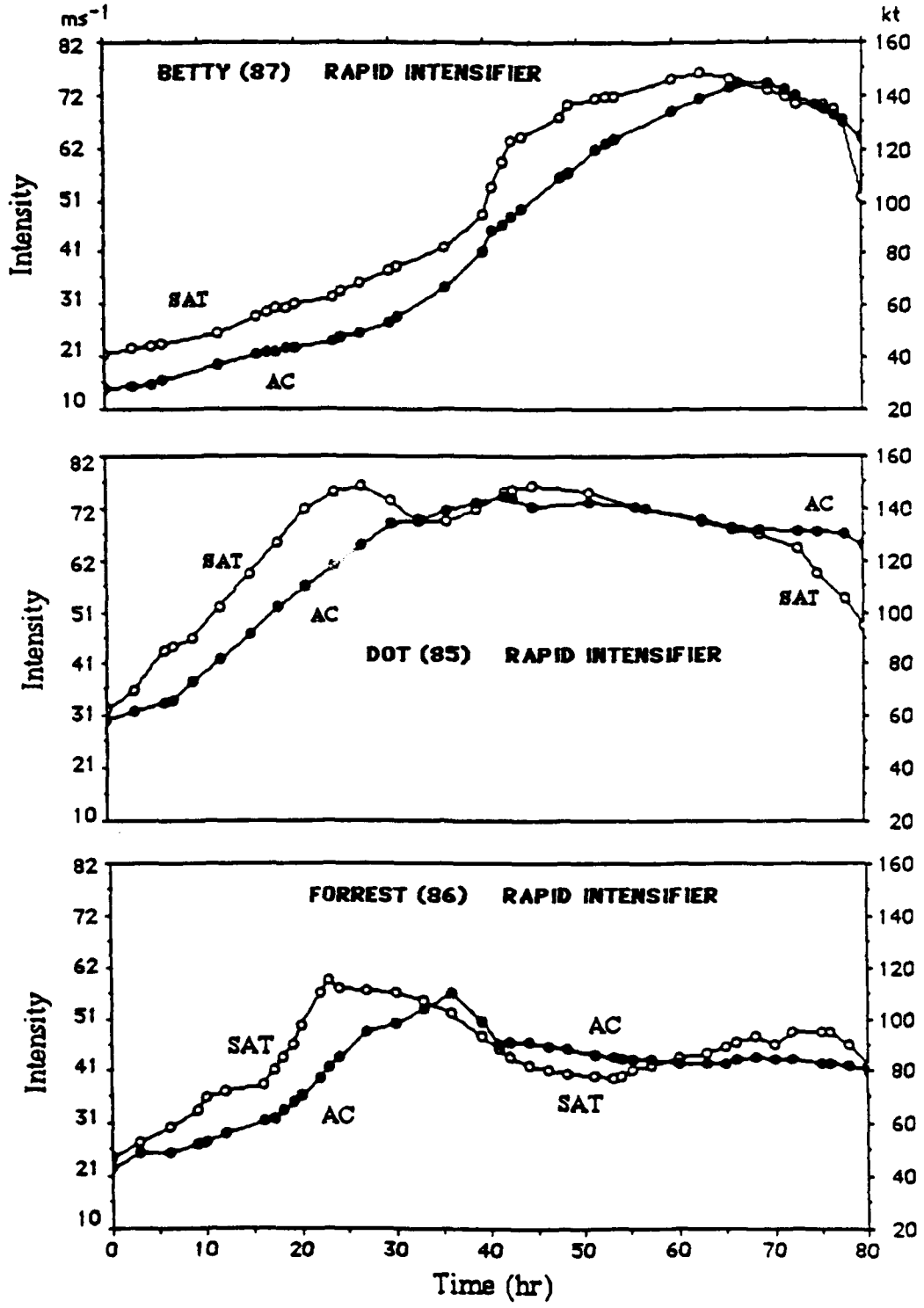

Figure 4.2: Representation of time versus intensity differences for rapidly intensifying tropical cyclones. Satellite (SAT) intensity is based on Dvorak data T-number estimates. Aircraft (AC) intensity is based on aircraft measurements of MSLP or 700 hPa height. Intermediate values have been interpolated.

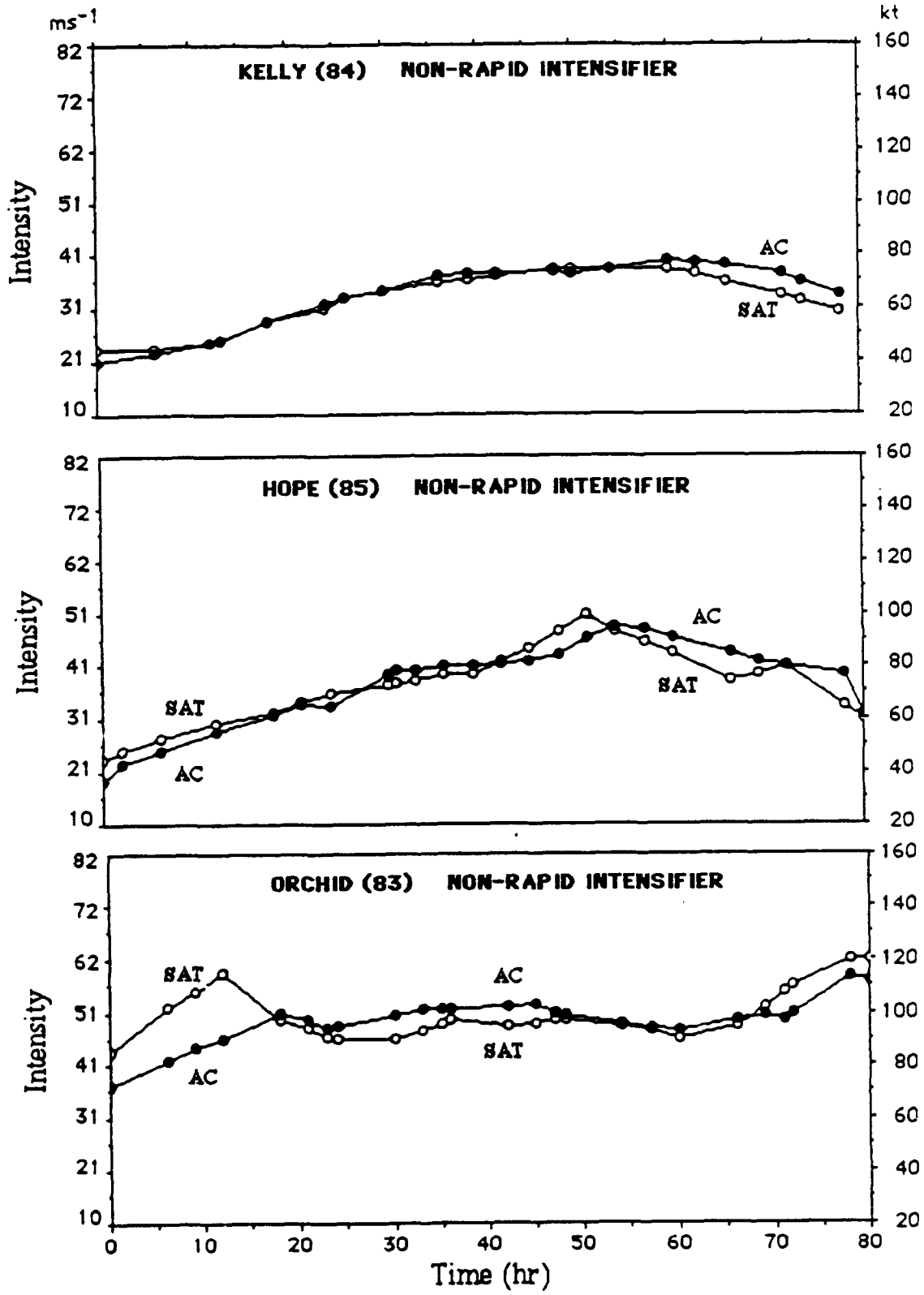

Figure 4.3: Same as Fig. 4.2 except for non-rapid intensification cases.

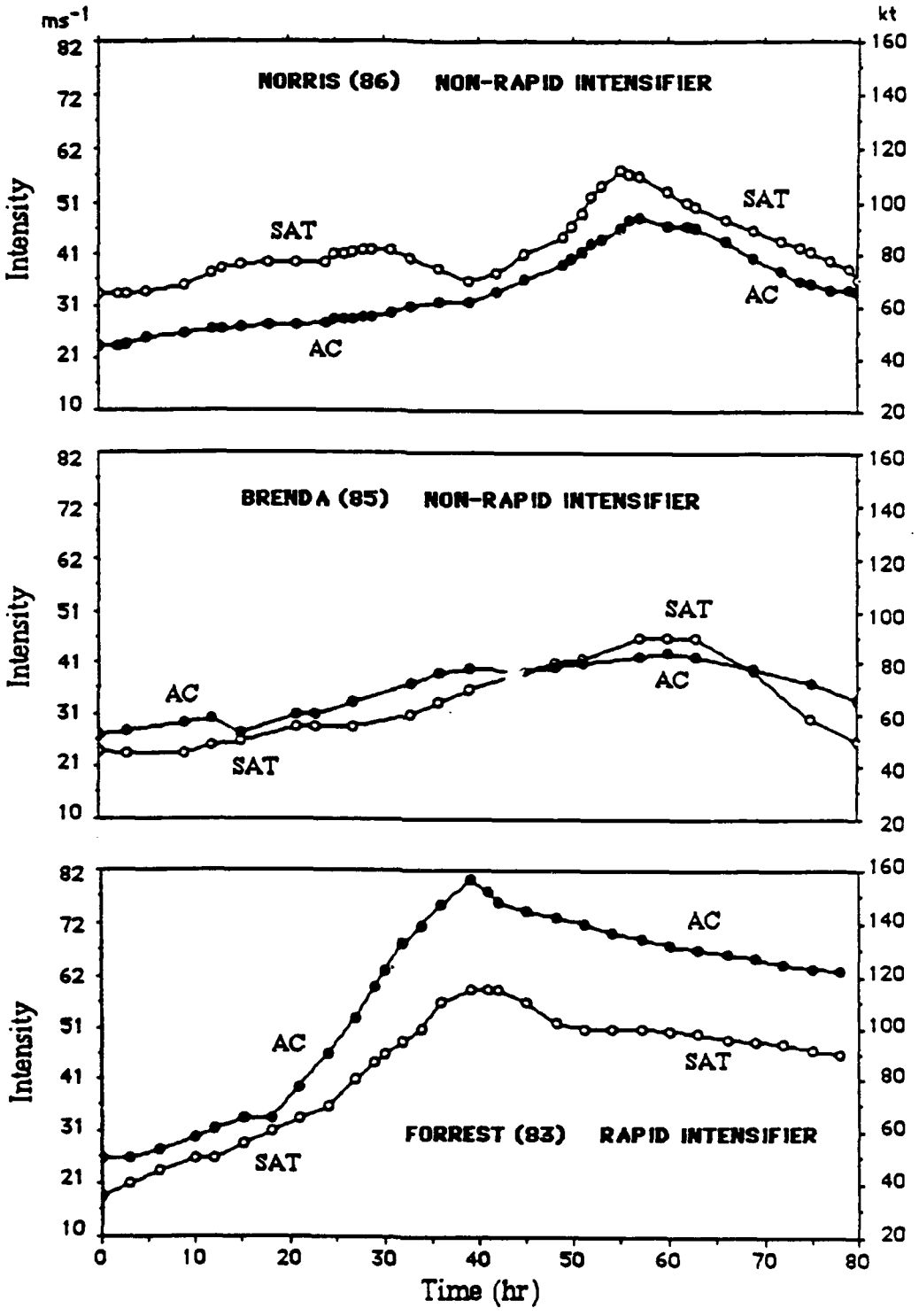

Figure 4.4: Time versus intensity differences for tropical cyclones that did not have a time lag between satellite observed intensity estimates and the aircraft measured MSLP or 700 hP_a height.

is considered possible to predict, on a short term basis, rapid intensification if such a 6 to 12 hour time lag exists between the Dvorak data T-number and actual intensity change in nearly all cases of rapid intensity change.

Most, but not all rapid intensifiers exhibit a time lag between the satellite data T-number and surface pressure change (see Fig. 4.4). There were also some cases (usually in the off season months of December and January) where the satellite data T-number indicated rapid intensification was occurring but it was not verified by the aircraft observations. The magnitude of the time lag between convection (as measured by the data T-number) and intensity change has large variability. Therefore, any prediction scheme which attempts to use the short-term time lag to predict future intensity change would not be 100 percent successful. The key question is whether large forecast intensity errors could be reduced in most cases even if it is not possible for all cases. At the least, this technique which attempts to predict rapid intensification should aid the decision process used by the operational forecaster.

In order to classify the magnitude of the time lag between the satellite intensity and the actual intensity for rapid intensifiers, the intensity and time differences were recorded for all rapid intensifiers in the satellite data set for the time period of 12 hours before period 1 until 12 hours after period 2. In addition, intensity and time differences for periods of non-rapid intensification were noted (Fig. 4.5). The objective was to determine if, during the period of rapid intensification, there are significant differences from periods of non-rapid intensification that can be used to predict rapid intensification when such differences are identified. Table 4.2 lists these intensity/time differences relative to the peaking hour (period 3), and stratified by rapid intensification and non-rapid intensification periods. On average, the rapid intensification period is typified by data T-number equivalent intensities which are 6.1 ms^{-1} (11.8 kt) higher than the actual intensity measured by aircraft within one hour of the satellite observation. The mean time lag when these higher satellite intensities are matched by aircraft observations is 6.3 hours later. In contrast, non-rapid intensification is characterized by a difference between the two measurement platforms of only 0.6 ms^{-1} with a time lag of 1.9 hours (Fig. 4.6).

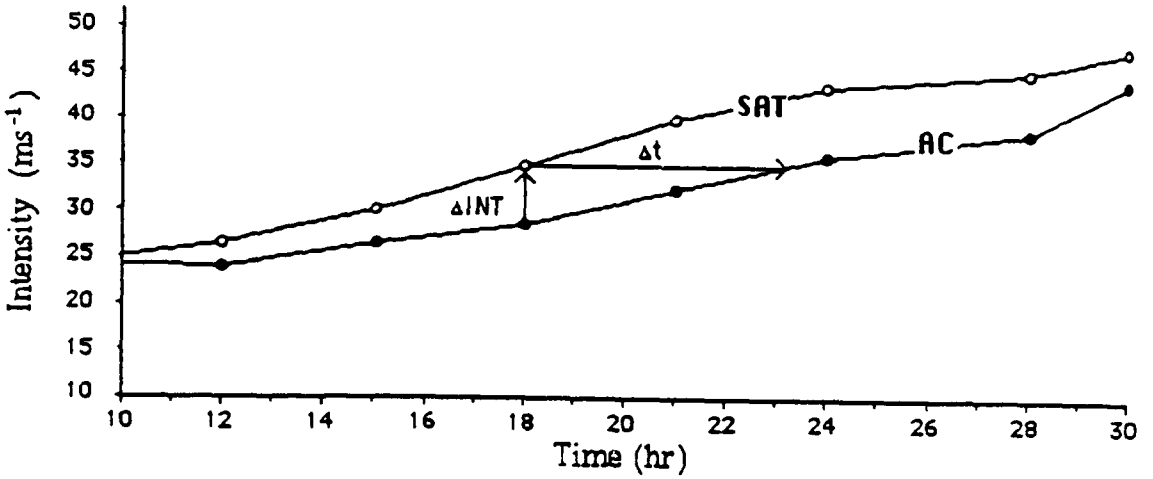

Figure 4.5: Illustration of the method used to determine intensity and time lag differences of the satellite data T-number intensity estimate and the actual intensity as measured by aircraft. Intermediate values were extrapolated when intensity measurements were not coincident.

Table 4.2: Description of the intensity and apparent time lag differences between satellite and aircraft intensity measurements. Time 0 is relative to the minimum central pressure measured by aircraft. A list of the tropical cyclones analyzed to obtain these mean values is given in Appendix D.

(a)

	TIME (hr)	SAT (ms^{-1})	A/C (ms^{-1})	ΔINT (ms^{-1})	Δt (hr)
NON RAPID INT	-36	32.4	32.5	-0.1	0
	-33	33.6	33.7	-0.1	0
	-30	35.3	35.0	0.3	3
	-27	36.0	35.4	0.6	2
	-24	36.9	36.6	0.3	1
	-21	38.3	37.9	0.4	2
	-18	39.4	38.8	0.6	1
	-15	41.1	40.2	0.9	3
	-12	42.9	41.3	1.6	4
	-9	43.6	42.4	1.2	3
	-6	44.6	43.6	1.0	2
	-3	45.8	45.4	0.4	1
	0	45.5	46.8	-1.3	1
	+3	43.3	43.9	-0.6	1
	+6	41.4	42.4	-1.0	2
	+9	38.4	40.0	-1.6	3
	+12	35.8	37.7	-1.9	3

(b)

	TIME (hr)	SAT (ms^{-1})	A/C (ms^{-1})	ΔINT (ms^{-1})	Δt (hr)
RAPID INT	-36	36.3	31.6	4.7	9
	-33	38.1	33.8	4.3	9
	-30	40.3	35.4	4.9	9
	-27	42.0	36.5	5.5	8
	-24	44.5	37.9	6.6	7
	-21	47.4	40.6	6.8	6
	-18	50.4	43.9	6.5	6
	-15	54.2	47.3	6.9	6
	-12	57.5	50.7	6.8	6
	-9	61.3	54.2	7.1	6
	-6	63.8	57.1	6.7	5
	-3	66.4	61.1	5.3	*
	0	67.2	64.6	2.6	*
	+3	65.1	64.0	1.1	*
	+6	61.9	62.6	-0.7	2
	+9	59.0	61.4	-2.4	6
	+12	55.8	60.2	-4.4	7

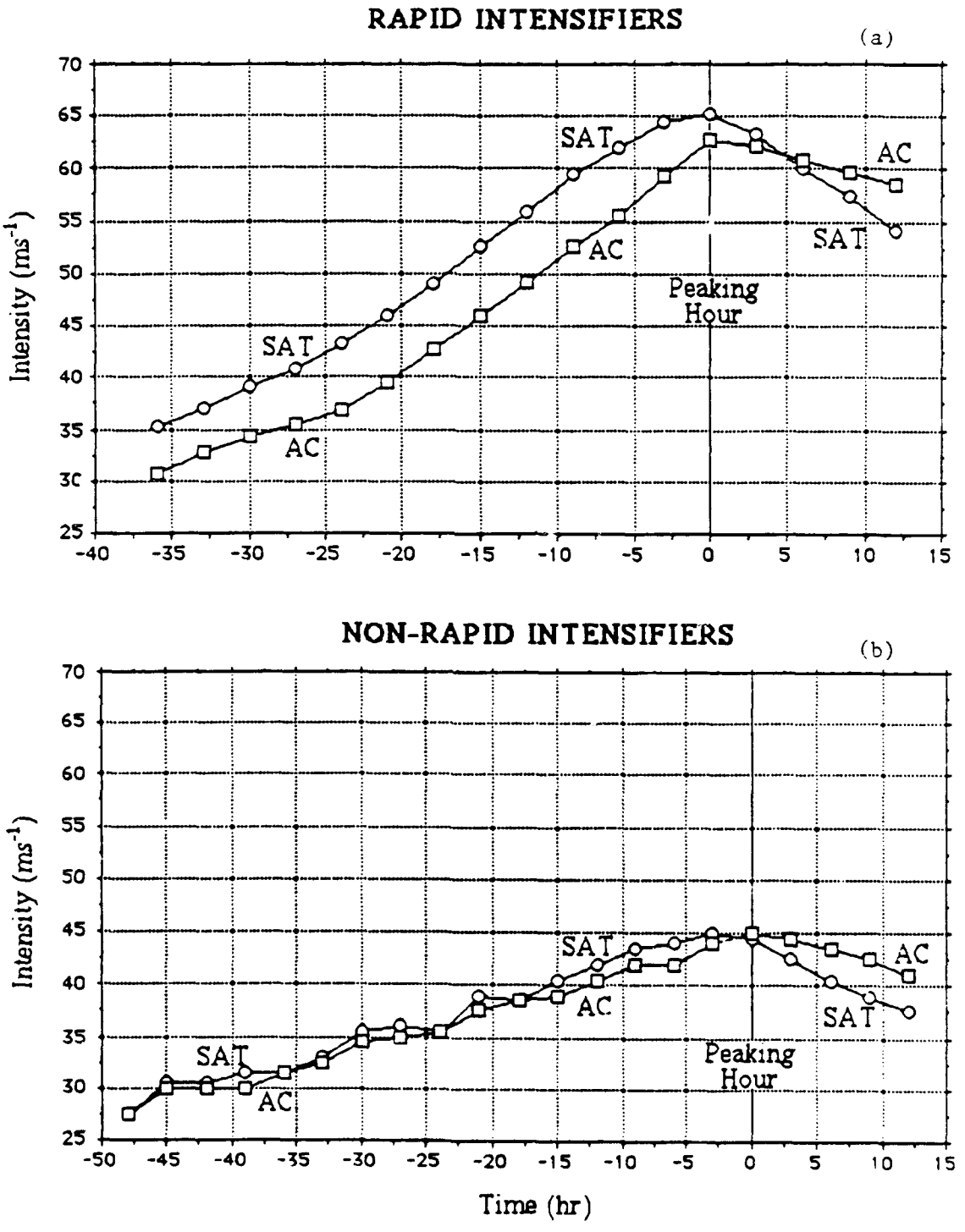

Figure 4.6: Illustration of the time versus intensity differences for satellite and aircraft measurements from the data presented in Table 4.2.

4.3 Prediction of Rapid Intensification From the Dvorak Data T-numbers

If we assume that a time lag exists between large increases in convection and subsequent drops in surface pressure (Steranka *et al.*, 1986), then the facts presented in the previous section can be utilized for short-term prediction of intensity change if the period of rapid intensification can be readily identified. If rapid intensification is suspected, then the actual intensity (final T-number) should be lower than the indicated data T-number intensity, and the data T-number intensity is then the predicted intensity value 6 to 12 hours later. An example of how the Data T-number intensity can be used to predict rapid intensification is summarized in Fig. 4.7.

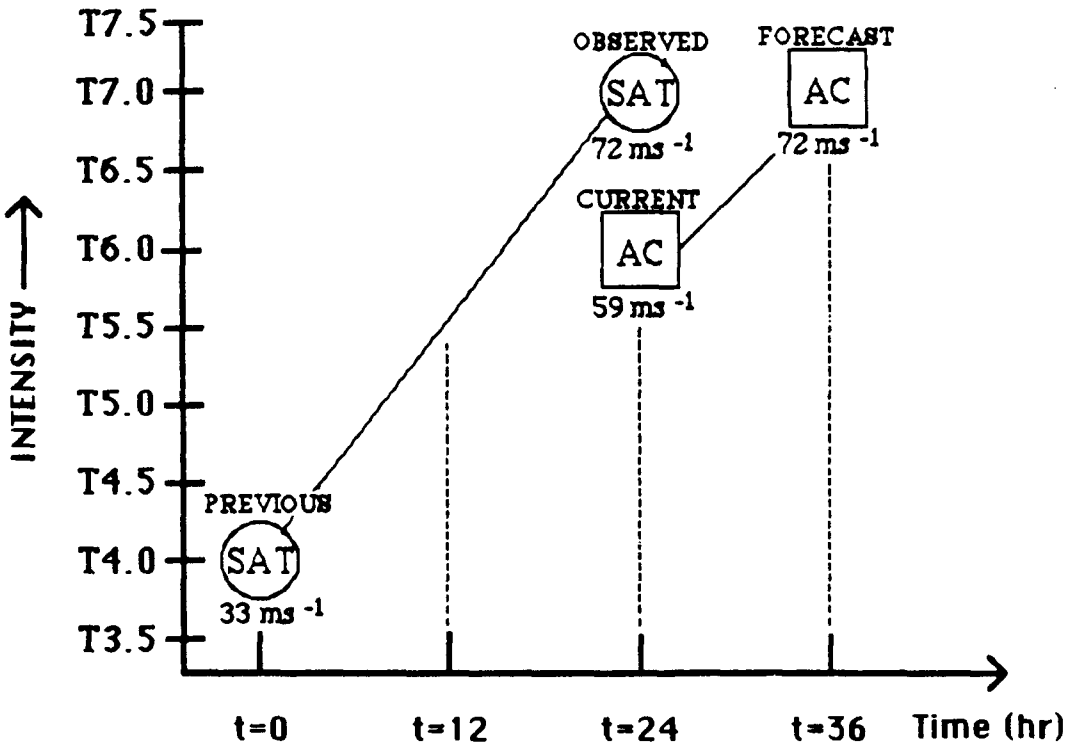

Figure 4.7: An example of a short term forecast technique used to reduce large intensity forecast errors. The apparent overestimate of intensity by the Dvorak data T-number during a period of rapid intensification is utilized to predict future intensity since a time lag of approximately 12 hours is assumed to exist between satellite estimates and actual intensity change.

In this example, the final T-number 24 hours ago was T4.0, which corresponds to an equivalent intensity of 33 ms^{-1}. The current data T-number, using the EIR Dvorak

method of comparing eye temperature to inner radii cloud top temperature, is T7.0 (72 ms^{-1}). This represents an apparent intensity change of 39 ms^{-1} over the past 24 hours. The actual intensity that an aircraft would measure at the same time would probably be about 13 ms^{-1} lower than this (59 ms^{-1}), or an equivalent Dvorak Final T-number of T6.0. Note that this would be a change of 2.0 T numbers in 24 hours, the maximum current intensity (CI) change allowed by the Dvorak model. However, given the assumption that during rapid intensification the Data T-number change precedes the measured intensity change by about 10 hours, the current Data T-number value of T7.0 is used to predict an intensity of 72 ms^{-1} 12 hours later. Since this would be a change of 13 ms^{-1} in only 12 hours, this would mean further rapid intensification is forecast for at least another 12 hours. This technique could then be extrapolated to predict a 24 hour intensity change, depending on other factors such as proximity to land masses, etc. In this example, the operational forecaster has not only indicated that the intensity has changed 26 ms^{-1} (50 kt) during the past 24 hours, but that further rapid intensification of 13 ms^{-1} (25 kt) is expected in the next 12 hours.

As noted earlier, this method to predict rapid rates of intensification relies upon timely identification that rapid change is actually occurring. This is possible if Dvorak data T-numbers are calculated more frequently than once or twice a day, as is commonly practiced at the present time. If hourly (or even half-hourly) digital infrared satellite data is available, it is relatively simple to affix a data T-number to each image if an eye is present, and keep a running record of hourly changes in the data T-number. If the data T-number changes by T1.0 in six hours or T1.5 in twelve hours, this is usually sufficient to identify the onset of a rapid intensification period. A major deficiency of this method is that it does not identify rapid intensification until it is well underway, since the observed time lag is only 6 to 9 hours. The Dvorak data T-numbers are, however, a strong signal that an unusual rate of intensity change is taking place.

4.4 Experimental Results of a Data T-number Prediction Method

A prediction experiment based on the apparent lag time between the satellite data T-number and aircraft measured intensities was supervised by the author in a quasi-

operational mode during the Modified Operations Evaluation Experiment (OPEVAL) conducted by joint efforts of the US Air Force Air Weather Service and the US Navy Oceanographic Command from June to August 1987 (JTWC, 1987). The objective of this trial was to develop new, useful techniques that could be used by satellite analysts at Detachment 1, First Weather Wing and forecasters at the JTWC to improve prediction of intensity change without benefit of aircraft while aerial reconnaissance was still available in the NWPAC for verification purposes.

In this experiment, data T-numbers were determined approximately once every six hours for all tropical cyclones which occurred during the OPEVAL period. If rapid changes ($\geq$ 1.0 in six hours or $\geq$ 1.5 in 12 hours) in the data T-number were noted, the data T-number was not considered the same as the final T-number and a lower intensity estimate was recorded for later verification. The data T-number was then used to predict what minimum sea level pressure the aircraft would measure 12 hours later. Sufficient verification data was available for five tropical cyclones, four of which had a visible eye; Typhoon Sperry, Supertyphoon Thelma, Typhoon Vernon, Supertyphoon Wynne and Supertyphoon Betty. Only Vernon and Sperry did not experience a period of rapid intensification, hence it was extremely fortunate that this experiment could be attempted on three different rapid intensifiers. Results of this experiment are summarized in Table 4.3.

Current intensity estimates were reasonably accurate; the mean error was 4.2 hP_a with a bias of +2.4 hP_a. The maximum error was +20 hP_a. Twelve hour intensity forecast errors had a mean of 6.1, a bias of +1.4, with a max error of 20 hP_a. A mean error of 6 hP_a in 12 hours is about average. However, since 4 of the 14 verified forecasts were rapid intensification events (identified by an asterisk in Table 4.3), then it would appear this short range forecast was much better than average. All satellite rapid intensification forecasts were verified by a rapid drop in surface pressure of at least 20 hP_a in 12 hours. The errors forecasting rapid intensity change 12 hours later were 2, -2, 5 and 13 hP_a. This is considerably less than a climatological ΔP forecast of -7 hP_a in 12 hours (Weatherford and Gray, 1988), which would yield errors of 18, 13, 23 and 18 hP_a, respectively. These limited results are encouraging but not convincing. It does appear possible, in some cases,

Table 4.3: Experimental verification statistics for a short term forecast method using the Dvorak data T-numbers such as in Fig. 4.7. This experiment was conducted during the Modified Operations Evaluation (OPEVAL) on Guam in 1987. CI and FI denote current and forecast intensity, respectively. All rapid intensification events, whether observed or forecast, are indicated by an asterisk.

CYCLONE NAME	DATE/TIME GMT	SATELLITE CI ESTIMATE (hPa)	AIRCRAFT CI MEASURED (hPa)	CI ERROR (hPa)	SATELLITE 12HR FCST (hPa)	AIRCRAFT 12HR OBS (hPa)	FI ERROR (hPa)
SPERRY	062700	996	1001	-5	994	991	+3
	062800	983	985	-2	974	994	-20
THELMA	070700	1004	1003	+1	997	none	n/a
	070800	1000	1002	-2	994	none	n/a
	071012	958	954	+4	940	936	+4
	071100	935*	936	-1	913*	911*	+2*
	071200	920	920	0	939	937	+2
VERNON	071700	998	999	-1	991	997	-6
	071800	997	997	0	997	994	+3
	071900	996	988	+8	992	987	+5
	072000	984	984	0	985	990	-5
WYNNE	072400	990	987	+3	965*	967*	-2*
	072500	944*	931*	+13*	939	926	+13
	072600	942	922	+20	950	none	n/a
BETTY	080900	1000	1000	0	995	993	+2
	081000	984	985	-1	960*	955*	+5*
	081100	927*	917*	+10*	905*	892*	+13*
	081200	905	909	-4	905	none	n/a

to predict short-term rapid intensity change if satellite observations indicate a rapid rate of change in the Dvorak data T-number.

4.5 Theory of Rapid Intensification as Observed By Satellite

During periods of rapid intensity change, satellite pictures of rapid intensifiers are strikingly different from those of non-rapid intensifiers. The two distinctive features observed by satellite are a concentration of the deep convection near the center and a small, symmetric eye. There are two primary patterns which are repeated in nearly all satellite-observed cases of rapid intensification. Either the eye becomes more symmetrical and decreases in size (Fig. 4.8) or there is a concentration of deep convection near the cyclone center (Fig. 4.9). In many rapid intensifiers, these two processes occur at the same time. Clearly, there must be an explanation why such a concentration of deep convection and/or shrinking of the eye happens.

From the gradient wind equation in cylindrical coordinates (Eq. 4.1), the velocity V is a function of the pressure gradient force $\frac{1}{\rho}\frac{\partial p}{\partial r}$ and the radius of maximum winds, r

$$\frac{V^2}{r} + fV = \frac{1}{\rho}\frac{\partial p}{\partial r} \tag{4.1}$$

For tropical cyclones a nearly cyclostrophic balance exists (Eq. 4.2). During rapid intensification, as the pressure gradient force at a given radius increases, the radius of maximum winds decrease or there is an increase in tangential wind velocity.

$$\frac{V^2}{r} = \frac{1}{\rho}\frac{\partial p}{\partial r} \tag{4.2}$$

The most efficient way to create large pressure gradients is to lower the pressure hydrostatically by concentrating the latent heat release from convection into a small area (Hack and Schubert, 1986). This is accomplished by a relative concentration of the deep convection to as close to the center as possible. In this scenario, the pressure gradient is steepest close to the eye wall, and the radial pressure gradient away from the center is relatively weak when compared to a more typical profile of pressure (Fig. 4.10). In the typical case of non-rapid intensification, there is a lack of deep convection concentration

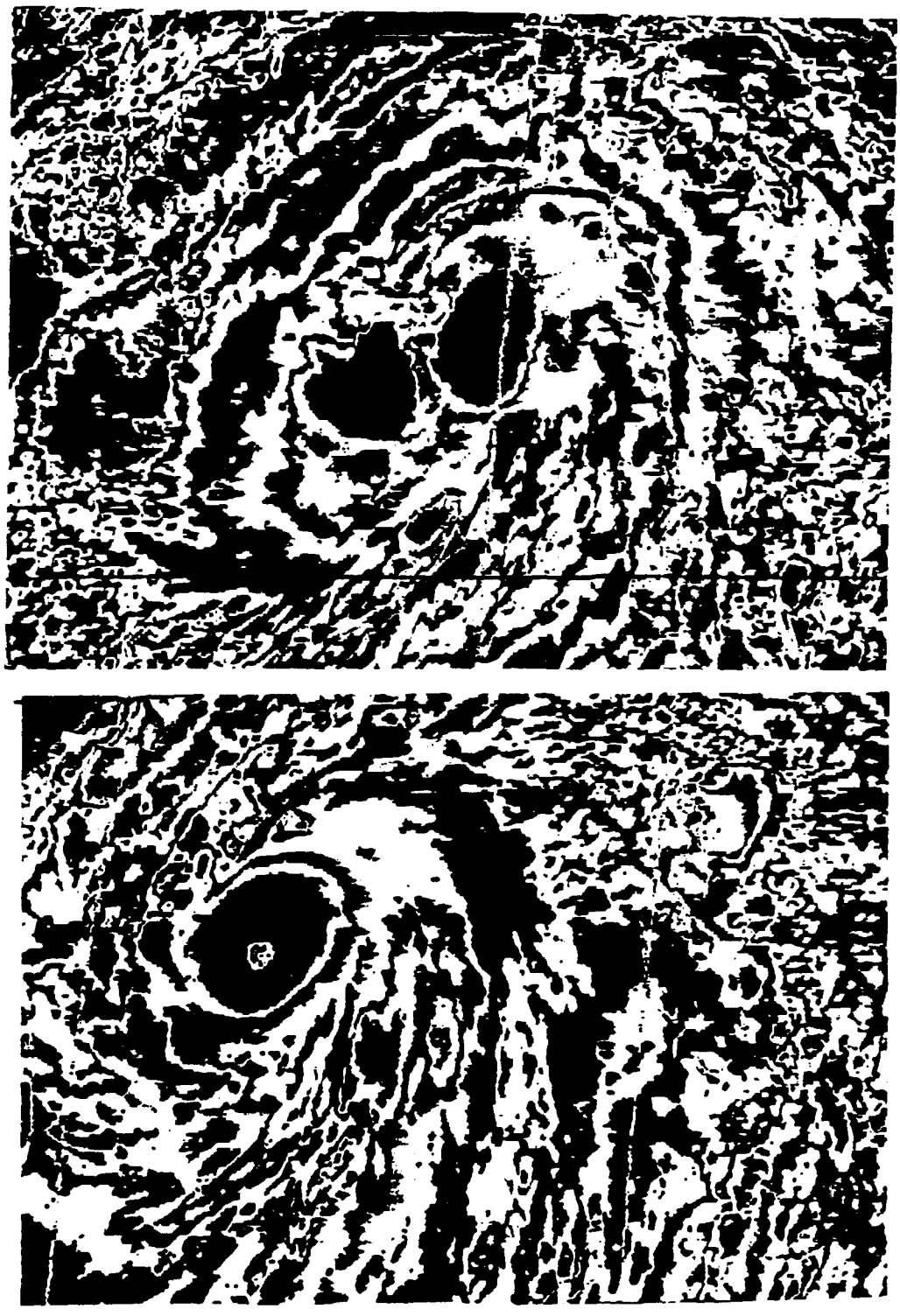

Figure 4.8: Enhanced Infrared (EIR) satellite imagery of Supertyphoon Thelma near the onset of rapid intensification at 09Z GMT on 10 July 1987 (a) and near the termination of rapid intensity change at 12Z GMT on 11 July (b). During rapid intensification there was a substantial decrease in eye size from 35 to 10 km. Enhancement is the MB curve (NOAA User's Guide) developed by Dvorak (1984).

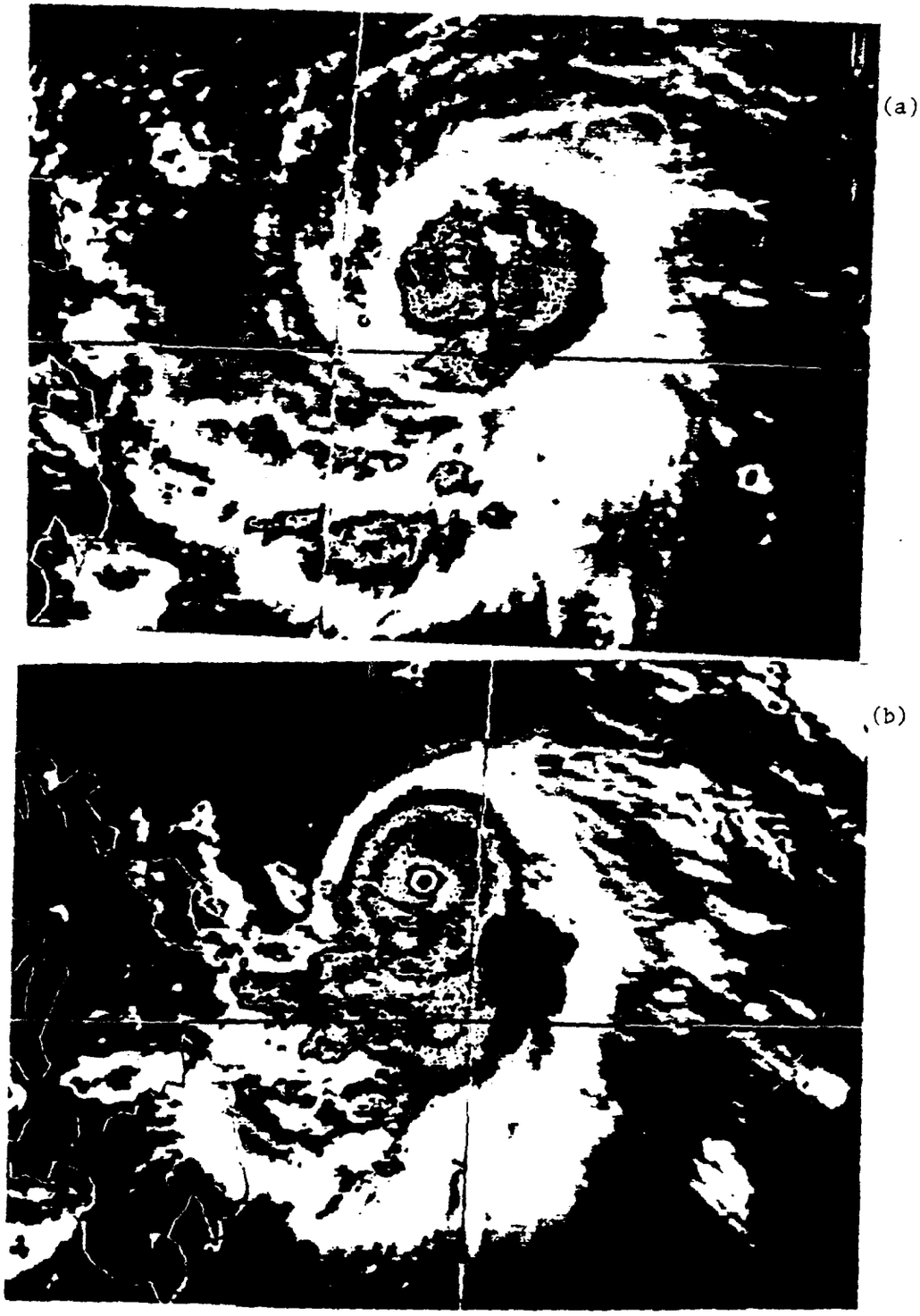

Figure 4.9: Infrared (IR) satellite imagery of Supertyphoon Betty (1987) at the onset (a) and termination (b) of rapid intensification at 03Z GMT on 10 and 11 August. A concentration of the deep cumulus convection at the inner core of Betty was evident during rapid intensity change.

(convection is spread out to a broader radius). A second way to cause large tangential wind increase and lower the surface pressure is to have a contraction of the eye. Note in Eq. 4.2 that if r is reduced to half of its original value, the pressure gradient force (neglecting friction) must double for the same velocity V. During rapid intensification, eyewall contraction and wind increase occur simultaneously. This results in larger values of V and a smaller radius of maximum wind. Weatherford and Gray (1988) stated that the most "intense" typhoons (as defined by MSLP) are not necessarily the "strongest" ones (based on outer winds). Thus the rapid intensifiers can be considered to be cyclones with extremely intense inner core regions and relatively weak outer wind distributions. Weatherford also found that these intense typhoons had large increases in outer winds after the end of a rapid intensification event at the inner core.

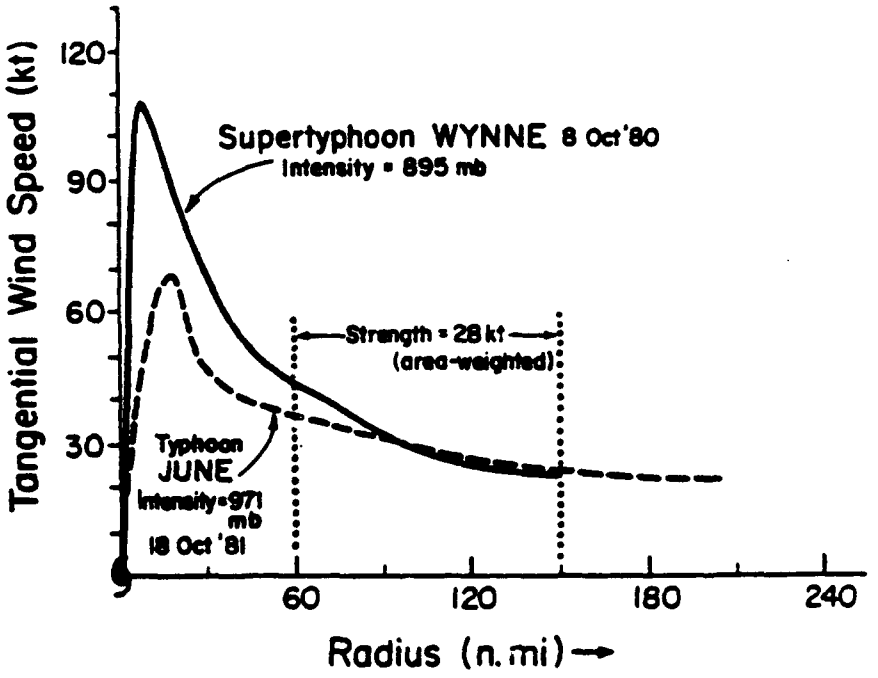

Figure 4.10: Two examples of tangential wind profiles after rapid intensification (Wynne) and after non-rapid intensification (June). Note that the outer winds are the same but the inner core winds are very different (Weatherford and Gray, 1988).

4.6 Relationship of Eye Size to Rapid Intensification

As noted in the previous section, one characteristic of rapid intensifiers is a small, symmetric eye. Weatherford and Gray (1988) examined aircraft reconnaissance missions and concluded that rapid deepeners tend to form an eye at a higher (985 hP_a) MSLP and to have eyes that are smaller than average. They stated that the onset of rapid deepening coincided closely with eye formation and that during rapid intensification the mean eye size was reduced by a factor of 2.0. Mean typhoon eye sizes were tabulated by Bell (1975). His results are shown in Fig. 4.11. Holliday and Thompson (1979) compared the eye sizes of rapid intensifiers at the onset of rapid deepening and 12 to 24 hours later. They found that rapid intensifiers developed smaller than average eyes. Mean eye size for rapid intensifiers decreased substantially during the rapid intensification period (Fig. 4.12). The mean radius of maximum wind 24 hours after rapid intensification was only 13 km ($\approx$ 7 n mi), an extremely small mean value. Note that there were no instances of eye size larger than Bell's mean eye diameter of 51.4 km (27.8 n mi) at 24 hours after the onset of rapid deepening. It is observed that rapid intensifiers either have small eyes at period 1 or that the eye diameter contracts during rapid intensification.

An estimate of the relative importance of contraction of eye size to rapid intensity change can be determined from the mean data presented in this and other research. At the onset of rapid deepening, the mean intensity is 33.5 ms^{-1} and the average eye radius is 20.4 km (Holliday and Thompson, 1979). Using regression curves which relate intensity and eye size (Weatherford and Gray, 1988), the mean OCS is initially 16.1 ms^{-1}. Twenty-four hours later, the mean values for intensity, eye radius and OCS are 64.3 ms^{-1}, 12.8 km, and 22.3 ms^{-1}, respectively. Mean values at onset of rapid intensification and 24 hours later are depicted in Fig. 4.13.

If we assume that the relationship between velocity and radius (Riehl, 1963) is given by:

$$V_r^x = constant \tag{4.3}$$

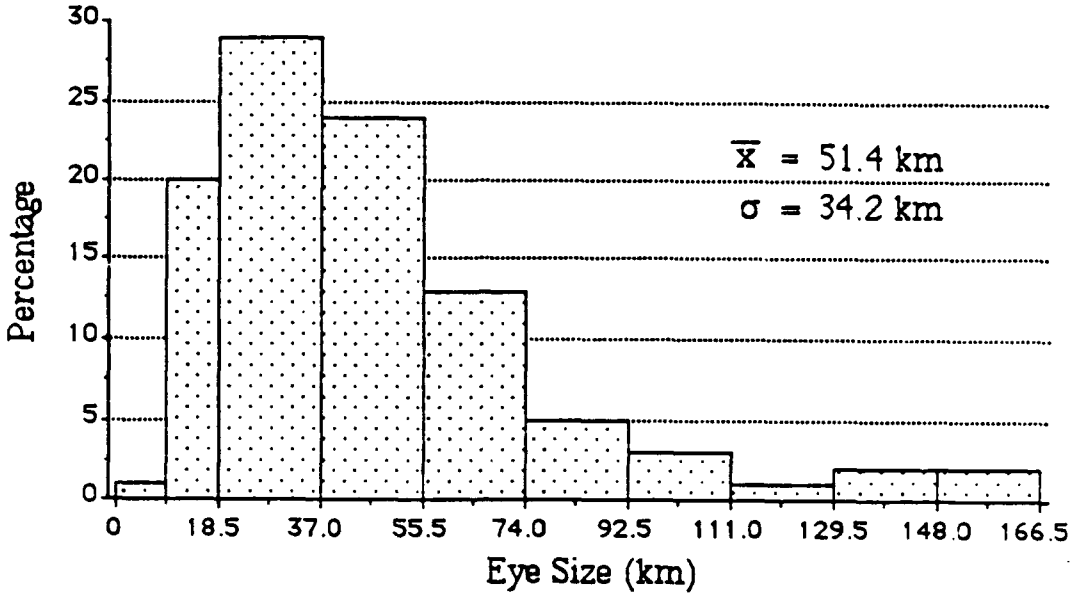

Figure 4.11: Relative frequency distribution of eye diameter for western North Pacific typhoons. Data consists of 2013 cases studied by Bell (1975).

with x = 0.5 is valid, then the constant value is 151.3 for the mean values of intensity and eye radius at the onset of rapid deepening. The expected value of V_{max} 24 hours later for x = 0.5 if r decreases to 12.8 km is 42.3 ms^{-1}. Thus, after rapid intensification, Eq. 4.3 is no longer valid for x = 0.5. Instead, the value of x is given by 0.34 if the constant is 151.3. If we consider the exponent x = 0.5 to be an accurate mean value (Shea and Gray, 1973), then the amount of tangential wind increase due strictly to the contraction of eye radius from 20.4 to 12.8 km is 8.8 ms^{-1}, or 22% of the total velocity increase from 33.5 to 64.3 ms^{-1} (Fig. 4.14a). If x = 0.5 at the end of the rapid intensification period, then x = 0.64 initially. In this case, 37% of the tangential wind increase is due to eye contraction (Fig. 4.14b). It would appear from the mean data that approximately one-fourth to one-third of the increase in wind speed during rapid intensification can be accounted for by reductions in mean eye size. The remaining 65 to 75% of the increase in wind speed for the mean rapid intensification case is due to wind spin up at all radii due to momentum imported to the core by concentrating the deep convection closer to the cyclone center.

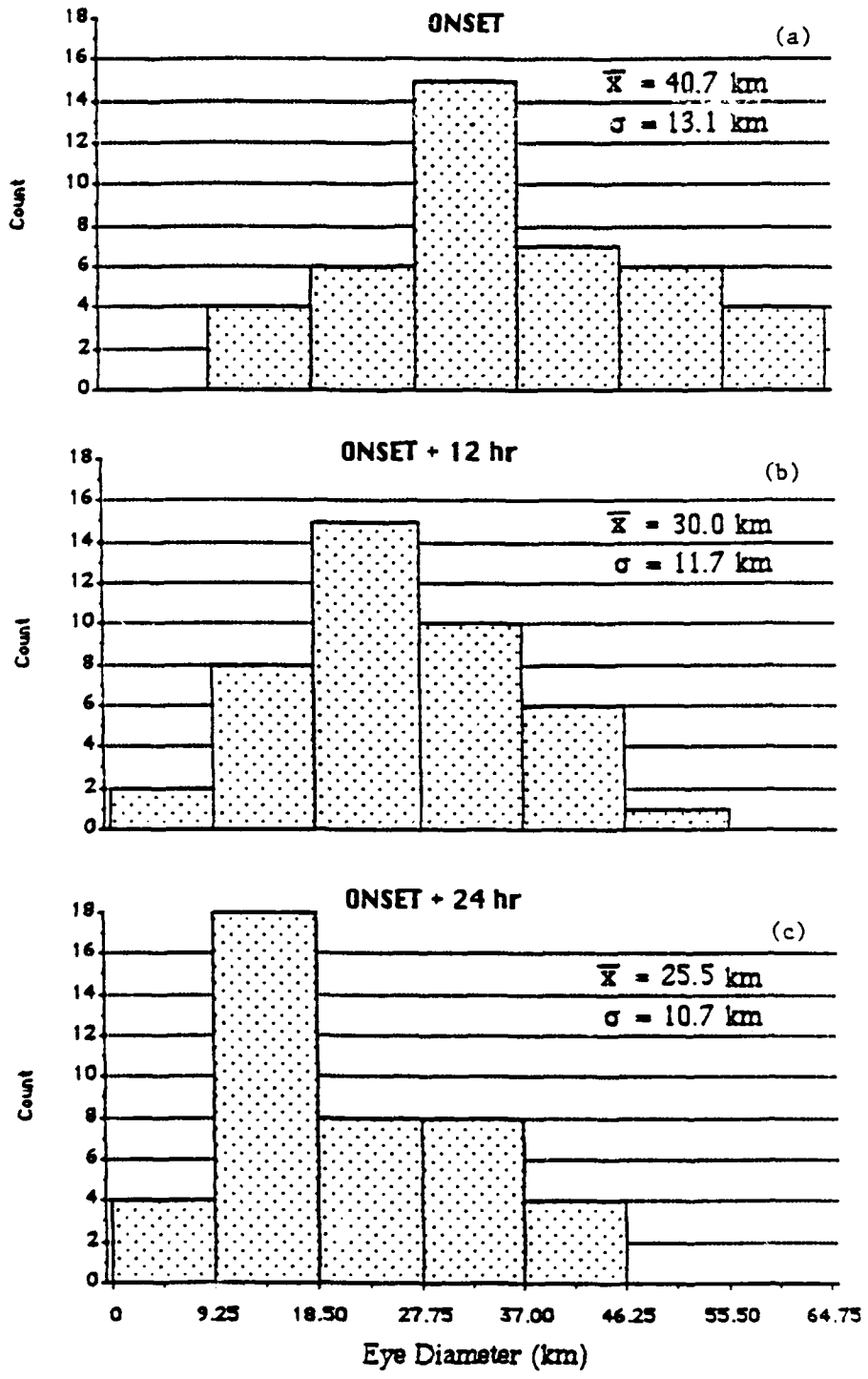

Figure 4.12: Frequency distribution of eye diameter at the onset of rapid intensification (a), 12 hours after onset (b), and 24 hours after onset (c). Data consists of 42 rapid intensification events studied by Holliday and Thompson (1979).

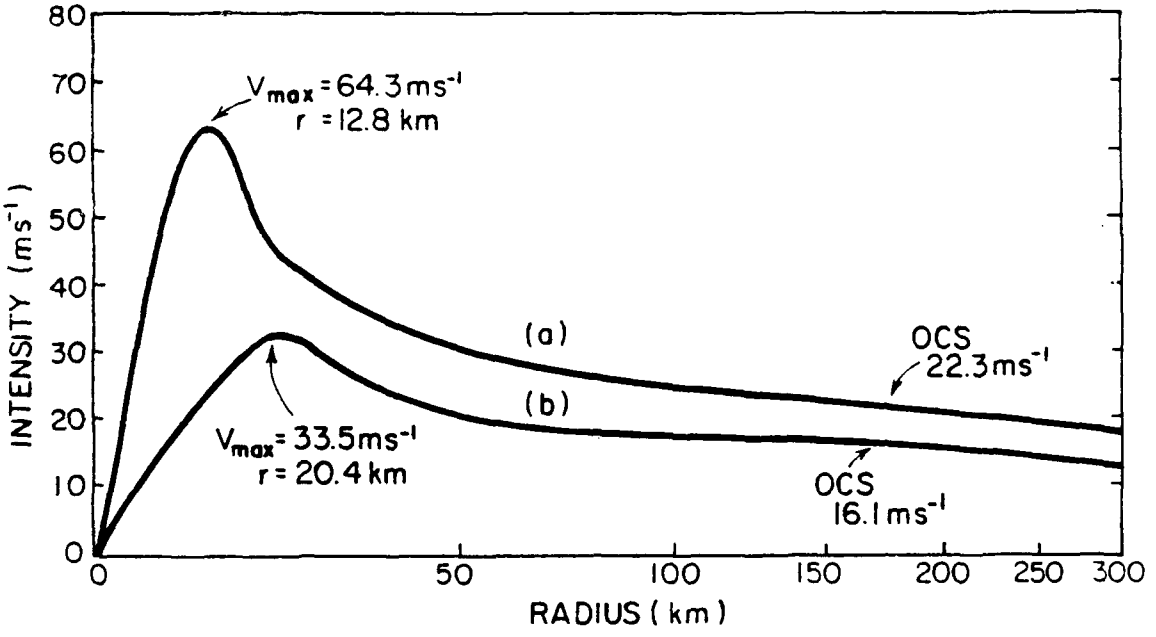

Figure 4.13: Mean tangential wind profiles of rapid intensifiers compiled from mean data at onset of rapid intensification and 24 hours after onset. Maximum intensities were derived from Fig. 3.13. Eye size was obtained from Fig. 4.10. Outer core winds were calculated from regression equations developed by Weatherford and Gray (1988) which correlated eye size and MSLP to outer wind strength.

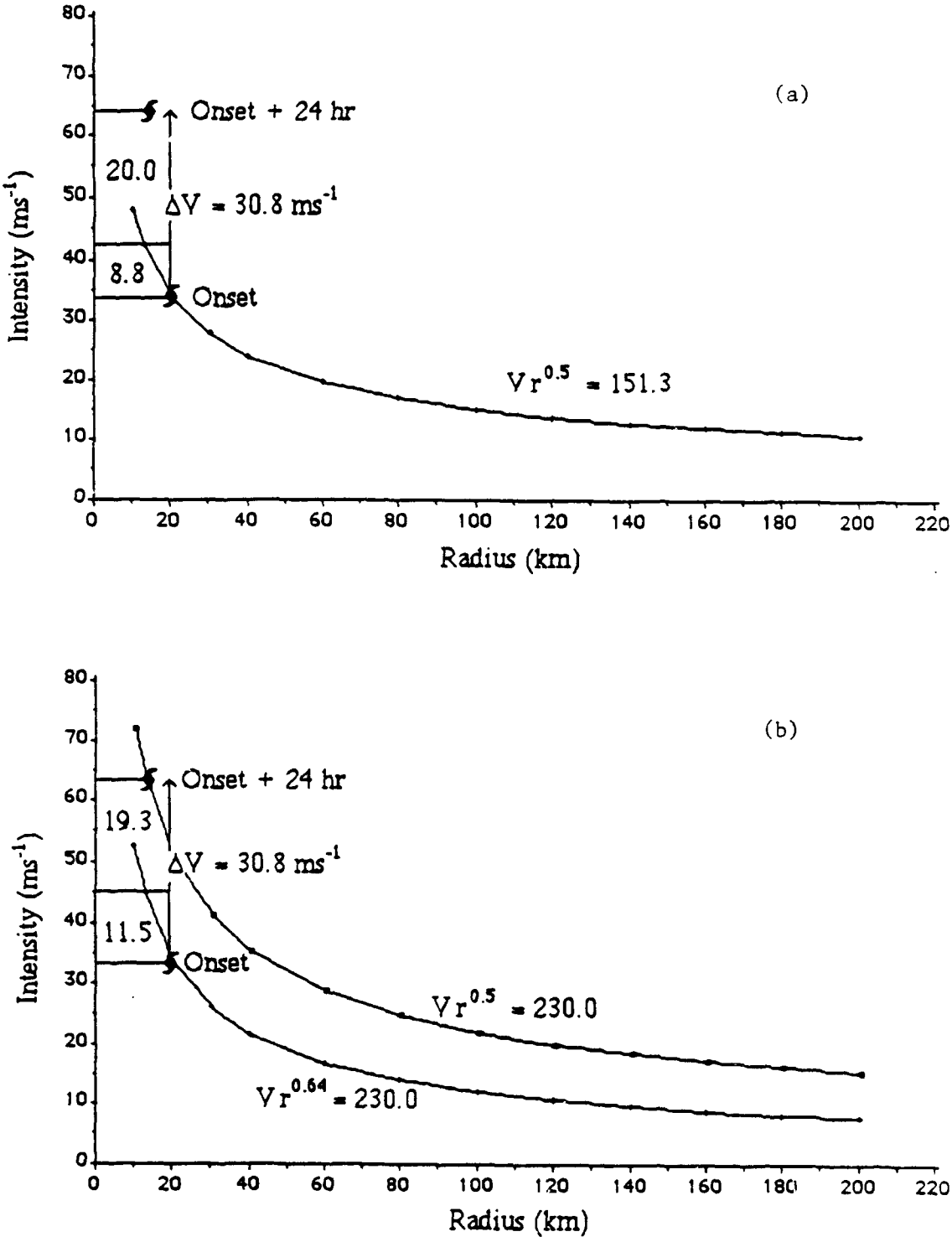

Figure 4.14: Illustration of the relative importance of the reduction of eye size during rapid intensification. The relationship $V_r^{0.5}$ = constant is assumed to approximate the actual tangential wind profile at either the onset of rapid intensity change (a), or at the termination of rapid deepening 24 hours later (b). One-fourth to one-third of the intensity increase is estimated to be due strictly from eye size contraction.

Measurement of eye size, particularly the changes of eye diameter, is an important aspect of tropical cyclone reconnaissance. In the NWPAC, measurement of eye size from aircraft radars is no longer possible. From the satellite perspective, eye size can often be estimated relatively well, but is not routinely measured or recorded by satellite analysts. A comparison of recorded eye diameters from US Air Force satellite analysts to aircraft measured eye size within $\pm$ 3 hr was made by Zehr (1990). He found the diameters were generally a good approximation in most cases, but some large differences are possible (Fig. 4.15). In a relative sense, the satellite is able to detect if the eye size is of a normal size, larger or smaller than average even if the actual value is suspect. If an eye is present, rapid intensification is more likely to occur if the satellite detects an eye smaller than normal or if the eye size is contracting from a normal size to a small size.

The best way to determine if contraction is actually occurring (without aircraft) is to develop a standardized method to measure eye diameter from satellite and record eye size on each observation if an eye is present. At present, no such standard exists, and the frequency of satellite measurements is irregular. Large variations in satellite measurements of eye size can occur for no other reason than individual differences between satellite analysts.

A lack of hourly high resolution IR data and the scarcity of satellite reports of eye diameter made further study of the practicality of such a standardized method impossible. The author believes satellite measurements of eye diameter could be effectively used to predict intensity change. Rapid intensifiers tend to have small eyes and that typhoons with eye diameters $\geq$ 65 km (35 n mi) will not intensify rapidly unless the eye substantially reduces in size. Increasing eye size is not characteristic of rapid intensifiers (Weatherford, 1989), although some rapid intensification events do occur without a significant decrease in eye size.

4.7 Relationship of Inner/Outer Convection Ratio to Rapid Intensification

In section 4.6, the importance of a concentration of the deep convection near the cyclone center was discussed. A way to measure the degree of concentration is to set up

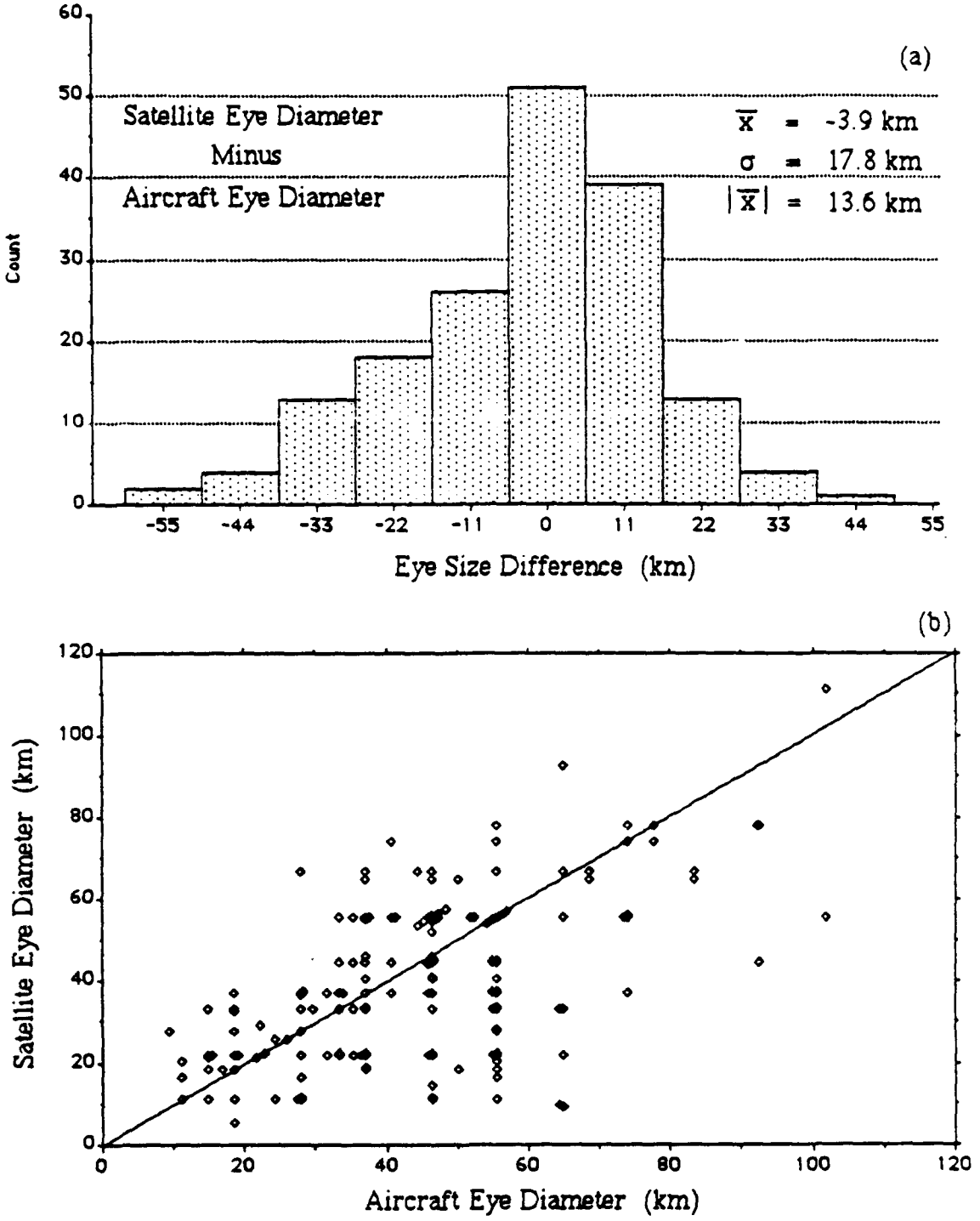

Figure 4.15: Histogram of satellite eye measurement accuracy as compared to aircraft measurements within ± 3 hours (a) and correlation between measurements of eye diameter by satellite analysis and by aerial reconnaissance radar (b). Data was obtained from fix data published in the JTWC Annual Tropical Cyclone Reports from 1983 to 1986 (Zehr, 1990).

a cylindrical grid, centered on the cyclone center, and count the number of pixels colder than a given threshold value for radial bands measured from the center point. The pixel counts for inner radial bands are then divided by the pixel counts of outer radial bands to derive a ratio of inner/outer convection (I/O ratio). High values of I/O ratio are thus indicative of concentrated deep convection. To determine if high values of I/O ratio are also predictors of rapid intensification, the temperature thresholds and radial bands listed in Table 4.4 were used to derive a variety of I/O ratios for a sample of digital IR GMS imagery which included both rapid intensifiers and non-rapid intensifiers from 1983 to 1985. Based on the results from several typhoons in the sample, the pixel count $\leq$ -75°C for 0-2° radius was selected as the "inner" value and the number of pixels $\leq$ -65°C at 2-6° was chosen as the "outer" value because these appeared to have the highest correlation between I/O ratio and the onset of rapid intensification. Due to large diurnal variations in the amount of deep convection (Zehr, 1988) it was necessary to smooth the raw data by using a 24 hour running mean. Examination of the 24 hour running means of convection colder than -75°C in the inner radius and -65°C in the outer radius showed a very good relationship with the onset of rapid intensity change. This lead to the development of a method to accurately predict rapid versus non-rapid intensity change based on the relative amounts of inner to outer deep convection.

4.8 An Intersection Technique to Predict Rapid Intensity Change

As noted in Chapter 1, the intersection technique developed by Dunnavan (1981) to predict intensity change based on the MSLP trace and the 700 hP_a equivalent potential temperature is no longer used in the NWPAC. Research involving the I/O ratios of 1983-5 rapid and non-rapid intensifiers revealed a strong, and somewhat surprising, correlation between the amount of inner (0-2°) convection with cloud top temperatures $\leq$ -75°C and the number of outer (2-6°) pixels $\leq$ -65°C. This research indicated that when these pixel counts are slightly modified in scale, an intersection of the "centered" 24 hour running means of inner and outer convection pixel counts was an excellent predictor of the onset of rapid intensification (Fig. 4.16). Note that the intersection occurs 12 hours prior to

Table 4.4: Depiction of the temperature thresholds and radial bands used to determine ratios of inner to outer deep convection. Paired inner to outer radial bands were 0-1 vs. 2-4, 0-1 vs. 2-6, 0-1 vs. 0-4, 0-2 vs. 2-4, 0-2 vs. 2-6, 0-2 vs. 0-6, 1-2 vs. 2-4, 1-2 vs. 2-6, and 0-4 vs. 4-8. A total of 16 temperature threshold combinations were examined for each pair of inner and outer radial bands. The circled temperature thresholds and radial bands yield the best intensity prediction signal for the NWPAC.

TEMPERATURE THRESHOLDS	INNER CONVECTION RADIAL BANDS	TEMPERATURE THRESHOLDS	OUTER CONVECTION RADIAL BANDS
-80° C	0 - 1°	-70° C	2 - 4°
(-75° C)	(0 - 2°)	(-65° C)	(2 - 6°)
-70° C	1 - 2°	-60° C	0 - 4°
-65° C	0 - 4°	-50° C	0 - 6°
			4 - 8°

the onset of rapid intensity change when the 24 hour running means are centered on the midpoint of the 24 hour period. In an operational sense, it is only possible to determine a 24 hour running mean from previous satellite data, thus there would be little or no leadtime from the point the two running mean plots intersect and the onset of rapid intensity change. However, the raw data should indicate a concentration of inner to outer convection at least 6 to 12 hours before the onset of rapid intensification. There was only one instance (Clara, 1984) of a non-rapid intensifier which had an intersection between the inner and outer pixel counts, once "climatological filtering" was done to eliminate cyclones whose geographic location and the time of year indicated they were not likely to rapidly intensify. Almost all of the non-rapid intensifiers did not have an intersection of the inner/outer pixel count plots, some examples of which are shown in Fig. 4.17.

The climatological filters used were: 1) Time of year. Storms occurring from Dec 15 to May 10 were eliminated in this manner. 2) Latitude. All cyclones poleward of 22°N and those occurring 2° (222 km) or more north of the mean latitude of initial typhoon intensity classification were not expected to rapidly intensify, even if an intersection occurred. 3) Intensity. Tropical cyclones with maximum sustained winds of 23 ms^{-1} (45 kt) or less and those with maximum winds $\geq$ 51 ms^{-1} (100 kt) were not deemed likely to rapidly

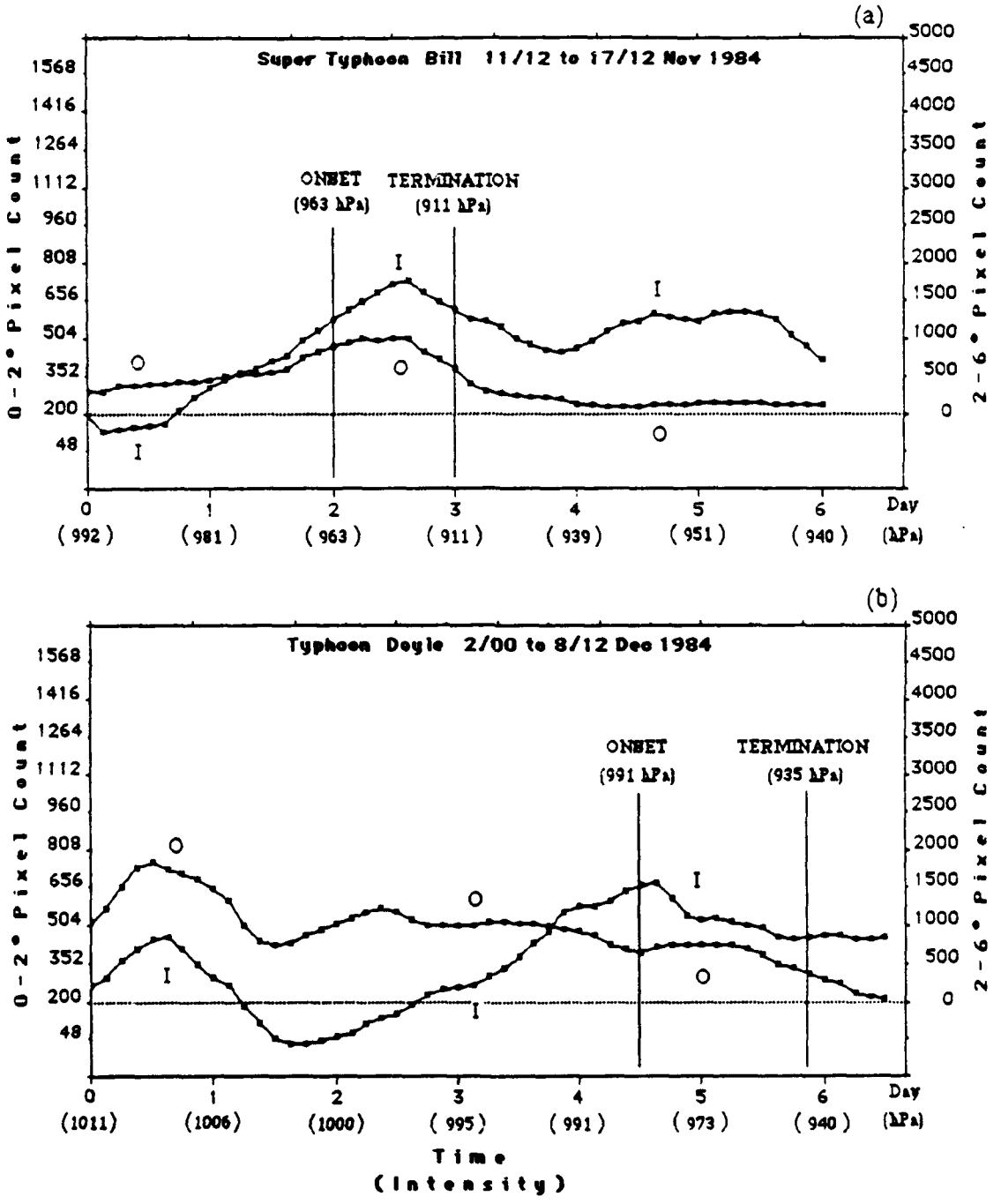

Figure 4.16: a to f: Relative concentrations of inner (0 to 222 km) and outer (223 to 666 km) deep convection versus time and intensity for six rapid intensification events from 1983 to 1985. Twenty-four hour running means of pixel counts colder than -75°C and -65°C are denoted by I (inner) and O (outer), respectively. Running means are plotted in the standard manner, relative to the midpoint (at 12 hours). The relative concentrations intersect about 12 hours prior to the onset of rapid intensity change.

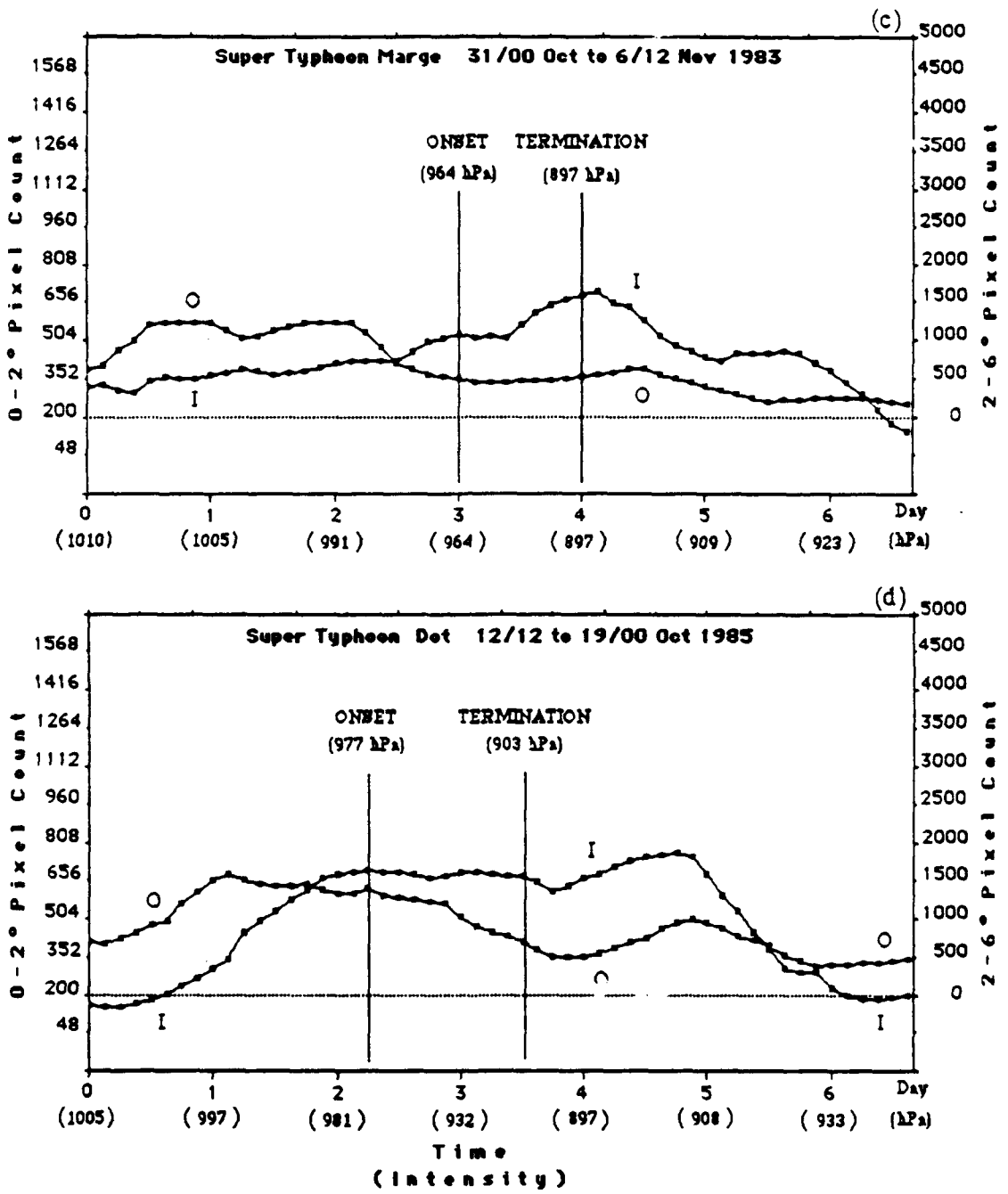

Figure 4.16: Continued.

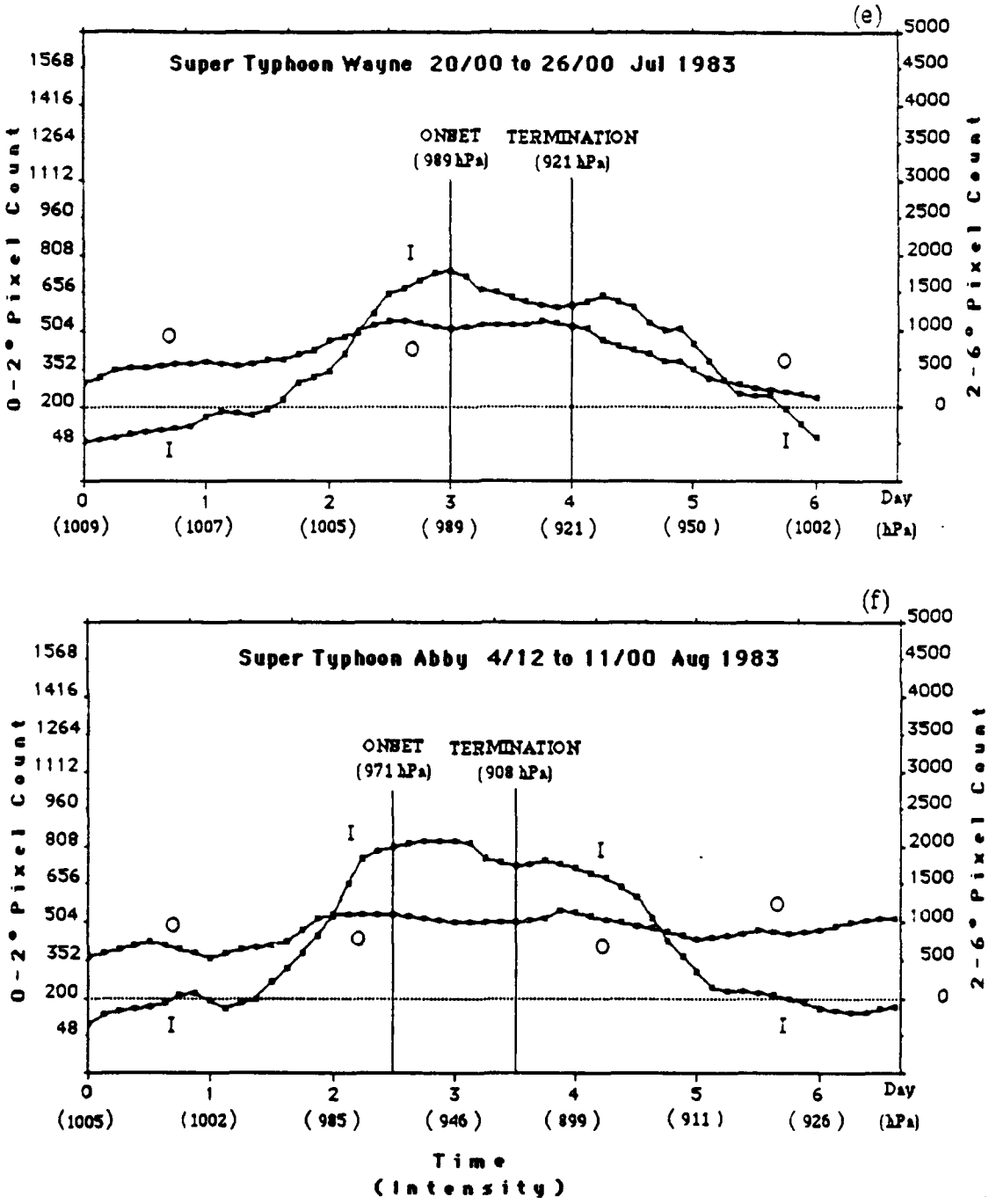

Figure 4.16: Continued.

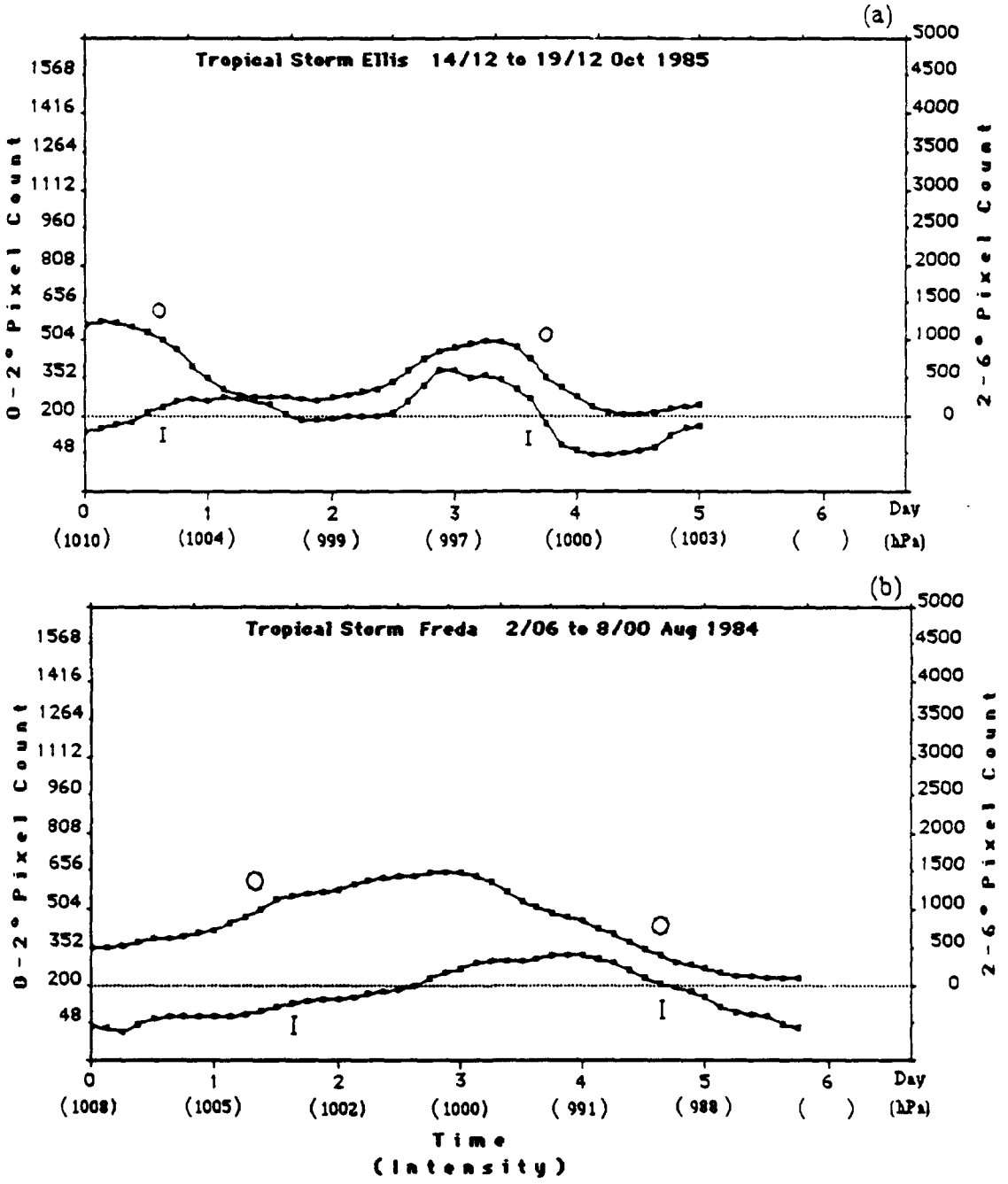

Figure 4.17: a to d: Same as Fig. 4.16 except for four non-rapid intensification events.

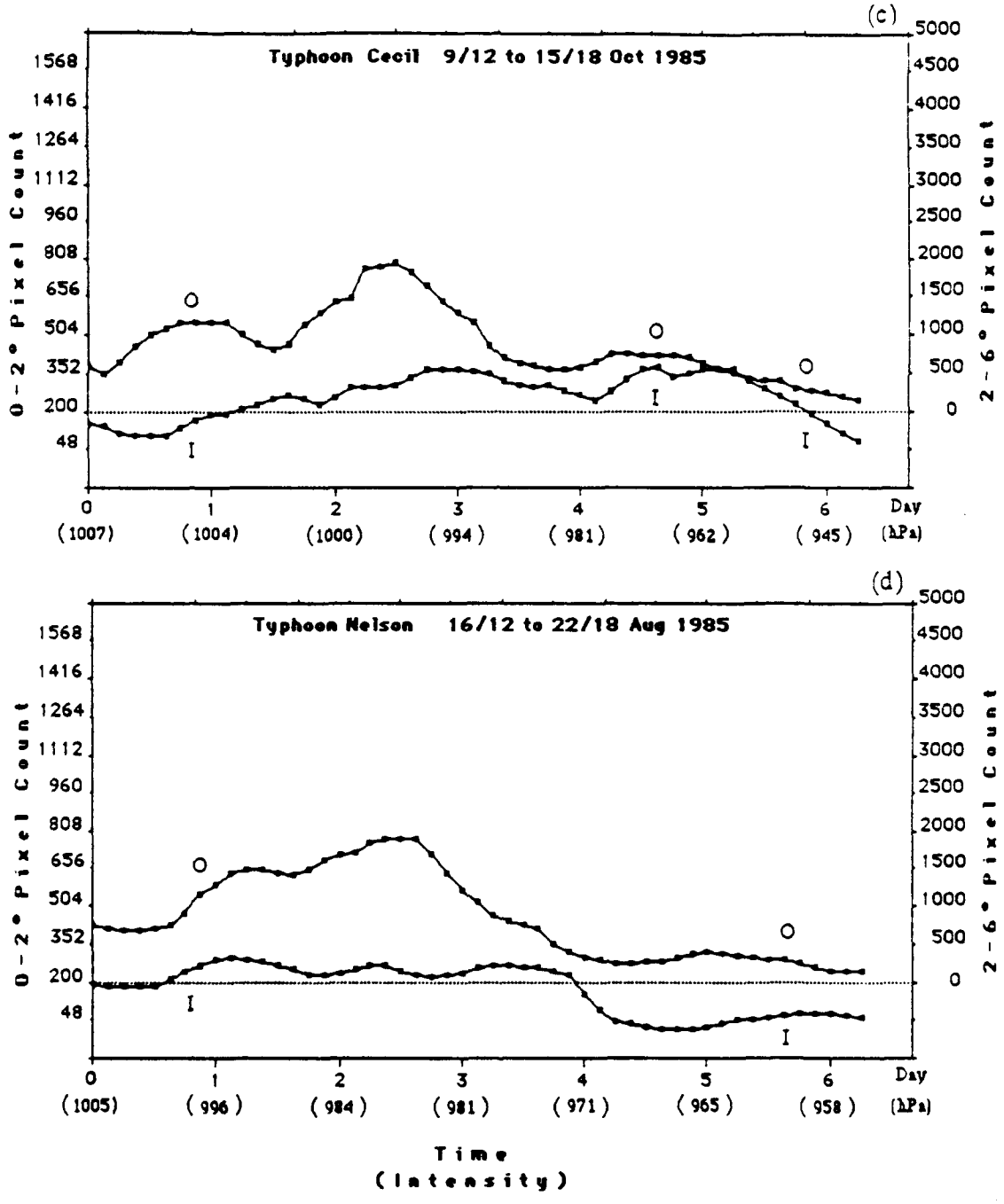

Figure 4.17: Continued.

intensify at that time. 4) Location. Storms in the South China Sea and in close proximity to large land masses were not expected to rapidly deepen. These climatological filters are based on the probabilities of the occurrence of rapid intensifiers expressed in Chapter 3. A total of 9 storms which had an intersection of the inner and outer convection plots were not included based on one or more negative climatological parameters listed above (Fig. 4.16).

This intersection technique for 10 km resolution GMS data is expressed visually as the 24 hour running means of the number of pixels colder than -75°C (full scale of 0 to 1520 pixels within 222 km of center), with a correction of -200 (200 inner radius pixels equal zero) and the number of pixels colder than -65°C on a modified scale of 0 to 5000 pixels (out of a total number of 12165 pixels within 222 to 666 km from the center).

Mathematically, this is expressed as

$$x = \frac{(3.29)(P_i - 200)}{P_o}$$

where P_i is the inner pixel count $\leq$ -75° and P_o is the outer pixel count $\leq$ -65°.

When x $\geq$ 1.0, this identifies an intersection of the relative amounts of convection. This is then used as a predictive signal to the operational forecaster that the concentration of deep convection near the cyclone center is sufficient to allow the central pressure to drop rapidly. Once this intersection occurs, as long as dx/dt is positive (i.e. the inner convection concentration is increasing), then the typhoon will continue to rapidly deepen. Once the 24 hour running mean plots begin to converge (dx/dt < 0), this means that the outer convection is increasing relative to the inner convection, the cyclone will not continue to intensify further. This is a predictive signal that the leveling off of the intensification process has started. This should also indicate Weatherford's "Phase 2", the point at which intensifiers begin to expand their outer radius winds, also known as its "strength" (Weatherford and Gray, 1988). Figure 4.19 is a diagram of an idealized time sequence of a rapid intensifier as indicated by the relative concentration of inner to outer deep convection and how it can be used to predict rapid intensification. This is important because this intersection technique can effectively replace the obsolete intersection method Dunnavan developed to predict rapid deepening.

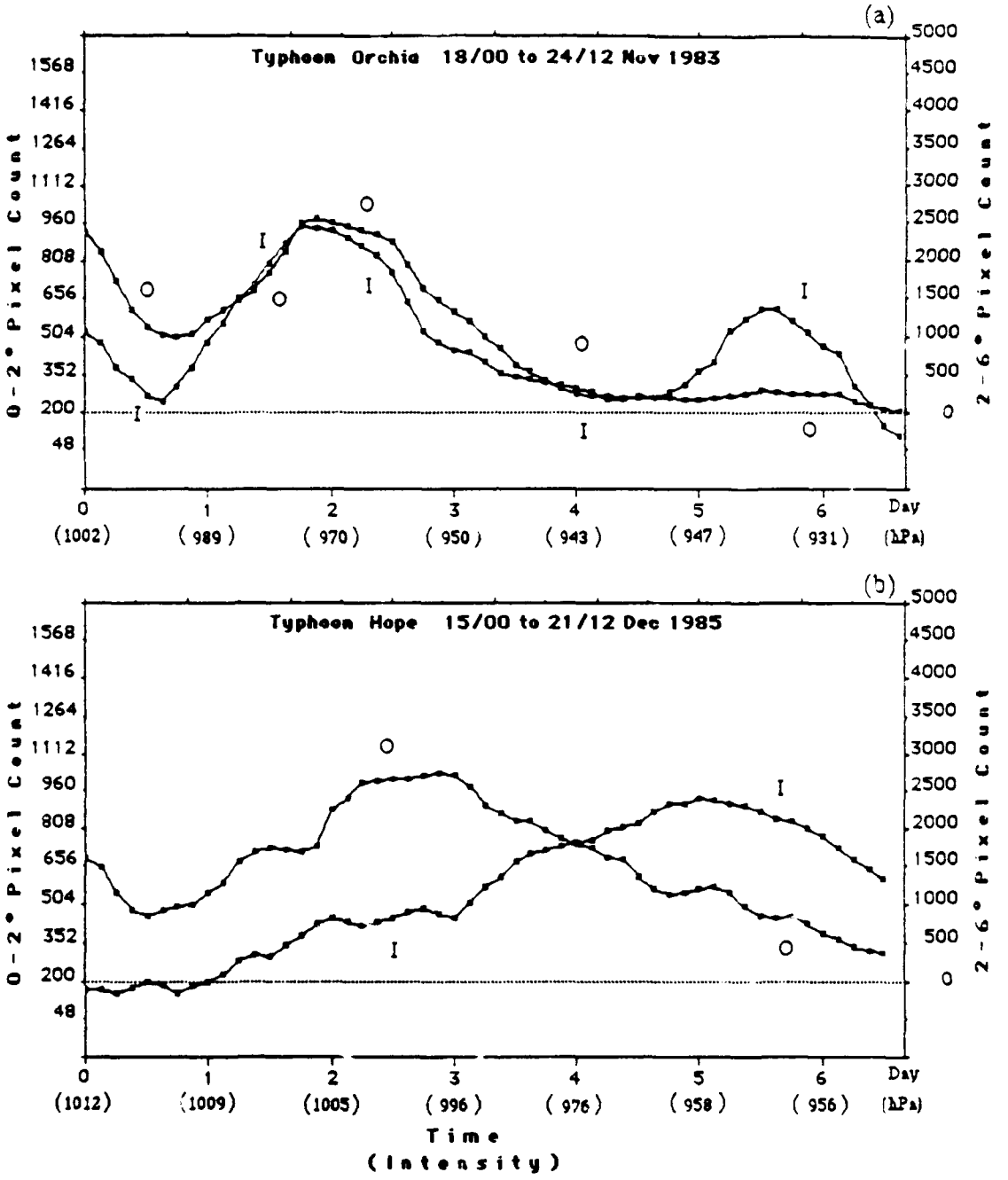

Figure 4.18: a to d: Depiction of four non-rapid intensification events in which an intersection of the inner and outer plots did not coincide with the onset of rapid intensity change, but were eliminated by climatological factors. Orchid's intersection occurred at 51 ms^{-1} (100 kt). Hope was an off season tropical cyclone. Joe and Percy developed in the South China Sea.

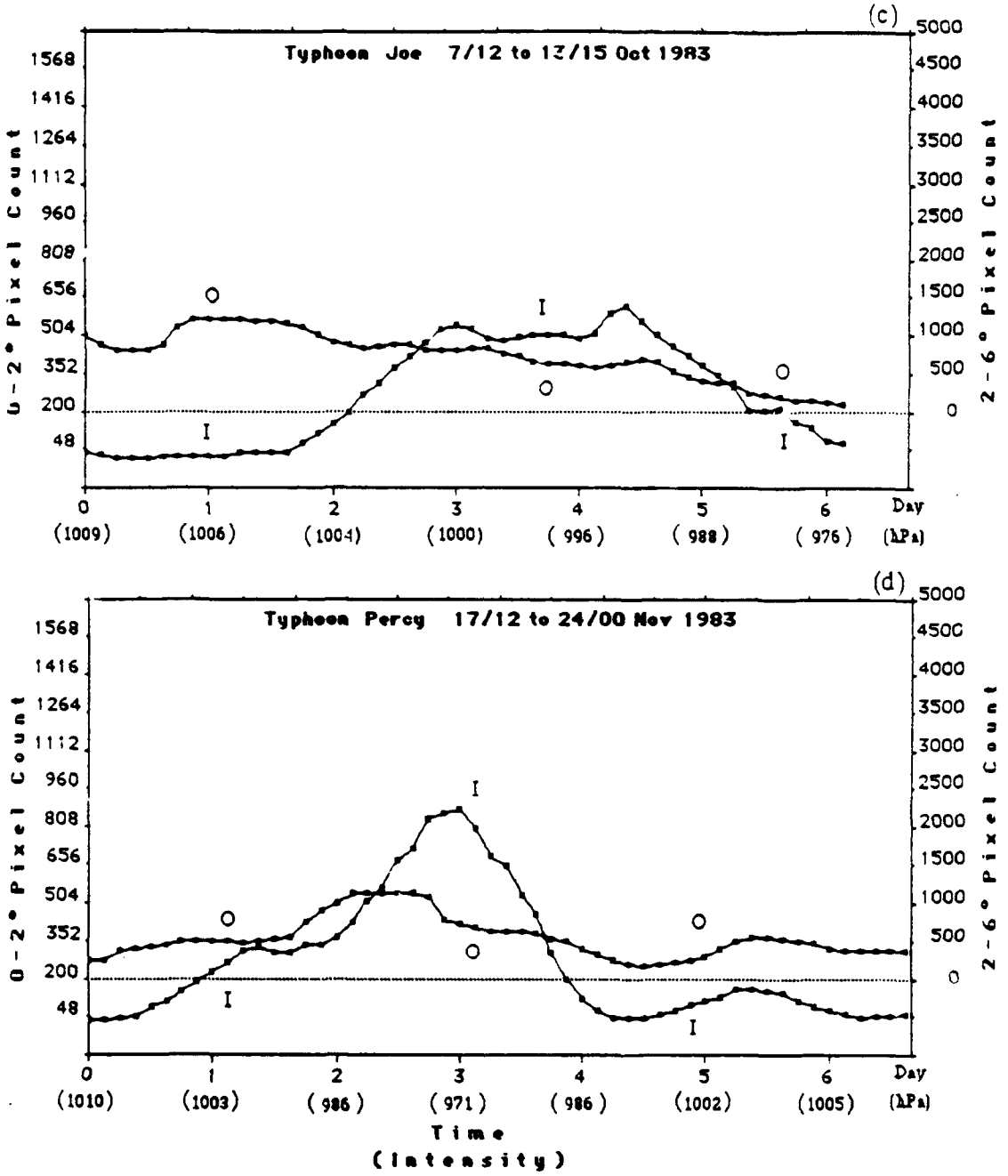

Figure 4.18: Continued.

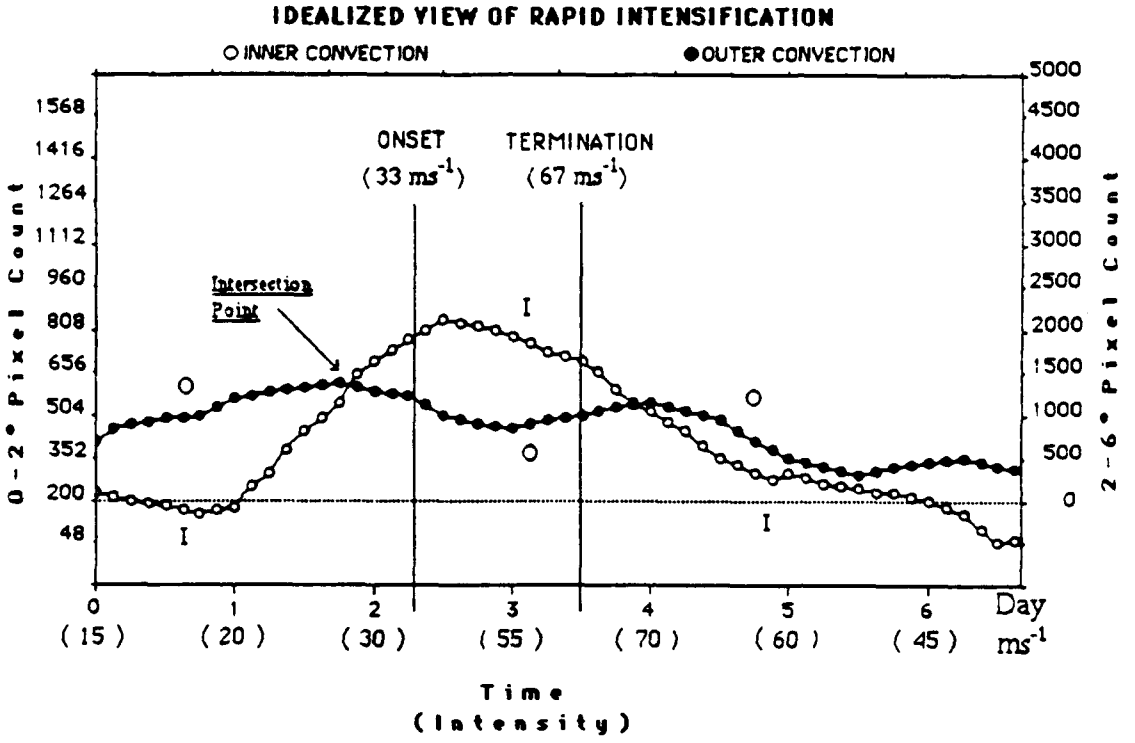

Figure 4.19: Illustration of an idealized rapid intensification event predicted by the intersection of the relative concentrations of inner (0 to 222 km) pixels colder than -75°C versus outer (223 to 666 km) pixels colder than -65°C. As long as all climatological parameters are favorable, the onset of rapid intensity change is very likely to occur within the next 12 hours.

Statistics of the success rate of this intersection technique are presented in Table 4.5. Of the 11 rapid intensifiers which occurred in the years 1983 to 1985, only three, Forrest (1983), Dinah (1984) and Agnes (1984) did not have an intersection take place near the onset of rapid intensification (Fig. 4.20). A possible explanation why Forrest and Agnes did not fit the pattern (i.e., a concentration of deep convection) is the fact that both had extremely small eyes. It is likely that rapid intensity change was primarily due to the contraction of eye size, not a concentration of deep convection towards the center. As evidence of this, the change of eye size over time versus intensity for both Forrest and Agnes are given in Table 4.6.

Table 4.5: Verification statistics of the method used to predict rapid intensification events discussed in section 4.8. There were a total of 70 named tropical cyclones in the NWPAC during the 1983-1985 seasons. Verification of TY Ed (84), TY Ike (84), TY Thad (84), TS Elsie (85), TY Fabian (85), and TY Gay (85) was not possible. "Eliminated by Climatology" means intersection events that occurred when climatological factors indicated the probability of rapid intensification was below .10. These were counted as successes.

1983 to 1985	TROPICAL CYCLONES	PIXEL PLOT INTERSECTIONS	ELIMINATED BY CLIMATOLOGY	SUCCESSFUL FORECASTS	%
RAPID INTENSIFIERS	10	7	0	7	70
NON-RAPID INTENSIFIERS	60	10	9	59	98
TOTAL	70	17	9	66	94

Satellite imagery of supertyphoon Forrest during rapid intensity change indicated the eye was so small that the satellite was unable to resolve warm temperatures in the eye. Thus the Dvorak data T-numbers for Forrest were significantly lower than the aircraft intensity measurements (Fig. 4.21).

In summary, the intersection technique presented in this section is a valuable tool to predict rapid intensification when used in conjunction with a good knowledge of the climatology of rapid intensifiers. It provides a standard of measurement to identify cyclones which are most likely to rapidly deepen as opposed to the majority of storms which do not rapidly intensify. It is not unexpected that such a relationship between the relative amounts of deep convection exists (Schubert and Hack, 1982), but it is of note that

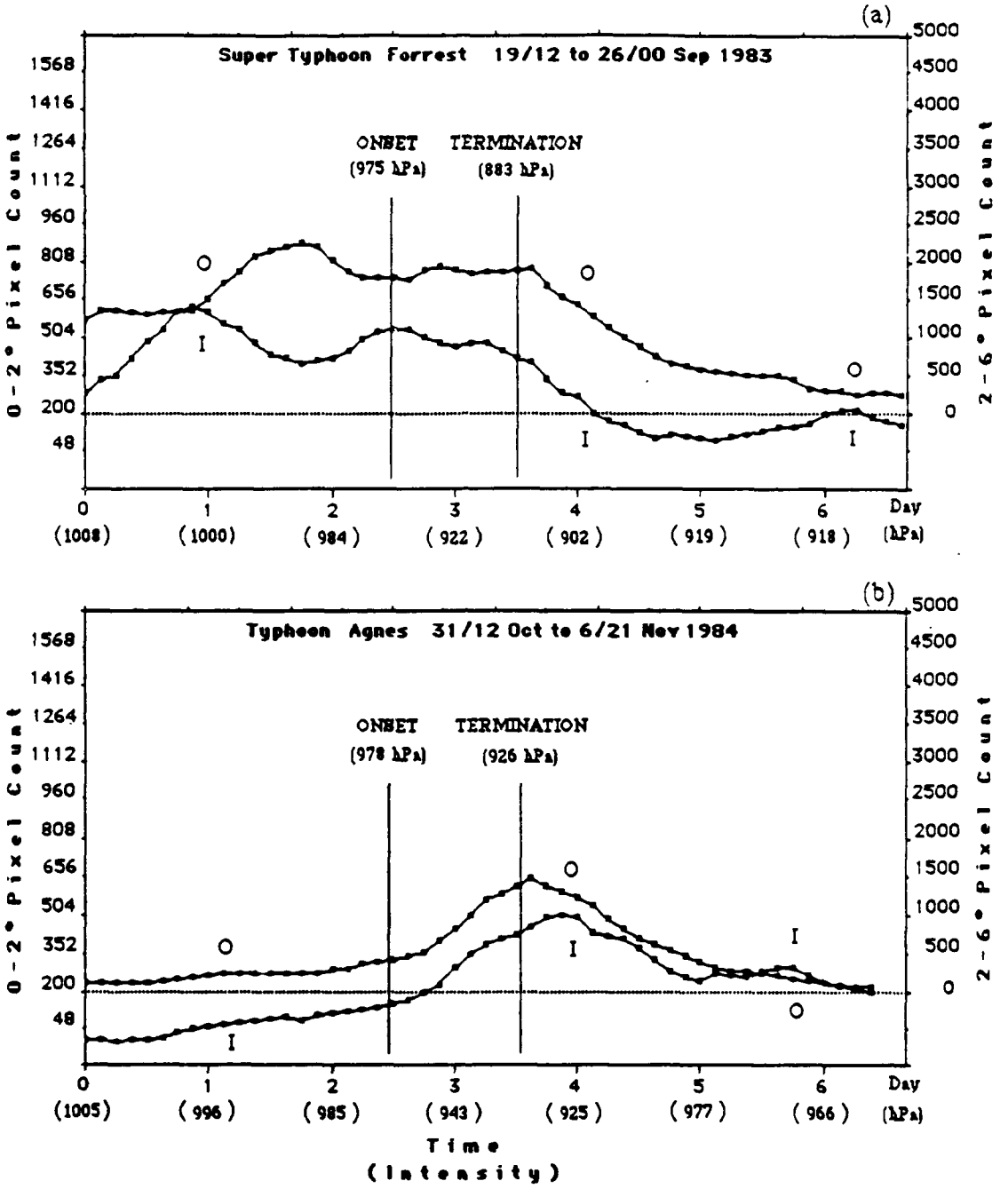

Figure 4.20: a to d: Depiction of the four non-verifying cases in which the relative concentrations of inner to outer deep convection either did not intersect close to the onset of rapid intensification (a, b, c), or did not rapidly deepen once intersection occurred (d). Both Forrest and Agnes experienced substantial contraction in eye size during rapid intensification. After intersection, Clara intensified at a non-rapid rate of 1.25 $hPa\ h^{-1}$.

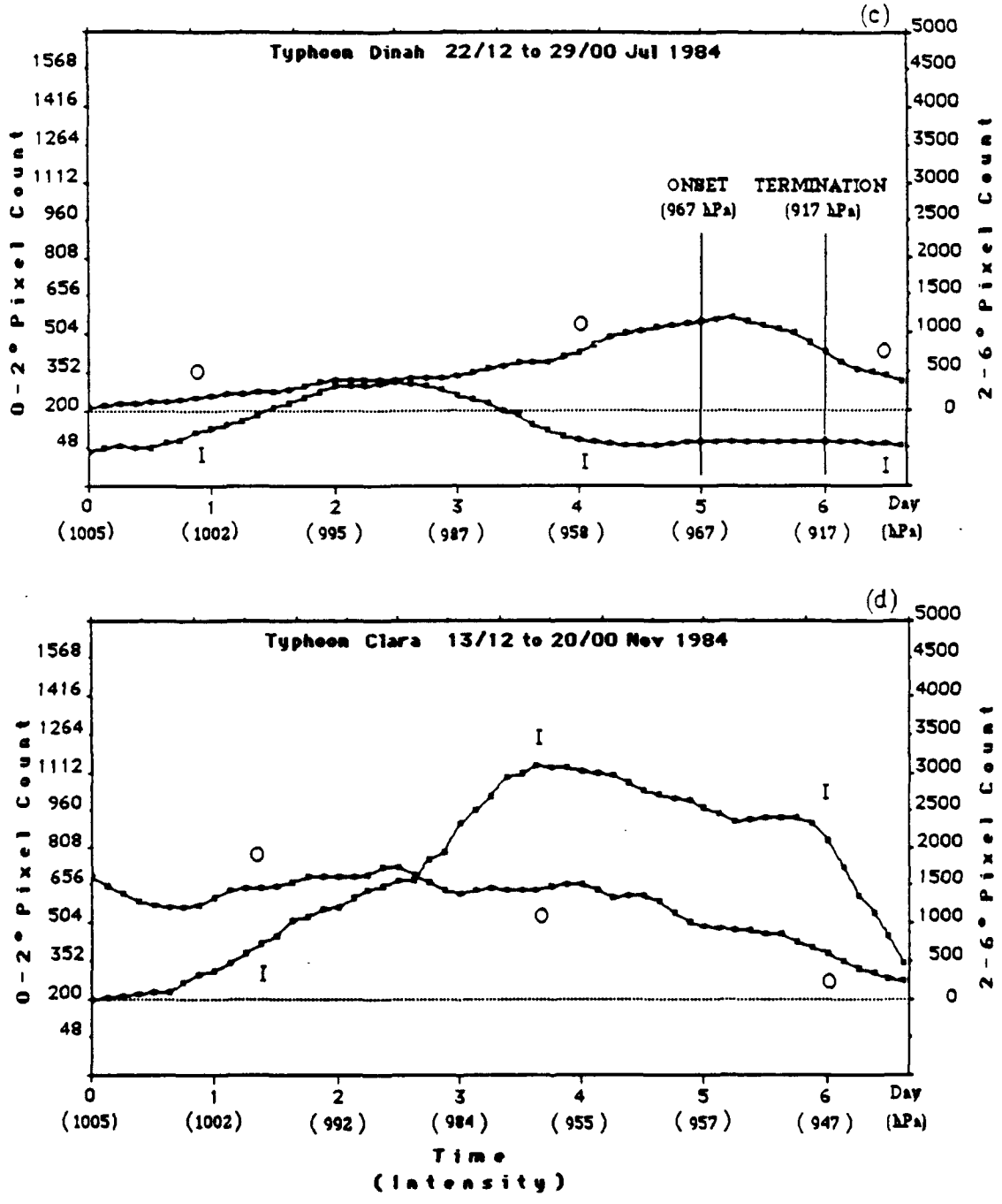

Figure 4.20: Continued.

Table 4.6: Relationship between rapid intensity change and eye size. Starting at the same initial intensity, the eye sizes of Forrest (Δ p = 107 hPa) and Agnes (Δ p = 61 hPa) decreased by factors of 7.0 and 3.3, respectively, during rapid intensification.

FORREST			AGNES		
TIME GMT	INTENSITY (hPa)	EYE RADIUS (km)	TIME GMT	INTENSITY (hPa)	EYE RADIUS (km)
092109	987	32.4	100209	987	18.5
092121	977	14.8	100221	980	13.9
092200	975	9.3	100223	978	9.3
092211	926	4.6	100306	956	9.3
092214	907	4.6	100308	951	9.3
092221	880	4.6	100320	937	7.4
092223	883	4.6	100323	926	5.6
092309	898	5.6	100409	932	9.3
092312	902	6.5	100411	925	7.4

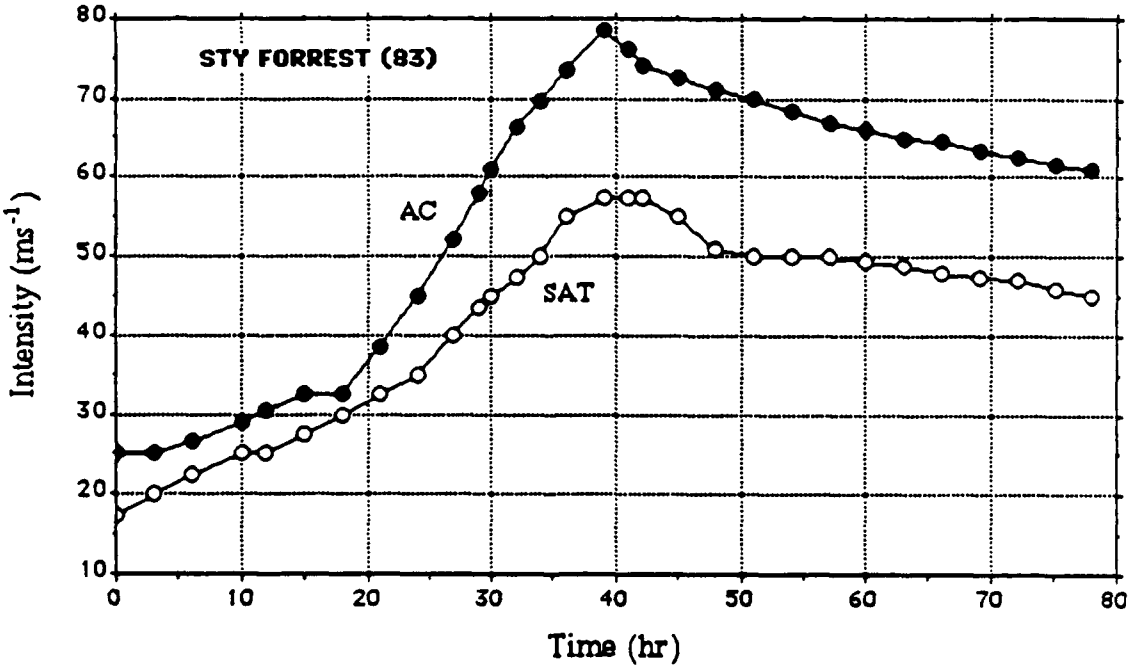

Figure 4.21: Illustration of the large intensity differences between satellite and aircraft measurements during rapid intensification caused, at least in part, by the unusually small eye of Super Typhoon Forrest.

prediction of one of the most difficult forecast situations in meteorology may indeed be possible.

Most rapid intensification events are not predicted. Even if, after further trials, this technique is found to predict rapid intensification with less skill than evidenced from the 1983-85 data, it will be an improvement over current forecast skill which is near zero. With the pixel counting technology currently available, it is possible to display the actual pixel counts for both 0-2° and 2-6°, and record the data to display running means of the data for various lengths of time. The author believes the values of -75°C for the inner radius of 0 to 222 km and -65°C for an outer radius of 222 to 666 km will provide the best results, but further refinements of this technique based on trial and error may give superior results. Application to other tropical cyclone basins would require calibration adjustments for satellite resolution and different inner/outer radial temperatures.

Chapter 5

OUTER CORE WIND STRENGTH AS A PREDICTOR OF RAPID INTENSITY CHANGE

5.1 Background

The relationship between outer core (1 to 2.5° radius) wind strength (OCS) and inner core minimum central pressure and maximum wind (intensity) was first discussed by Weatherford and Gray (1988). They found one of the most notable differences between intensifiers and fillers of the same MSLP was a stronger OCS of the filling storms.

Weatherford stated that, for the same central pressure, the stronger outer core of filling cyclones prevents low-level momentum from reaching the inner core due to inertial stability arguments and concluded that if the OCS value was > 20 ms^{-1}, the likelihood of continued rapid intensity change diminishes quickly. In Fig. 5.1, most of the rapid intensity changes of -20 mb or more correspond to an OCS value of 22 ms^{-1} or less. Rapid intensifiers as a group tended to have significantly lower OCS values for the same central pressure (Fig. 5.2). Weatherford and Gray did not establish a predictive link between OCS and rapid intensity change, so a re-examination of the reconnaissance data they used was conducted to determine if such a link existed.

5.2 Objective

The time and intensity aspects of the OCS data should reveal whether it is possible, given a certain MSLP and an OCS value, to predict rapid intensity change based on Figs. 5.1 and 5.2. To investigate Weatherford's data set, the aircraft mission data was stratified into several categories based on the criteria shown in Table 5.1. The objective was to correlate initial intensity and OCS with subsequent 12 and 24 hour intensity change (as measured by aircraft observations of MSLP and/or 700 hPa height).

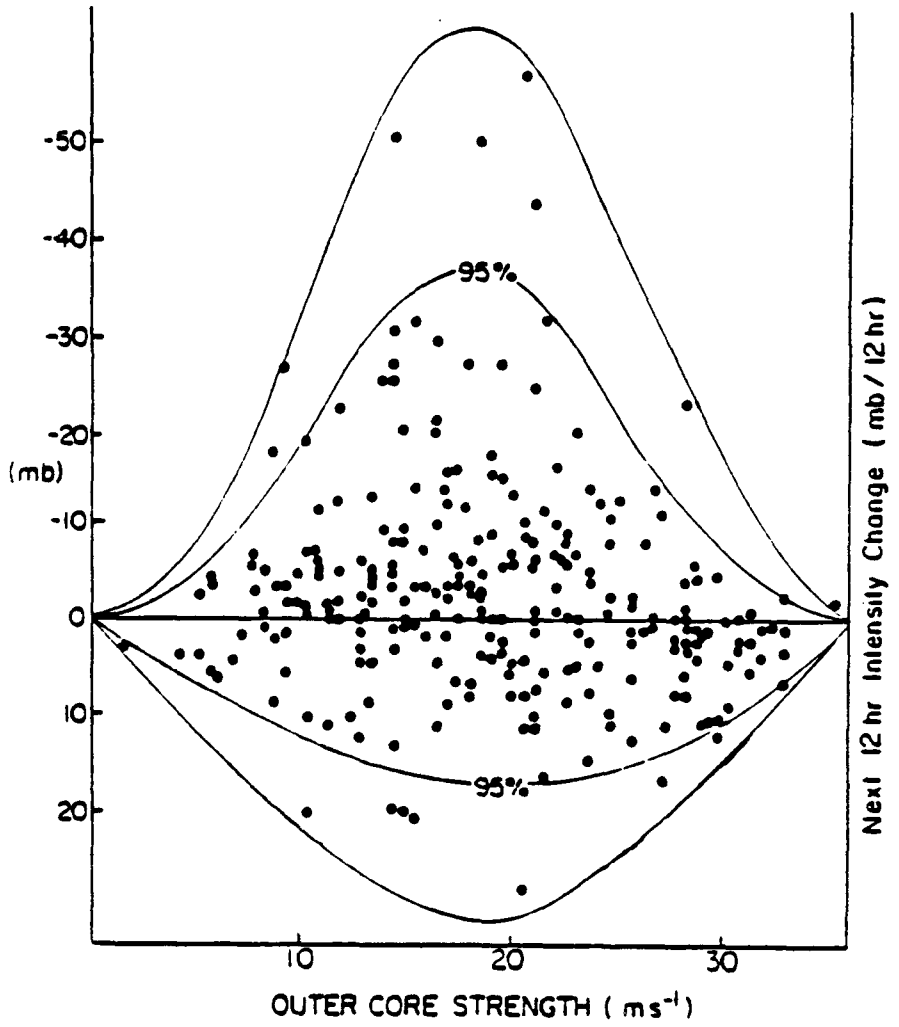

Figure 5.1: Scatter diagram showing the relationship between outer core strength (OCS) and intensity change during the subsequent twelve hours (Weatherford, 1989).

Table 5.1: Criteria used to determine intensification classifications.

CLASSIFICATION	CRITERIA
Rapid Intensifiers	**$\Delta p \leq$ -42 hPa next 24 hr**
Non-Rapid Intensifiers	**-10 hPa $\leq \Delta p \leq$ -41 hPa next 24 hr**
Non-Intensifiers	**+9 hPa $\leq \Delta p \leq$ -9 hPa next 24 hr**
Fillers	**$\Delta p \geq$ +10 hPa next 24 hr**

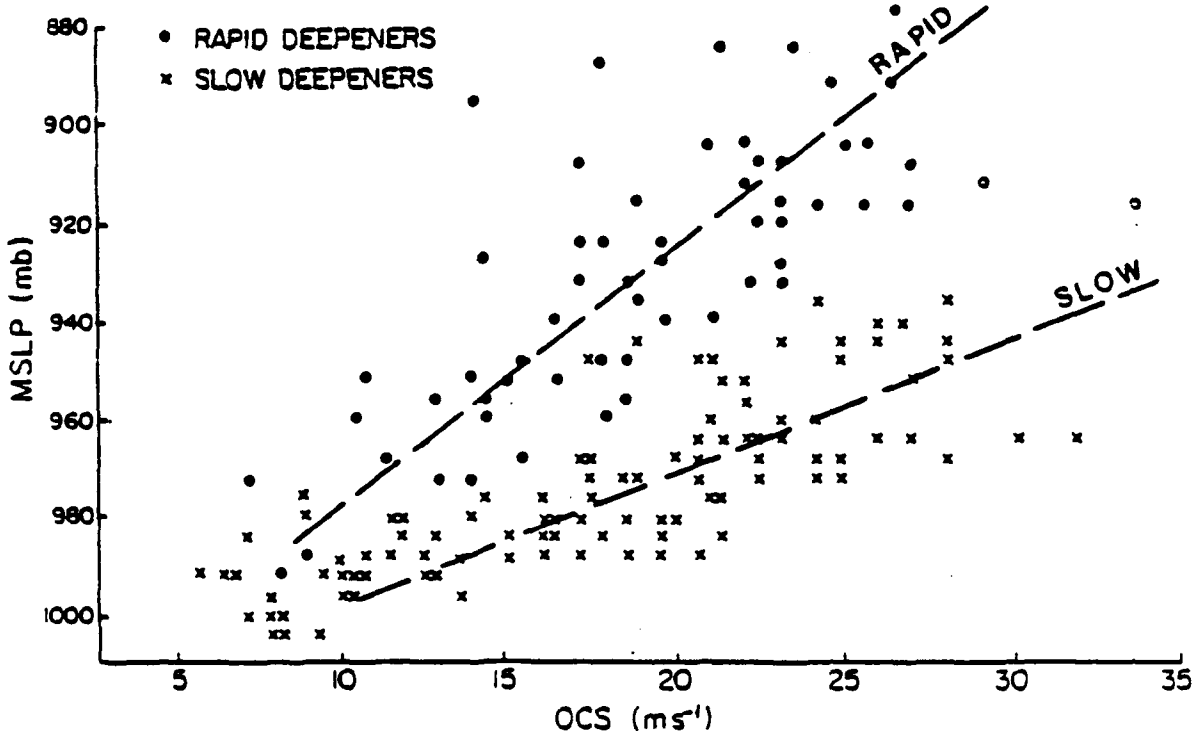

Figure 5.2: Scatter diagram of intensity vs. outer core strength for rapid ($\leq$ 42 hPa d^{-1}) deepeners and slow ($\leq$ 10 hPa d^{-1}) deepeners (Weatherford, 1989).

5.3 Methodology and Results

The following comparisons were made between stratification categories: 1) intensifiers versus fillers, 2) intensifiers versus non-intensifiers, 3) intensifiers versus rapid intensifiers, and 4) non-intensifiers versus rapid intensifiers. These comparisons of OCS values for a given central pressure are given in Fig. 5.3 (a to d).

Figure 5.3 clearly indicates that no predictive relationship exists between OCS and future intensity change. Assuming that only aerial reconnaissance data were available such that the central pressure and OCS were known, it would not be possible to accurately predict if a cyclone will rapidly intensify or even if it will intensify at all in the next 24 hours (see Fig. 5.3 c,d). Thus, the lack of measurement of outer core wind strength caused by the removal of reconnaissance aircraft in the Pacific appears to have not degraded any potential for intensity change forecasts based on OCS information, since no predictive signal appears to exist.

5.4 Summary

Further analysis of Weatherford's data showed that rapid intensifiers have rather ordinary outer core wind strength (OCS) for any given pressure prior to period 1. No distinctive differences in OCS were noted for rapid intensifiers prior to onset. The significant differences which Weatherford showed between rapid and slow deepeners were at the end of period 2 (Fig. 5.4).

It is found that rapid intensifiers have a distinctly different outer wind structure for a given central pressure and after rapid intensity change, but not before. The average rapid intensifier has a large ($\approx$100%) increase in intensity as measured by inner core maximum winds, but only a small ($\approx$30%) increase in strength as measured by outer core winds (see Fig. 4.13). The OCS transitions from normal strength to one that is relatively weak for a given central pressure. During rapid intensification, a contraction of the maximum wind field likely occurs, so that most of the energetics of the tropical cyclone can be concentrated as close as possible to the circulation center.

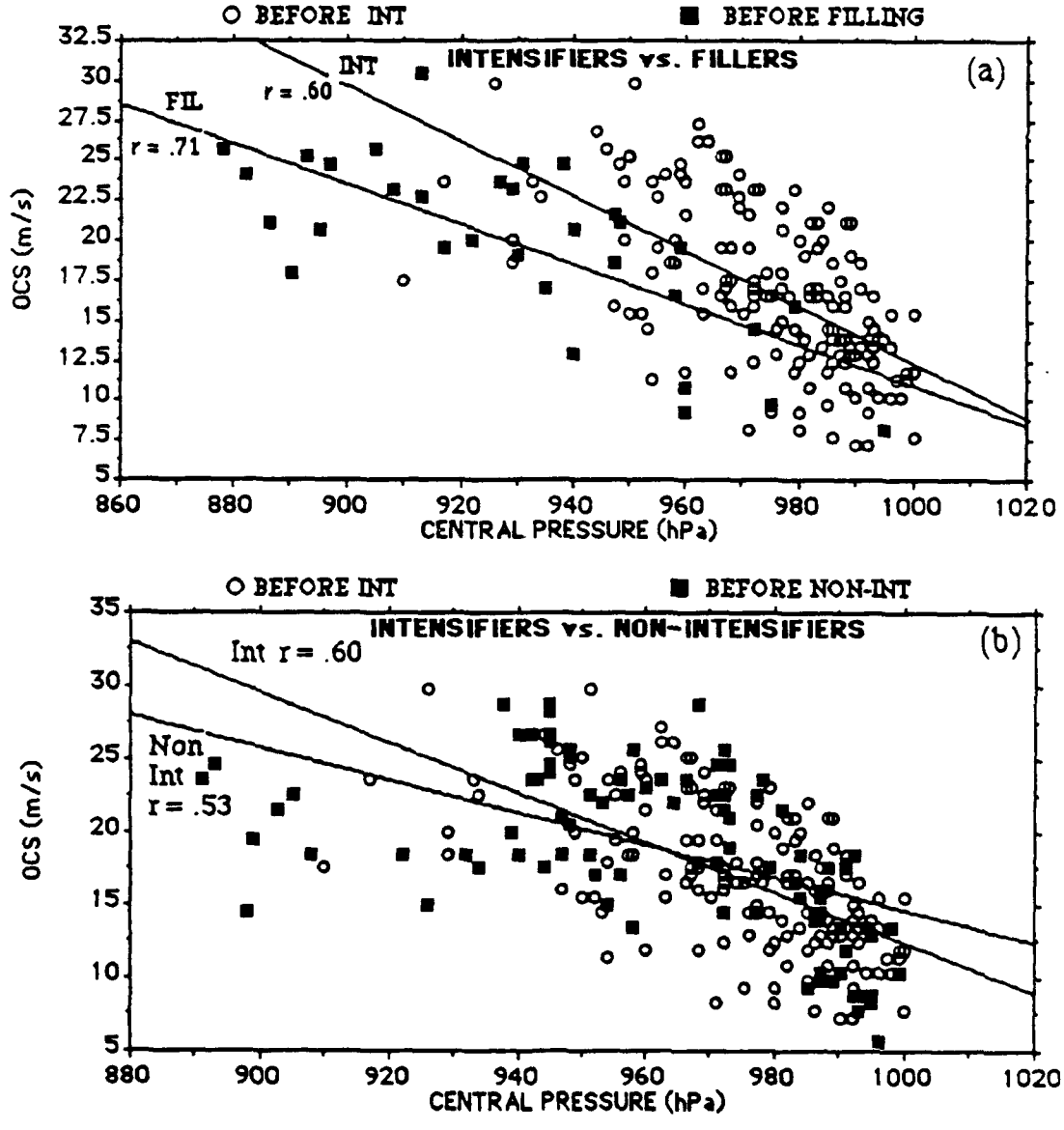

Figure 5.3: Representation of measured outer core strength (OCS) and MSLP for (a) before intensification versus before filling, (b) before intensification versus before non-intensification, (c) before intensification versus before rapid intensification, (d) before non-intensification versus before rapid intensification. The best fit regression lines and their correlation values are also shown.

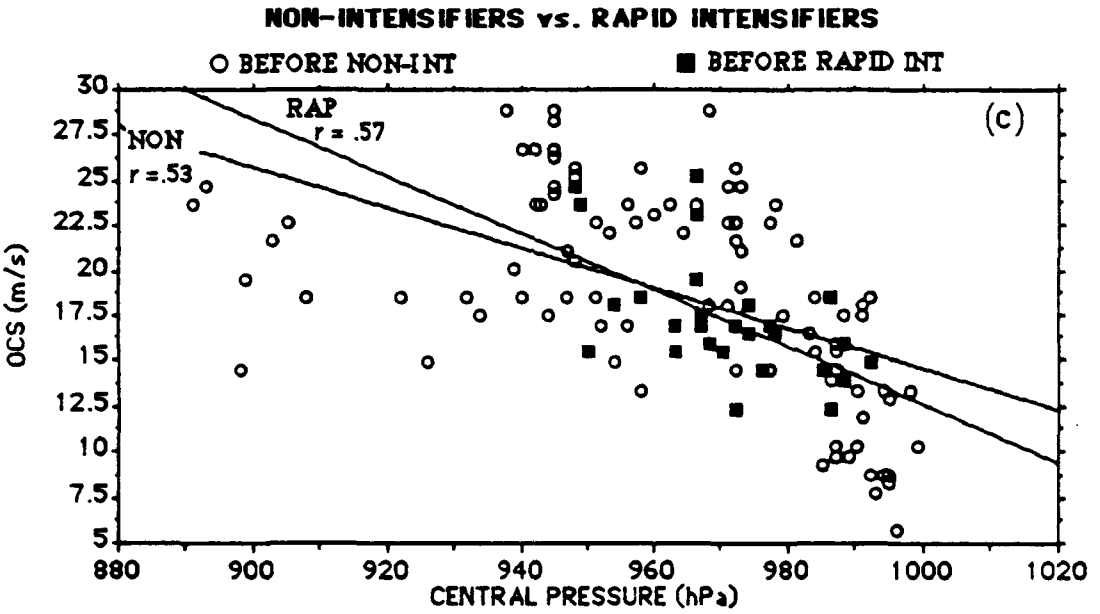

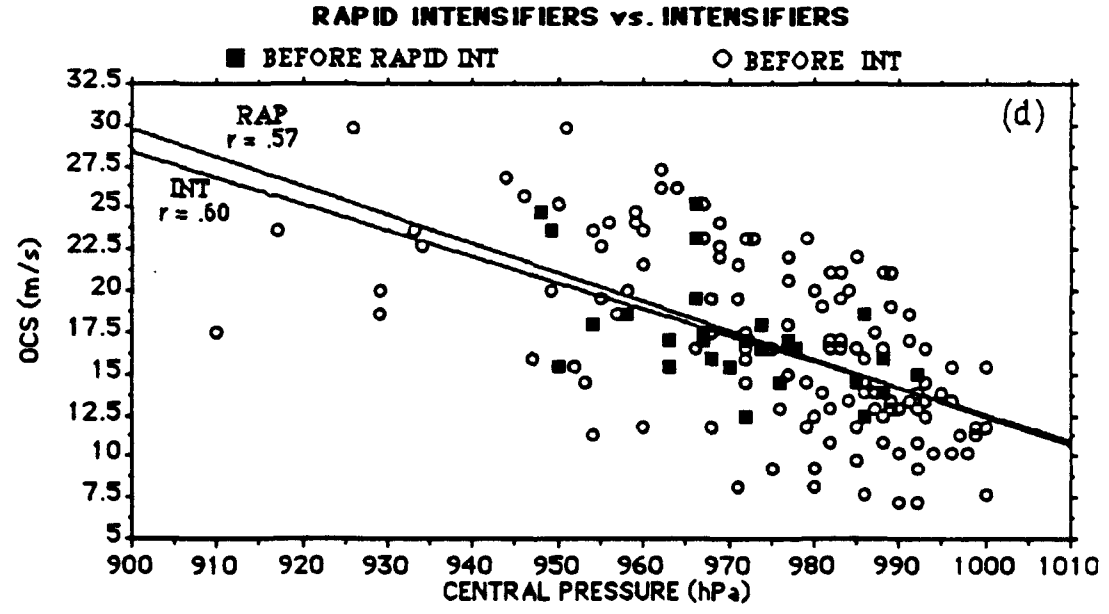

Figure 5.3: Continued.

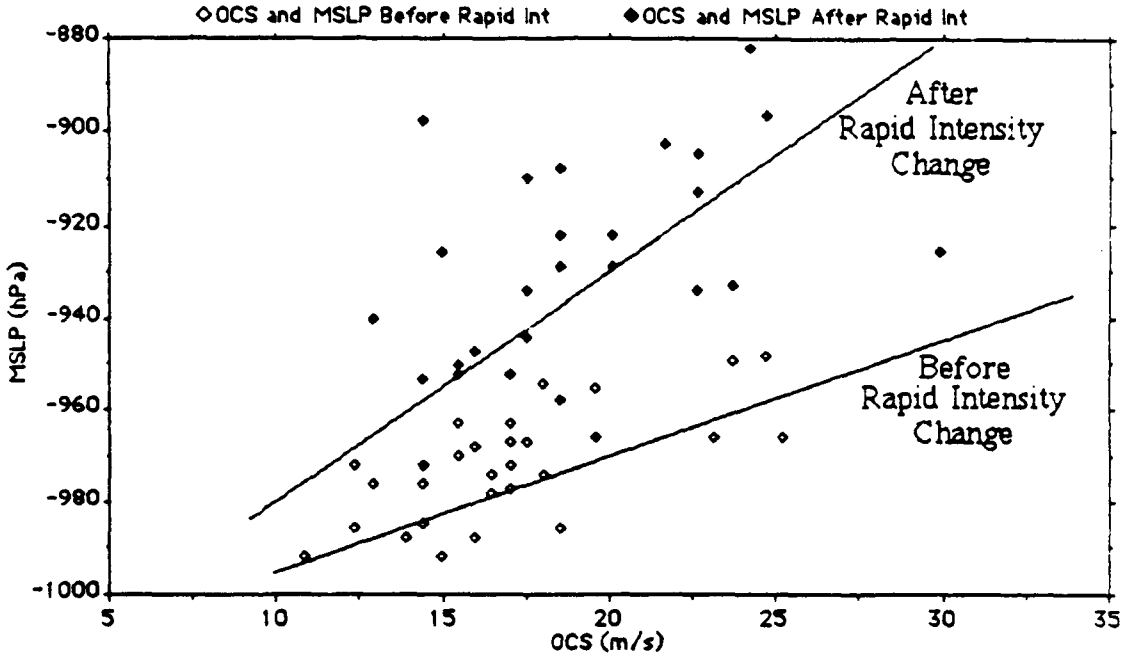

Figure 5.4: Scatter diagram of OCS and MSLP values for rapid intensifiers before and after the onset of rapid deepening. B represents the centroid of the data points for both before rapid intensification and non-rapid intensification. R is the centroid of data points after rapid deepening. NR is the centroid after non-rapid intensification and is shown for comparison. The regression lines shown closely approximate the regression lines for rapid and slow deepeners shown in Fig. 5.2.

A most unusual aspect of Weatherford's research is that immediately after rapid intensification, the OCS is relatively unchanged from its previous value before the onset of rapid deepening (Fig. 5.5b). The values of OCS and central pressure before a rapid intensification event are approximately equal to OCS and central pressure values prior to non-rapid intensification. After rapid and non-rapid intensification, the central pressure values are considerably different but the OCS values are nearly the same (see Fig. 5.5). It may seem surprising to some that rapid intensifiers are not initially characterized by relatively weak outer winds during the tropical storm and minimal typhoon stages which would then strengthen as intensification proceeded. It is possible to have strong outer winds as a tropical storm just before rapid intensification, but this is not usually the case. As long as inflow proceeds to near the center, rapid deepening can still occur.

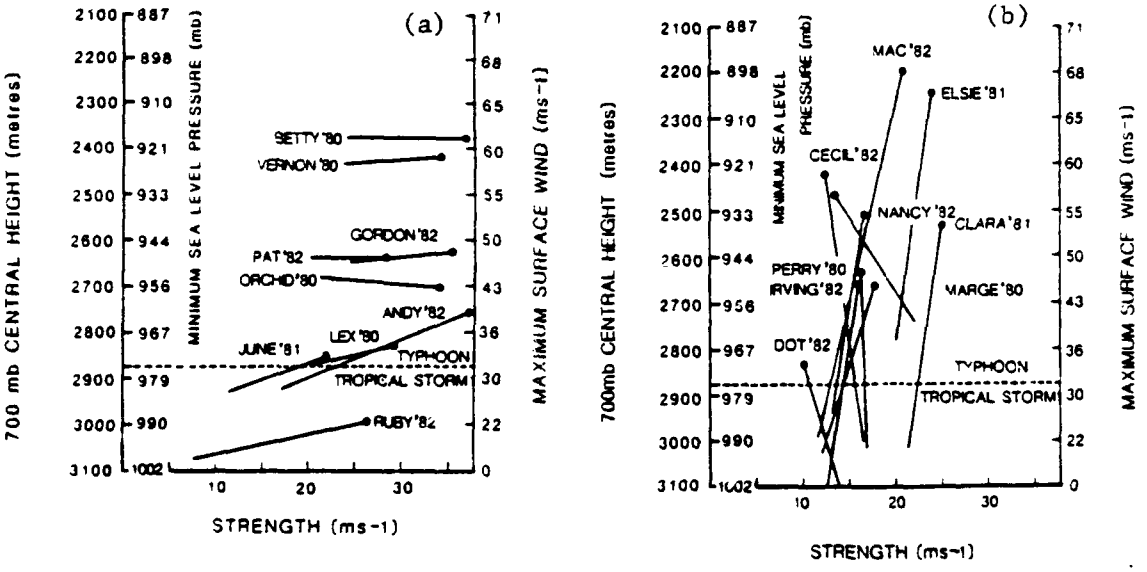

Figure 5.5: Depiction of strength and intensity changes observed during non-rapid intensification (a) and rapid intensification (b) (from Weatherford and Gray, 1988).

Chapter 6

THEORETICAL ASPECTS OF RAPID INTENSITY CHANGE

6.1 Vertical Momentum Transport in a Low Shear Environment

One of the critical factors for intensification of tropical cyclones is vertical alignment between the lower inflow layers and the upper outflow layers. The amount of upper level ventilation or "blowthrough" is believed to be directly related to maximum intensity (Zehr, 1976; Lunney, 1987). Merrill (1988) showed that the outflow characteristics of intensifying hurricanes typically did not have unidirectional flow (ie., ventilation) over their center (Fig. 6.1).

In an environment of low vertical shear, a strong cyclonic circulation can be developed at the inner core all the way up to the tropopause. The relationship between intensity and cyclonic winds aloft will be explained in the next section. An upper level cyclonic circulation exists, in theory, due to the upward transport of cyclonic momentum by strong vertical motion in the inner core deep convection. The few upper tropospheric research flights which were conducted in the late 1950's and early 1960's revealed small, intense, cyclonic vortices close to their centers. Senn *et al.* (1960) compared aircraft measurements of wind velocity versus radar echoes of cloud motion in the upper levels of Hurricane Daisy (1958) and found evidence of cyclonic momentum being transported by the updrafts at the 250 hPa level (Fig. 6.2). Note that 65 kt (33 ms^{-1}) cyclonic winds were measured in the eyewall less than 19 km from the center of Daisy. Even larger values of radar echo velocities (up to 57 ms^{-1}) were reported outside the eyewall.

6.2 Thermal Considerations of Intense Upper Level Cyclones

Assuming environmental conditions of low vertical wind shear near the cyclone center, the vertical updrafts in the inner core region are presumed to transport cyclonic

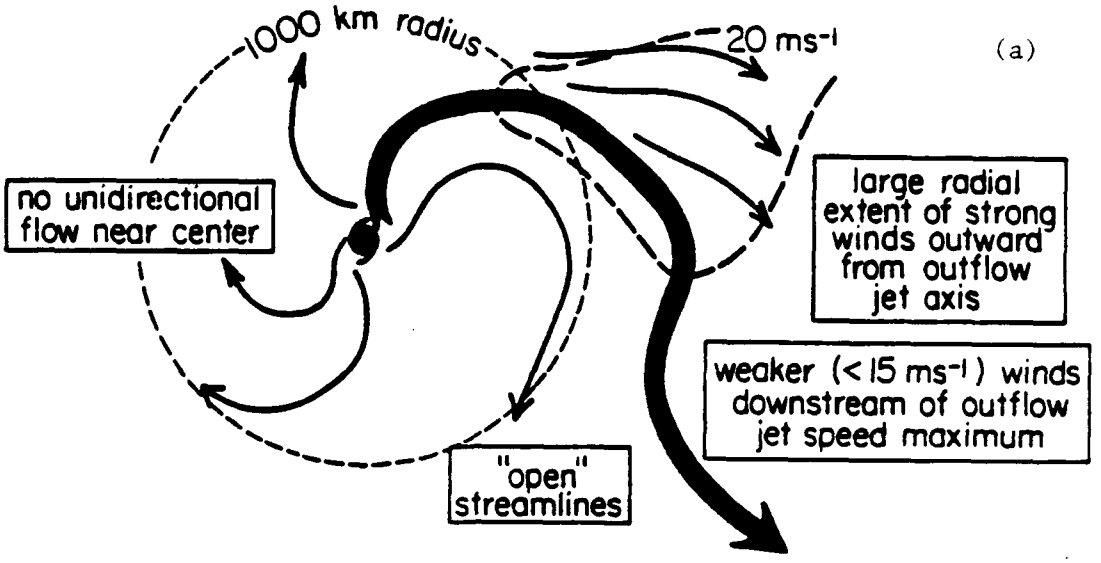

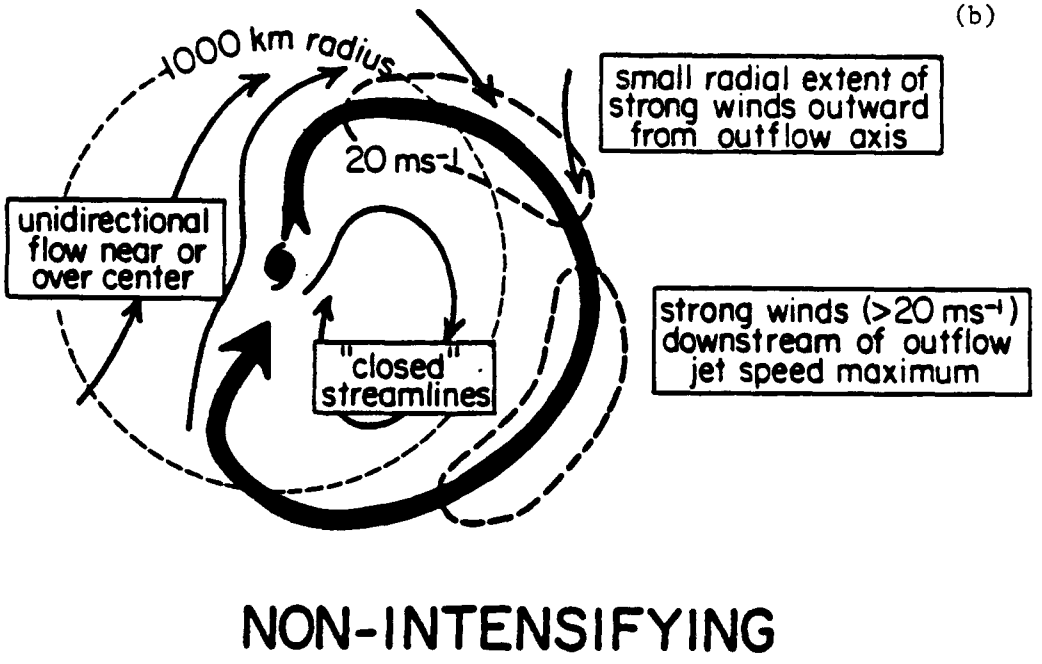

Figure 6.1: Summary of outflow and ventilation differences between intensifying and non-intensifying Atlantic hurricanes (Merrill,1988).

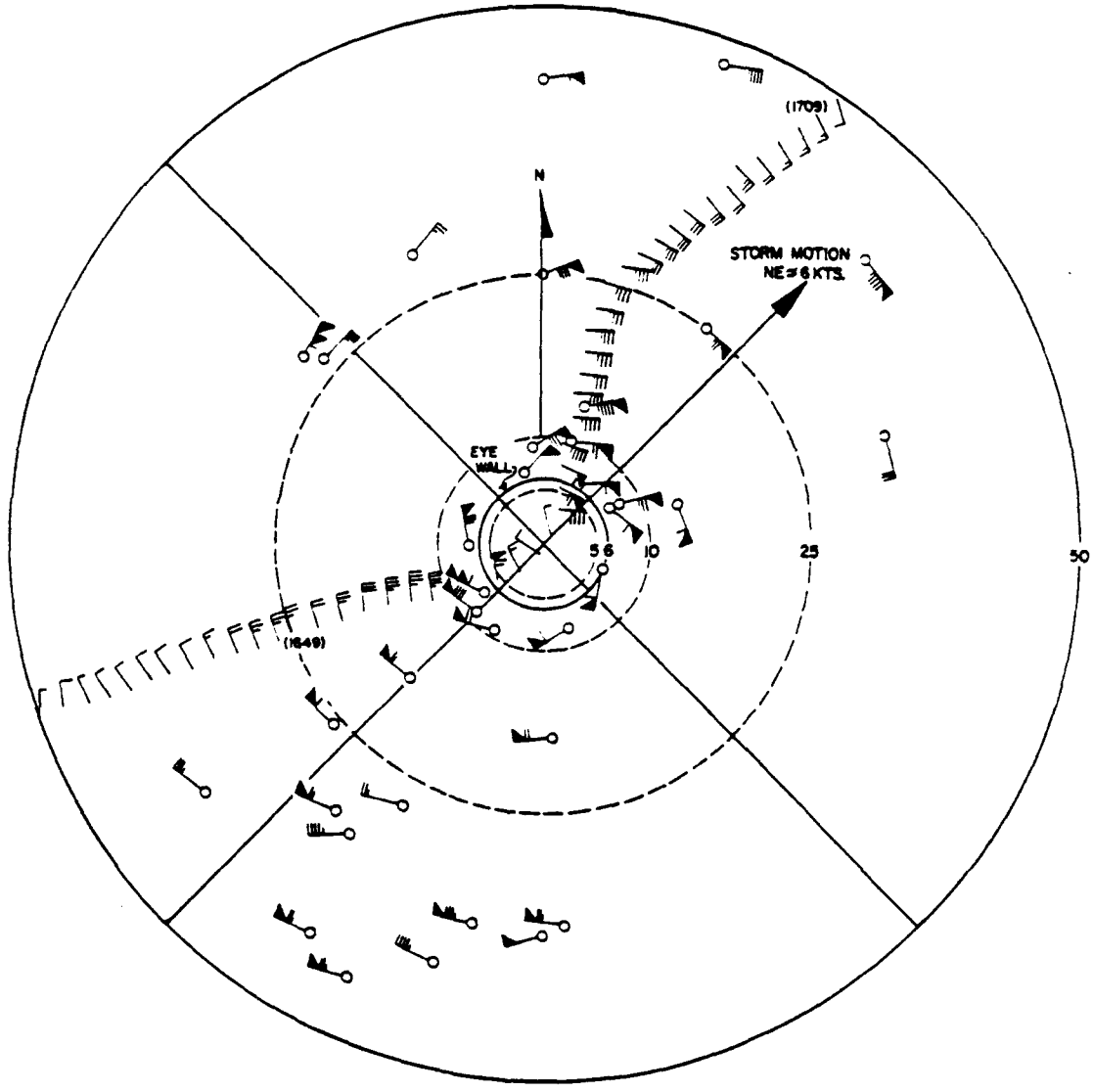

Figure 6.2: Measured inner core flight level winds and radar echo velocities at 35,000 ft (10.7 km) of Hurricane Daisy. An intense inner core cyclonic circulation is still present at the 250 hPa level. Intensity at the time of observation was 942 hPa, which is equivalent to a maximum sustained wind of about 62 ms^{-1} (Gray, 1989).

momentum to the upper level circulation. If there is a lack of unidirectional flow across the tropical cyclone across the center of the upper level vortex, the strength and vertical extent of the updrafts should directly act to increase the cyclone's inner core upper level cyclonic circulation. As observed from satellite, rapid intensifiers typically have very high, cold cloud tops that often penetrate into the stratosphere. This would indicate that the vertical velocities of updrafts in rapid intensifiers should be greater than non-rapid intensifiers. This would imply, from the preceding arguments, that rapid intensifiers should have cyclonic circulations that extend through the entire depth of the troposphere, as indicated by profile a in Fig. 6.3. In theory, the vertical shear of tangential winds up to 150 hPa ($\partial V_\theta / \partial p$) would be relatively small in comparison to the vertical shear typical of most intensifying and stead-state typhoons (profile b). Assuming that the wind velocity goes to zero near the tropopause, most of the vertical wind shear would be limited to near the tropopause level.

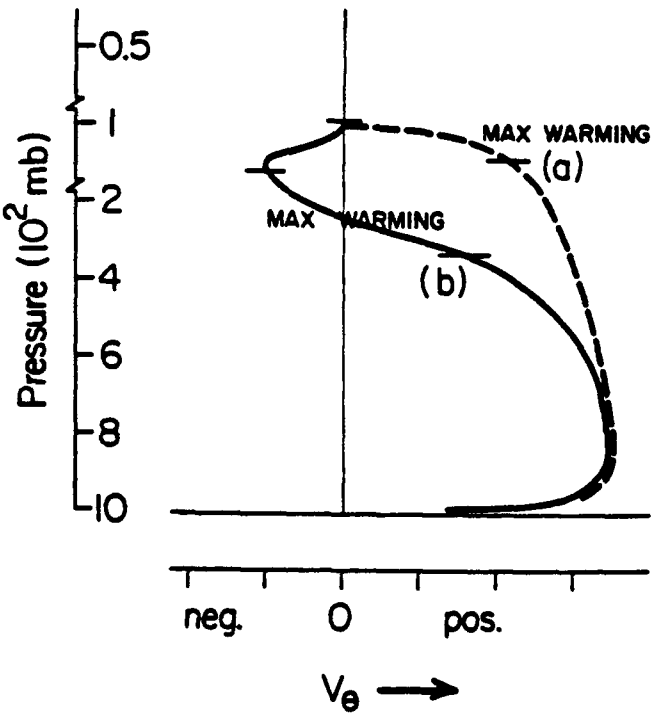

Figure 6.3: Idealized vertical tangential wind profiles of (b) vertical shear usually found in intensifying tropical cyclones and (a) vertical shear placed higher in the atmosphere due to upward momentum transport (Chen and Gray, 1985).

A concentration of tangential wind shear at the top of the troposphere has important thermal consequences. The thermal wind equation in cylindrical coordinates is given by,

$$\left(f + \frac{2V_\theta}{r}\right)\frac{\partial V_\theta}{\partial p} = \frac{-R}{p}\frac{\partial T}{\partial r}\Big|_p - \frac{\partial F_r}{\partial p} + \frac{\partial}{\partial p}\left(\frac{dV_r}{dt}\right) \tag{6.1}$$

where f is the coriolis parameter, V_θ the tangential wind velocity, r the radius from a fixed center, R is the gas constant, ρ the density, T the virtual temperature, F_r equals the radial component of friction and V_r is the radial wind velocity.

In the upper atmosphere, the last two terms are small in comparison to the others in Eq. 6.1, which gives the following thermal wind balance:

$$\left(f + \frac{2V_\theta}{r}\right)\frac{\partial V_\theta}{\partial p} = \frac{-R}{p}\frac{\partial T}{\partial r}\Big|_p \tag{6.2}$$

(1) (2) (3)

According to Gray (1967), the first term is an "inertial parameter", W_r, the second term a vertical wind shear parameter, S, and the third expresses the horizontal baroclinicity, B. For simplicity, Gray uses the equation

$$W_r S = B \tag{6.3}$$

Figure 6.4 is an illustration of the thermal effects of intensification for two different types of tangential wind profiles. We assume that both plots of tangential wind are initially the same (curve 0), but in the first case (curve 1) the increase in tangential wind occurs in the lower troposphere. This is considered by many authors to be the most common intensification process. In the other intensification process (curve 2), the majority of the increase in tangential wind is concentrated in the upper troposphere. The vertical wind shear parameter, $\partial V_\theta/\partial p$, for curve 2 is much higher in the atmosphere than it is for curve 1. In order to maintain thermal wind balance in the region of maximum vertical wind shear, increases in vertical shear (S) would require a decrease of the inertial parameter (W_r) or an increase the horizontal baroclinicity (B). A decrease in W_r would mean a reduction in the tangential component of the wind or an increase in the size of the eye

since f is assumed constant. Weaker winds and larger eye size are not characteristic of intensifying tropical cyclones, hence thermal wind balance in the region of maximum vertical wind shear is most likely achieved by an increase in horizontal baroclinicity. Shea and Gray (1973) demonstrated that the most intense hurricanes have large temperature and pressure gradients across the eyewall and minimum vertical wind shear at the radius of maximum wind (Fig. 6.5). Upper level reconnaissance flights into the inner core of Atlantic hurricanes (Gray and Shea, 1976) showed that cyclones with the lowest surface pressure tended to be warmer than average in the upper troposphere eye region, but also were cooler than average in the upper level wall cloud.

Merrill (1988) found intensifying NWPAC tropical cyclones were cooler than non-intensifiers at larger radii (Fig. 6.6). These data demonstrate that baroclinicity is the key factor to explain why deep cumulus convection can be maintained in the inner core region as the eye undergoes strong warming (see Fig. 6.7).

Decreases of horizontal baroclinicity below the level of maximum shear (due to reduction of $\frac{\partial V}{\partial p}$ from curve 0 to curve 2 in Fig. 6.4) most likely result in subsidence warming in the eye while the region of most intense convection in the eyewall remains relatively cool.

If the vertical wind shear is concentrated as high as possible in the atmosphere (as in curve 2 of Fig. 6.4), warming of the inner core outside the subsidence eye region will also be concentrated near the tropopause level, as indicated by the temperature deviation profiles of Fig. 6.4. In a more common type of intensification (curve 0 to curve 1 in Fig. 6.4) where the bulk of the tangential wind increase is in the lower troposphere, the inner core warming outside the eye is located in the middle troposphere where the vertical wind shear is the greatest. In general, deep convection acts to warm and stabilize the upper troposphere of tropical cyclones, which over time tends to reduce further deep convection. Rapid intensifiers are believed to limit the stabilizing effects of deep convection by concentrating the vertical shear of tangential wind near the tropopause so that warming is as high in the atmosphere and close to the center as possible.

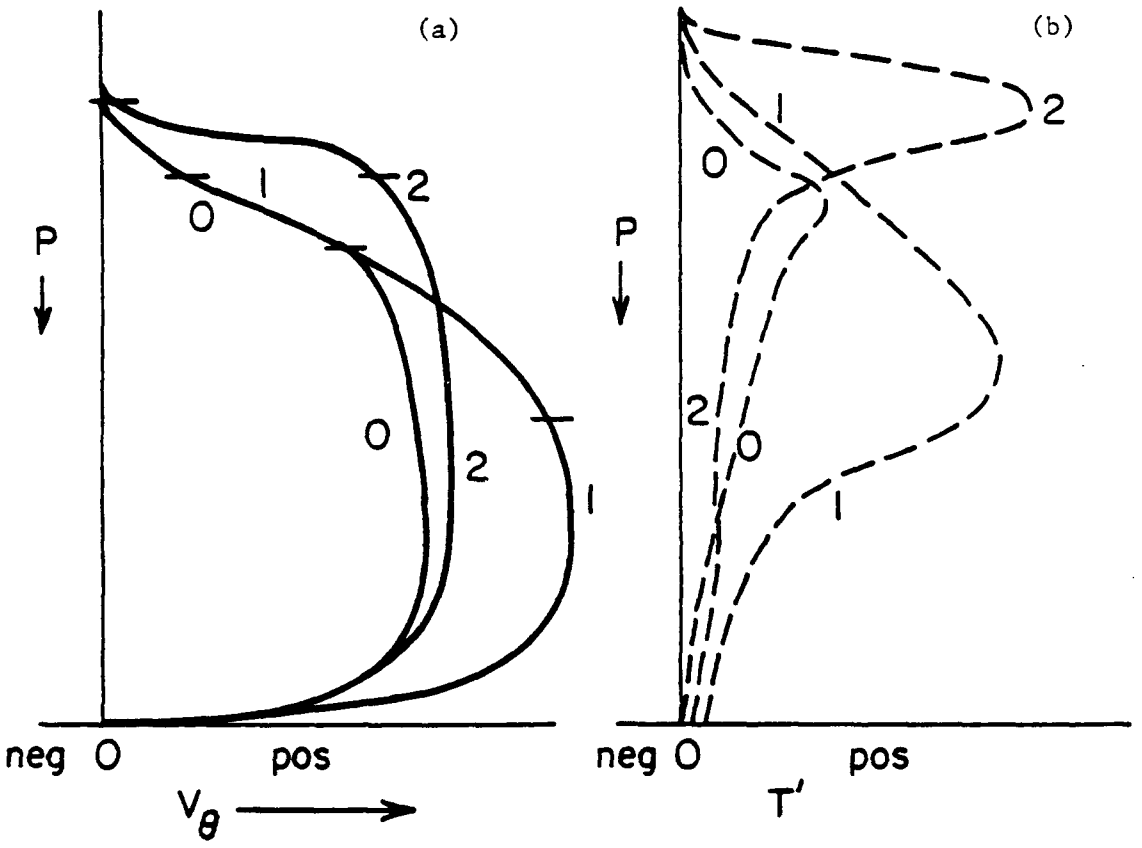

Figure 6.4: Vertical profiles of tangential wind (V_θ) and temperature anomalies (T') for two idealized typhoons initially with the same vertical profiles of wind and temperature (curve 0). Curve 1 represents a spin up of the low level cyclonic circulation during intensification. Curve 2 represents a spin up of the upper level vortex during intensification. The temperature anomalies corresponding to each wind profile needed for thermal wind balance are shown on the right.

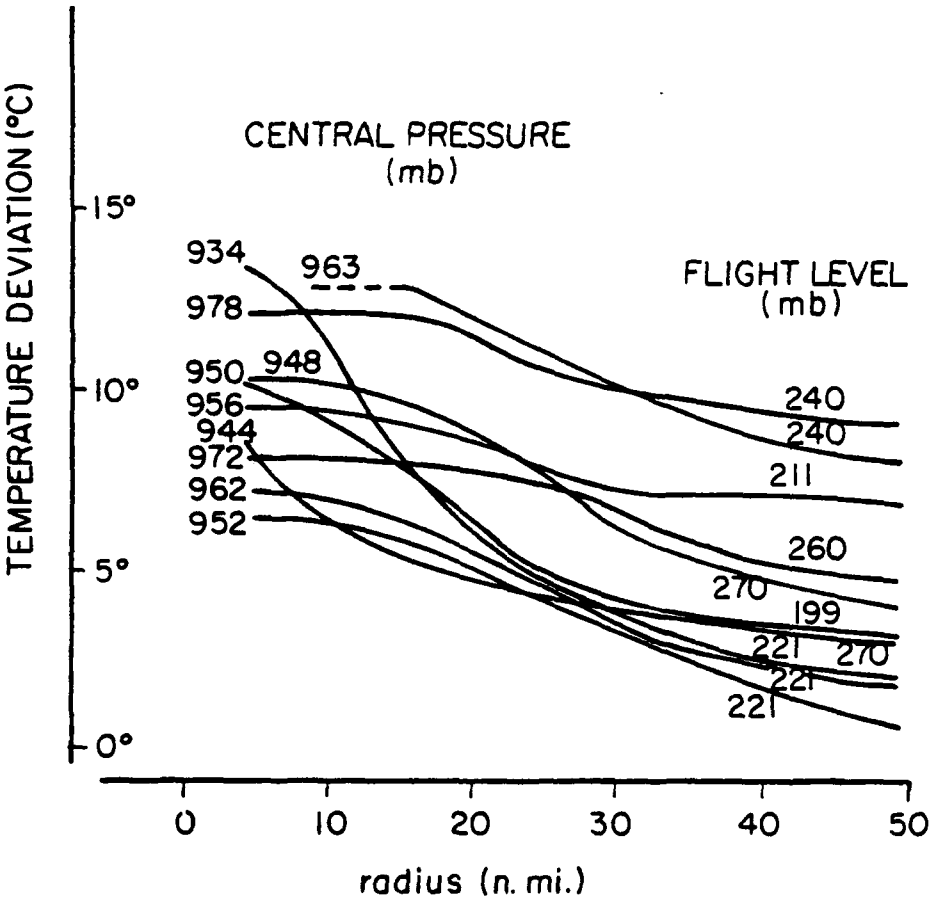

Figure 6.5: Inner core upper tropospheric temperature anomaly from the mean summertime tropical atmosphere as measured by National Hurricane Research Laboratory upper level reconnaissance flights (from Gray and Shea, 1976).

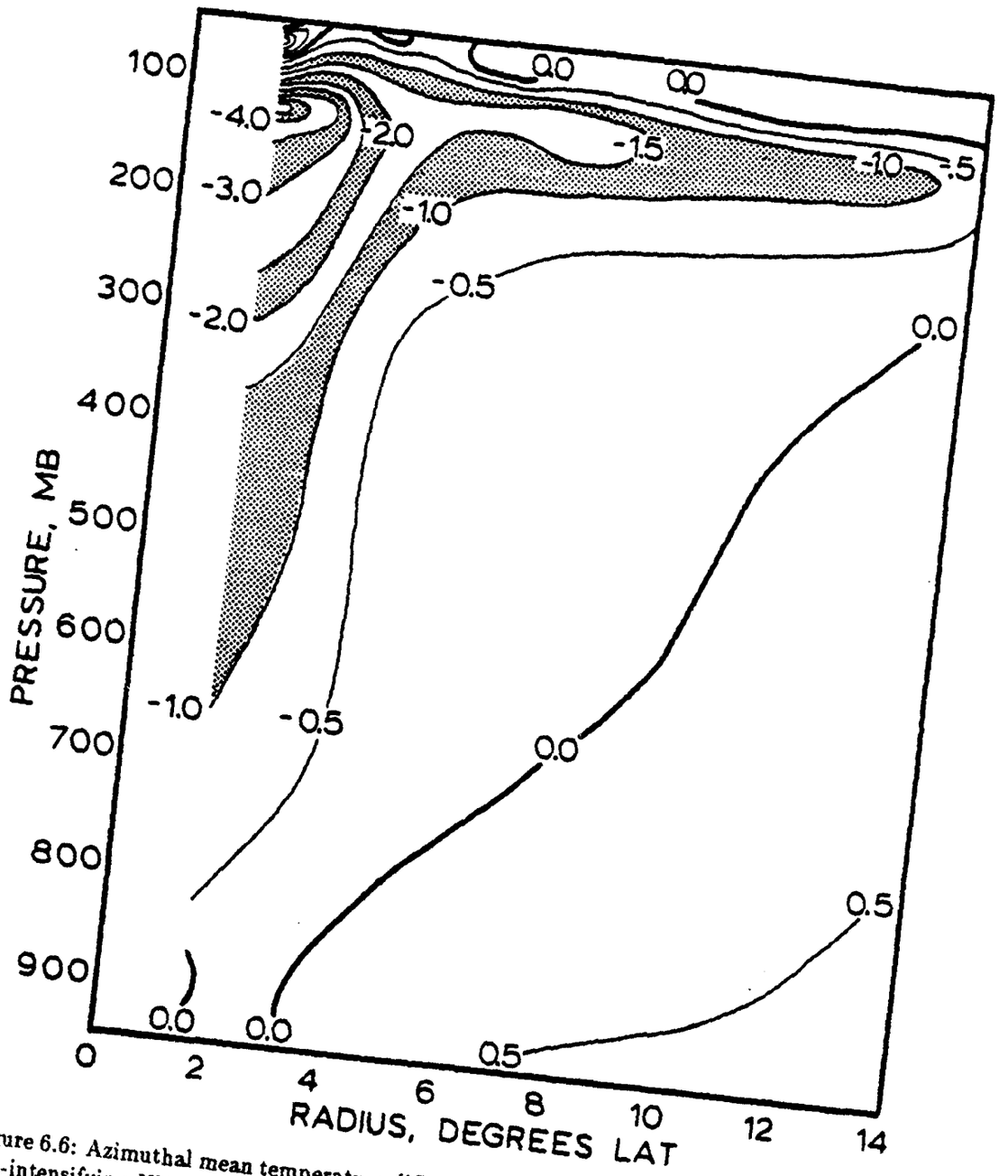

Figure 6.6: Azimuthal mean temperature differences between a composite intensifying and non-intensifying NWPAC typhoon of similar current intensity. Negative values indicate where the intensifying typhoon is cooler (from Merrill, 1988).

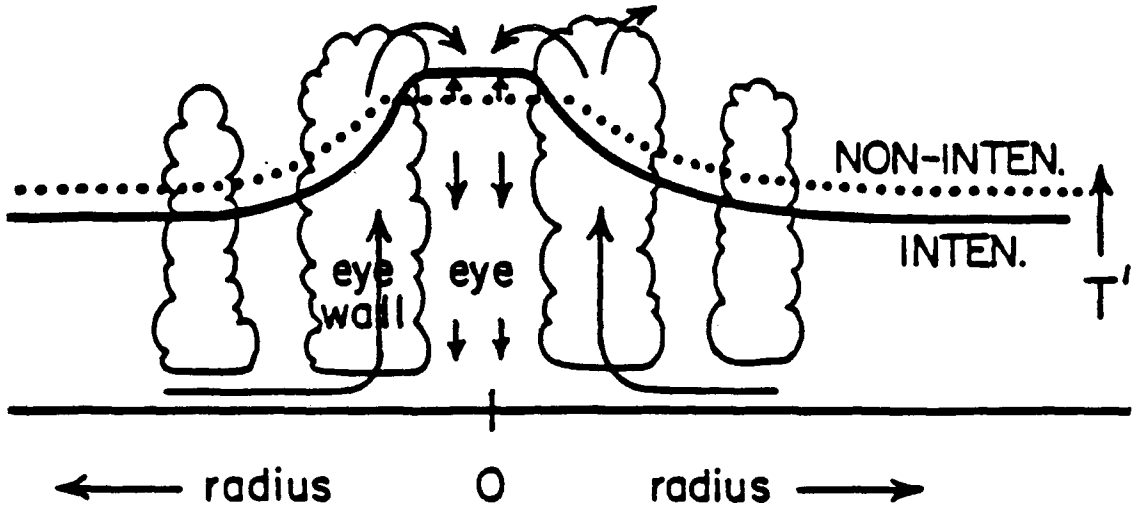

Figure 6.7: Cross sectional illustration of upper tropospheric temperatures of both intensifiers and non-intensifiers. By extension, rapid intensifiers are believed to be cooler outside the eyewall region and warmer in the subsidence eye region of the upper troposphere.

6.3 Application of the Hydrostatic Approximation to Upper Level Temperature Change

Inward warming of the tropical cyclone necessary for thermal wind balance in the region of maximum vertical shear brings up some rather interesting theoretical conclusions. Rapid intensification is favored by the upper level cyclone being as intense and as high as possible in the troposphere. This leads to a concentration of tangential vertical wind shear and the largest temperature gradients across the eyewall near the tropopause. This indicates that the most intense tropical cyclones would have a warmer eye and a relatively cold wall cloud region in the upper atmosphere. The change in thickness ΔZ for a given ΔT in the pressure layer p_1 to p_2 is given by:

$$\Delta Z = \frac{R}{g} \Delta \bar{T} \left(\frac{\Delta p}{\bar{p}} \right) \tag{6.4}$$

where $\Delta p = p_2 - p_1$ and $\bar{p} = \frac{p_1 + p_2}{2}$. Greater thickness changes are possible if the same amount of warming in an equal pressure layer occurs as high as possible in the atmosphere due to the fact that $\frac{\Delta p}{\bar{p}}$ is much larger in the upper than lower pressure layers. As an example, in a standard tropical atmosphere, if 5°C warming occurs the 400 to 350 hPa

layer, this will produce a net thickness change, ΔZ, of 19.5 m. If, however, the same 5° warming is placed in the 150 to 100 hPa layer, ΔZ equals 59.3 m, larger than the 400-350 hPa thickness change by a factor of 3. This is graphically illustrated in Fig. 6.8.

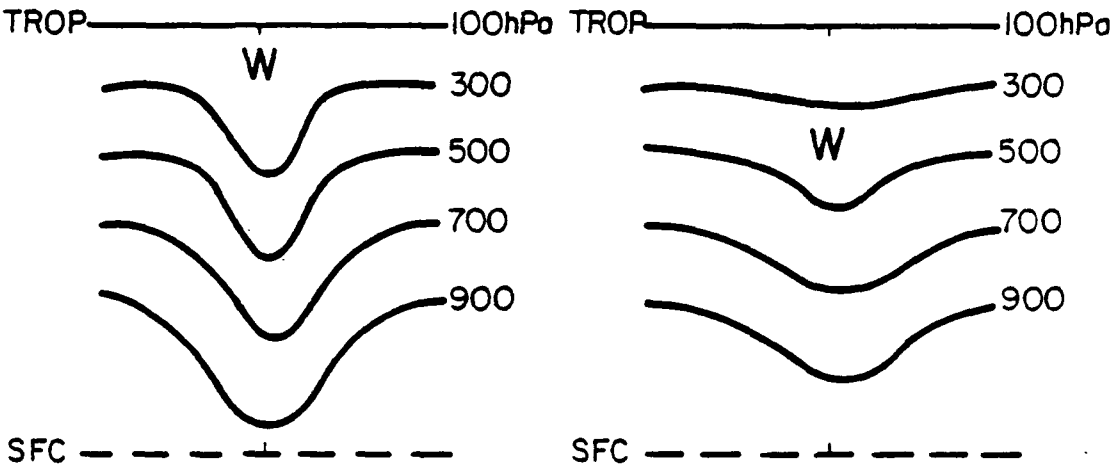

Figure 6.8: Relative pressure thickness differences for an equal amount of inner core warming due to the placement of warm temperature anomalies in the vertical. Larger pressure falls are possible at the surface if the warming occurs near the tropopause.

Equal in importance for rapid intensification is the need to maintain a relatively cold inner core environment at upper levels. It is necessary that favorable lapse rate buoyancy conditions be maintained at the inner core to maintain the "in-up-and-out" transverse circulation of the intensifying tropical cyclone. A primary factor that inhibits intensification is the fact that the warming needed to reduce the surface pressure will also tend to stabilize the middle and upper troposphere, reducing further convection. Rapid intensity change is considerably more likely if the warming generated by the tropical cyclone is as high and as close to the center as possible so that the warm inner core does not, over time, reduce the amount of deep convection.

6.4 Frictional Dissipation Effects

Another inhibiting factor is the increase in frictional dissipation that occurs along with the increase of tangential wind in the boundary layer.

Frictional dissipation is a function of the square of the wind velocity so any increase in tangential winds near the surface will also have larger values of frictional dissipation.

Frictional effects also offer a better understanding of the process involved in the concentration of deep convection close to the center and the decrease of the radius of maximum winds during rapid intensification.

The simplified equation of motion for the tangential component of the wind in cylindrical coordinates (including friction) is given by:

$$\frac{\partial V_\theta}{\partial t} = -V_r \zeta_a - \omega \frac{\partial V_\theta}{\partial p} + F_\theta \tag{6.5}$$

where V_θ is the tangential wind, V_r the radial wind, ζ_a the absolute vorticity, r is the radius of curvature, ω the vertical wind component, and F_θ denotes frictional dissipation. The absolute vorticity and frictional dissipation terms are given by:

$$\zeta_a = f + \frac{\partial V_\theta}{\partial r} + \frac{V_\theta}{r} \text{ and } F_\theta = -KV^2{}_\theta, \text{ where } K = \frac{g}{\Delta p}(pC_D) = \text{constant.}$$

g (gravity) equals 9.8 ms^{-2} and C_D (drag coefficient) taken to be 2 x 10^{-3}. After substitution in Eq. 6.5,

$$\frac{\partial V_\theta}{\partial t} = -V_r(f + \frac{\partial V_\theta}{\partial r} + \frac{\partial V_\theta}{r}) - \omega \frac{\partial V_\theta}{\partial p} - KV^2{}_\theta \tag{6.6}$$

We define $V_r = -\alpha V_\theta$, where α is the inflow angle and assume f constant. Let $\frac{\partial V_\theta}{\partial r} = 0$ at the radius of maximum wind and approximate $\frac{\partial V_\theta}{\partial p}$ to be relatively small in the boundary layer such that $\omega \frac{\partial V_\theta}{\partial p} \approx 0$, then the equation of motion is given by:

$$\frac{\partial V_\theta}{\partial t} = V^2{}_\theta(\frac{\alpha}{r} - K) \tag{6.7}$$

GEN DIS

Interpretation of Eq. 6.7 implies that in order to intensify (increase the tangential wind), it is necessary that the generation term (α/r) be greater than the frictional dissipation constant, K. An increase of the inflow angle α or a decrease in radius r is necessary for a larger generation term. There is no such radial dependence for the frictional dissipation term.

A fundamental process of tropical cyclone intensification is a pressure gradient force larger than required to balance frictional dissipation. If the tangential winds are subgradient, then there must be an increase in the radial wind component (larger inflow angle α) in order for the gradient wind to be larger than needed to balance friction. A large inflow angle implies that there would be more net radial convergence into the radius of maximum winds, which in turn would concentrate the deep cumulus convection closer to the center. A contraction of deep convection is considered necessary, if there is no significant decrease in eye size, for rapid intensity change.

Gray (1981) showed that the boundary layer inflow angle required to balance frictional dissipation is substantially less at inner radii because of the geometric characteristics of the inner core in a cylindrical coordinate system (Fig. 6.9). Wind accelerations at the inner core are related to the fact that generation is a function of the inflow angle, radius, and the square of the tangential wind while frictional dissipation is a function only of V^2. Closer to the cyclone center (smaller r) the generation term is much larger than the frictional dissipation term for an equal inflow angle. The inflow angle needed to balance friction for small r is also small. Larger inflow angles would increase the generation term and act to spin up the inner core and concentrate the deep convection even closer to the center.

6.5 Summary

The theoretical aspects of rapid intensity change are summarized in Fig. 6.10. The primary environmental condition necessary for rapid intensification to occur appears to be minimal upper level ventilation, assuming sea surface temperatures at least 28°C. In theory, rapid intensifiers are able to spin up the upper level cyclonic circulation and place the level of maximum shear higher in the atmosphere. As a result, inward warming near the tropopause can more efficiently reduce the surface pressure without stabilizing the middle and upper tropospheric environment. Enhanced radial inflow (down the pressure gradient) would increase low level convergence and drive even more vigorous convection in the eyewall/inner core region and continue spin up of the upper level cyclonic vortex.

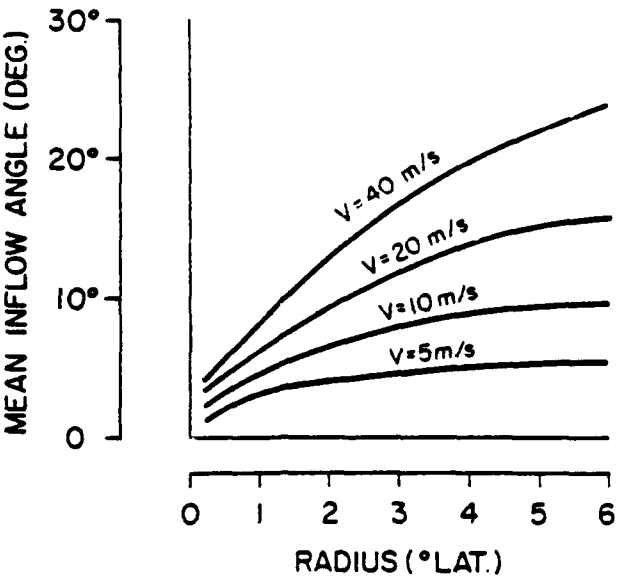

Figure 6.9: Depiction of the relationship between the mean inflow angle required to balance frictional dissipation at the radius of maximum winds where $\frac{\partial V_\theta}{\partial r} = 0$ (Gray, 1981).

The net effect is that, in order for tropical cyclones to rapidly intensify, the energetic processes of the cyclone must be concentrated as close to the center and as high as possible in order to spin up the rapidly intensifying typhoon. As long as the convection is concentrated close to the center and the inward warming necessary for thermal wind balance is near the tropopause, the upper level inner core region is exceptionally warm while the outer core region is relatively cold. Hydrostatically, this creates a large pressure gradient at the surface which is confined very close to the center. A small radius of maximum winds and a steep pressure gradient allows the vigorous in-up-and-out circulation of rapid intensifiers to continue by reducing the inflow angle required to balance friction and still spin up the tangential winds.

The following factors are believed to be necessary for rapid intensification to occur (Fig. 6.11):

1. Low vertical wind shear through the troposphere. An absence of strong, (relatively) unidirectional wind flow across the upper level center allows for vertical alignment of the tropical cyclone so that upward transport of cyclonic momentum can occur and result in a more efficient drop in surface pressure within the inner core region

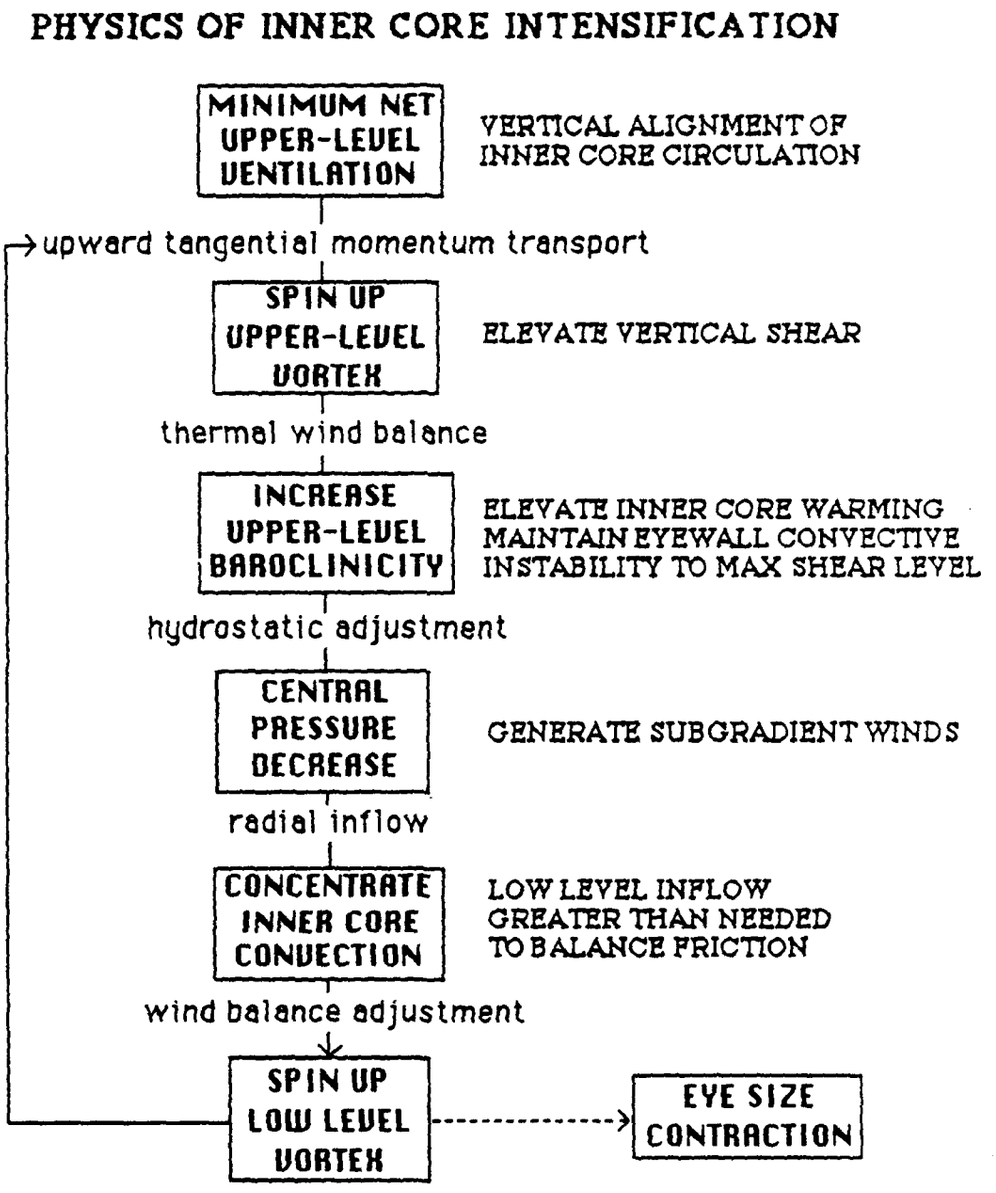

Figure 6.10: Idealized view of the step-by-step process of inner core rapid intensification and the theoretical reasoning used to explain rapid intensification. Minimum ventilation across the inner core is considered to be a necessary, but not sufficient, initial condition in order for rapid intensification to occur. Favorable sea surface temperatures are implicitly assumed.

due to upper level warming. The outer core region would not have a large decrease in surface pressure if warming effects are confined to the inner core.

2. A deep layer cyclonic circulation. If the intense cyclonic circulation extends all the way to the tropopause, such that the vertical shear of the tangential wind is concentrated at the very top of the troposphere, then the inward heating of the cyclone needed for thermal wind balance occurs as high as possible. In a deep, intense cyclonic circulation upward momentum transport spins up the upper level cyclonic circulation. If there is less of a spin up of the low level circulation (relative to upper levels), then larger radial inflow and concentration of the deep cumulus convection closer to the center are more likely to occur.

3. Large temperature gradients across the upper level eyewall region. Hydrostatically, concentrated warming near the tropopause is the most effective process to produce a rapid drop in surface pressure. It is necessary that the eye of the typhoon be as warm as possible but that the upper troposphere of the eyewall be as cool and convectively unstable as possible to rapidly decrease surface pressure.

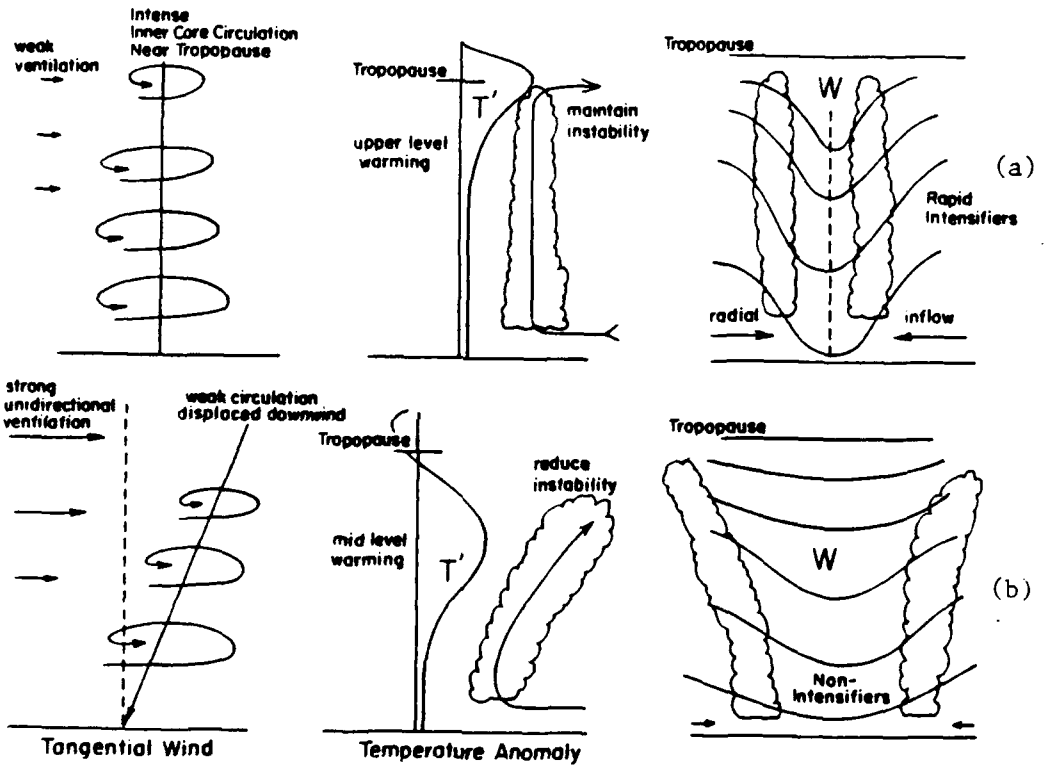

Figure 6.11: Generalization of the factors considered necessary for rapid intensification (a) compared to the environmental conditions typical of non-intensification (b). Weak ventilation permits vertical alignment of the inner core, which is more favorable to spin up the cyclonic circulation near the tropopause. An intense inner core near the tropopause concentrates inner core warming higher in the atmosphere and produces a larger hydrostatically induced pressure fall at the surface.

Chapter 7

DISTINCTIVE CHARACTERISTICS OF RAPID INTENSIFIERS

7.1 Composite Data Set Stratifications

In order to determine the distinctive differences of rapid intensifiers, it was necessary to stratify the composite data into rapid intensifiers (R), non-rapid intensifiers (I) and non-intensifiers (N). The non-rapid and non intensifiers were further classified as either tropical storms (TS) or typhoons (TY), based on intensity before the intensification event. These stratifications and the mean MSLP for each classification are listed in Table 7.1. These composite data sets were used, along with individual soundings within 111 km of the center, to explore the mean characteristics of the inner (0 to 2° radius) and outer (3 to 5°) circulation regions of each intensification class.

7.2 Upper Level Ventilation

A fundamental hypothesis upon which the theory of rapid intensification discussed in chapter 6 is based is minimum ventilation, or "blowthrough". Minimum ventilation allows maximum tangential momentum transport into the upper troposphere and is necessary if large surface pressure gradients are caused by upper level thickness changes. Ventilation is not a quantity directly measured by rawinsondes, but must be calculated indirectly from the relative magnitudes of the radial component of the wind.

The method used to compare the amount of net ventilation for each of the different stratifications is rather simple and straightforward. The total wind for each of the eight octants for a given radial band in the cylindrical composite grid with the storm motion removed (MOT) were calculated. Then the difference between the MOT radial inflow and outflow components were expressed as vectors along each of four major axes (see

Table 7.1: Description of the various composite stratifications used in this study to identify unique features of both rapid and non-rapid intensifiers.

COMPOSITE	DESCRIPTION TIME PERIOD	$\overline{\text{MSLP}}$ (hPa)
I1	Before Intensification / Tropical Storms 0 to 24 Hours Before Onset	993
I2	After Intensification / Tropical Storms 0 to 24 Hours After Onset	967
I3	Before Intensification / Typhoons 0 to 24 Hours Before Onset	966
I4	After Intensification / Typhoons 0 to 24 Hours After Onset	945
$\overline{\text{I}}$	Intensifiers $15\ \text{hPa} \leq \Delta p \leq 35\ \text{hPa}$ / day 24 Hours Before to 24 Hours After Onset	967
N1	Before Non-Intensification/Tropical Storms 0 to 24 Hours Before Onset	998
N2	After Non-Intensification/ Tropical Storms 0 to 24 Hours After Onset	993
N3	Before Non-Intensification/ Typhoons 0 to 24 Hours Before Onset	963
N4	After Non-Intensification/ Typhoons 0 to 24 Hours After Onset	962
$\overline{\text{N}}$	Non - Intensifiers $\Delta p \leq 10\ \text{hPa}$ / day 24 Hours Before to 24 Hours After Onset	977
R1	Before Rapid Intensification $\Delta p \geq 42\ \text{hPa}$ 12 to 24 Hours Before Onset	983
R2	After Rapid Intensification $\Delta p \geq 42\ \text{hPa}$ 0 to 12 Hours After Onset	956
$\overline{\text{R}}$	Rapid Intensifiers $\Delta p \geq 42\ \text{hPa}$ /day 24 Hours Before to 12 Hours After Onset	969

Fig. 7.1). This difference is termed "asymmetric outflow" relative to the center. In Fig. 7.1, two units of asymmetric outflow across the center are indicated along the E-W axis due to what is usually termed "blowthrough". Three units along the NE-SW axis is the result of stronger outflow to the SW. No net ventilation is indicated along the NW-SE axis because of symmetric outflow. Vector addition of the four axial vectors yielded a single "*asymmetric relative wind vector*" (ARW Vector) with a magnitude given by the square root of the sum of u and v components squared. Thus, the ARW vector is the resultant (relative) wind and a measure of the magnitude and direction of unidirectional wind flow across the cyclone center for a given radial belt, such as 1 to 3° (111 to 333 km). Based on this definition, cyclones with perfectly symmetrical inflow or outflow patterns would have an ARW vector of zero, regardless of the magnitude of radial inflow/outflow components (Fig. 7.2). Divergence into and out of a particular radial belt or pressure level is assumed to be near zero for a composite set of data. This is a valid argument only if ventilation across the cyclone center is desired and the data is a composite of many different tropical cyclones. In particular, if the composite data indicated inflow along one axis and outflow along the opposite axis, the radial wind components would add together and is assumed to be a measure of unidirectional flow (ie., "blowthrough").

It was desirable to obtain ARW vectors for as close to the center as possible, while maintaining a sufficient number of soundings in each octant for reliable vector calculation. The 1-3° (111 to 333 km) and 3-5° (333 to 555 km) radial belts were selected for analysis in the upper troposphere at the 300, 250, 200, 175, 150, 125 and 100 hPa pressure levels. Insufficient sounding data at all octants in the R1 (before rapid intensification) and R2 (after rapid intensification) composites in the 1-3° region precluded the use of these stratifications. However, since composites R1 and R2 are subsets of composite R (rapid intensifiers), the latter was used for comparison with other composite stratifications since R1 and R2 combined together had at least 3 soundings per octant (Fig. 7.3).

7.3 Magnitude of Net Ventilation

Vertical profiles of net ventilation (ARW vector magnitude) for a set of stratifications initially at tropical storm intensity for the 1-3° and 3-5° belts are shown in Fig. 7.4. The

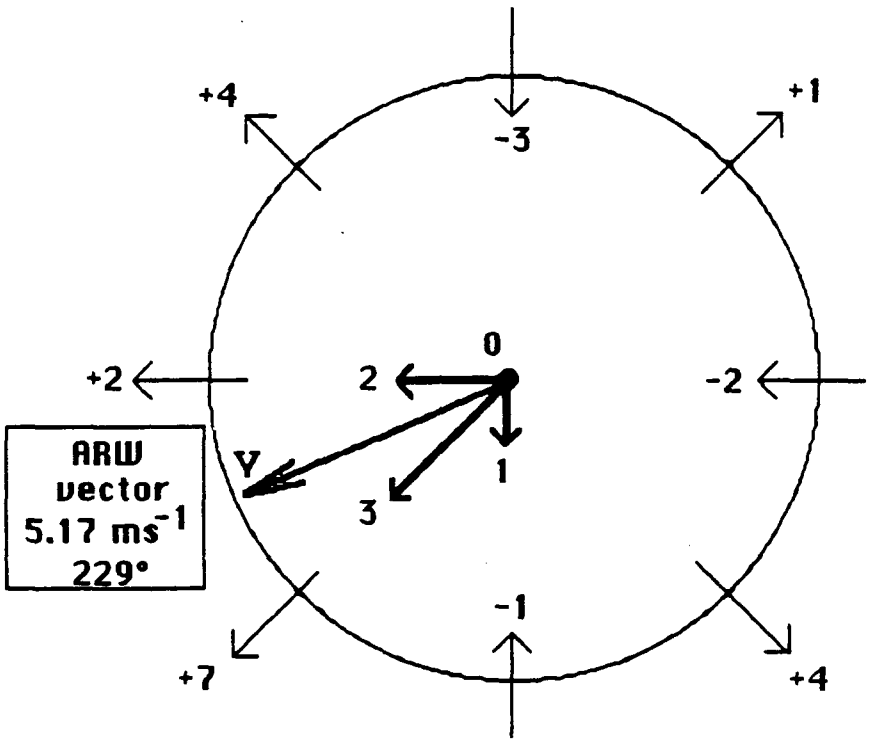

Asymmetrical Relative Wind (ARW) Vector = **Asymmetical Outflow (A)** + **Blowthrough (B)**

Figure 7.1: Illustration of the method used to calculate net ventilation. The asymmetric relative wind (ARW) vector is the resultant wind of the radial wind components at each octant. The heavy arrows indicate the asymmetric outflow along each of the four major axes. The ARW vector V is derived from vector addition of the four axial vectors.

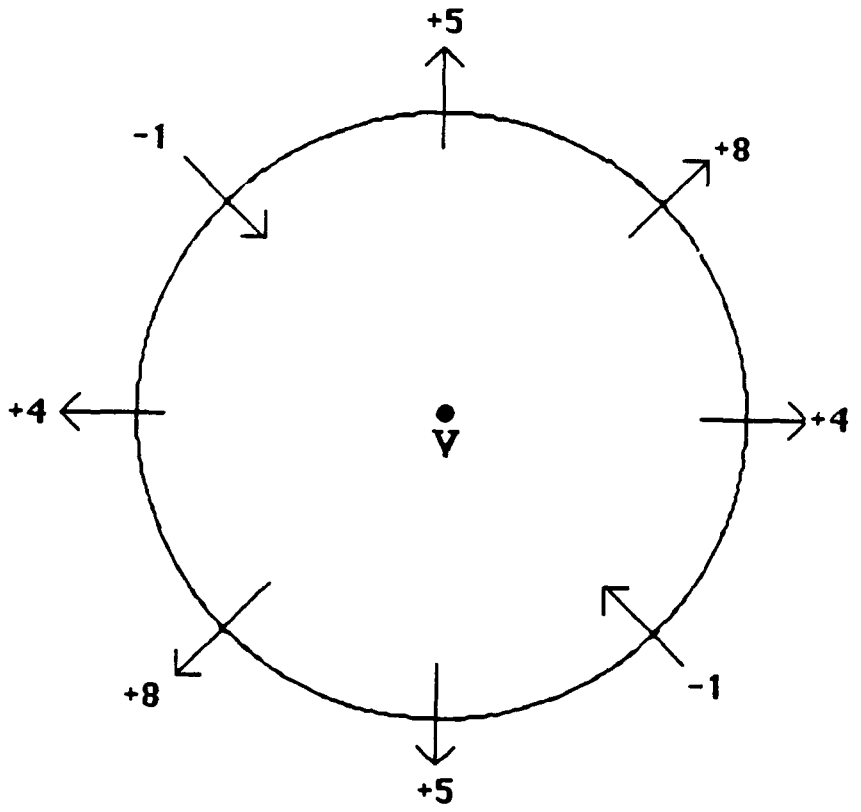

Figure 7.2: An example of zero net ventilation. There is zero asymmetric outflow along each of the four major axes. In this example, strong outflow channels are oriented to the northeast and to the southwest. Dual outflow channels may enhance intensification by reducing unidirectional ventilation.

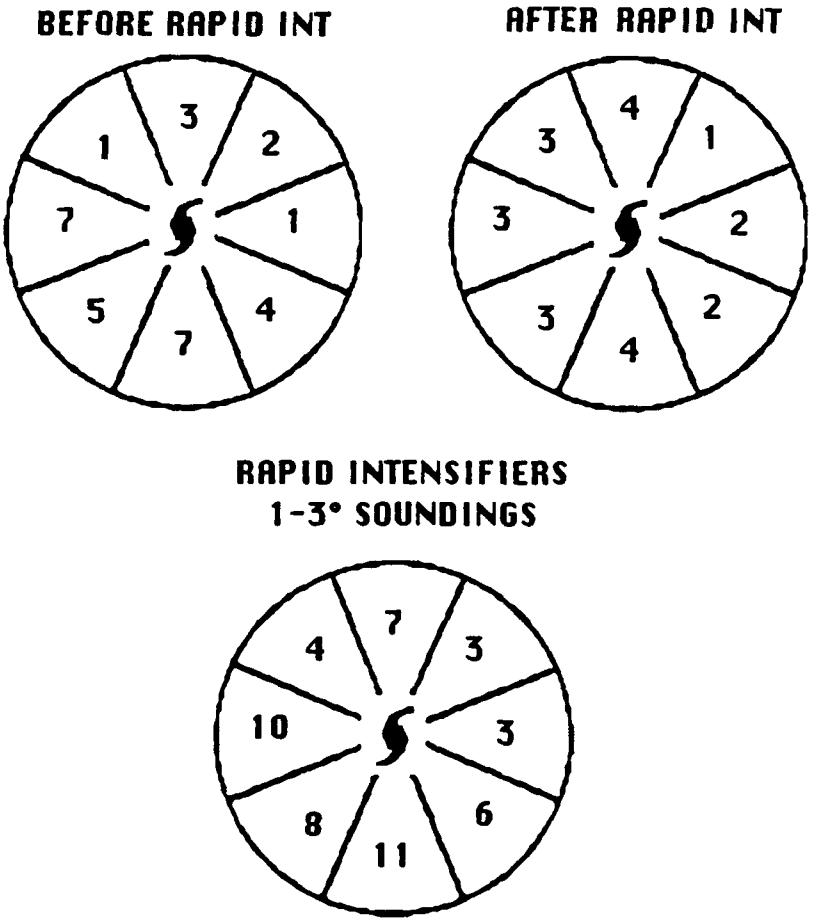

Figure 7.3: Representation of the number of soundings, by octant, in the before, after, and combined rapid intensification composite stratifications at the 1-3 ° radial belt.

most significant differences are between rapid intensifiers and N1 (before non-intensification). For the 1-3° radial belt below 150 hPa, the non-intensifiers in composites N1 and N2 had an asymmetrical relative wind three times as large as the net ventilation across the center of the rapid intensifiers. It appears likely that one reason these tropical storms did not intensify is larger upper level "blowthrough" which would act to prevent vertical alignment of the tropical cyclone circulation. Conversely, minimum net ventilation for composites R and I1 (before intensification) would be a favorable factor for further development to typhoon intensity. The data for the 3-5° belt also indicated relatively large ARW vector differences across the centers of rapid intensifiers and non-intensifiers.

When a comparison is made between composite stratifications of typhoon intensity (Fig. 7.5), only small differences between intensifiers and non-intensifiers are apparent in the 1-3° region. Only typhoons which intensified at a non-rapid rate (I4) had significantly larger values of asymmetric relative wind. At 3-5°, no large differences are apparent, but the rapid intensifiers tended to have less net ventilation below 150 hPa.

The relative differences in net ventilation are more apparent when the individual composites are grouped together into three major categories; rapid intensifiers (R), intensifiers (I), and non-intensifiers (N). A comparison for both the inner (1-3°) and outer (3-5°) ARW vectors is given in Fig. 7.6. Note that the rapid intensifiers have less unidirectional wind flow across the center than the non-rapid cases. No distinct magnitude differences are indicated between the averaged non-intensifiers and non-rapid intensifiers, especially at the 3-5° radial belt.

7.4 Direction of Net Ventilation

The direction of the ARW vector was also investigated to determine if rapid intensifiers have distinctly different directional ventilation patterns than non-rapid intensifiers. As shown in Fig. 7.7, the direction of the 1-3° ARW vector for the rapid intensifier stratification varies greatly with height. Note that the 200 hPa vector is nearly 180° opposite of the 100 hPa vector as the direction of the asymmetric relative wind tends to

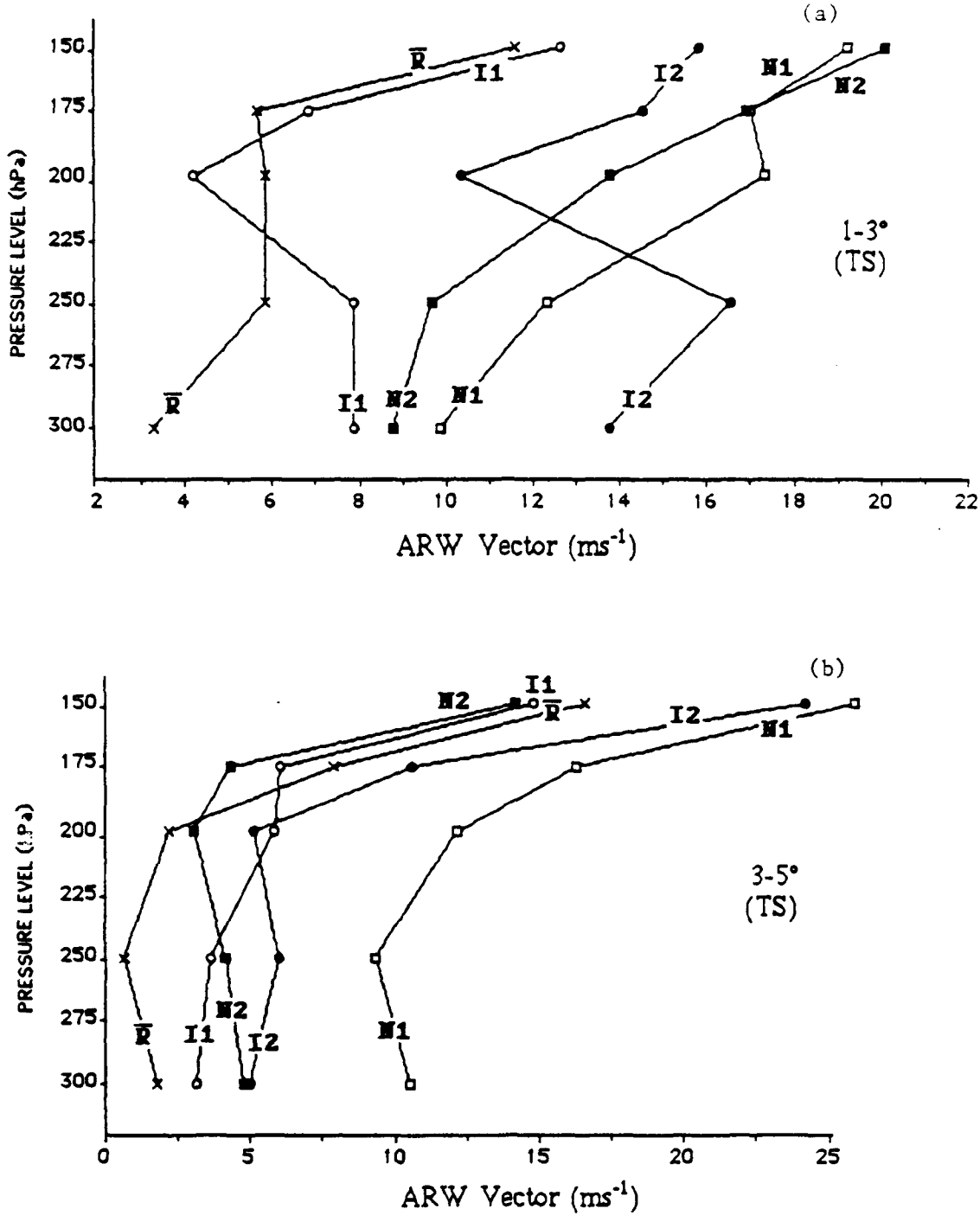

Figure 7.4: Upper level profiles of asymmetric relative wind (ARW) vectors for composite stratifications initially at tropical storm intensity at the 1-3° and 3-5° radial belts for rapid intensifiers (R), intensifiers (I), and non-intensifiers (N). The numbers represent before (1) and after (2) classifications.

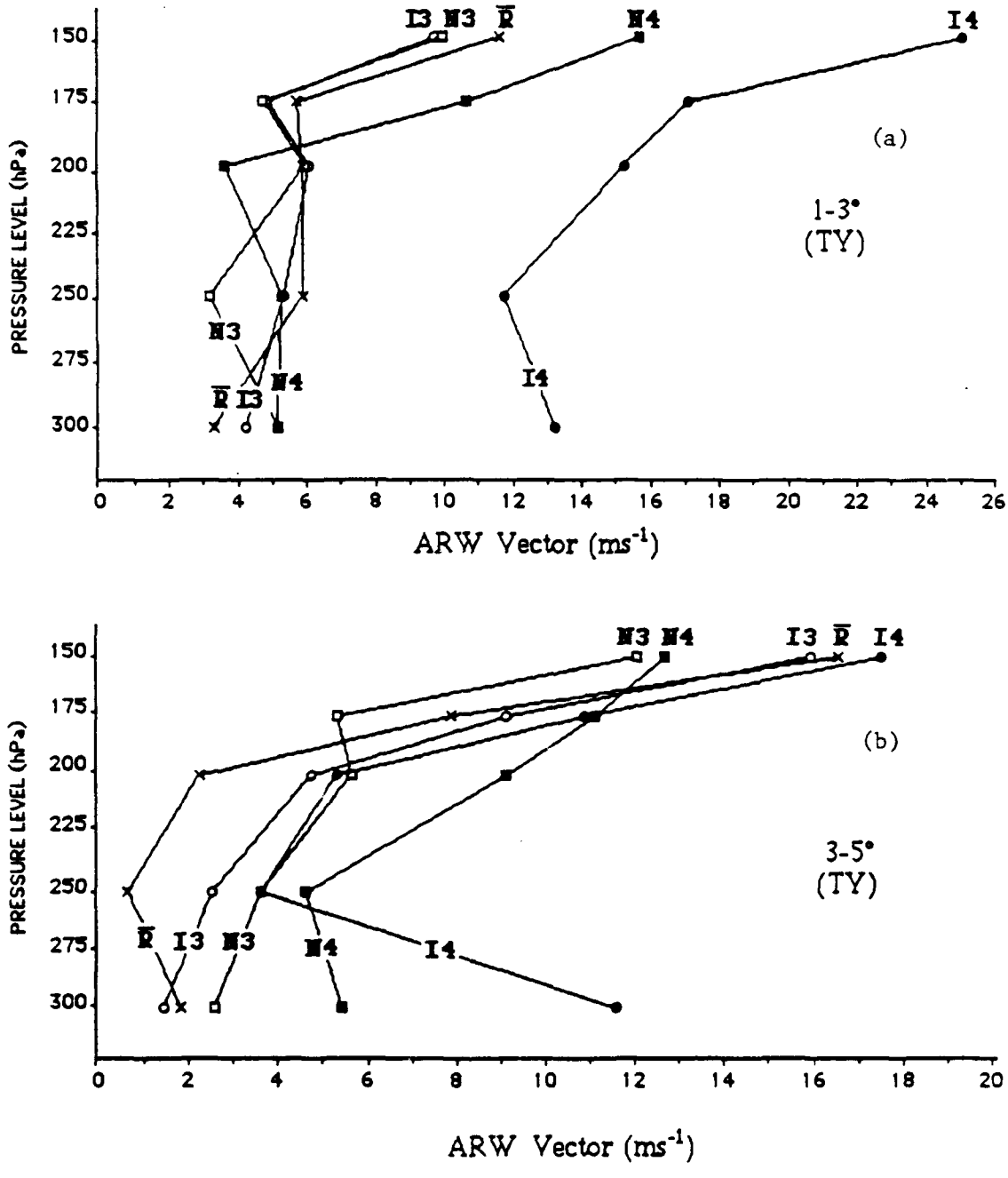

Figure 7.5: Same as Fig. 7.4 except for composite stratifications initially at typhoon intensity.

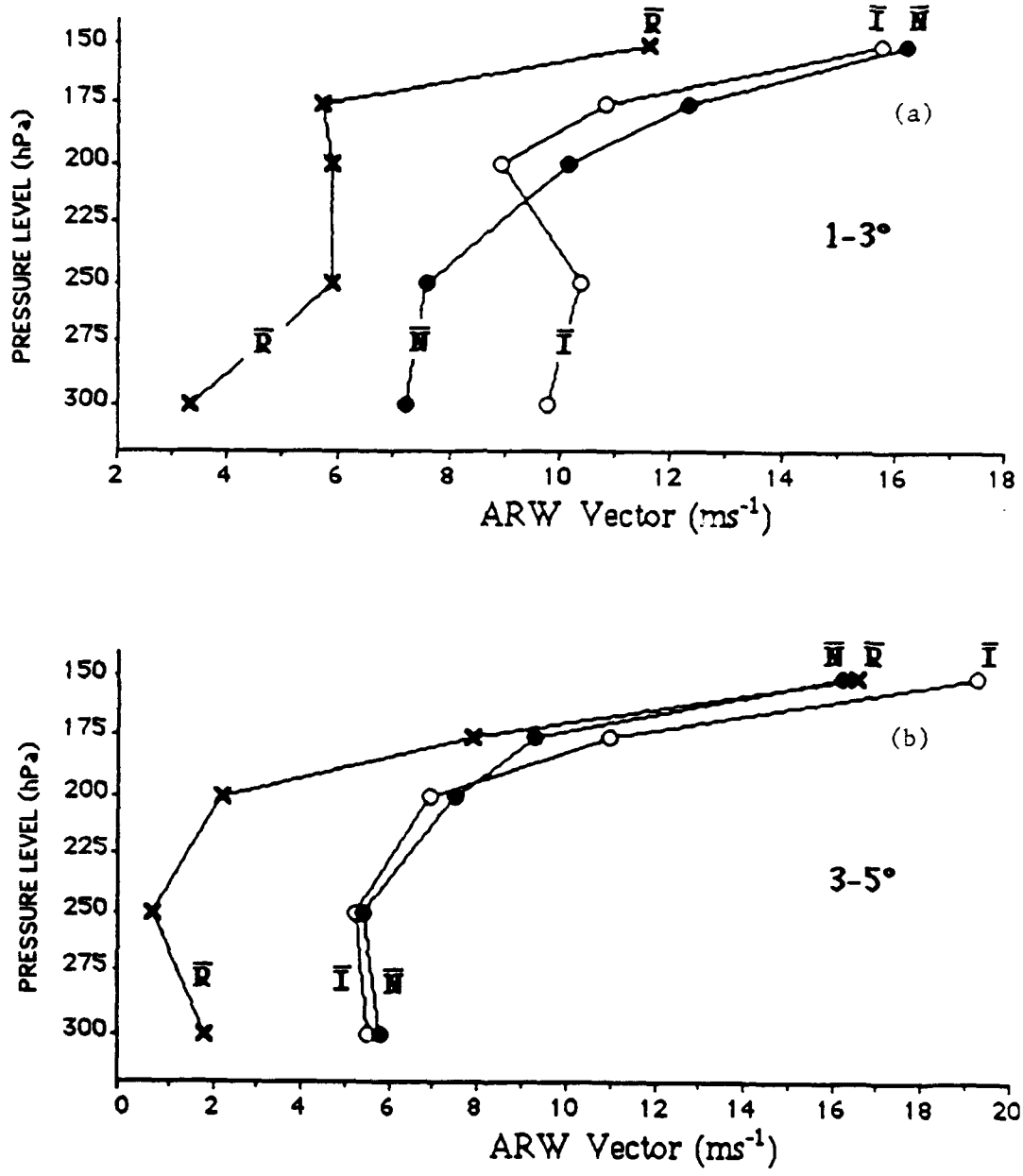

Figure 7.6: Mean upper level asymmetric relative wind (ARW) at the 1-3° and 3-5° radial belts for combined composite stratifications of rapid intensifiers (R), intensifiers (I), and non-intensifiers (N).

veer (anticyclonic) with height. In contrast, the directional profile of composite N1 (before non-intensification, TS intensity), also shown in Fig. 7.7, which indicates a nearly uniform direction of the ARW vector with height.

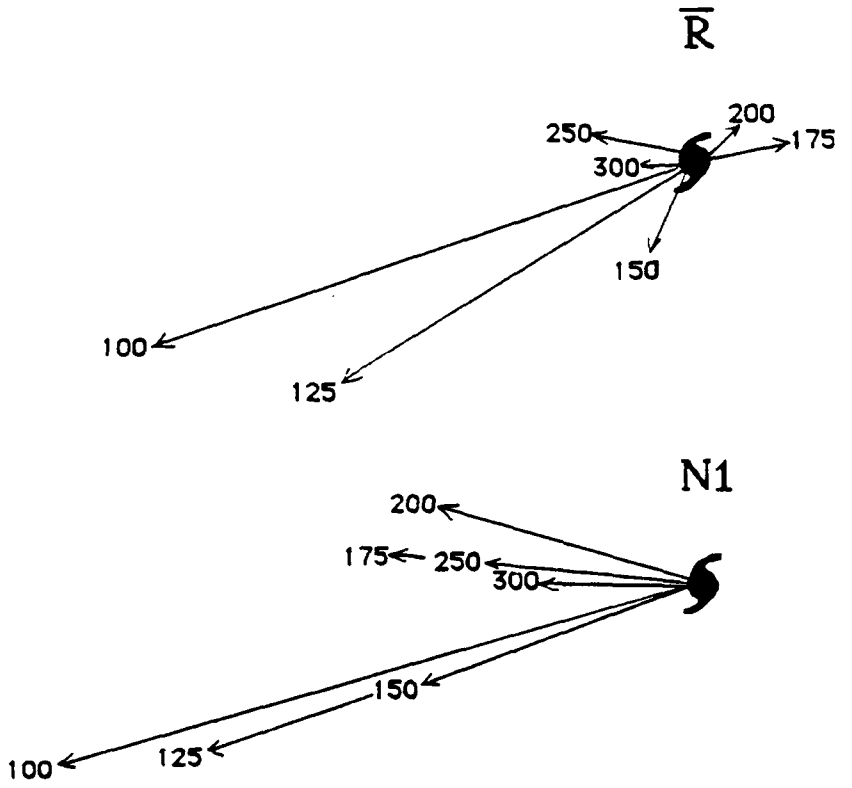

Figure 7.7: Comparison of upper level directional vectors at the 1-3° radial belt for rapid intensifier (R) and before non-intensification (N1) TS intensity composites.

Conceptually, it is important that the direction of the ARW vector not be constant with height. As parcels ascend in the core of the cyclone, they would be displaced further and further from the center if the ventilation vector direction is constant and the vector magnitude increases with height. Anticyclonic veering of the ventilation vector with height, as in the case of composite R, would allow ascending parcels to have lower outward momentum and maintain proximity to the center as they encounter relative winds that are directed back toward the cyclone center. Apparently, the ARW vectors of rapid intensifiers are distinctly different from those of tropical storms which fail to intensify. Strong, unidirectional wind flow across the center of the cyclone at upper levels acts to prevent intensification while weaker, multidirectional winds across the center tends to minimize

vertical wind shear in the rapidly intensifying storms. It should be noted that the while the concept of asymmetric outflow as a measure of ventilation is fairly straightforward, actual measurement of unidirectional ventilation (blowthrough) based on composite data is extremely difficult. The data presented here demonstrates, in a relative sense, that the resultant wind across the center of rapid intensifiers is at least the same, if not less than, the resultant wind across the center of non-rapid intensifiers and non-intensifiers.

7.5 Tangential Wind Profiles

Based on the ventilation results presented in this chapter, it is reasonable to assume that rapid intensifiers have relatively weak wind flow across their center in the upper troposphere, especially below 150 hPa. The 150 hPa level is also the approximate level to which Cb clouds penetrate. Vertical transport of cyclonic momentum by the deep cumulus convection near the center is therefore possible since rapid intensifiers do not appear to have strongly unidirectional flow across the center to disrupt vertical alignment. To examine the depth of the composite cyclonic wind fields, the tangential component of the wind in a cylindrical coordinate system with the motion of the storm removed (MOT) was calculated for each composite pressure level and out to 555 km from the center. Vertical profiles of the tangential wind were plotted for the radial belts of 0-2° (0 to 222 km) and 3-5° (333 to 555 km) to determine relative differences between the inner and outer circulations of the various composite data sets.

The 0-2° tangential wind profiles of rapid intensifiers and non-rapid intensifiers is shown in Fig. 7.8. When a comparison is made between composites of tropical storm intensity in the inner circulation region (Fig. 7.8a), the tangential wind differences due to initial intensity are clearly indicated. The mean MSLP of tropical cyclones in R1 is 983 hPa, compared to 993 for I1 and 998 hPa for N1 (see Table 7.1). The tangential wind profiles after the intensification or non-intensification event are also shown in Fig. 7.8a. Note the large increase in tangential winds for composites I1,I2 (non-rapid intensification) and N1,N2 (non-intensification). This is in contrast to the before versus after profiles of R1,R2 (rapid intensification), where lower troposphere tangential winds remained nearly

constant while the upper level winds increased (Fig. 7.8b). This means that, over time, the vertical wind shear of the non-rapid and non-intensifiers increased but decreased for rapid intensifiers in the inner (0-2°) region. In the outer (3-5°) region, the pickup in tangential winds after the intensification/non-intensification event is similar for all three of the composite classifications (Fig. 7.9). Figure 7.9b shows that there is less of an increase in vertical wind shear for rapid intensifiers below 125 hPa, and a spin-up of cyclonic tangential winds near the tropopause and in the lower stratosphere at 3-5° radius.

Similar comparisons between rapid intensifiers and non-rapid intensifiers of typhoon intensity at 0-2° radius are shown in Fig. 7.10. The tangential winds in composite R1 are weaker than those in composites I3 (before intensification) and N3 (before non-intensification), and this is to be expected due to mean MSLP differences (see Table 7.1). Large tangential wind differences exist in the "after" composite stratifications. Note that there was little pickup in the winds for composites N4 and R2, as opposed to composite I4 (Fig. 7.10a). As shown in Fig. 7.10b, the net effect is to increase the mid-tropospheric vertical wind shear of intensifiers and non-intensifiers over time at 0-2° radius.

Tangential wind data in the 3-5° radial belt for typhoon intensity composites (Fig. 7.11a) reveal only small differences in the before/after stratifications. Figure 7.11b shows a similar increase in tangential winds in the lower troposphere by both rapid and non-rapid intensifiers. Non-intensifiers had no apparent increase or decrease of tangential wind in the vertical.

It is evident that distinctive differences exist in the inner tangential wind profiles of rapid intensifiers. Typically, as a tropical cyclone intensifies, the tangential component of the wind increases. The pickup in tangential winds is largest in the lower troposphere since tropical cyclones are warm core systems with the strongest winds near the surface which weaken with height. For rapid intensifiers, the opposite occurs. Apparently, even though there is a large decrease in the central surface pressure, no substantial increase in the low level tangential wind velocity occurs. In fact, the 0-2° data indicated the tangential winds near the surface actually decreased (Fig. 7.12). At 0-2° radius, there is an increase of upper level tangential winds, resulting in a net reduction of vertical wind shear at the

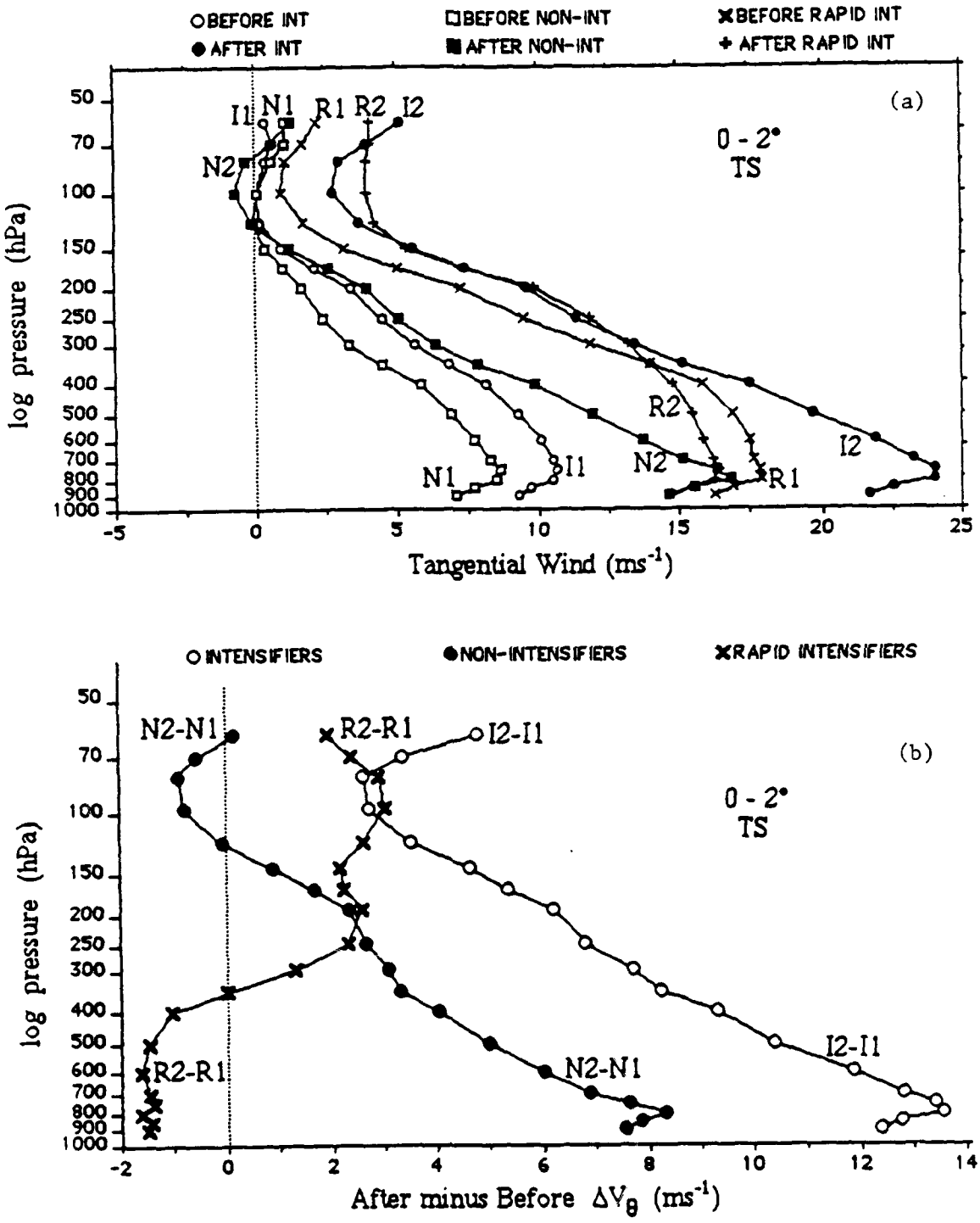

Figure 7.8: Tangential wind profiles at the 0-2° radial belt for composite stratifications initially at tropical storm intensity (a) and the change of tangential wind after the intensification or non-intensification event (b).

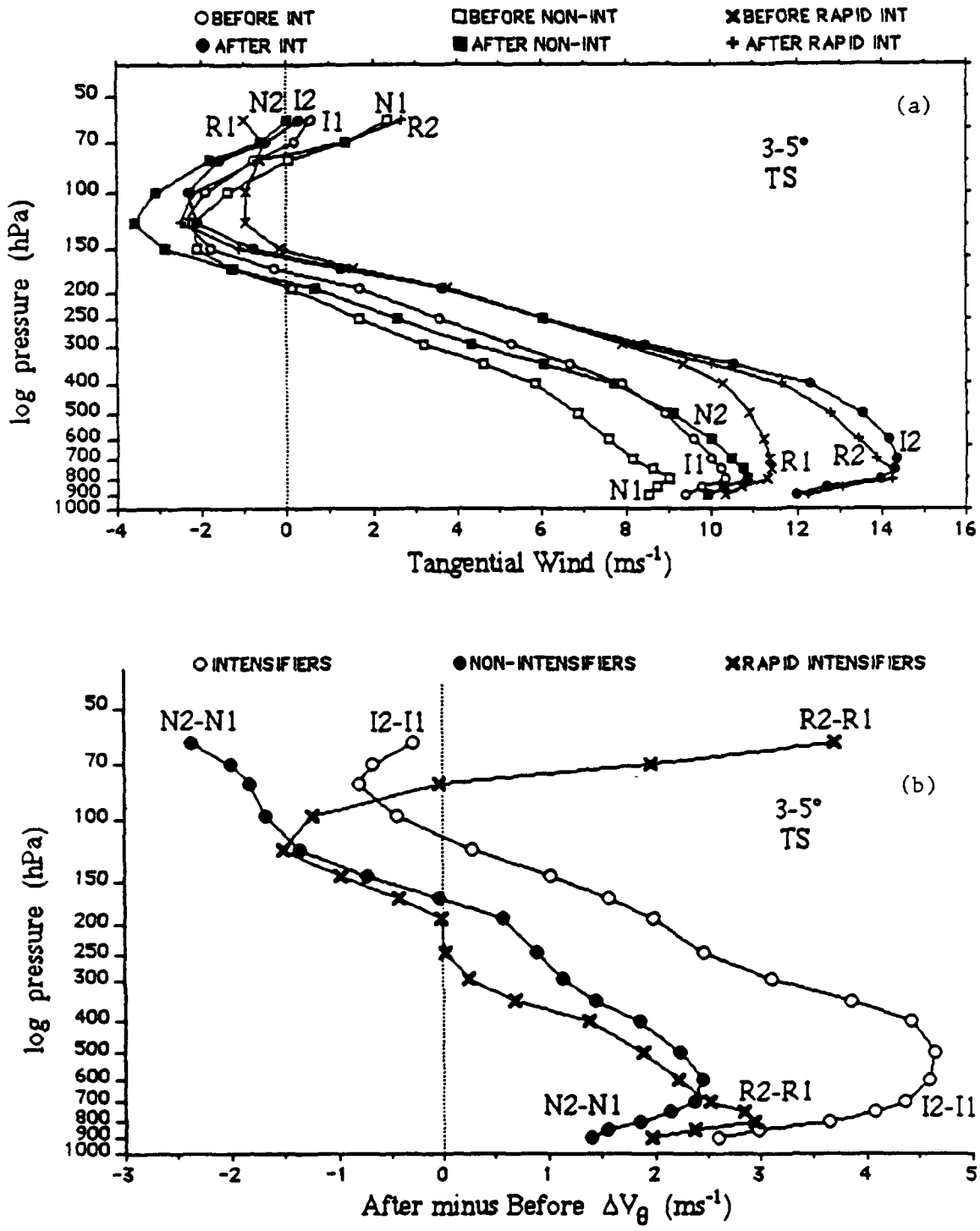

Figure 7.9: Tangential wind profiles at the 3-5° radial belt for composite stratifications initially at tropical storm intensity (a) and the change of tangential wind after the intensification or non-intensification event (b).

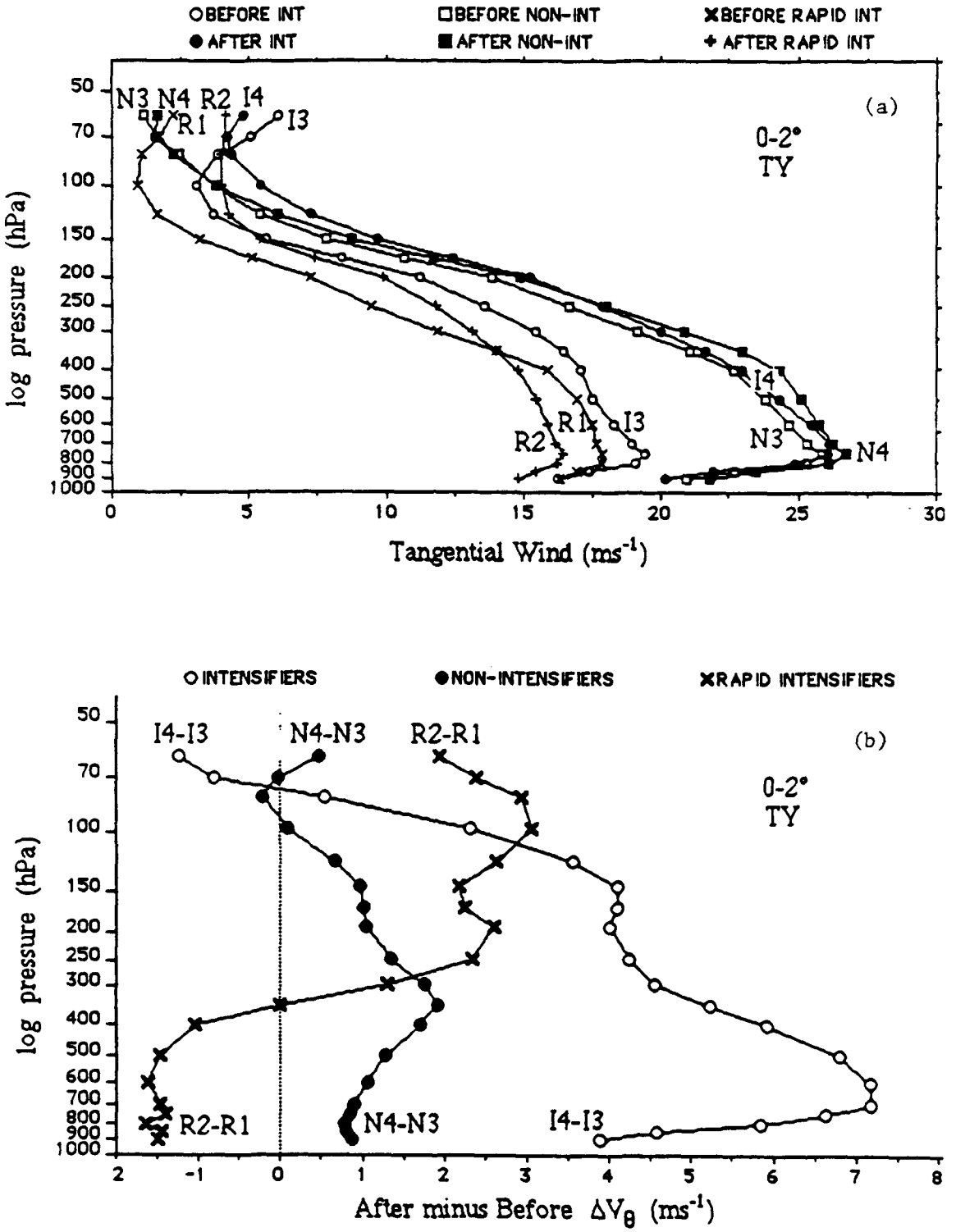

Figure 7.10: Tangential wind profiles at the 0-2° radial belt for composite stratifications initially at typhoon intensity (a) and the change of tangential wind after the intensification or non-intensification event (b).

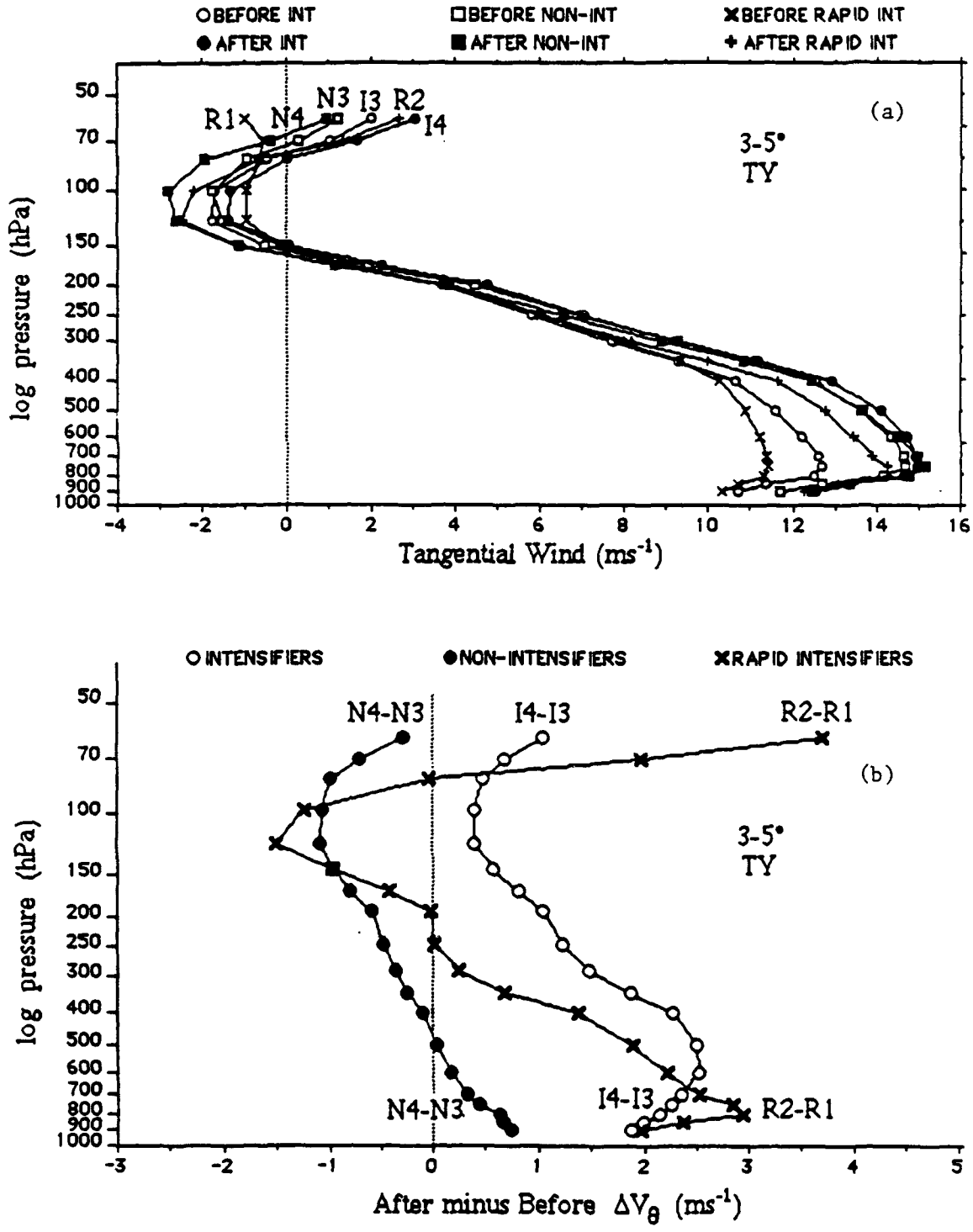

Figure 7.11: Tangential wind profiles at the 3-5° radial belt for composite stratifications initially at typhoon intensity (a) and the change of tangential wind after the intensification or non-intensification event (b).

inner core of rapidly intensifying tropical cyclones. From the thermal wind equation, the inward heating of the inner core due to vertical wind shear must occur above 300 hPa, where the thickness changes are larger for the same amount of heating. By the same argument, inner core warming of non-rapid and non-intensifiers should take place below 200 hPa (Fig. 7.13).

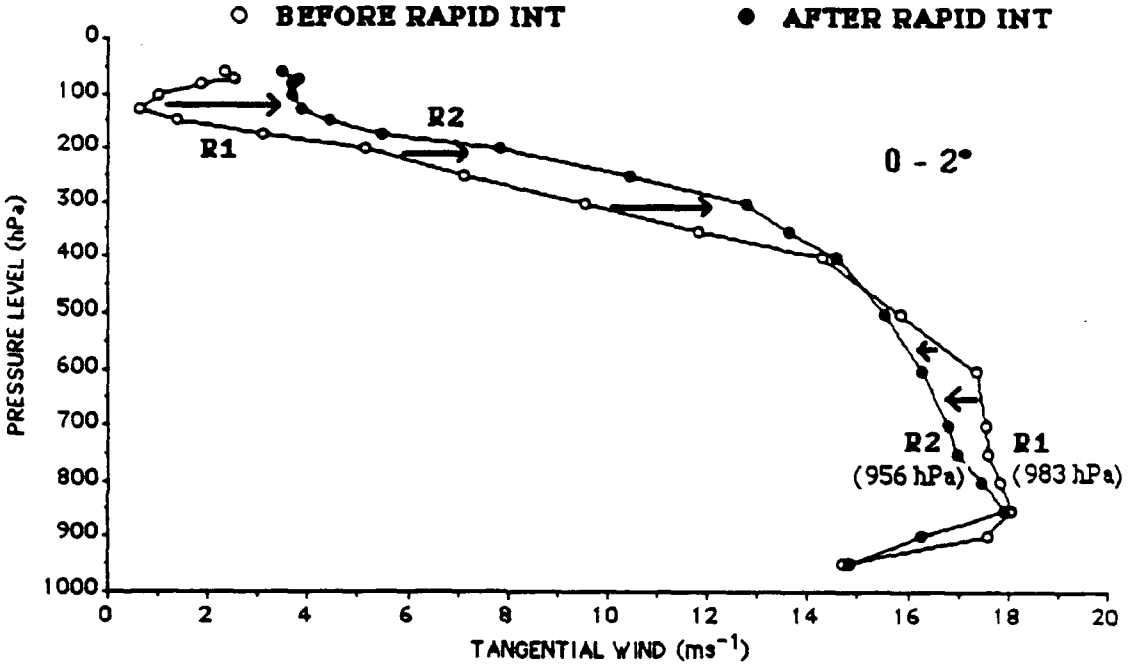

Figure 7.12: Comparison of the inner core composite tangential wind profiles and mean MSLP before (R1) and after (R2) rapid intensification.

7.6 Temperature Anomalies

To determine whether the tangential wind profiles discussed in the previous section did, as theorized, affect the upper level thermal structure of rapid and non-rapid intensifiers, composited rawinsonde temperature sounding data for the various stratifications were taken at 0-2° (0 to 222 km) and 3-5° (333 to 555 km) radial belts. In order to compare the relative temperature differences of each composite stratification, it was necessary to subtract the mean temperature from the data to obtain temperature anomalies. A mean tropical cyclone sounding at 2° (222 km) radius given by Frank (1977) was used

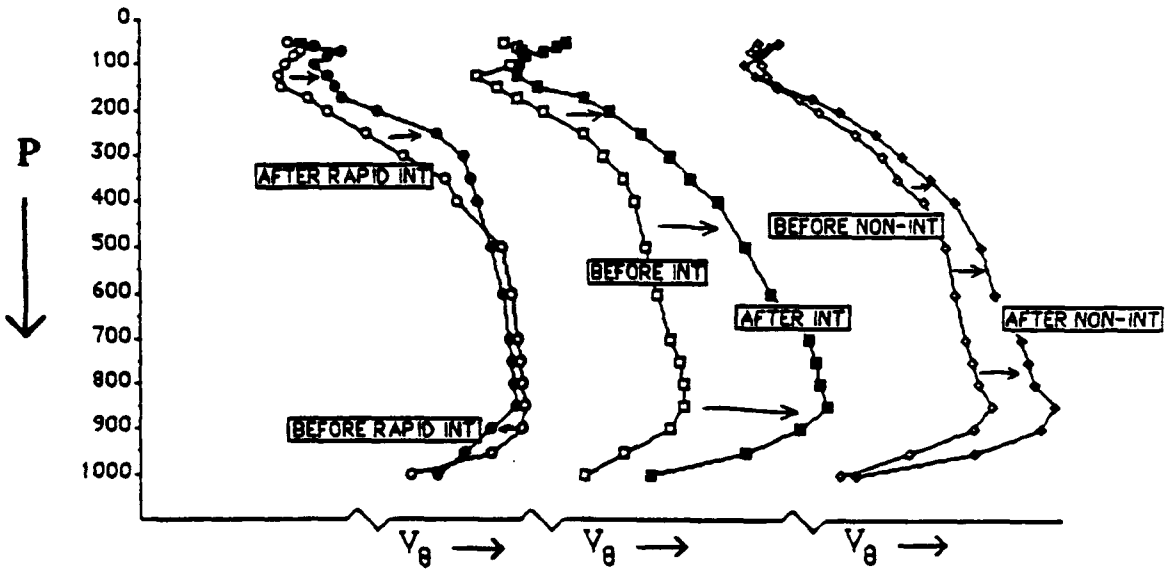

Figure 7.13: Illustration of the relative differences of inner core tangential wind profiles for rapid intensifiers, intensifiers, and non-intensifiers. Increases in tangential wind below 200 hPa for intensifiers and non-intensifiers acts to increase the vertical shear of tangential winds in the middle and upper troposphere.

to determine the composite temperature anomaly at each pressure level. Temperature anomalies were plotted with pressure as the vertical axis.

When a comparison is made between composites of tropical storm intensity in the inner region (Fig. 7.14a), the before rapid intensification composite (R1) is initially warmer than the before intensification (I1) and before non-intensification (N1) composites in the middle and upper troposphere and much warmer in the stratosphere. After the intensification or non-intensification event, temperature anomaly profiles are as shown in Fig. 7.14a. Note the large differences in middle and upper tropospheric warming apparent in the non-rapid (I2) and non-intensifying (N2) composites. In contrast, the rapid intensifier temperature profile changed very little after the onset of rapid intensification (Fig. 7.14b). The mid level inner core warming indicated for composites I2 and N2 would tend to stabilize the tropical cyclone environment and act to suppress deep convection. On the other hand, rapid intensifiers would maintain buoyant instability if no mid-level warming occurs.

At the outer circulation (333 to 555 km), rapid intensifiers are relatively cool in the middle and upper troposphere both before and after onset (Fig. 7.15a). Note the

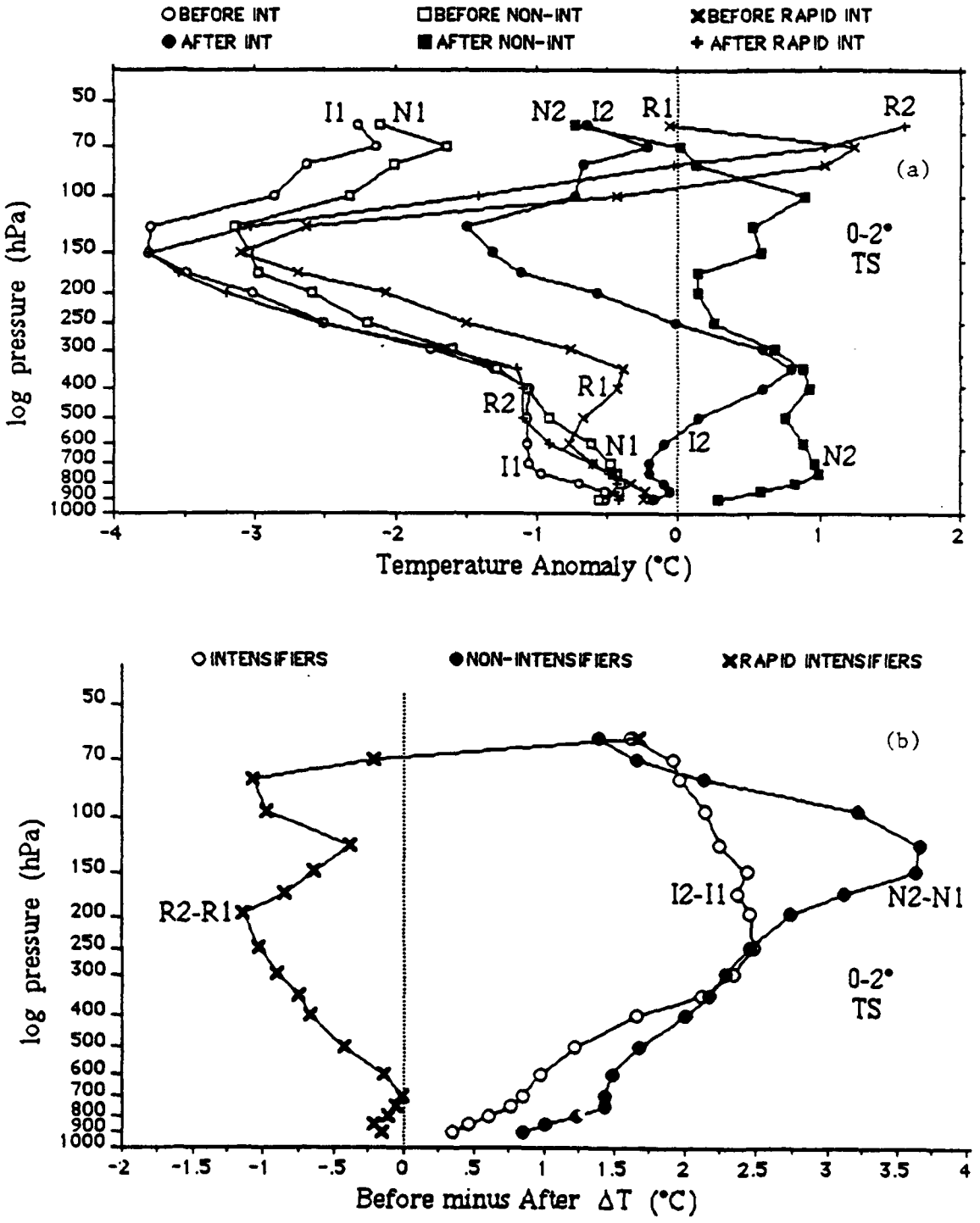

Figure 7.14: Temperature anomaly profiles at the 0-2° radial belt for composite stratifications initially at tropical storm intensity (a) and the change of temperature after the intensification or non-intensification event (b).

warming that occurs in composites I2 and N2 in the 300 to 100 hPa pressure layer (Fig. 7.15b). Hydrostatically, this should be reflected as a pressure fall at the surface. However, since it occurs relatively far from the center, a concentration of the pressure gradient near the center, believed to be necessary for rapid intensity change, is not likely to occur (Weatherford, 1989).

Inner region temperature anomaly profiles for composites I3 and N3, initially at typhoon intensity, are shown along with the before rapid intensification composite (R1) in Fig. 7.16a. Clearly, non-intensifying typhoons are much warmer and more stable in the middle and upper troposphere than non-rapid and rapid intensifiers. The largest temperature differences between the composite stratifications is at 150 hPa. The before and after temperature profile composites for both intensifiers and non-intensifiers are not considerably different as is shown in Fig. 7.16b. Some upper tropospheric warming is apparent during rapid intensification, but what is remarkable about the rapid intensifiers are the cooler temperatures in the middle troposphere after the onset of rapid intensity change. The temperature profiles of rapid intensifiers are more unstable in the inner core, both before and after onset.

Some upper tropospheric heating occurs in the outer (3-5°) region of rapid intensifiers, as is shown in Fig. 7.17a. But the outer heating during rapid intensification is nearly equal to the heating that occurs during intensification and non-intensification (Fig. 7.17b). Investigation of upper level temperature anomalies outside 5° radius revealed that rapid intensifiers are consistently cooler than intensifying and non-intensifying typhoons. Thus, even though rapid intensifiers generate large amounts of latent heat released in vigorous convection, the mid- and upper troposphere of the inner core remains relatively cool during a rapid intensification event.

7.7 Temperature Anomalies Within 1° of the Center

Data in the previous section revealed the inner region (0 to 222 km) temperatures of rapid intensifiers were anomalously warm in the stratosphere but relatively cold below the tropopause. To examine further whether this temperature profile was an actual inner core

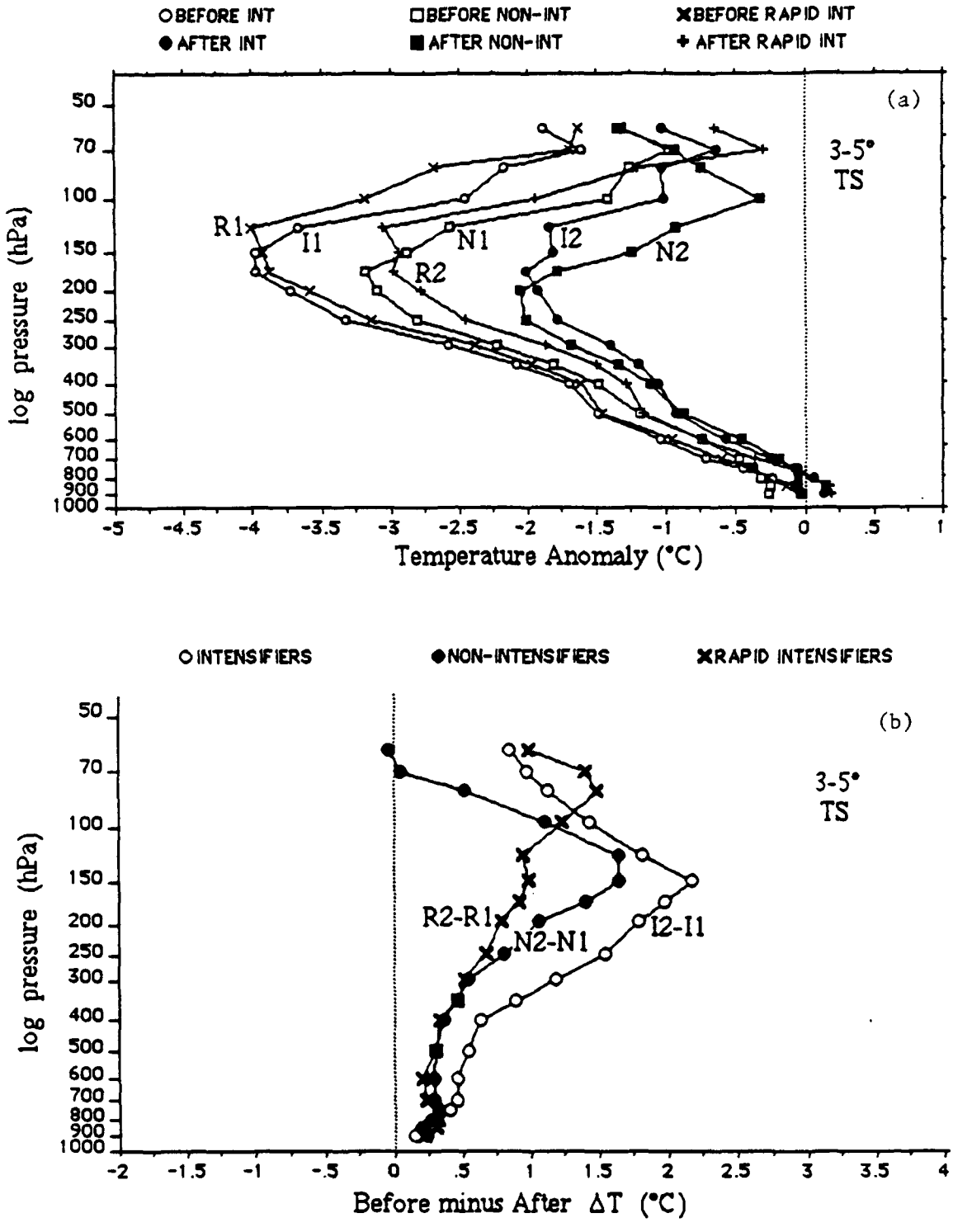

Figure 7.15: Temperature anomaly profiles at the 3-5° radial belt for composite stratifications initially at tropical storm intensity (a) and the change of temperature after the intensification or non-intensification event (b).

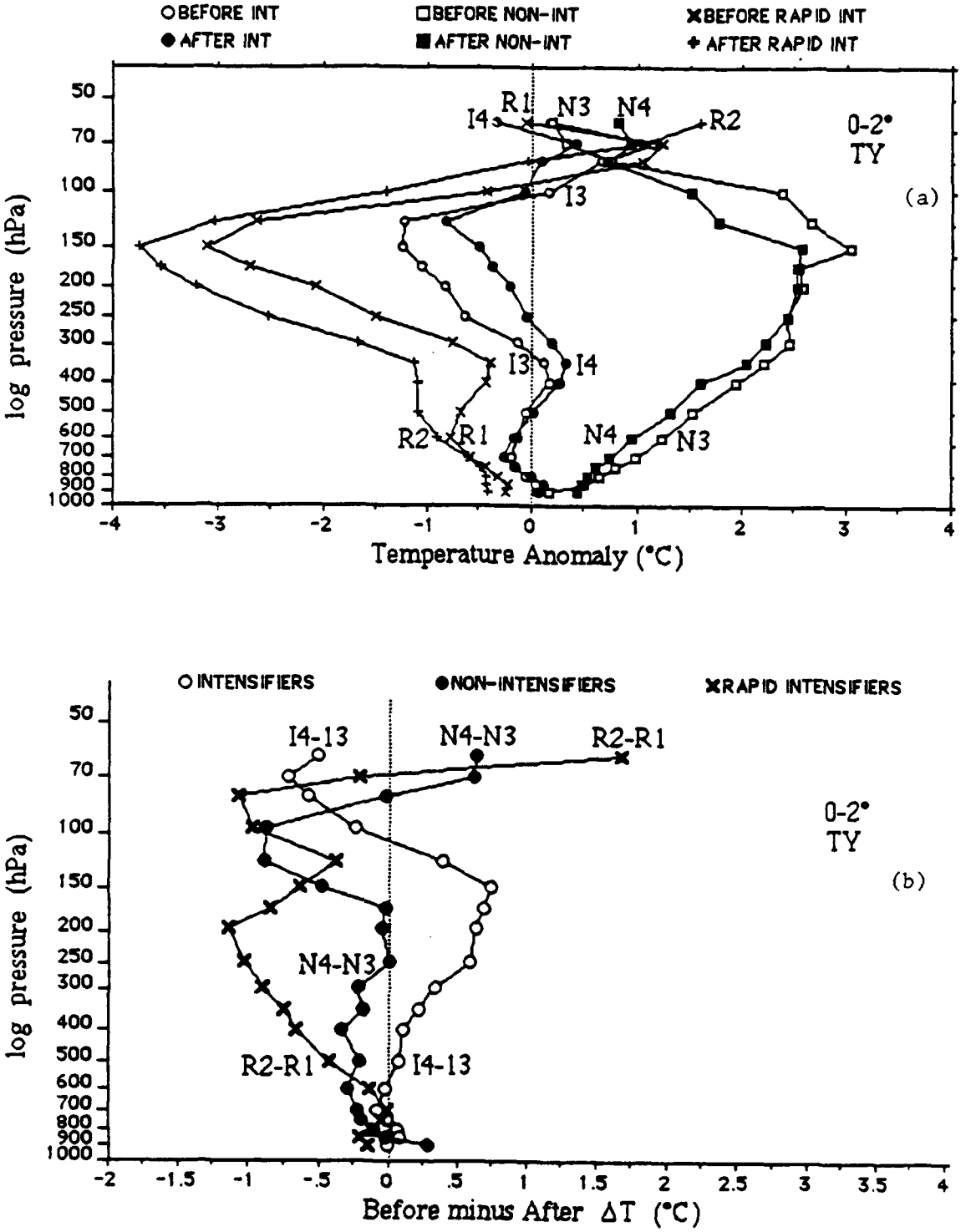

Figure 7.16: Temperature anomaly profiles at the 0-2° radial belt for composite stratifications initially at typhoon intensity (a) and the change of temperature after the intensification or non-intensification event (b).

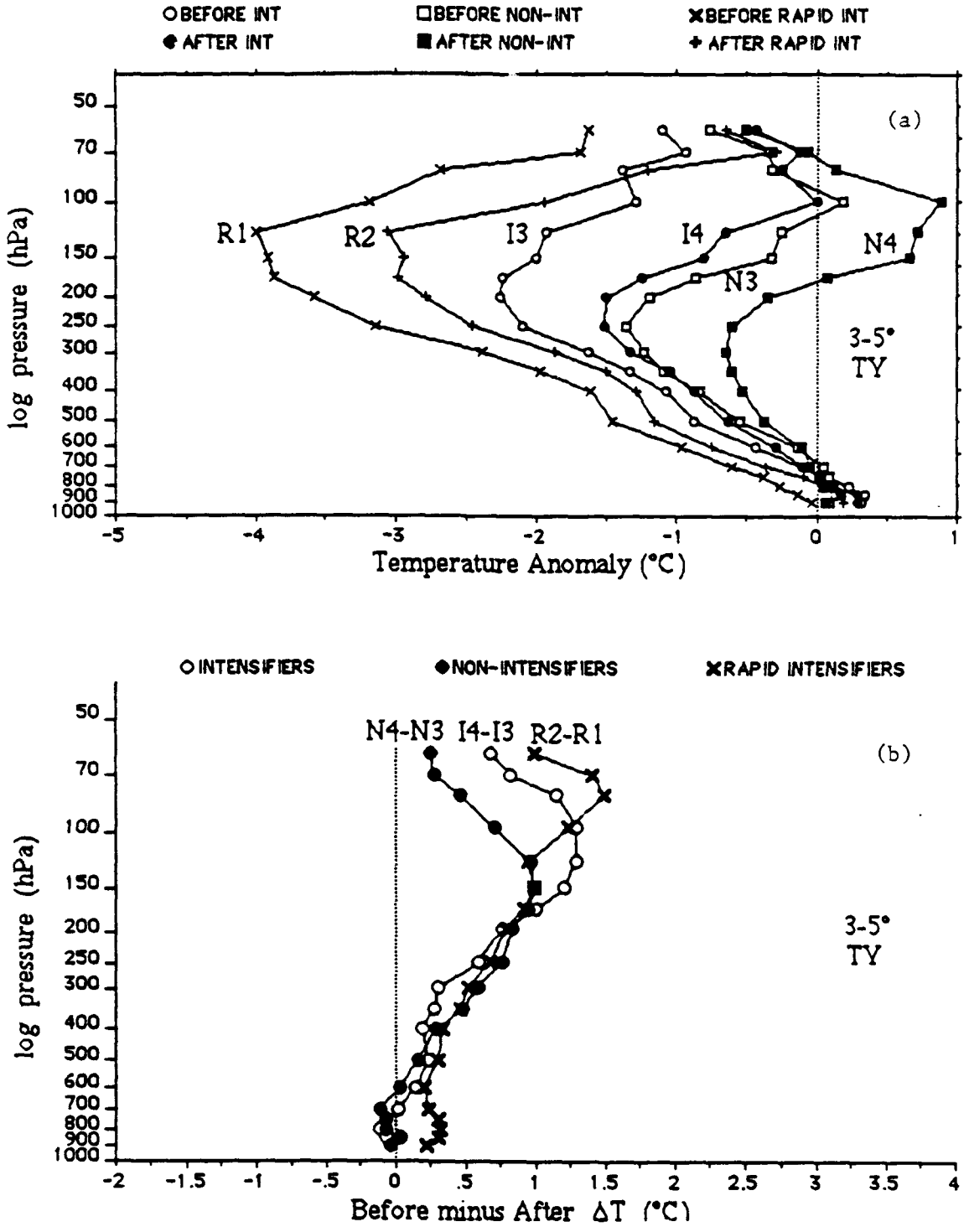

Figure 7.17: Temperature anomaly profiles at the 0-2° radial belt for composite stratifications initially at tropical storm intensity (a) and the change of temperature after the intensification or non-intensification event (b).

feature of rapid intensity change, individual soundings within 111 km (1°) of the center were obtained from the composite data sets. The number of soundings within 1° of the center is quite small; a total of only 23 complete (stratosphere included) soundings were available from a total of 10 composite data sets (Table 7.2). Of particular interest are the two soundings in composite R1, taken within 24 hours of the onset of rapid intensification. This is the only data available which directly measures, in the vertical, the distinctive tropospheric and lower stratospheric characteristics of the inner core eyewall region in rapidly intensifying typhoons. There were no 0-1° soundings in the lower stratosphere less than 12 hours after the onset of rapid intensity change (composite R2).

Table 7.2: Upper level temperature of soundings within 111 km of the tropical cyclone center. Soundings are grouped according to composite classification (see Table 7.1). Boxed values are 90th percentile of warmest temperatures. Circled values are 10th coldest percentile.

COMP	DATE	MSLP	50	60	70	80	100	125	150	175	200
R1	05 SEP 71	989	-60.8	-62.4	[-63.8]	[-66.4]	[-72.5]	-75.5	-67.9	-59.1	-51.8
R1	28 JUL 77	997	[-53.6]	[-57.1]	[-60.3]	[-64.3]	[-66.6]	-70.7	-63.0	-54.0	-47.0
I1	22 OCT 68	992	-66.0	-68.5	-70.5	-78.1	-76.4	-75.1	-65.6	-57.1	-49.8
I1	11 JUL 57	1006	-60.0	-62.8	-66.9	-70.2	-75.0	-74.7	-66.6	-59.0	-51.8
I1	20 APR 69	989	-66.0	-69.9	-78.0	(-84.1)	-76.4	-73.9	-64.9	-56.1	-48.6
I1	15 MAY 76	1004	-61.5	-67.5	-74.7	-77.0	-77.4	-76.2	-67.5	-58.8	-51.3
I3	23 FEB 70	961	-64.0	-69.0	(-78.5)	-82.0	-81.9	-72.1	-64.1	-57.3	-50.5
I3	17 AUG 64	975	-58.8	-64.5	-68.0	-67.0	-72.7	-72.7	-64.5	-56.0	-48.0
I4	05 AUG 59	971	[-56.0]	[-59.3]	-64.9	-69.6	[-72.5]	-71.4	-62.0	-53.5	-45.6
I4	31 JUL 77	[932]	-60.5	-62.4	-64.0	-68.9	-73.0	[-64.5]	-58.3	-51.0	-44.3
N1	08 OCT 64	(1005)	-66.7	-68.4	-68.6	-68.5	-80.1	(-76.9)	(-70.6)	(-61.0)	(-52.8)
N1	14 NOV 65	1002	-66.4	-69.2	-70.5	-77.1	-79.4	-75.7	-67.2	-58.8	-51.3
N1	14 NOV 65	1001	-62.5	(-70.6)	-72.0	-76.9	(-82.0)	(-76.7)	-68.4	-60.1	(-52.8)
N1	15 NOV 65	1000	(-67.0)	-69.9	-69.6	-75.9	-81.5	-75.4	-67.5	-59.8	-51.3
N1	19 NOV 68	1004	(-67.7)	-69.5	(-80.0)	-81.0	(-85.0)	-75.0	-66.0	-57.1	-49.8
N1	17 SEP 75	(1008)	-61.8	-63.5	-67.7	-72.2	-76.5	-75.7	(-70.5)	(-61.8)	(-54.3)
N1	06 OCT 59	997	-58.3	-63.8	-69.2	-74.0	-76.0	-71.4	-67.9	-58.5	-50.1
N3	15 AUG 73	980	-61.3	-64.7	-67.7	-72.2	-75.5	-68.5	-60.5	-52.0	-44.3
N3	18 AUG 74	974	-63.8	-65.8	-67.4	-72.6	-77.4	-67.5	[-57.6]	[-49.8]	[-43.0]
N4	13 NOV 67	935		(-70.0)	-75.2	(-86.0)	-79.5	-69.5	-63.3	-55.3	-47.8
N4	20 AUG 60	978	-58.1	-60.6	-65.0	-68.6	-73.1	-72.9	-64.0	-55.3	-47.5
N4	23 SEP 72	934	-59.0	-62.4	-65.4	-70.1	-73.7	[-65.7]	[-55.6]	[-49.0]	[-38.8]
N4	29 AUG 71	[920]	-61.8	-63.8	-65.4	-69.7	-72.7	-68.7	-62.6	-54.3	-46.5
MEAN		981	-61.9	-65.6	-69.3	-73.6	-76.4	-72.5	-64.6	-56.3	-48.7
ST. DEV.		27	3.8	3.8	5.1	5.9	4.2	3.6	3.9	3.5	3.7

The most distinct differences for rapid intensifiers is in the vicinity of the tropopause. Even though there are only two stratospheric soundings available before the onset of rapid intensity change, these two are warmer in the lower stratosphere at 70 to 100 hPa than any of the other 21 intensifying and non-intensifying soundings. Below the troposphere at 125 and 150 hPa, the temperatures before rapid intensity change were close to average. Therefore, the 70-125 hPa pressure layer near the tropopause was unusually warm for both cases prior to the onset of rapid intensity change. Upon close examination of the data in Table 7.2, it would appear that the tropopause levels of the two soundings prior to the onset of rapid intensity change were lower than the other soundings taken within 111 km. The coldest temperatures for the rapid intensifiers were at 125 hPa, while all of the other 21 soundings had the coldest temperatures at 100 hPa or higher. This is not due to initial MSLP differences or the time of year. Other soundings of approximately the same central pressure in the same months had higher tropopause levels.

Perhaps the most interesting feature of the rapid intensifier soundings is the unusually large warm anomalies near the tropopause (Fig. 7.18). In the first sounding, taken on 5 September 1971 by Wake Island in Super Typhoon Wendy, the 125 hPa temperature is 3.0° colder than the mean, but at 100 hPa the temperature is 3.9° warmer than the mean and 7.2° warmer than average at 80 hPa. The minimum central pressure of Wendy dropped 49 hPa in 24 hours, with an onset 21 hours after the sounding was taken. The second sounding, taken on 28 July 1977 by Kadena AB, Okinawa, on Typhoon Vera, the 125 hPa temperature is 1.8° warmer than the mean, and 9.8° warmer than the average at 100 hPa. The central pressure of Vera decreased by 46 hPa in 24 hours, commencing 14 hours after the sounding.

These warm anomalies may be due simply to the fact that the tropopause level appears to be lower in these two particular cases, but it is equally likely that there is unusually strong subsidence in the lower stratosphere prior to the onset of rapid intensity change which would tend to bulge the tropopause level downward. Regardless of the reason, the 0-1° soundings prior to the onset of rapid intensification tend to support the hypothesis that the inner core of rapid intensifiers is unusually warm in the vicinity of the tropopause

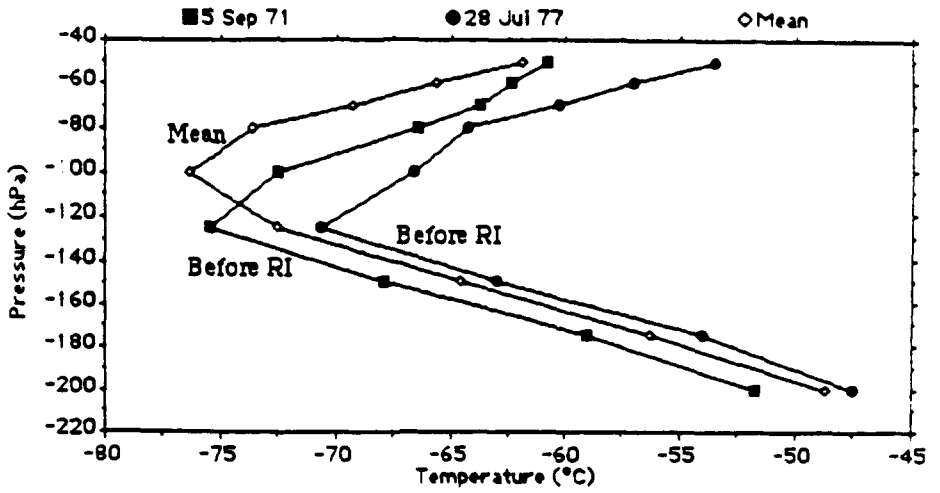

Figure 7.18: Vertical temperature profiles of two soundings taken within 1° of the center of rapidly intensifying tropical cyclones less than 24 hours prior to the onset of rapid intensity change. The mean sounding for 23 NWPAC rawinsondes within 1° of the cyclone center is also shown.

level. This has important consequences in relation to changes in surface pressure. The higher and more intense the inner core warming, the larger the drop in central pressure.

It is uncertain if the inner core of rapid intensifiers remains anomalously warm near the tropopause as intensification proceeds or whether their vigorous deep convection would act to force the tropopause higher and colder (Simpson, 1947; Palmén, 1948; Arakawa, 1950; Gentry, 1967; Koteswaram, 1967; Sugg, 1967) .

While there is a lack of data to support it, a hypothesis of what triggers rapid intensity change may be found in the lower stratosphere. Overshooting cumulonimbus towers that penetrate into the stratosphere transport energy and momentum out of the troposphere. If we assume that prior to rapid intensification, the relatively cold upper troposphere found to be characteristic of rapid intensifiers acts to destabilize the environment, then the vertical motion at the tropopause would be greater for rapid intensifiers than for non-rapid intensifiers and convection could penetrate to a greater depth in the stratosphere before subsiding.

Enhanced subsidence could significantly increase the temperature of the lower stratosphere (Holland, *et al.*, 1984). Higher stratospheric temperatures could then act to trigger rapid pressure change at the surface. It is possible that rapid intensifiers are initially warm

core in both the troposphere and stratosphere. After intensification, rapid intensifiers may remain unusually warm near the tropopause, but it is more likely that they develop a cold core aloft in the lower stratosphere due to mixing of colder air from the troposphere. A cold core near the tropopause is more typical of an intense tropical cyclone (La Suer and Hawkins, 1963; Koteswaram, 1967; Gentry, 1967).

7.8 Rapid Intensification in the North Atlantic Region

In the North Atlantic, there is one well documented case of the inner core characteristics of Inez in 1966 near the onset of rapid intensity change (Hawkins and Imbembo, 1976). Concurrent research flights by three aircraft at different levels into Hurricane Inez before and after a period of "rapid intensification" ($\approx 40\ hPa\ d^{-1}$) also revealed the same general tangential wind and temperature anomaly features as the 0-1° soundings and the 0-2° composited rawinsonde data set of rapid intensifiers discussed in this chapter. During the rapid intensification period of Inez (Fig. 7.19a), there was a large increase in tangential winds in the upper troposphere and very little spin up of the low level winds outside a radius of 0.5° (55 km). The largest temperature increases occurred in the upper troposphere in the region of maximum vertical wind shear and concentrated within the eye (Fig. 7.19b).

There is a lack of data between the 180 hPa and 500 hPa flight levels and near the tropopause level. Hawkins and Imbembo interpolated the flight data to create vertical cross sections of Inez which may have significant errors. But if the cross sections of Inez are generally correct before and after the onset of rapid intensification, these data tend to support the hypothesis that rapid intensifiers are characterized by a relatively large increase in tangential winds at upper levels and that the spin up of the upper level cyclonic circulation produces large inner core temperature anomalies near the tropopause.

7.9 Geopotential Thickness Anomalies

Corresponding to the temperature anomalies discussed in sections 7.6 and 7.7, warm temperatures in a given pressure layer would be indicated by a greater thickness in that

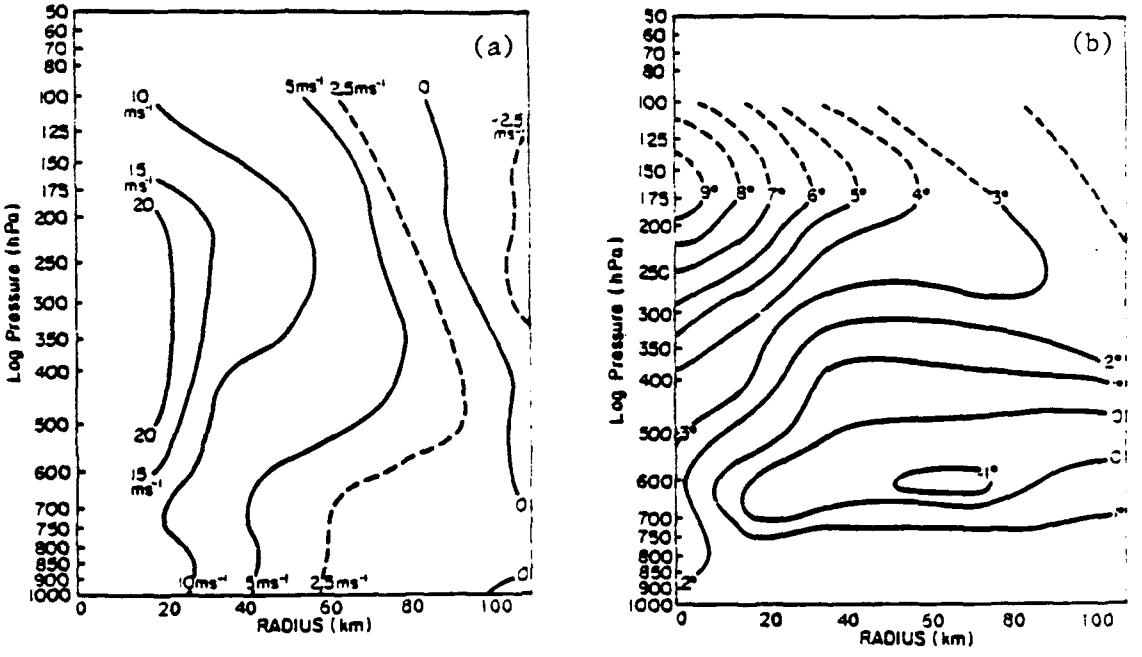

Figure 7.19: Cross sections of wind velocity (a) and temperature (b) changes observed within 1° of the center of Hurricane Inez during its rapid intensification period from 27 to 28 September, 1966. Concurrent aircraft missions were performed at the 180, 500, 650, 750 and 900 hPa pressure levels to obtain a rather complete horizontal and vertical depiction of the inner core of Inez during a rapid intensity change from 970 to 927 hPa central pressure (from Hawkins and Imbembo, 1976).

layer. The 300 hPa level was chosen to delineate the upper (100 to 300 hPa) and middle (300 to 500 hPa) troposphere layers. A thickness layer of 50 to 100 hPa represented the lower stratosphere. Composite thicknesses at 0-2° and 3-5° were computed for the following before/after classifications: rapid intensifiers, intensifiers, and non-intensifiers. Composites initially at tropical storm (I1, I2, N1, N2) and typhoon (I3, I4, N3, N4) intensity were averaged together to simplify the comparison and create stratifications of nearly equal initial intensity.

Rapid intensifiers have negative thickness anomalies in the middle and upper troposphere, but large positive inner core anomalies in the lower stratosphere (Fig. 7.20). This sharp reversal of thickness anomaly near the tropopause is another strong indication that an unusually warm layer exists in the inner core near the tropopause of rapid intensifiers. By contrast, non-intensifiers also have relatively large positive inner core thickness anomalies near the tropopause, but since the thickness anomalies are also positive at lower layers, this is an indication of a deep warm core that extends to the tropopause. This is typical for mature tropical cyclones (Arakawa, 1950; LaSuer and Hawkins, 1963; Gentry, 1967; Koteswaram, 1967; Hawkins and Imbembo, 1976).

Figure 7.21 is a depiction of the 3-5° (outer core) thickness anomalies for before and after composites. Note that before rapid intensification, negative thickness anomalies persist at all layers, but that after rapid intensification there is a large thickness anomaly in the 50-100 hPa layer. Conceptually, if the basic compositing assumptions made earlier are accurate, the warm anomaly near the tropopause is initially confined to the inner region and as rapid intensification proceeds, the warm layer spreads out at the tropopause to larger radii. The resulting hydrostatic balance would cause surface pressures to fall in the 3-5° outer core region. Over time, this would reduce the inward pressure gradient force in the boundary layer unless the inner core is able to sustain heating as high as possible in the atmosphere at a rate greater than the outer core. It is very difficult to maintain this rate of upper level heating in the inner core tropopause level for extended periods of time because the warm anomaly does not remain confined to the inner core, but extends out to larger radii and hydrostatically weakens the pressure gradient force at the surface.

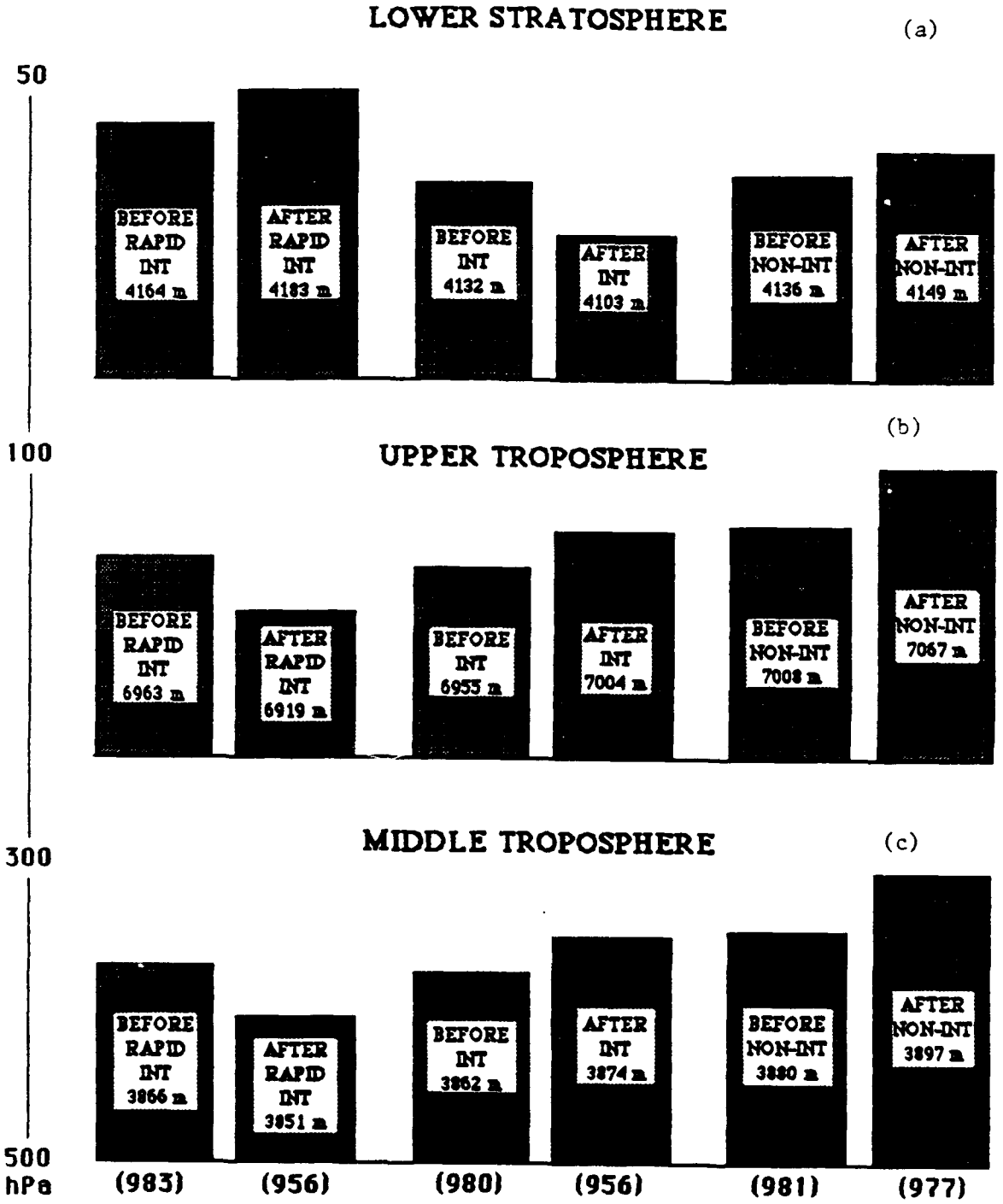

Figure 7.20: Depiction of pressure thickness values for before and after classifications of rapid intensifiers, intensifiers, and non-intensifiers at the 0-2° radial belt in the lower stratosphere (a), upper troposphere (b), and the middle troposphere (c). Mean central pressure for each composite classification is shown in parentheses at the bottom.

Without a sharp pressure gradient at the inner core, the rapidly intensifying tropical cyclone is unable to continue to deepen at a rapid rate. This is a possible explanation why rapid intensifiers deepen so quickly in the first few hours after onset and rarely intensify at a rapid rate for longer than 24 hours (Holliday and Thompson, 1979).

7.10 Horizontal and Vertical Cross-Sections of Temperature and Tangential Winds

Discussion of the distinctive characteristics of rapid intensifiers in this chapter has been confined to the inner (0-2°) and outer (3-5°) circulation regions. This is because most of the large differences between rapid and non-rapid intensifiers occur at the inner core. The 3-5° radial belt was considered representative of the mean environmental conditions that would be altered by the presence of a tropical cyclone, while sounding data outside 5° radius would not be expected to yield significant differences.

Mean values of the data used in this research from the stratified composite sets was organized in tabular form by pressure level and radial belt, hence it is possible to get a more complete picture of the distinctive characteristics of each stratification from horizontal and vertical cross sections of the mean data. Temperature anomalies before intensification or non-intensification, along with the changes of temperature and the tangential component of the wind during the intensification or non-intensification event are presented in Figs. 7.22 to 7.24.

The cross sections illustrate how (and why) the upper level temperature structure of rapid intensifiers, non-rapid intensifiers, and non-intensifiers are distinctly different. In Fig. 7.22, note that before the intensification or non-intensification event, non-intensifiers are much warmer than intensifiers and rapid intensifiers in the middle and upper troposphere. At the inner core, rapid intensifiers have progressively warmer temperature anomalies in the lower stratosphere. Non-intensifiers and intensifiers have colder inner core temperature anomalies above the tropopause. The temperature structure of rapid and non-rapid intensifiers is strikingly similar outside the inner core region at radii >150 km.

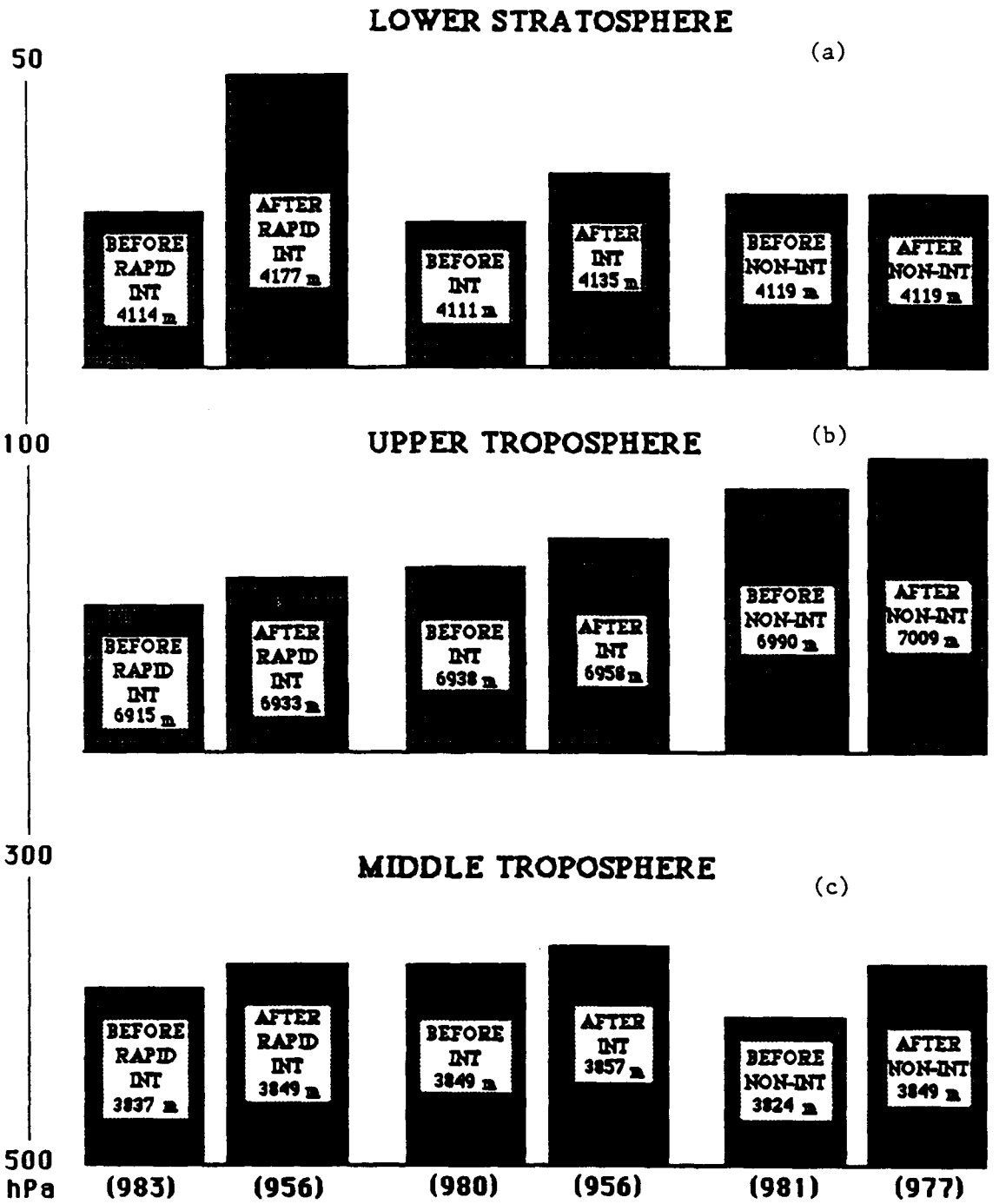

Figure 7.21: Same as Fig. 7.20 except at the 3-5° radial belt.

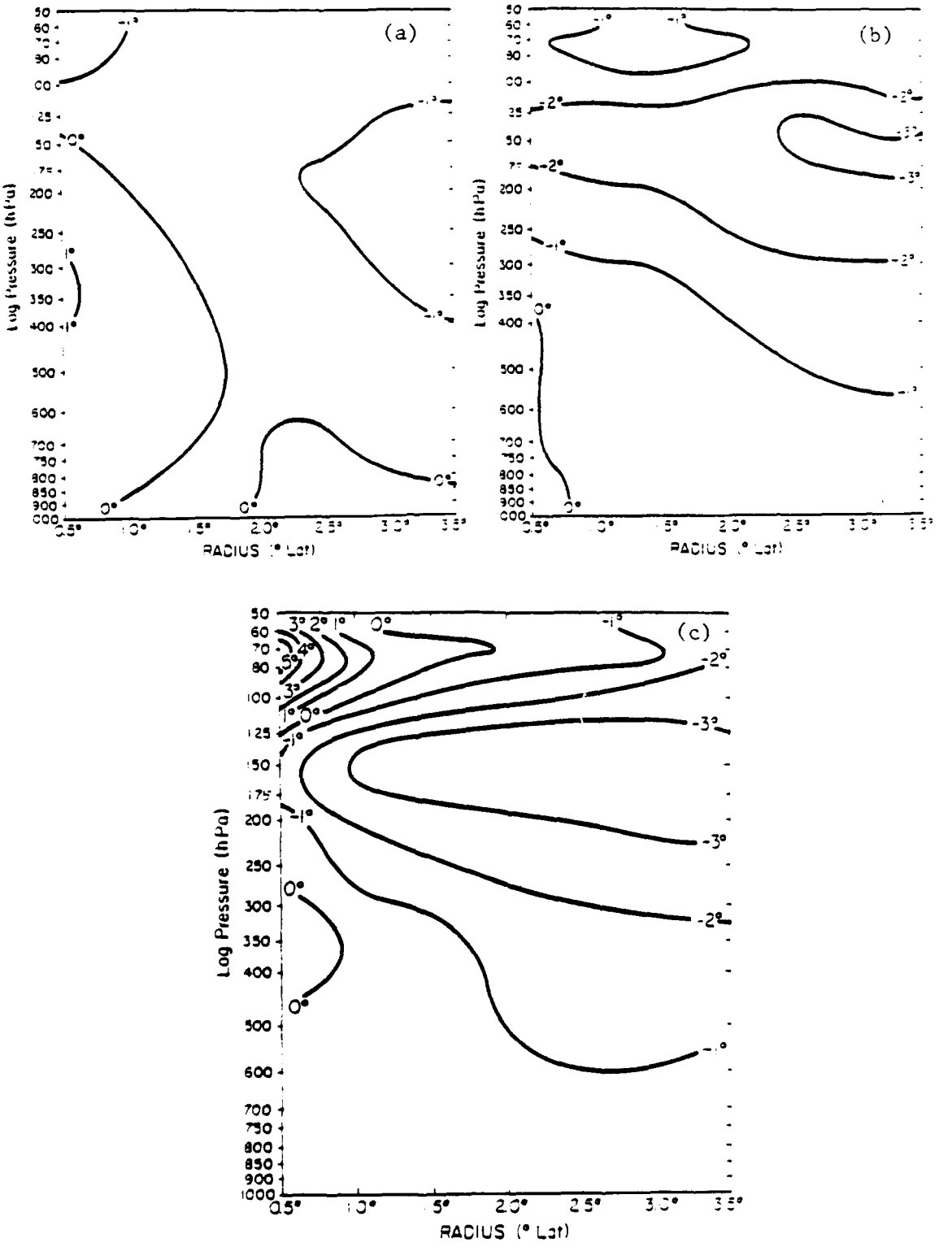

Figure 7.22: Composite cross sections of temperature anomalies before rapid intensification (a), before intensification (b), and before non-intensification (c). Temperature anomalies were determined by subtracting a mean 0-4° tropical cyclone sounding given by Frank (1977).

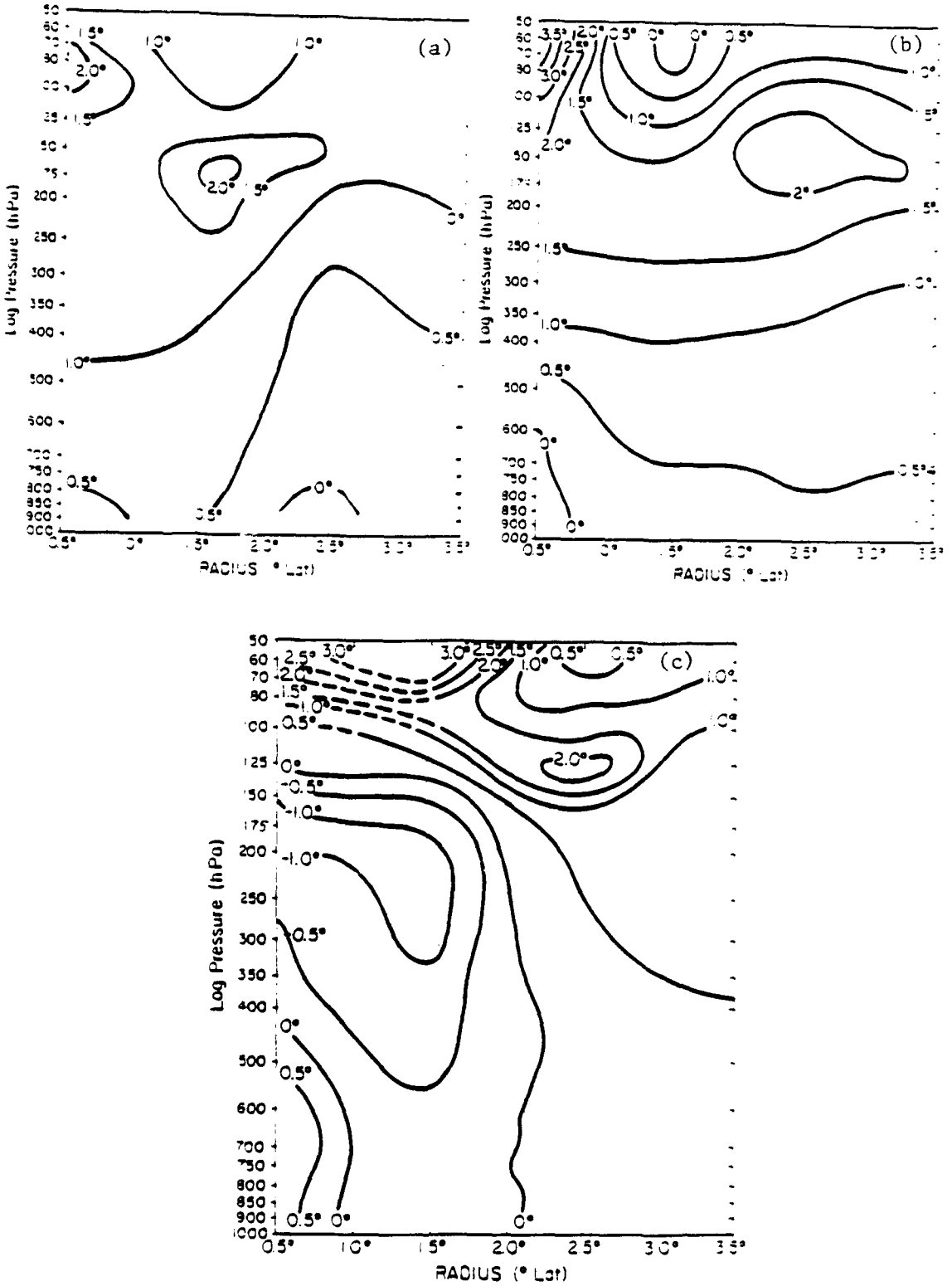

Figure 7.23: Composite cross sections of temperature change after rapid intensification (a), after intensification (b), and after non-intensification (c).

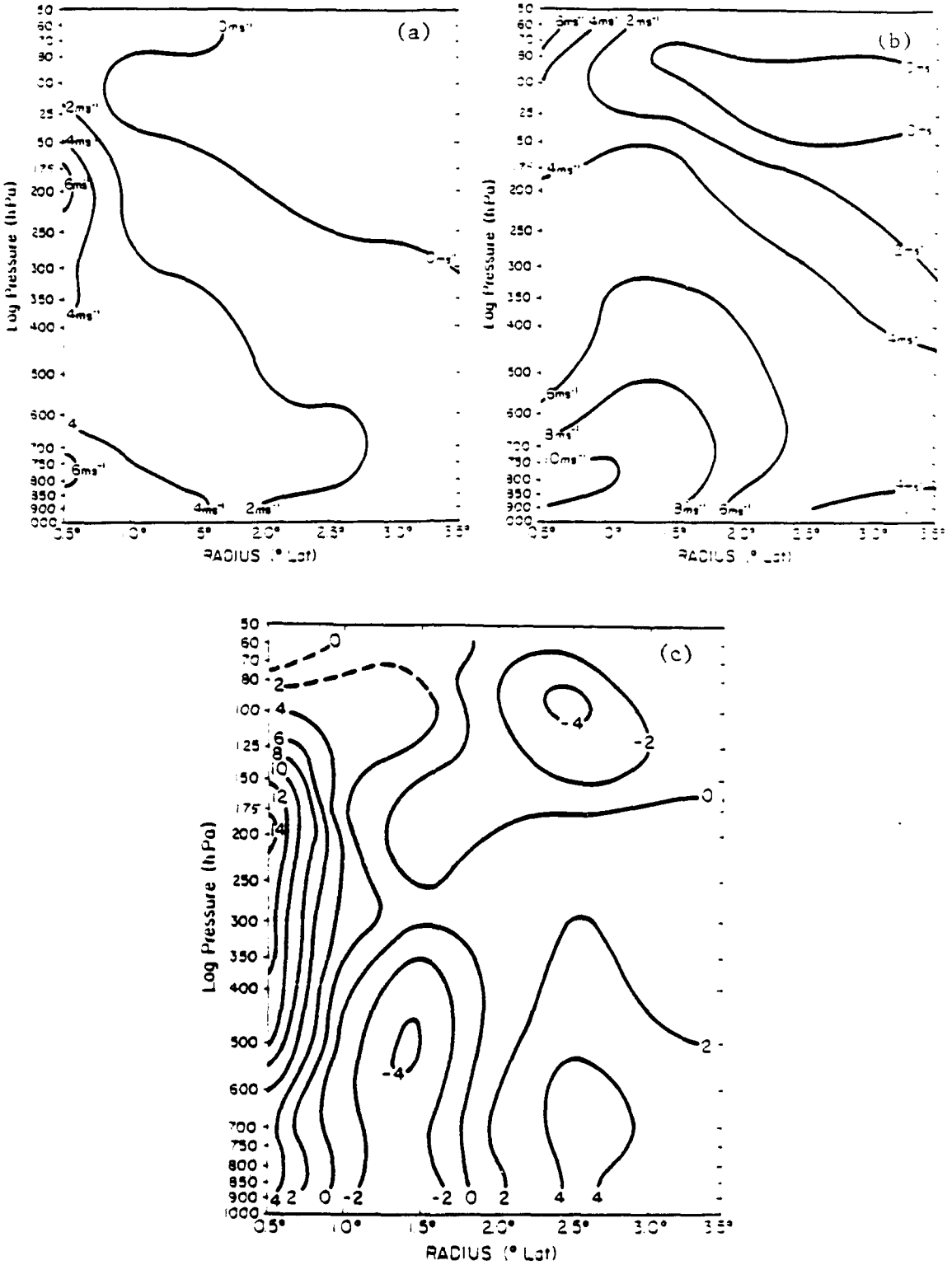

Figure 7.24: Composite cross sections of change of the tangential wind component after rapid intensification (a), after intensification (b), and after non-intensification (c).

Less similarity exists between rapid and non-rapid types after intensification. During rapid intensification, the middle and upper troposphere of the inner core is considerably colder than for non-rapid intensifiers. Within 2° (222 km) of the center, there is no significant inner core warming is apparent below the tropopause level of rapid intensifiers (Fig. 7.23). The inner core environment of rapid intensifiers maintains buoyant instability. The inner core upper level warming of the intensifiers and non-intensifiers acts to stabilize the tropical cyclone environment and would reduce subsequent deep convection. Rapid intensifiers appear to concentrate their inner core warming as high and as close to the cyclone center as possible.

The most distinctive feature of rapid intensifiers is the inner core increase in tangential winds which occurs, not near the surface, but in the upper troposphere (Fig. 7.24). The tangential wind increase during rapid intensification is nearly uniform in the 150 to 500 hPa layer. This is evidence that vertical transport of low level cyclonic momentum does take place at the inner core during rapid intensity change. Vertical momentum transport has spun up the upper level circulation and forced the region of maximum vertical shear to very high levels (above 150 hPa). When we refer back to the change of temperature profile of rapid intensifiers in Fig. 7.24, it is likely that the largest inner core temperature increases are above 150 hPa. This correlates exactly with the region of maximum vertical wind shear.

7.11 Summary

A picture of the distinctive characteristics of rapid intensifiers is beginning to emerge. It has been obtained from examination of composited rawinsonde data at radial belts of 0-2° and 3-5° and cross sections out to 400 km.

Rapid intensifiers are found to have less unidirectional flow across their upper level center, and thus better vertical alignment, than other stratifications that intensified in a non-rapid manner.

Vertical profiles of the tangential component of the wind revealed that, in the 0-2° inner circulation region, rapid intensifiers have less vertical wind shear in the middle and

upper troposphere than similar profiles of non-rapid intensifiers. Even though the intensity, as measured by the MSLP, changes rapidly during intensification, a corresponding increase in the low level tangential winds and outer core wind strength (OCS) was not observed. During rapid intensification, the tangential winds in the inner core region of the upper troposphere increase. Most of the inward heating is concentrated near the tropopause at the level of maximum shear.

Rapid intensifiers are relatively cool through most of the troposphere but relatively warm above 150 hPa. This allows deep Cb convection to continue due to minimal stabilization in the middle and upper troposphere.

The results of this chapter highlight that distinctive differences exist at the inner core of rapidly intensifying tropical cyclones. While the lack of soundings close to the center of rapidly intensifying tropical cyclones makes it difficult to draw any conclusions from the individual soundings within 111 km of the center, it is important to note that of the available soundings, rapid intensifiers had the warmest temperatures of all near the tropopause. The data compiled by Hawkins and Imbembo (1976) of a rapid intensifier in the Atlantic add further support to the relatively few 0-1° soundings obtained from the western North Pacific. There were, however, more soundings available at the 1-2° radial belt. These soundings support the presence of unusual warm inner core anomalies near the tropopause of rapid intensifiers.

The data presented here offers a physical explanation for rapid intensification and is believed to be useful for numerical models which are developed to understand the physical processes of intensity change. Finer resolution of the inner core structure of rapid intensifiers should demonstrate the effectiveness of the inner core warming near the tropopause level caused by placing the vertical shear of the tangential wind as high and as close to the center as possible.

Chapter 8

DISCUSSION AND APPLICATIONS

8.1 Conclusion

The largest forecast intensity errors are due to under-forecasting rapid rates of intensification. The objective of this research was to determine if prediction of rapid intensification is possible and to provide operationally useful techniques that can be applied by the forecaster to reduce large forecast errors.

Climatological factors are important in assessing whether rapid intensification is likely or not. The best and most operationally significant prediction technique is based on the relative concentration of inner to outer deep convection. A prediction method which uses the 24 hour running mean pixel count values of inner radius (0-2°) convection colder than -75°C and outer radius (2-6°) convection colder than -65°C appears to be an effective prediction tool. An intersection of the two pixel count plots is an indication that extreme concentration of inner core convection was occurring and that the onset of rapid intensification was imminent. If this method were used in the western Pacific during 1983 to 1985, it would have correctly predicted the onset of rapid intensification in 7 of 10 rapid intensifiers and nearly all non-rapid intensification periods. A complete description of the methods used to predict rapid intensity change and their application to operational forecasting is given in Appendix A.

The prediction technique tends to support the hypothesis that intensification is preceded by enhanced convection, and not vice versa. A lag appears to exist between increases in deep cumulus convection and intensity change. For rapid intensification events, the perceived lag is more readily apparent because of (relatively) large increases in inner core convection over a shorter period of time. Large increases in inner core convection

compared to outer core convection would indicate that a relatively large increase in pressure gradient at the surface would be concentrated at the inner core in the near future. This is believed to be the reason why the relative concentrations of inner and outer core convection, as observed from satellite, can effectively predict the onset of rapid intensity change.

Minimal undidirectional flow across the cyclone center is considered necessary for spin up of the inner core at upper levels. A cyclonic circulation as high in the atmosphere as possible results in a level of maximum shear near the tropopause. In theory, inner core warming occurs near the tropopause at the level of maximum shear. This results in more rapid intensity change due to the fact that for a given temperature change between equal pressure layers, there is a larger pressure thickness change if the warming is placed higher in the atmosphere.

Observational evidence of the distinctive characteristics of rapid intensifiers appears to agree with the theory of rapid intensification. Rapid intensifiers have less net ventilation (asymmetrical outflow) across their cyclone center than other composite stratifications of intensifiers and non-intensifiers. Vertical shear and warm inner core temperature anomalies are concentrated near the tropopause level.

Rapid intensity change is believed to be directly linked to the physical processes occurring only within the inner core. Outside of 2° radius, very little structural change is apparent during rapid intensification. The outer core response would seem to be independent of the substantial changes occurring within 2° of the center. The relative concentration of convection within 2° which occurs prior to the onset of rapid deepening would also seem to clearly indicate the physical processes of the inner core are of greater importance than outer core features in regards to the rate of intensification. Thus, we can consider rapid intensity change to be limited to a very small, intense inner core and not directly linked to environmental conditions at larger radii, such as outflow channels and tropical upper tropospheric trough (TUTT) interactions.

The most widely accepted physical explanation for rapid intensity change has been the existence of strong asymmetrical (single or multiple) outflow channels (Sadler, 1978;

Holliday and Thompson, 1979; Holland and Merrill, 1984; Chen and Gray, 1985; Merrill, 1988). A double outflow channel exporting heat and mass in opposite directions away from the upper levels of the intensifying tropical cyclone is generally considered to be the most effective way to maintain upper level buoyant instability necessary for continued deep convection.

Although intensification is frequently associated with multiple outflow channels, the author does not believe intensification is directly linked to a special dynamic response of the deep convection to the outflow as has been hypothesized by Holland and Merrill (1984) and numerous other authors (Alaka, 1962; Sadler, 1978). The primary link would appear to be the relationship of such asymmetric outflow "jets" to the development of minimum net ventilation across the tropical cyclone inner core region.

Multiple outflow channels appear to play an important indirect role in the intensification process by reducing unidirectional shear across the center of the developing tropical cyclone. Any environmental conditions which would minimize the magnitude of net ventilation across the top of the tropical cyclone would be more favorable for intensification. It is very likely that if there is a lack of unidirectional shear (relative to storm motion) across the center of the rapid deepener, multidirectional outflow will follow as a natural consequence, regardless whether or not strong outflow channels initially exist.

Previous research has determined that the most favorable environmental conditions for rapid intensification are outflow "jets" on the poleward and equatorward sides of the cyclone or a tropical upper tropospheric trough (TUTT) located in a favorable position poleward of the disturbance. In Fig. 8.1, it is evident that these outflow patterns would create a region of minimum ventilation in the transition zone from easterly winds on the equatorward side (relative to the moving center) to (relatively) westerly winds on the poleward side (Fig. 8.2). It is in this region of minimal unidirectional shear that rapid intensification is possible if a spin up of the upper level tangential winds at the inner core occurs.

Enhanced outer radius outflow may cause a spin up of the outer core winds. As previously discussed, inner and outer core tangential winds are not well related to each

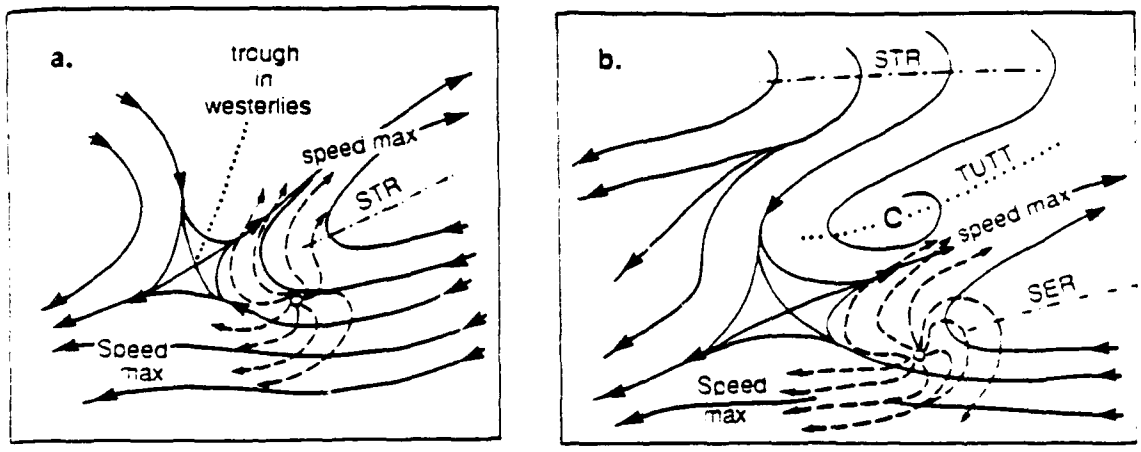

Figure 8.1: Illustration of two synoptic streamline models of upper level environmental flow patterns associated with enhanced tropical cyclone intensification. "STR" is the subtropical ridge, "SER" the subequatorial ridge, and "TUTT" is the tropical upper tropospheric trough (*et al.*, 1987).

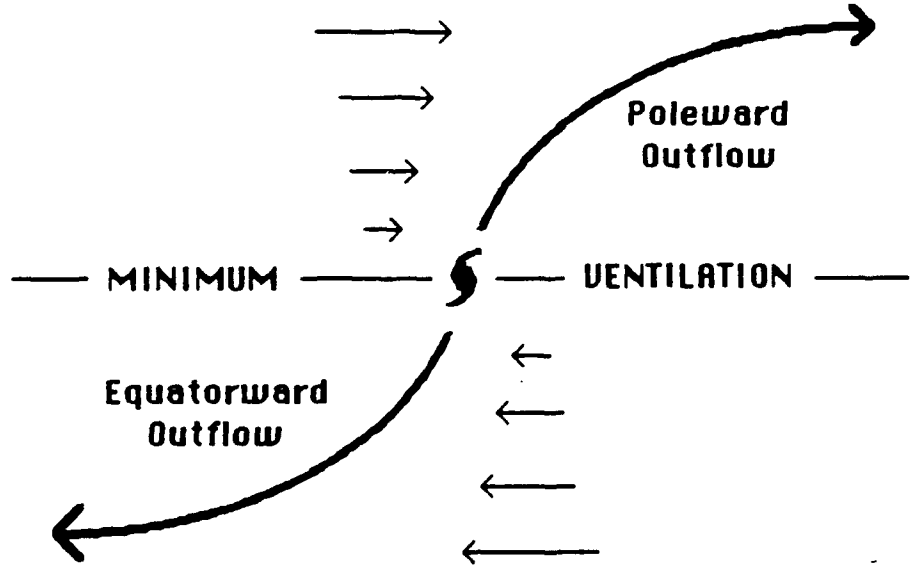

Figure 8.2: Illustration of the effect (relative to storm motion) dual outflow channels associated with mid-latitude troughs and TUTTs have in reducing the amount of net ventilation (unidirectional shear) across the top of an intensifying tropical cyclone. Minimum net ventilation occurs in a region of weak easterly winds for a cyclone moving at a moderate rate to the west- northwest.

other. The concept of outflow channels being necessary for removal of excess heat in order for rapid intensification to occur appears flawed. In the opinion of the author, it is necessary to *retain* as much heat as possible close to center without stabilizing the eyewall deep convection (which is most crucial).

The theory and observations presented in this study offer a more plausible physical explanation of the process of rapid intensification.

8.2 Recommendations

The pixel plot intersection technique discussed in this thesis should be adopted immediately in the western Pacific in order to predict the onset of rapid intensity change. Operational application of this prediction method should dramatically reduce the magnitude of 24 hour forecast intensity errors caused by under forecasting rapid intensity change while at the same time not increasing the false alarm rate. There has been only limited success in previous attempts to predict rapid intensification even with the availability of aircraft (Dunnavan, 1981), so the fact that aerial reconnaissance of tropical cyclones is no longer performed in the western Pacific is not a major factor except that verification of rapid intensification events will be more difficult without "ground truth" aircraft measurements of minimum sea level pressure changes.

The focus of this research has been the western Pacific, which is the most active tropical cyclone basin in the world and where the majority of rapid intensifiers occur. Application of this prediction technique (based on 10 km resolution GMS infrared imagery) for higher resolution GMS data and to the Atlantic and the Southern Hemisphere would require additional calibration.

The distinctive characteristics of rapid intensifiers considered in Chapter 7 are also based on a small set of rawinsonde data obtained from the northwest Pacific basin. While the theoretical concepts discussed here are thought to be valid at other locations, other additional factors may have to be considered in the other tropical cyclone regions. The key is availability of rawinsonde data within 2° of the center of rapidly intensifying tropical cyclones and stratification into proper categories. Future research of the distinctive

characteristics of rapid intensifiers should attempt to obtain more inner core soundings of rapid intensifiers than was available to the author in the 1957-77 composited rawinsonde data set at Colorado State University.

The unusually warm inner core temperature anomalies in the upper troposphere and lower stratosphere typical of rapid intensifiers might also be measured by specially designed research aircraft (Gray, 1979) or by the satellite microwave data (Kidder, *et al.*, 1978; Veldon and Smith, 1983), which is currently available on the DMSP and NOAA polar orbiting spacecraft. Aerial reconnaissance of rapid intensifiers using jet aircraft would provide a more complete description of their upper level structure than is available from compositing the relatively rare inner core rawinsonde soundings taken near the onset of rapid deepening. In particular, measurement of asymmetrical relative wind across the cyclone center out to 2-3° radius would determine the relative importance of minimal ventilation to rapid intensity change. Improvements in the resolution and capabilities of satellite-based microwave sensors should yield more evidence of unusually warm temperatures near the tropopause of rapidly intensifying tropical cyclones (Veldon, 1989).

REFERENCES

Alaka, M. A., 1962: On the occurrence of dynamic instability in incipient and developing hurricanes. *Mon. Wea. Rev.*, 90, 49-58.

Anthes, R. A., 1982: Tropical cyclones, their evolution, structure and effects. *Meteor. Monogr.*, American Meteorological Society, Boston, MA, 208 pp.

Atkinson, G. D. and C. R. Holliday, 1977: Tropical cyclone minimum sea level pressure maximum sustained wind relationship for the western North Pacific. *Mon. Wea. Rev.*, 105, 421-427.

Arakawa, H., 1950: Vertical structure of a mature typhoon. *Mon. Wea. Rev.*, 78, 197-200.

Arnold, C. P., 1977: Tropical cyclone cloud and intensity relationships. Dept. of Atmos. Sci. Paper No. 277, Colo. State Univ., Ft. Collins, CO, 154 pp.

Bell, G. J., 1975: Observations on the size of the typhoon eye. Proceedings of WMO Technical Conference on Typhoon Modification, World Meteorological Organization Pub., 408, 19-29.

Brand, S., 1973: Rapid intensification and low-latitude weakening of tropical cyclones in the western North Pacific. *J. Appl. Meteor.*, 12, 94-103.

Brand, S. and R. F. Gaya, 1971: Intensity changes of tropical storms and typhoons of the western North Pacific Ocean. Navy Wea. Res. Fac., Norfolk, VA, Tech. Paper No. 5-71, 201 pp.

Chen, L. and W. M. Gray, 1985: Global view of the upper level outflow patterns associated with tropical cyclone intensity changes during FGGE. Dept. of Atmos. Sci. Paper No. 392, Colo. State Univ., Fort Collins, CO, 126 pp.

Dunnavan, G. M., 1981: Forecasting intense tropical cyclones using 700 mb equivalent potential temperature and central sea-level pressure, NOCC/JTWC Tech. Note 81-1, U. S. Naval Oceanography Command Center / Joint Typhoon Warning Center, FPO San Francisco, 96630, 12 pp.

Dvorak, V. F., 1972: A technique for the analysis and forecasting of tropical cyclone intensities from satellite pictures. NOAA Tech. Memo. NESS 36, U. S. Department of Commerce, National Oceanic and Atmospheric Administration, National Earth Satellite Service, Washington, DC, 15 pp.

Dvorak, V. F., 1984: Tropical cyclone intensity analysis using satellite data. NOAA Tech. Memo. NESDIS 11, US Department of Commerce, Washington, DC. 47 pp.

Edson, R., 1985: Synoptic scale view of the differences in tropical cyclone intensity vs. strength change. Extended Abstacts Volume, 16th Conf. on Hurricanes and Tropical Meteorology, AMS, Houston, TX, May 14-17, 1985.

Elsberry, R. L., W. M. Frank, G. H. Holland, J. D. Jarrell and R. L. Southern, 1987: *A Global View of Tropical Cyclones.* Univ. of Chicago Press, 185 pp.

Fleet Weather Central, 1957-59: Annual Typhoon Reports 1956-58. Fleet Weather Central, FPO San Francisco, 96630.

Frank, N. L. and C. L. Jordan, 1960: Climatological aspects of the intensity of typhoons. *Geophys. Mag.*, 30, 131-148.

Frank, W. M., 1977: The structure and energetics of the tropical cyclone. I. Storm Structure. *Mon. Wea. Rev.*, 105, 1119-1135.

Gentry, R. C., 1967: Structure of the upper troposphere and lower stratosphere in the vicinity of Hurricane Isabell, 1964. Papers in *Meteor. and Geophys.*, 18, 293-310.

Gentry, R. C., E. B. Rodgers, J. Steranka and W. E. Shenk, 1980: Predicting tropical cyclone intensity using satellite measured equivalent blackbody temperatures of cloud tops. *Mon. Wea. Rev.*, 108, 445-455.

Gray, W. M., 1967: The mutual variation of wind, shear, and baroclinicity in the cumulus convective atmosphere of the atmosphere. *Mon. Wea. Rev.*, 95, 55-74.

Gray, W. M., 1970: A climatology of tropical cyclones and disturbances of the western Pacific with a suggested theory for their genesis/maintenance. U. S. Navy Weather Research Facility Tech. Paper 19-70, Norfolk, VA, 224 pp.

Gray, W. M., 1979: Tropical cyclone intensity determination through upper tropospheric aircraft reconnaissance. *Bull. Amer. Meteor. Soc.*, 60, 1069-1074.

Gray, W. M., 1981: Recent advances in tropical cyclone research from rawinsonde composite analysis. World Meteorological Organization, Geneva, 407 pp.

Gray, W. M. and D. J. Shea, 1976: Data summary of NOAA's hurricane inner-core radial leg flight penetrations 1957-1967 and 1969. Dept. of Atmos. Sci. Paper No. 257, Colo. State Univ., Ft. Collins, CO, 126 pp.

Gray, W. M. and R. W. Jacobson, Jr., 1977: Diurnal variation of deep cumulus convection. *Mon. Wea. Rev.*, 105, 1171-1188.

Hack, J. J. and W. H. Schubert, 1986: On the nonlinear response of atmospheric vortices to heating by organized cumulus convection. *J. Atmos. Sci.*, 43, 1559-1573.

Hawkins, H. F. and S. M. Imbembo, 1976: The structure of small intense hurricane–Inez 1966. *Mon. Wea. Rev.*, 104, 418-442.

Hawkins, H. F. and D. L. Rubsam, 1968: Hurricane Hilda, 1964, II: Structure and budgets of the hurricane on October 1, 1964. *Mon. Wea. Rev.*, 96, 617-637.

Holland, G. J. and R. T. Merrill, 1984: On the dynamics of tropical cyclone structural changes. *Quart. J. Roy. Meteor. Soc.*, 110, 723-745.

Holland, G. J., T. D. Keenan and G. D. Crane, 1984: Observations of a phenomenal temperature perturbation in Tropical Cyclone Kerry (1979). *Mon. Wea. Rev.*, 112, 1074-1082.

Holliday, C. R., 1977: On the rapid intensification of typhoons. MS Thesis, Texas A and M Univ. Department of Meteorology, College Station, TX.

Holliday, C. R. and A. H. Thompson, 1979: Climatological characteristics of rapidly intensifying typhoons. *Mon. Wea. Rev.*, 107, 1022-1034.

Jarvinen, B. R. and C. J. Neumann, 1979: Statistical forecasts of tropical cyclone intensity for the North Atlantic basin. NOAA Tech. Memo. NWS-NHC-10, 22 pp.

Joint Typhoon Warning Center, 1960-80: Annual Typhoon Reports 1959-79. Fleet Weather Central/Joint Typhoon Warning Center, FPO San Francisco, 96630.

Joint Typhoon Warning Center, 1981-89: Annual Tropical Cyclone Reports 1980-88. US Naval Oceanography Command Center/Joint Typhoon Warning Center, FPO San Francisco, 96630.

Joint Typhoon Warning Center, 1987: Modified Operations Evaluation. US Naval Oceanography Command Center/Joint Typhoon Warning Center, FPO San Francisco, 96630.

Kidder, S. Q., W. M. Gray and T. H. Vonder Haar, 1978: Estimating tropical cyclone central pressure and outer winds from satellite microwave data. *Mon. Wea. Rev.*, 106, 1458-1464.

Koeteswaram, P., 1967: On the structure of hurricanes in the upper troposphere and lower stratosphere. *Mon. Wea. Rev.*, 95, 541-564.

LaSuer, N. E. and H. F. Hawkins, 1963: An analysis of Hurricane Cleo (1958). *Mon. Wea. Rev.*, 91, 694-709.

Lunney, P. A., 1987: Environmental and convective influence on tropical cyclone development vs. non-development. Dept. of Atmos. Sci. Paper No. 436, Colo. State Univ., Fort Collins, CO, 105 pp.

Martin, J. D., 1988: Tropical cyclone observation and forecasting with and without aircraft reconnaissance. Dept. of Atmos. Sci. Paper No. 428, Colo. State Univ., Fort Collins, CO, 102 pp.

Merrill, R. T., 1987: An experiment in statistical prediction of tropical cyclone intensity change. *NOAA Tech. Memo.*, NWS NHC-34, 32 pp.

Merrill, R.T., 1988: Environmental influences on hurricane intensification. *J. Atmos. Sci.*, 45, 1678-1687.

Palmén, E., 1948: On the formation and structure of tropical hurricanes. *Geophysica*, 3, 26-38.

Penn, S., 1966: Temperature and ozone variations near tropopause level over Hurricane Isbell October 1964. *J. Appl. Meteor.*, 4, 212-216.

Pike, A. C., 1985: Geopotential heights and thicknesses as predictors of Atlantic tropical cyclone motion and intensity. *Mon. Wea. Rev.*, 113, 931-939.

Riehl, H., 1948: A radiosonde observation in the eye of a hurricane. *Quart. J. Roy. Meteor. Soc.*, 74, 194-196.

Riehl, H., 1954: Some aspects of Hurricane Daisy. *Tellus*, 13, 181-213.

Schubert, W. H. and J. J. Hack, 1982: Inertial instability and tropical cyclone development. *J. Atmos. Sci.*, 39,1687-1697.

Shea, D. J. and W. M. Gray, 1973: The hurricane's inner core region. I: Symmetric and asymmetric structure. *J. Atmos. Sci.*, 30, 1544- 1564.

Shewchuk, J. D. and R. C. Wier, 1980: An evaluation of the Dvorak technique for estimating tropical cyclone intensities from satellite imagery. NOCC/JTWC Tech. Note 80-2, U. S. Naval Oceanography Command Center/Joint Typhoon Warning Center, FPO San Francisco, 96630, 25 pp.

Simpson, R. H., 1947: A note on the movement and structure of the Florida hurricane of October 1946. *Mon. Wea. Rev.*, 75, 53-58.

Simpson, R. H., 1955: On the structure of tropical cyclones as studied by aircraft reconnaissance. Proceedings, UNESCO Symposium on Typhoons, Tokyo, 1954.

Stear, J. R., 1965: Sounding in the eye of Hurricane Arlene to 108,760 feet. *Mon. Wea. Rev.*, 93, 380-382.

Steranka, J., E. B. Rodgers and R. C. Gentry, 1986: The relationship between satellite measured convective bursts and tropical cyclone intensification. *Mon. Wea. Rev.*, 114, 1539-1546.

Sugg, A. L., 1967: The hurricane season of 1966. *Mon. Wea. Rev.*, 95, 131-142.

Veldon, C. S., 1989: Observational analyses of North Atlantic tropical cyclones from NOAA polar-orbiting satellite microwave data. *J. Appl. Meteor.*, 28, 59-70.

Veldon, C. S. and W. L. Smith, 1983: Monitoring tropical cyclone evolution with NOAA satellite microwave observations. *J. Climate Appl. Meteor.*, 22, 714-724.

Weatherford, C. L., 1985: Typhoon structural variability. Dept. of Atmos. Sci. Paper No. 391, Colo. State Univ., Ft. Collins, CO, 77 pp.

Weatherford, C. L., 1989: The structural evolution of typhoons. Dept. of Atmos. Sci. Paper No. 446, Colo. State Univ., Ft. Collins, CO, 198 pp.

Weatherford, C. L. and W. M. Gray, 1988: Typhoon structure as revealed by aircraft reconnaissance. Part II: Structural variability. *Mon. Wea. Rev.*, 116, 1044-1056.

Willoughby, H. E., J. A. Clos and M. G. Shoreibah, 1982: Concentric eye walls, secondary wind maxima, and the evolution of the hurricane vortex.

J. Atmos. Sci., 39, 395-411.

Zehr, R. M., 1976: Tropical disturbance intensification. Dept. of Atmos. Sci. Paper No. 259, Colo. State Univ., Ft. Collins, CO, 91 pp.

Zehr, R. M., 1988: Satellite diagnosis of tropical cyclones. Extended Abstacts Volume, 3rd Conf. on Satellite Meteorology and Oceanography, AMS, Anaheim, CA, Jan 31 - Feb 5, 1988.

Zehr, R. M., 1990: Tropical cyclone genesis. Extended Abstracts Volume, 44th Interdepartmental Hurricane Conference, Homestead AFB, FL, Jan 9-12, 1990.

Appendix A

OPERATIONAL APPLICATION AND FORECAST RULES

Once a disturbance develops into a tropical storm, the latitude at which initial tropical storm classification occurs (TS Lat) is used in the first few forecasts for a long range forecast of maximum intensity and the number of hours required to reach peak intensity (Fig. A.1). For example, if a storm intensifies to tropical storm intensity (18 ms^{-1}) at 20°N in the western Pacific during the months of July to November, the mean (most likely) maximum intensity will be 41 ms^{-1} (80 kt) in 60 hours, an intensification rate of 9.2 ms^{-1} per day (0.75 $kt\ hr^{-1}$). If, for example, the cyclone reaches 33 ms^{-1} (64 kt) intensity at 23°N in 30 hours, then the relationship between initial typhoon latitude (TY Lat) and intensity would predict a maximum intensity of 46 ms^{-1} with an overall (TS to max) intensification rate of 9.6 ms^{-1} per day (Fig. A.2). Thus, the long range forecast at this point would be a further increase in intensity of 13 ms^{-1} (25 kt) in the next 42 hours. Actual forecasts would be based on several other environmental factors, but the relationship between tropical storm latitude and mean maximum intensity would probably be an improvement on any other prediction method based strictly on climatology and, in most cases, better than the official intensity forecast. The advantage of this long range prediction scheme is that it can provide an good initial intensity forecast for the first few tropical cyclone warnings until a more definite rate of intensification is established. A verification experiment demonstrated that a long range prediction method based strictly on the latitude of TS and TY development can outperform the official JTWC intensity forecasts during the primary season months of July to November, particularly for rapid

intensification events. Most tropical cyclone forecasters would agree that the most difficult intensity forecasts are during the first 24 hours of development, and a forecast method based on TS Lat would likely reduce the magnitude of long range intensity forecast errors.

Climatological parameters can also be used to determine the probability that a given tropical cyclone would rapidly intensify or not. Rapid intensification is very unlikely to occur if a tropical cyclone is north of 22°N latitude or located in the South China Sea region. Rapid intensification is not likely to occur during the months of December to June. Most rapid intensification events occur at initial intensities close to 33 ms^{-1} (65 kt), so the latitude and julian date at which minimal typhoon intensity occurs is useful to determine the probability that a certain typhoon will begin to rapidly intensify (Fig. A.3). The first step is to determine if the TS Lat and the TY Lat were at latitudes south of the seasonal mean (Fig. A.4). Rapid intensification is not likely if tropical storm and/or typhoon development occurs more than 1° (111 km) north of the seasonal mean. The next step is to determine the probability of rapid intensification based on julian date (Fig. A.5). Climatological parameters clearly show that typhoons which reach minimal typhoon intensity at low latitude in the primary season of July to November are more likely to experience a rapid intensification event.

The rate of change of the satellite data T-numbers once an eye was apparent in the satellite data was also found to be a strong indication of rapid intensification. Changes of more than 1.0 T-numbers in 6 hours or 1.5 in 12 hours are short term predictors of rapid intensity change since a 6 to 12 hour lag appears to exist between intensity estimates based on satellite measurements and minimum sea level pressure intensities measured by aircraft. The accuracy of any prediction method for rapid intensification based on the Dvorak data T-numbers is questionable due to observed storm-to-storm variability in the magnitude of the satellite overestimate and the apparent time lag. An experimental test of the ability to predict minimum sea level pressure measurements 12 hours later yielded encouraging results. Assuming a lag of about 12 hours between intensities observed by

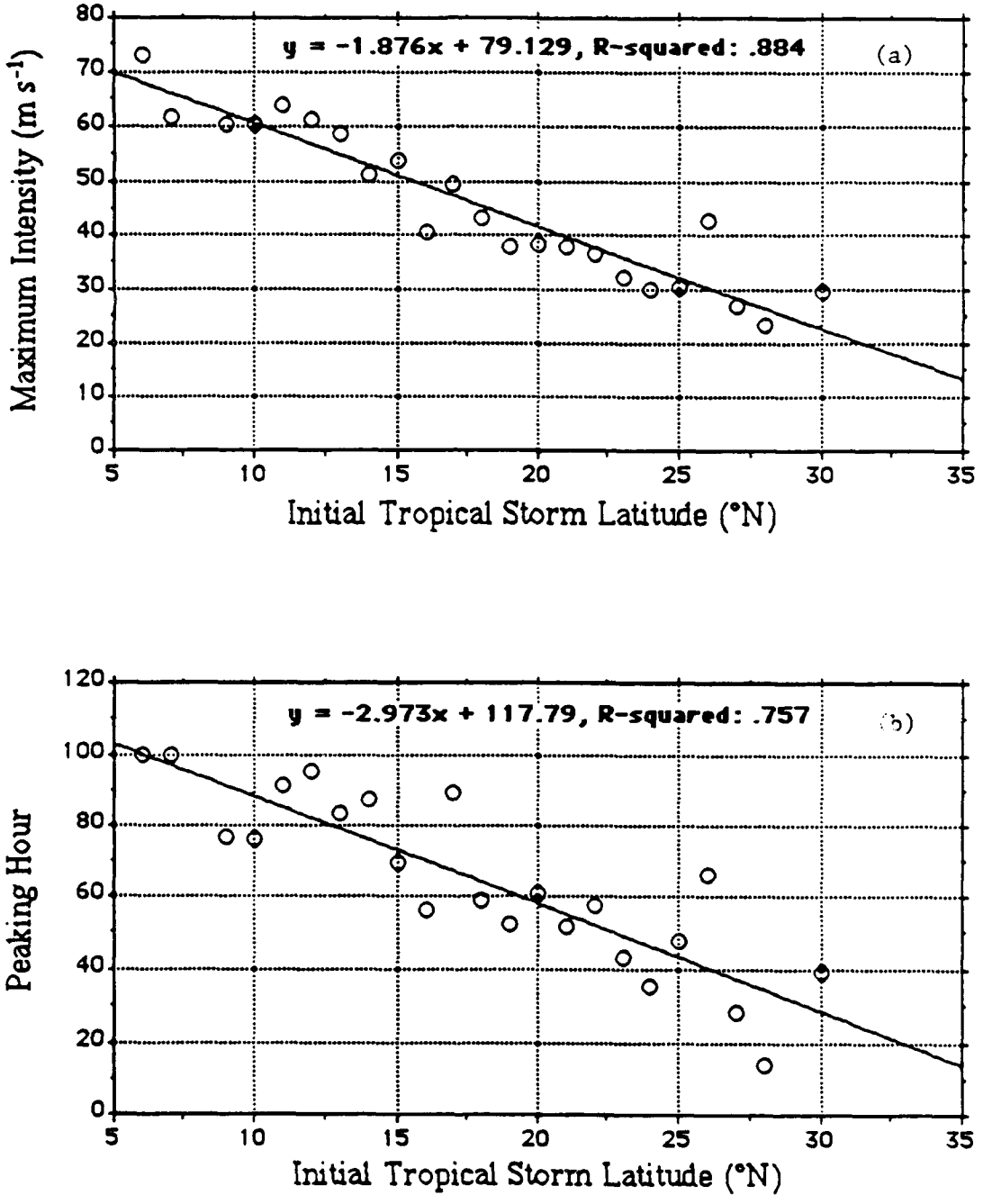

Figure A.1: Relationships between mean maximum intensity (a), mean peaking hour (b), and the latitude of initial classification as a tropical storm. The correlation coefficients are given by r and the regression equations by y.

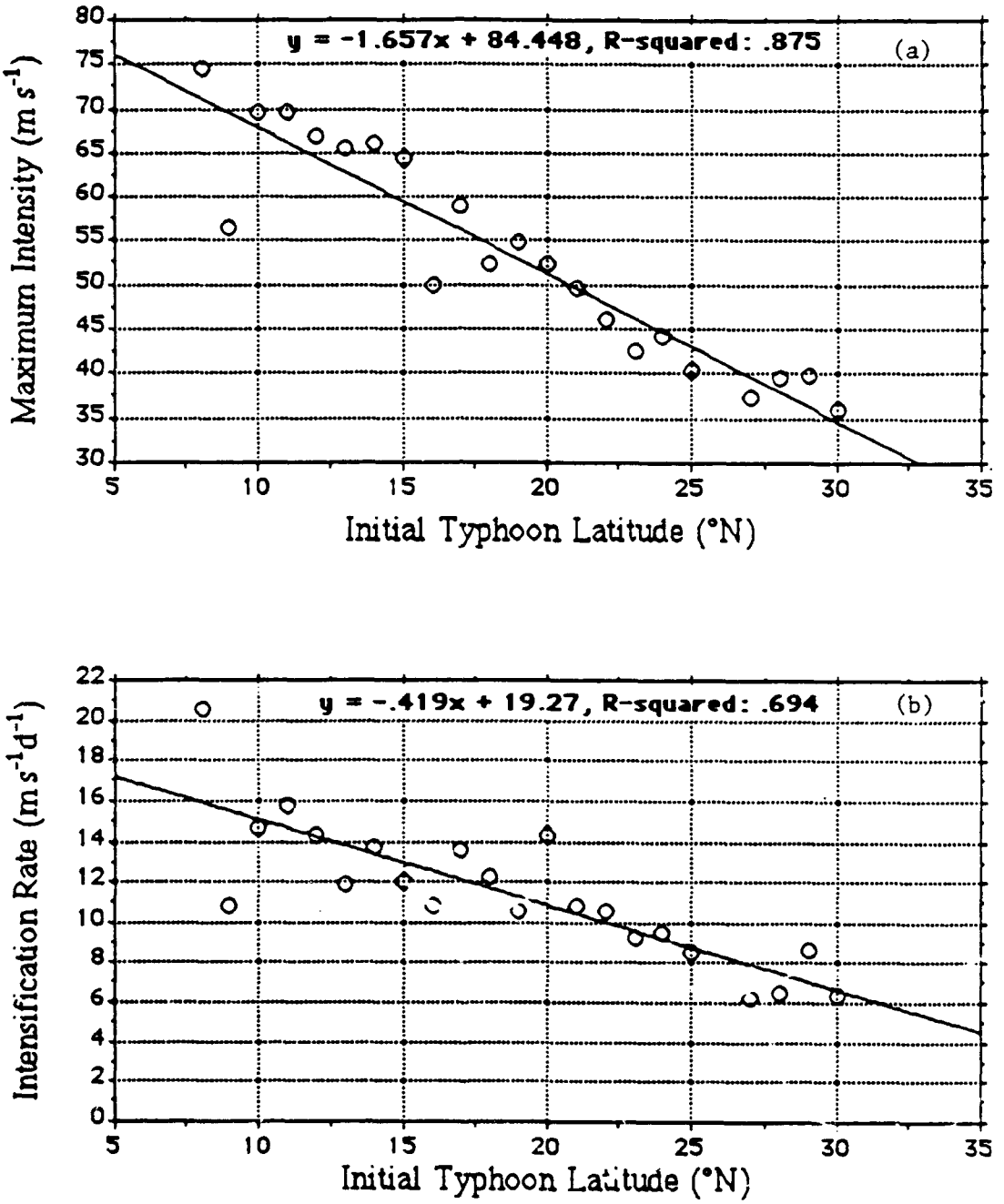

Figure A.2: Relationships between mean maximum intensity (a), mean rate of intensification (b), and the latitude of initial classification as a typhoon. The correlation coefficients are given by r and the regression equations by y.

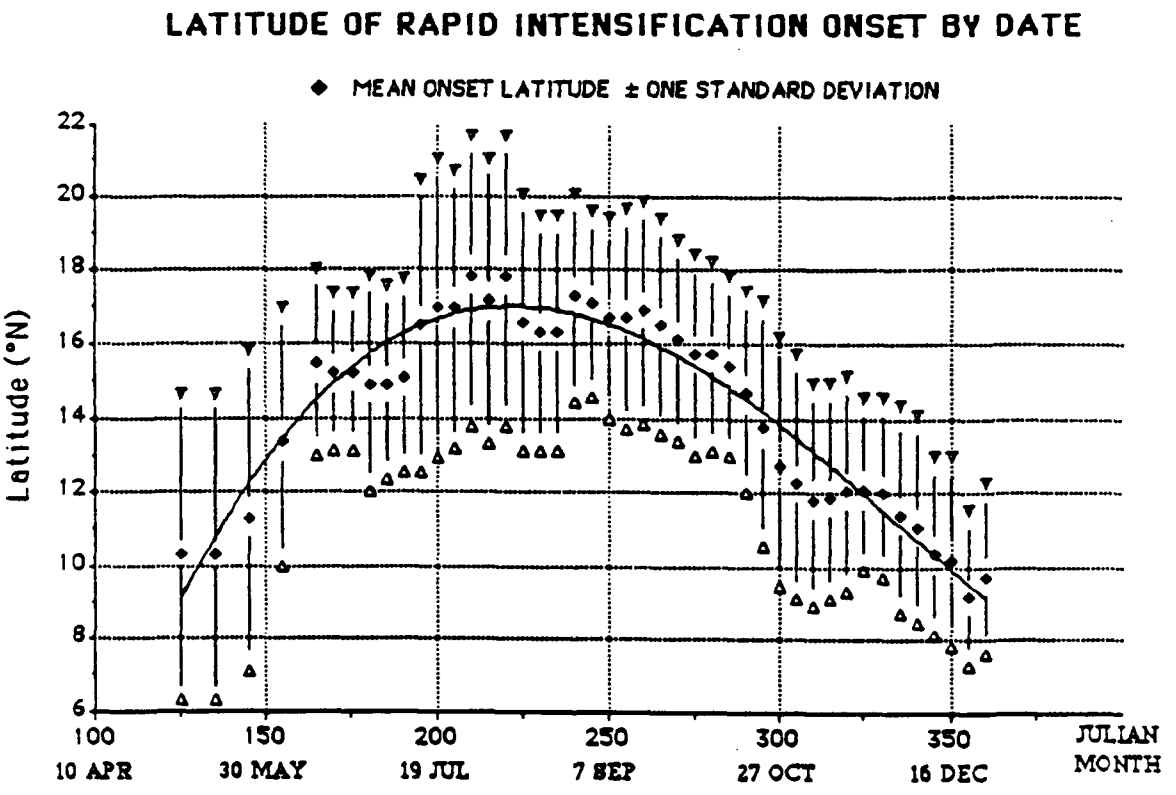

Figure A.3: Mean latitude of onset of rapid intensity change stratified by date. Mean values and standard deviations for each multiple of five julian days are shown along with the best fit regression line.

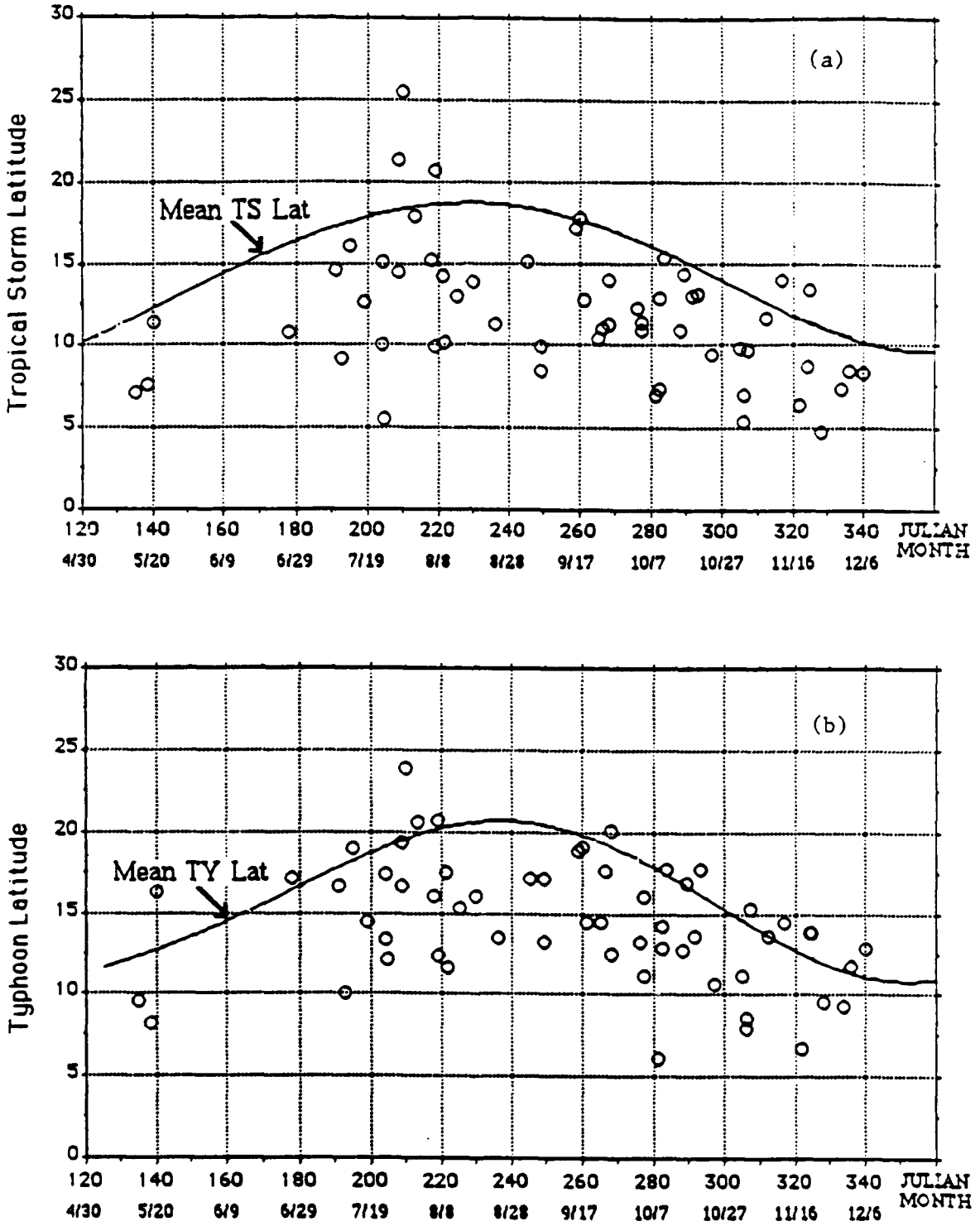

Figure A.4: Relationships between the latitude of initial classification as a tropical storm (a), latitude of initial typhoon classification (b) for rapid intensifiers (open circles), and the mean latitude (by julian date) of TS and TY development for all NWPAC tropical cyclones (solid lines).

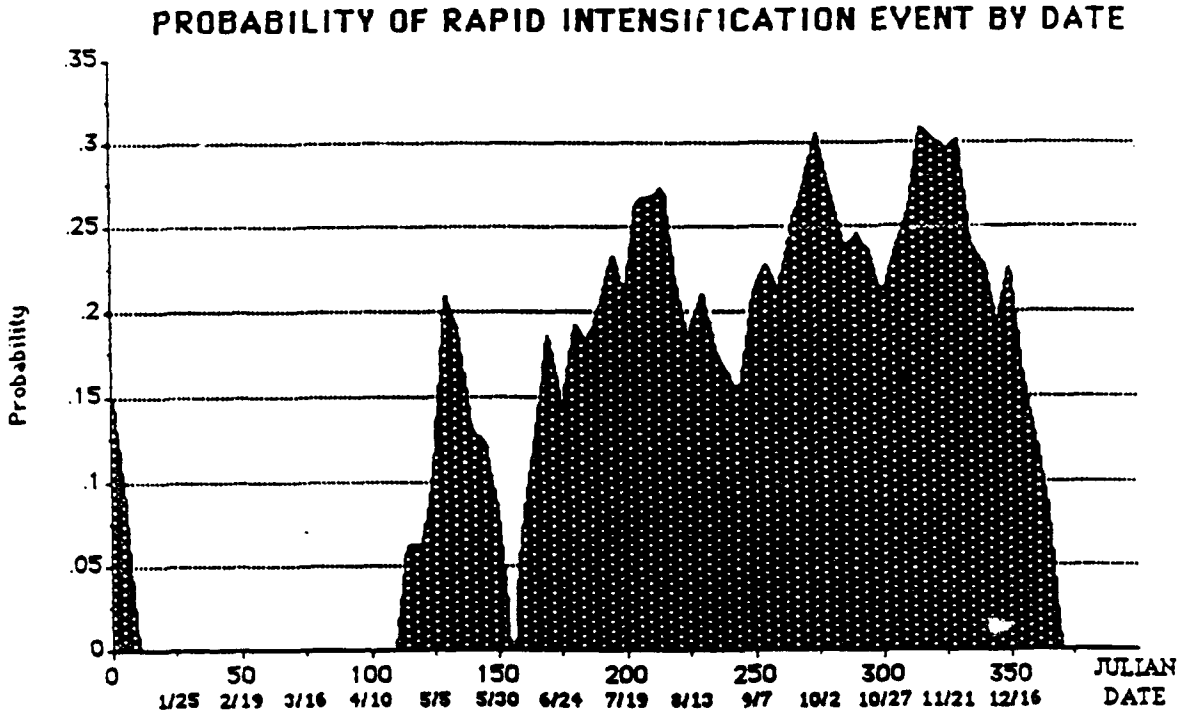

Figure A.5: Relative probability (by julian date) that a tropical cyclone of minimal typhoon intensity will rapidly intensify. Relative probabilities were determined by dividing the number of rapid intensification events by the number of minimal typhoon events for each 30 day overlapping "julian month" periods.

satellite and actual intensity changes at the surface during rapid intensification, unusually large increases in the data T-number for tropical cyclones with an eye can be used to predict the intensity currently indicated by the data T-number at a point 12 hours later (Fig. A.6).

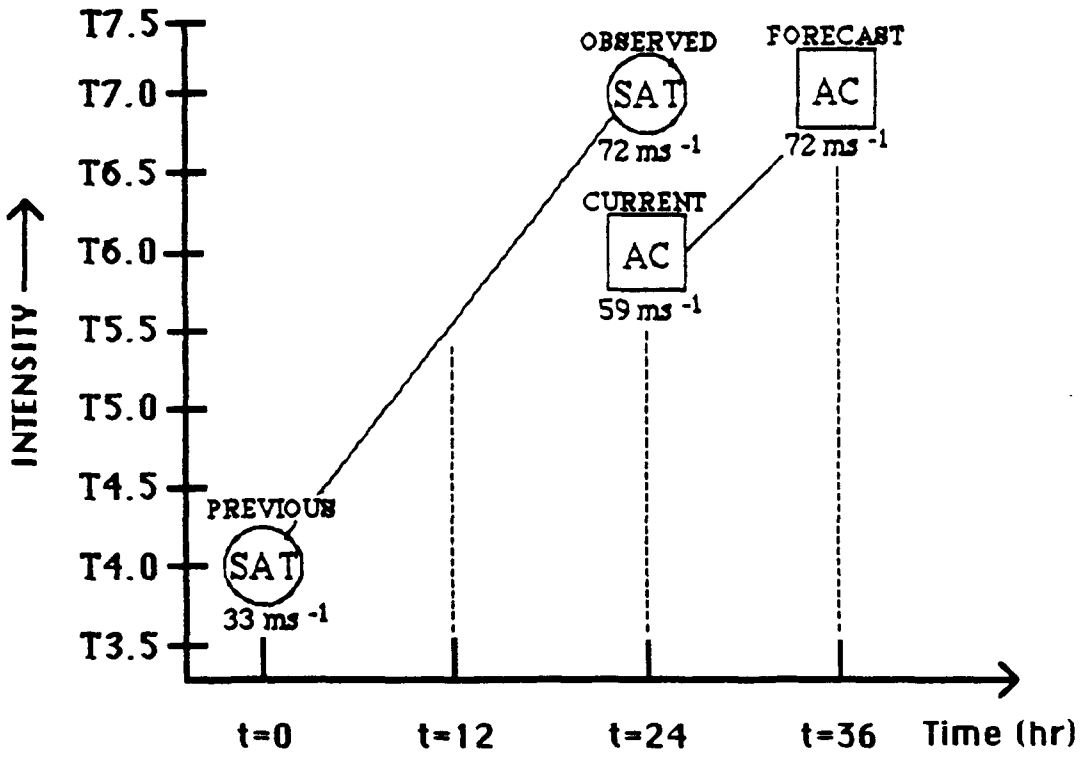

Figure A.6: An example of a method to predict short term intensity changes based on a lag of approximately 12 hours observed between rapid changes of satellite (SAT) intensity estimates and rapid intensity change as measured by aircraft (AC).

Prediction of rapid intensification based on the relative concentration of deep convection is most promising. The first step in this prediction method is to determine the number of pixels within 222 km of the center whose brightness temperature is -75°C or less and the pixel count colder than -65°C in the 222 to 666 km radial belt. A running mean of the previous 24 hours of data is taken to reduce diurnal effects. The running means are plotted along a modified scale given in Fig. A.7.

When the two plots intersect, or when X in the equation given by

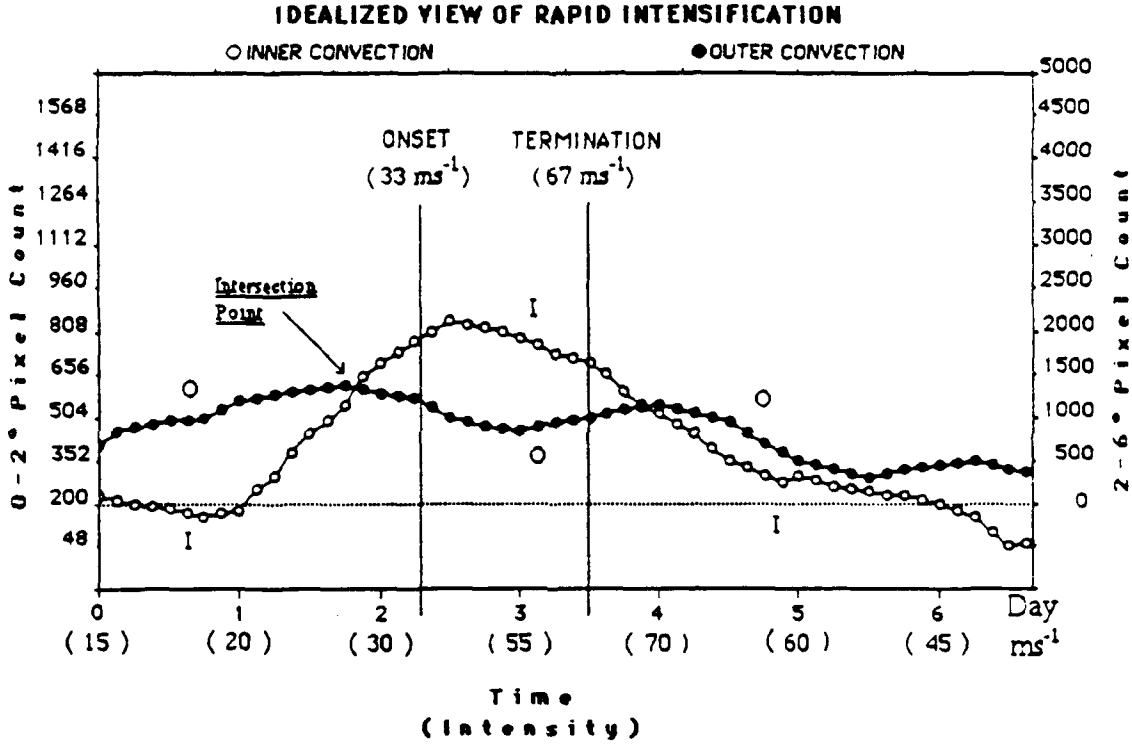

Figure A.7: Idealized view of the method used to predict the onset of rapid intensity change (for 10 km GMS infrared data) based on the relative concentrations of inner core (0-2°) and outer core (2-6°) deep convection. When climatological conditions are favorable, an intersection of the 24 hour running mean pixel count values occurs approximately 12 hours prior to the onset of rapid intensification.

$$x = \frac{(3.29)(P_i - 200)}{P_o}$$

is greater than 1.0, then the onset of rapid intensification is imminent and should be predicted within the next six hours as long as the climatological parameters of rapid intensification such as location, julian date and latitude indicate the probability of rapid intensification is relatively high. This prediction method correctly predicted the rapid intensification events of Wayne (83), Abby (83), Marge (83), Vanessa (84), Bill (84), Doyle (84) and Dot (85) and non-rapid intensification in 59 of 60 tropical storms and typhoons which occurred during the 1983-85 seasons. Prediction of rapid intensification for Clara (84) was not verified and the rapid intensification events of Forrest (83), Dinah (84) and Agnes (84) were not forecast, yielding an overall success rate of 94% (Table A1).

Table A.1: Verification statistics of a technique which uses relative concentrations of inner and outer core deep convection to predict the onset of rapid ($\geq$ 42 hPa d^{-1}) intensity change. Data is based on 70 named tropical cyclones in the NWPAC from 1983 to 1985.

1983 to 1985	Tropical Cyclones	Pixel Plot Intersections	Eliminated By Climatology	Successful Forecasts	%
Rapid Intensifiers	10	7	0	7	70
Non-Rapid Intensifiers	60	10	9	59	98
TOTAL	70	17	9	66	96

The inability of this intersection technique to forecast the rapid intensification of Forrest and Agnes can be explained by the contraction of the eye diameter in both typhoons to an extremely small size (2 11 km). It is likely that rapid intensity change primarily occurred due to the contraction of the radius of maximum winds and not due to the more

typical process of concentrating the deep convection closer to the cyclone center. The forecast rules discussed in this section are summarized in Fig. A.8.

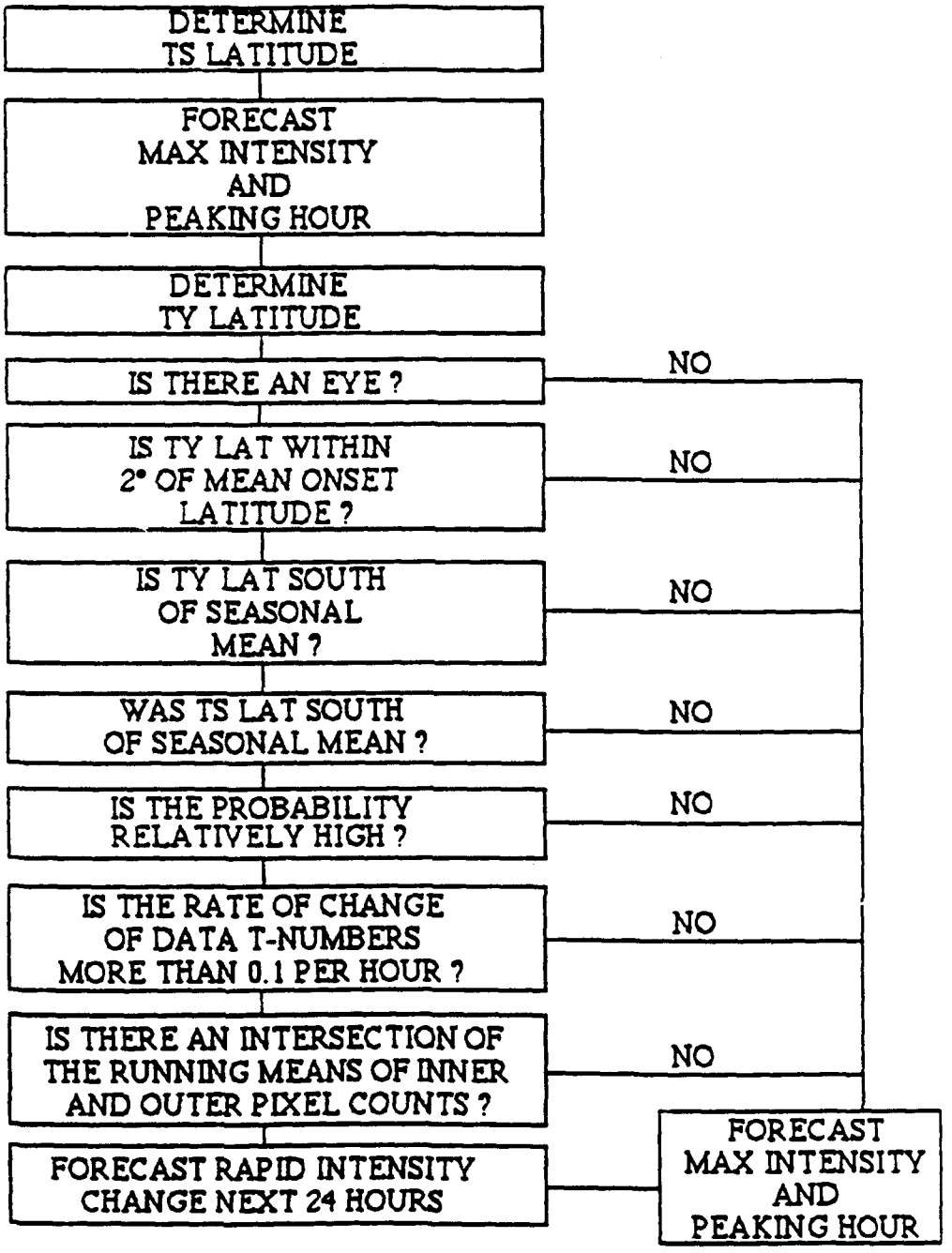

Figure A.8: Summary of climatological and satellite forecasting rules used to predict future intensity and the onset of rapid intensification. A long term forecast of maximum intensity and peaking hour is made at initial tropical storm classification. Once a tropical cyclone develops an eye or reaches minimal typhoon intensity, climatological factors such as time of year and location are the criteria used to determine the likelihood of rapid intensification once the pixel count curves of inner and outer convection (see Fig. A.7) intersect.

Appendix B

LIST OF RAPID INTENSIFIERS

Listing of the tropical cyclones that experienced a period of rapid intensification at a rate of at least 42 mb per day for the years 1956 to 1987. Climatological statistics of the date, location, intensity, and number of hours after tropical storm classification that the onset of rapid intensity change occurred is shown in the ONSET column. Changes in intensity (for both maximum winds and minimum sea level pressure) and the time period involved are shown in the INT RATE column. Latitudes of initial classification as a tropical storm and a typhoon are also shown.

		ONSET					INT RATE				
YEAR	NAME	JULIAN DATE	LAT °N	LON °E	V_{max} (kt)	HR	ΔV_{max} (kt)	ΔHR	ΔP_{max} (mb d^{-1})	TS Lat °N	TY Lat °N
56	WANDA	209	20.1	140.3	60		50	24	47		
57	VIRGINIA	171	13.3	135.6	50		80	28	76		
57	AGNES	228	20.6	133.2	65		60	36	66		
57	FAYE	261	10.8	145.3	80		45	23	49		
57	HESTER	280	18.0	141.9	60		80	24	81		
57	LOLA	317	09.0	152.6	85		55	25	64		
58	GRACE	243	13.7	137.1	75		60	25	65		
58	IDA	265	13.8	137.3	55		80	24	81		
58	NANCY	327	14.5	129.0	65		60	24	60		
59	JOAN	239	16.5	136.1	75		60	27	66		
59	VERA	265	16.8	146.7	75		70	23	73		
59	CHARLOT	285	15.8	129.0	65		65	32	70		
59	GILDA	348	07.4	140.2	60		45	24	42		
59	HARRIET	361	11.4	140.7	65		50	24	50		
60	TRIX	218	16.3	134.7	75		55	24	57		
61	PAMELA	253	22.2	133.7	70		45	24	43		
61	VIOLET	279	17.2	143.2	80		60	24	64		
62	OPAL	216	19.3	128.1	80		55	24	56		
62	RUTH	227	18.0	146.0	55		70	24	65		
62	EMMA	276	16.1	146.9	75		45	24	43		
62	KAREN	312	07.8	152.4	70		45	24			
63	WENDY	192	12.0	145.0	45		55	24	49		
63	BESS	215	18.5	137.7	70		50	25	53		
63	CARMEN	223	10.1	131.8	80		45	24	48		
63	JUDY	274	18.5	146.5	60		55	24	53		
64	HELEN	210	22.6	145.8	70		50	24	53		
64	IDA	217	15.0	131.0	70		45	24	45		
64	SALLY	249	14.3	140.7	80		60	24	60		
64	WILDA	263	19.4	142.3	85		50	24	58		
64	OPAL	343	07.9	138.8	55		60	23	53		
65	BESS	272	17.6	143.8	75		55	24	66		
65	CARMEN	279	16.6	147.0	70		60	29	59		
66	KIT	175	13.7	131.8	65		85	29	89		
66	CORA	244	15.3	138.3	45		70	27	63		
67	OPAL	245	19.0	162.8	60		60	24	57		
67	CARLA	286	11.8	136.6	60		75	30	78		
67	EMMA	305	09.0	135.7	70		55	29	55		
67	GILDA	316	13.5	146.3	85		45	30	49		
68	LUCY	180	16.8	138.0	50		60	24	52		
68	WENDY	240	16.1	146.8	70		45	24	48		
68	AGNES	245	17.3	142.4	85		50	24	52		
68	CARMEN	260	17.1	148.6	60		55	30	56		
68	ELAINE	269	13.5	128.6	55		75	30	76		
68	FAYE	276	15.5	158.3	70		45	24	43		
69	VIOLA	204	14.5	136.4	60		70	24	71		
69	IDA	289	16.0	144.8	40		75	30	78		
69	KATHY	310	14.2	132.0	60		65	30	60		
70	OLGA	181	14.3	132.4	65		60	24	60		
70	ANITA	230	21.9	138.3	75		50	24	47		
70	GEORGIA	252	14.7	131.5	70		60	33	63		
70	HOPE	265	17.5	151.6	65		80	24	81		
70	JOAN	284	11.5	130.7	60		60	24	54		
70	PATSY	320	14.6	135.7	50		50	24	42		
71	AMY	121	07.4	151.7	60		85	28	83		
71	HARRIET	185	15.0	115.9	65		50	24	45		
71	LUCY	198	15.6	130.1	85		45	24	46		
71	NADINE	203	17.1	133.7	80		50	24	53		
71	WENDY	248	20.7	165.5	75		50	24	49		
71	BESS	261	18.3	146.8	70		55	24	56		
71	IRMA	314	12.8	137.4	60		90	24	97		

		ONSET					INT RATE				
YEAR	NAME	JULIAN DATE	LAT °N	LON °E	V_{max} (kt)	HR	ΔV_{max} (kt)	ΔHR	ΔP_{max} (mb d^{-1})	TS Lat °N	TY Lat °N
72	KIT	6	10.2	132.8	60	18	60	24	53	09 5	10 7
73	BILLIE	195	17 9	125.4	50	24	80	36	65	16 0	19 0
73	NORA	277	13.0	131 3	80	60	80	30	72	11 4	11 [illegible]
73	PATSY	282	15.1	135.9	80	48	65	24	61	12.9	14 2
74	IVY	199	14 1	130.9	55	24	45	24	42	12.6	14 4
75	NINA	213	20.3	130.8	60	18	75	24	63	17 9	20 6
75	PHYLLIS	225	14.1	136.5	45	12	75	48	52	13 0	15 3
75	ELSIE	283	17 8	129.0	60	24	75	24	69	15 3	17 8
75	JUNE	322	08.8	142.5	75	42	85	30	90	06 4	06 [illegible]
76	OLGA	140	16.1	124.5	60	162	50	24	46	11 4	16 3
76	SALLY	178	18.1	133.8	75	60	45	24	48	10 8	17 [illegible]
76	THERESE	193	10.3	150.6	65	30	70	30	66	09 2	10 [illegible]
76	BILLIE	218	17.5	139.5	75	60	50	24	54	15 2	16 [illegible]
76	FRAN	249	17.1	140.7	65	48	60	24	61	09 9	17 [illegible]
76	LOUISE	305	11.2	138.6	65	36	70	30	50	09 8	11 2
77	VERA	210	24.9	128.1	65	24	45	24	47	25 5	23 9
77	BABE	249	16.7	128.6	85	108	45	24	53	08 5	13 2
77	KIM	312	13.3	146.1	55	36	50	24	42	11 6	13 6
77	LUCY	336	11.4	134.5	55	24	55	24	53	08 4	11 [illegible]
78	FAYE	245	17.0	147 5	55	60	50	30	42	15 0	17 [illegible]
78	VIOLA	324	13.8	136.5	65	60	60	24	54	08 7	13 3
79	JUDY	230	15.7	139.0	55	24	75	24	69	13 8	16 0
79	OWEN	268	21.0	130.7	75	36	45	24	49	13 9	20 [illegible]
79	TIP	282	13.7	141.1	95	114	45	24	55	07 3	12 9
79	VERA	306	08.0	140.9	65	24	70	24	64	07 0	08 0
80	ELLEN	135	09.5	142.0	65	54	45	24	42	07 1	09 5
80	KIM	204	13.6	128.6	70	48	60	24	61	10.0	13 4
80	MARGE	221	15.4	156.1	45	24	55	24	56	14 2	17 5
80	PERCY	259	19 5	125.9	75	66	50	24	48	17 1	18 8
80	WYNNE	281	17.4	141.2	70	120	80	24	85	07 0	06 [illegible]
81	CLARA	261	15.7	126.3	75	48	45	24	45	12.7	14 4
81	ELSIE	268	12.2	142.2	50	18	80	36	59	11 3	12 5
81	IRMA	325	13.8	140.3	70	42	55	24	51	13 4	13 9
82	BESS	209	16.8	149.6	95	114	45	24	47	14 4	16 [illegible]
82	CECIL	219	20.9	123.7	70	30	50	24	50	20.7	20 [illegible]
82	KEN	260	18.7	130.0	60	18	45	24	43	17 8	19 1
82	MAC	276	12.6	145.4	50	18	75	42	46	12 3	13 2
83	WAYNE	204	16.8	130.2	55	18	75	30	68	15 0	17 4
83	ABBY	219	12.8	135.8	70	30	60	24	65	09 9	12 4
83	FORREST	265	15.2	137.9	65	36	85	24	92	10 4	14 4
83	MARGE	307	17.0	139.1	80	66	60	24	67	09 7	15 3
84	DINAH	209	21.0	151.5	80	84	45	24	46	21 3	19 3
84	THAD	293	17 8	145.6	65	24	45	24	40	13.1	17 8
84	VANESSA	297	12.3	142.2	70	42	75	30	67	09 4	10 6
84	AGNES	306	08.6	137.3	65	48	50	24	52	05 4	08 6
84	BILL	317	12.5	138.4	80	114	50	24	52	13 9	14 5
84	DOYLE	340	12.9	133.4	60	48	45	24	43	08 3	12 9
85	DOT	288	12.7	139.0	65	36	75	30	67	10 9	12 7
86	LOLA	138	08 2	159 0	65	30	65	30	58	07 6	08 2
86	BEN	266	17.8	146.0	70	102	45	24	43	11 0	17 6
86	CARMEN	277	16.7	141.7	55	60	45	30	43	10 9	16 1
86	FORREST	289	16.3	151 9	50	12	50	24	42	14 3	16 9
86	KIM	334	11 4	154.3	65	54	50	24	44	07 4	09 3
87	THELMA	191	17.7	134.0	90	48	40	24	43	14 6	16 6
87	WYNNE	205	12.1	157 6	50	54	55	24	52	05 5	12 1
87	BETTY	222	11 3	131.7	55	24	85	36	68	10.2	11 6
87	DINAH	236	14 6	133.7	75	72	55	30		11 3	13 5
87	LYNN	291	15.1	145.0	80	60	60	30		13 0	13 6
87	NINA	328	12.1	129.6	90	114	55	24		04 8	09 5

Appendix C

LIST OF TROPICAL CYCLONES INCLUDED IN CLIMATOLOGICAL FORECASTING EXPERIMENT

Listing of the tropical cyclones used in a series of three verification experiments to determine the accuracy of a climatological forecast intensity method based on the latitude of initial tropical storm or typhoon classification. Forecast intensity errors were based on the official JTWC "best track" and compared to the errors of the official JTWC intensity forecasts at 24, 48, and 72 hours. There were four types of storm classifications: primary season (P), off season (O), rapid intensifiers (R), and South China Sea (S).

CLIMO EXPER 1

NAME	MONTH	TYPE
Marie	Jun 72	O
Susan	Jul 72	S
Joan	Aug 73	S
Harriet	Jul 74	P
Carmen	Oct 74	P
Lola	Jan 75	O
Phyllis	Aug 75	R
Grace	Oct 75	P
Violet	Jul 76	S
Nora	Dec 76	O
Patsy	Mar 77	O
Emma	Sep 77	P
Virginia	Jul 78	P
Ora	Oct 78	P
Cecil	Apr 79	O
Lola	Sep 79	P
Norris	Aug 80	P
Betty	Oct 80	P
Holly	Apr 81	O
Clara	Sep 81	R
Kit	Dec 81	O
Dot	Aug 82	P
Pamela	Nov 82	P
Sarah	Jun 83	S
Forrest	Sep 83	R
Gerald	Aug 84	S
Agnes	Oct 84	R
Hal	Jun 85	O
Winona	Sep 85	S
Vera	Aug 86	P
Herbert	Nov 86	S
Thelma	Jul 87	R
Freda	Aug 87	P

CLIMO EXPER 2

NAME	MONTH	TYPE
Cora	Aug 72	S
Therese	Dec 72	O
Billie	Jul 73	R
Opal	Oct 73	S
Wanda	Jan 74	O
Rose	Aug 74	P
Mamie	Jul 75	P
Flossie	Oct 75	S
Lorna	Feb 76	O
Hope	Sep 76	P
Sarah	Jul 77	S
Ivy	Oct 77	P
Olive	Apr 78	O
Irma	Sep 78	P
Gordon	Jul 79	P
Sarah	Oct 79	S
Ben	Dec 79	O
Forrest	May 80	O
Percy	Sep 80	R
Roy	Aug 81	S
Fabian	Oct 81	S
Ruby	Jun 82	O
Hope	Sep 82	P
Dom	Aug 83	P
Orchid	Nov 83	P
Wynne	Jun 84	O
Kelly	Sep 84	P
Mamie	Aug 85	P
Gordon	Nov 85	S
Peggy	Jul 86	P
Ben	Sep 86	R
Cary	Aug 87	P
Nina	Nov 87	R

CLIMO EXPER 3

NAME	MONTH	TYPE
Roy	Jan 88	O
Susan	May 88	O
Thad	Jun 88	O
Vanessa	Jun 88	O
Warren	Jul 88	P
Agnes	Jul 88	P
Bill	Aug 88	P
Clara	Aug 88	P
Doyle	Aug 88	R
Elsie	Aug 88	P
Fabian	Aug 88	P
Gay	Sep 88	P
Hal	Sep 88	P
Irma	Sep 88	P
Jeff	Sep 88	P
Kit	Sep 88	S
Lee	Sep 88	P
Nelson	Oct 88	R
Odessa	Oct 88	P
Pat	Oct 88	P
Ruby	Oct 88	P
Skip	Nov 88	P
Tess	Nov 88	S
Val	Dec 88	O

Appendix D

LIST OF TROPICAL CYCLONES USED FOR SATELLITE ANALYSIS

Listing of the tropical cyclones used to determine differences between satellite-derived estimates of intensity from the Dvorak Data T-number and aircraft measurements of intensity from minimum sea level pressure or 700 hPa height. Rapid intensifiers were defined to be tropical cyclones that intensified at a rate greater than 42 hPa per day for a period of at least 24 hours.

NON-RAPID INTENSIFIERS	
Vera	Jul 83
Ellen	Sep 83
Ida	Oct 83
Orchid	Nov 83
Alex	Jul 84
Cary	Jul 84
Kelly	Sep 84
Irma	Jun 85
Nelson	Aug 85
Pat	Aug 85
Brenda	Oct 85
Cecil	Oct 85
Faye	Oct 85
Hope	Dec 85
Peggy	Jul 86
Joe	Nov 86
Norris	Dec 86
Orchid	Jan 87

RAPID INTENSIFIERS	
Wayne	Jul 83
Abby	Aug 83
Forrest	Sep 83
Marge	Nov 83
Dinah	Jul 84
Thad	Oct 84
Vanessa	Oct 84
Agnes	Nov 84
Bill	Nov 84
Doyle	Dec 84
Dot	Oct 85
Lola	May 86
Ben	Sep 86
Carmen	Oct 86
Forrest	Oct 86
Kim	Dec 86
Thelma	Jul 87
Wynne	Jul 87
Betty	Aug 87